AD-A153 254 GROUND AND FLIGHT TESTING FOR AIRCRAFT GUIDANCE AND CONTROL(U) ADVISORY GROUP FOR AEROSPACE RESEARCH AND DEVELOPMENT NEUILLY-SUR-SEINE (FRANCE) R ONKEN ET AL. 1/3

UNCLASSIFIED DEC 84 AGARD-AG-262 F/G 1/4 NL

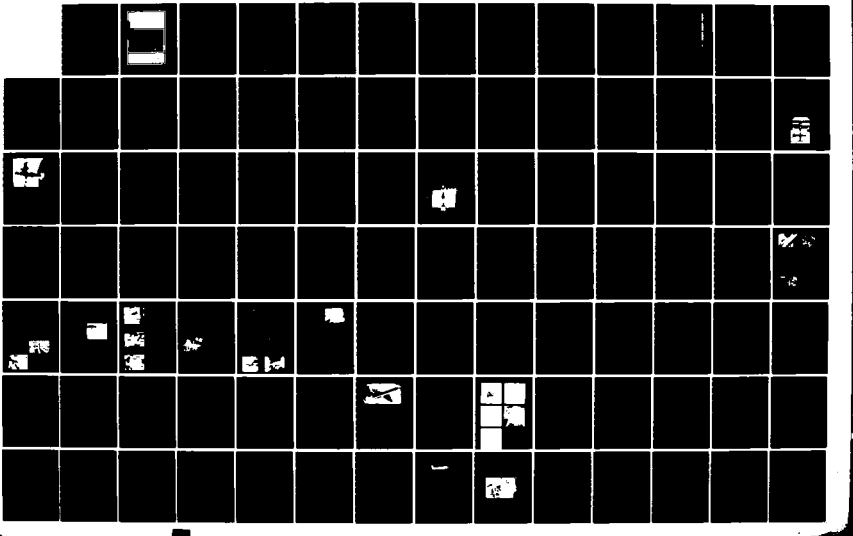

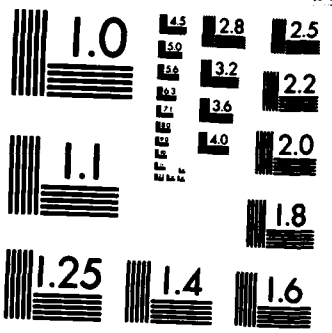

AGARD-AG-262

AGARD-AG-262

AGARD

ADVISORY GROUP FOR AEROSPACE RESEARCH & DEVELOPMENT

7 RUE ANCELLE 92200 NEUILLY SUR SEINE FRANCE

AGARDograph No. 262

Ground and Flight Testing for Aircraft Guidance and Control

Edited by

R.Onken and H.A.Rediess

NORTH ATLANTIC TREATY ORGANIZATION

AGARD-AG-262

NORTH ATLANTIC TREATY ORGANIZATION

ADVISORY GROUP FOR AEROSPACE RESEARCH AND DEVELOPMENT

ORGANISATION DU TRAITE DE L'ATLANTIQUE NORD

AGARDograph No.262

GROUND AND FLIGHT TESTING FOR AIRCRAFT GUIDANCE AND CONTROL

Edited by

Dr Ing. Reiner Onken
DFVLR
Institut für Flugführung
Postfach 32 67
D-3300 Braunschweig

and

Dr Hermann A.Rediess
HR Textron Inc
2485 McCabe Way
Irving, CA 92714
United States

This AGARDograph has been prepared and edited at the request of the Guidance and Control Panel of AGARD.

THE MISSION OF AGARD

The mission of AGARD is to bring together the leading personalities of the NATO nations in the fields of science and technology relating to aerospace for the following purposes:

- Exchanging of scientific and technical information;
- Continuously stimulating advances in the aerospace sciences relevant to strengthening the common defence posture;
- Improving the co-operation among member nations in aerospace research and development;
- Providing scientific and technical advice and assistance to the North Atlantic Military Committee in the field of aerospace research and development;
- Rendering scientific and technical assistance, as requested, to other NATO bodies and to member nations in connection with research and development problems in the aerospace field;
- Providing assistance to member nations for the purpose of increasing their scientific and technical potential;
- Recommending effective ways for the member nations to use their research and development capabilities for the common benefit of the NATO community.

The highest authority within AGARD is the National Delegates Board consisting of officially appointed senior representatives from each member nation. The mission of AGARD is carried out through the Panels which are composed of experts appointed by the National Delegates, the Consultant and Exchange Programme and the Aerospace Applications Studies Programme. The results of AGARD work are reported to the member nations and the NATO Authorities through the AGARD series of publications of which this is one.

Participation in AGARD activities is by invitation only and is normally limited to citizens of the NATO nations.

Published December 1984

ISBN 92-835-1482-3

Printed by Specialised Printing Services Limited
40 Chigwell Lane, Loughton, Essex IG10 3TZ

PREFACE

With the advent of many innovations in the realm of aircraft guidance and control systems technology (functions, components and system integration) along with the extension of system tasks and increase in cost, appropriate assessment of system performance becomes an increasingly necessary but also more difficult task during the development of new equipment.

The objective of this AGARDograph, assembled by the Guidance and Control Panel of AGARD, is to bring together the benefits in use of major test facilities and techniques in evaluating aircraft guidance and control functions, components and systems. The emphasis will be on specific examples of user oriented test programs rather than descriptions of the facilities.

The AGARDograph is organized into five parts. Part I deals with control handling and active control testing; Part II covers tests on flight path control; Part III focusses on navigation system testing; Part IV embarks on combat guidance and control evaluation and Part V gives some insight in testing of flight-crucial digital systems in guidance and control. We have been fortunate to put together a representative number of very knowledgeable contributions covering a great span of what is in use for ground and flight testing today. The editors wish to express their appreciation to the authors for their extensive efforts to share their valuable experiences and views.

The editors are also indebted to the panel colleagues who assisted in the identification of authors and selection of topics from their respective countries. In addition many individuals participated in this AGARDograph which is gratefully acknowledged, in particular the invaluable support of the AGARD staff.

K.Onken
Editor

CONTENTS

SPACE SHUTTLE PILOT-INDUCED-OSCILLATION RESEARCH TESTING

Bruce G. Powers
NASA Ames Research Center
Dryden Flight Research Facility
P.O. Box 273
Edwards, California 93523
U.S.A.

SUMMARY

Five approach and landing tests of the space shuttle were made to evaluate low-speed characteristics. During the last flight of this series, a pilot-induced-oscillation (PIO) tendency was noted during the landing. As a result, several piloted simulations were used to evaluate the handling qualities of the orbiter during landing. The testing included simulation of the orbiter with a fixed-base ground simulator, with moving-base ground simulations, and with in-flight simulation. The two moving-base ground facilities that were used, the flight simulator for advanced aircraft (FSAA) and the vertical motion simulator (VMS), are at the NASA Ames Research Center, Moffett Field, California. The in-flight simulation was performed on the Calspan total in-flight simulator. Additional studies on the effect of time delay were performed on the F-8 digital fly-by-wire airplane at NASA Ames-Dryden.

This paper, based on the results of those tests, discusses the simulation requirements for investigation of PIO characteristics during the landing phase. The general conclusion is that in-flight simulation is the only reliable method of evaluating the landing characteristics of aircraft with PIO tendencies; even then some form of artificial task needs to be introduced to produce pilot workload levels similar to those encountered in the actual flight environment.

SYMBOLS

ALT	approach and landing test	PIO	pilot-induced oscillation
DFBW	digital fly-by-wire	TIFS	total in-flight simulator
FSAA	flight simulator for advanced aircraft	VMS	vertical motion simulator
L/D	lift-to-drag ratio	τ	time delay, sec

1.0 INTRODUCTION

Five approach and landing tests (ALT) of the space shuttle (Ref. 1) were made to evaluate low-speed characteristics. The orbiter was launched from a B-747 aircraft and the flight regime from about 6100 m (20,000 ft) to touchdown was investigated. The first four landings were on the Edwards dry lakebed and no particular handling problems were exhibited. A tendency for pilot-induced oscillation (PIO) in both pitch and roll was exhibited near touchdown during the fifth landing, which was on the 4570-m (15,000-ft) concrete runway. As a result, the cause and significance of the PIO tendency were investigated. Analysis indicated that the problem was primarily in the pitch axis, which resulted in rate limiting of the elevons. Because of the priority rate-limiting logic that allocates elevon surface rate for both pitch and roll commands, the rate limiting in the pitch axis produced rate limiting in the roll axis, which resulted in roll oscillations. Several piloted simulations were conducted to evaluate the longitudinal landing handling qualities of the orbiter in the ALT configuration and with control system modifications that were developed to improve the landing characteristics (Ref. 2).

The testing included simulation of the orbiter with a fixed-base ground simulator, with moving-base ground simulations, and with in-flight simulation. A fixed-base simulation with a tracking task as the primary maneuver was used to evaluate the PIO characteristics of control system modifications. The moving-base ground facilities used were the two high-fidelity simulators at the NASA Ames Research Center, Moffett Field, California: the flight simulator for advanced aircraft (FSAA, Ref. 3), and the vertical motion simulator (VMS, Ref. 4). The in-flight simulation was performed on the Calspan total in-flight simulator (TIFS, Ref. 5). Additional in-flight studies on the effect of time delay were performed on the F-8 digital fly-by-wire (DFBW) airplane at NASA Ames-Dryden (Ref. 6).

The simulation of the landing task has always been difficult, particularly with a vehicle with PIO tendencies. This paper presents some of the results obtained from these tests concerning the simulation requirements for the investigation of PIO characteristics during the landing phase. Pilot evaluations of the PIO characteristics and the handling qualities are presented and compared.

2.0 ORBITER SIMULATIONS

2.1 Background

In 1978, after the ALT experience, a simulation program was conducted to study the cause and significance of the PIO characteristics observed in flight. The study was conducted on the FSAA moving-base simulator (Ref. 3), which has good motion and visual fidelity characteristics. A television model-board visual display was used to depict the runway landing scene. In general, the results indicated that the tendency toward PIO was not significant in the normal landing task. In a simulated formation tracking task, there was an indication of a PIO tendency similar to that observed during the ALT flight. At this point, the results were inconclusive: There was not a definite PIO tendency in the simulated landing task as had been observed in the ALT flight, but it was not known if this was the result of an inadequate model or of a simulation deficiency. As a result, a flight simulation program was conducted using the Calspan

TIFS to validate the FSAA results. The TIFS (Ref. 5) is an in-flight simulator that can reproduce the six-degree-of-freedom cockpit motions in addition to providing the actual visual scene. This simulation established that the PIO tendencies that were observed in the ALT flight could be reproduced in the in-flight simulator with the predicted model of the orbiter.

Following these simulations, control system improvements were developed and evaluated on a fixed-base simulator using a simple tracking task to evaluate the PIO characteristics. One of these systems was an adaptive stick gain (Ref. 7) which was designed to reduce the PIO tendencies. This system reduced the stick gain as the frequency of the pilot inputs approached the frequency of the PIO. After developing this system on the ground-based simulator, another series of simulations was made in 1979 and 1980 with the VMS (Ref. 4) and the TIFS. The VMS was designed to provide very good vertical motion simulation capabilities and has a vertical motion range of ±9 m (30 ft) and an acceleration capability of ±1g. The same visual display that was used on the FSAA was also used on the VMS.

In the following section, these simulations are compared based on pilot ratings of the PIO characteristics and pilot ratings of the handling qualities. During all of these tests, the pilots evaluated the PIO tendencies using the rating scale shown in Fig. 1; they evaluated the handling qualities using the rating scale shown in Fig. 2.

2.2 Comparison of Simulator Results

2.2.1 FSAA and TIFS landing evaluations

Normal landings with and without lateral offsets were made in the evaluation of the landing characteristics using the FSAA and TIFS. The results of these two tests are summarized in Fig. 3 in terms of a histogram of the ratings of the PIO characteristics. The FSAA ratings of the PIO characteristics indicate that the orbiter had, for the most part, no undesirable pilot-induced motions and only occasional occurrences of undesirable motions. On the other hand, the TIFS ratings indicate that undesirable motions are quite prevalent. It is clear from this figure that landings using the FSAA produced very little PIO tendency compared to those in the TIFS.

2.2.2 FSAA and TIFS formation task evaluations

The formation tracking task was also evaluated on the FSAA and the TIFS. This task consisted of close formation flying in a simulated aerial refueling position behind the lead aircraft. The objective was to tightly track this position. The results of these tests are shown in Fig. 4. In these cases, both simulations had indications of undesirable motions with PIO ratings around the 3 level. There was excellent agreement between the two simulations in terms of the evaluation of the vehicle PIO tendencies.

2.2.3 Comparison of formation and landing task evaluations

A comparison of the PIO tendencies obtained from the formation tracking task and the landing task with the TIFS is shown in Fig. 5. The results indicate that these two tasks produced similar evaluations of the PIO tendencies. These results are significant for both ground-based simulation and in-flight evaluations because of the ease and safety in performing formation tracking tasks as compared to performing the actual approach and landing task. Since the ground-based and in-flight simulation results from the tracking task were quite similar, this would suggest that a reasonable preliminary assessment of the PIO potential could be made for the landing condition by using a ground-based motion simulator and a tight-formation tracking task.

2.2.4 VMS and TIFS landing evaluations

Three control system configurations were evaluated using the VMS and TIFS. The PIO ratings from these tests are summarized in Fig. 6. The VMS and TIFS correlation is about the same or slightly better than that of the FSAA and TIFS, but there is still a rather significant difference between the moving-base simulation and the in-flight simulation. In both the VMS and TIFS tests, a very demanding task was used to accentuate the PIO tendencies. A 45-m (150-ft) lateral offset was performed at 30 m (100 ft) above the runway and a 4.6-m/sec (15-ft/sec) vertical gust was introduced at an altitude of about 15 m (50 ft). This produced a task that would be unreasonable to expect in actual landings, but it did provide a situation that produced a pilot gain high enough to make the PIO tendencies of the vehicle apparent to the pilot. On both of these simulators, a normal straight-in approach and landing could be made with little evidence of a PIO tendency after the pilot became familiar with the simulator.

Although the PIO tendencies were not the same for the two simulations, the ratings of the basic handling qualities were quite similar. The pilot ratings for the previous three configurations are shown in Fig. 7. The pilot rating distributions are quite similar, and the average pilot ratings are within 1/2 of a pilot rating of each other. This agreement may be fortuitous, however. The pilot comments generally indicated that PIO was a significant concern in addition to the flightpath control for the in-flight simulations, whereas the flightpath control alone was the dominant factor in the ground simulations. It appears that the ground simulations are adequate to assess the lower workload tasks associated with flightpath control, but the evaluation of the higher frequency, higher workload tasks require the fidelity of inflight simulation.

2.2.5 Fixed-base simulator tracking task evaluations

The correlation between the tracking task and the landing task evaluations has proved extremely useful in the evaluation of alternate control system concepts for the orbiter since the PIO tendencies can be evaluated on a relatively simple fixed-base simulation using the tracking task. The tracking task does not provide any information about the adequacy of the response characteristics for the actual landing task, but only gives an indication of the PIO tendencies. The task for the fixed-base ground simulation studies was to rapidly stabilize on a target that was initially displaced. Ten seconds was allowed for this task.

To more nearly simulate an actual landing situation, it was also required that the pilot not overshoot the target, as would be required if the target represented the ground plane.

The closed-loop response characteristics are a function of the pilot gain and lead compensation and of the distance between the tracking aircraft and the target. The closed-loop response results in two modes of interest: a relatively high frequency mode associated with pitch attitude response, and a lower frequency mode associated with flightpath reponse. The procedure used in the fixed-base simulation was to adjust the target distance and the time available for the task so that the closed-loop frequencies seen on the simulator matched those seen in the shuttle ALT flight tests. This resulted in a tracking distance of 30 m (100 ft) and a 10-sec time span for acquiring and stabilizing on the initially displaced target. With this task, the PIO conditions observed in flight could be repeatedly reproduced, which made it feasible to evaluate control system changes with a relatively simple simulation. This technique was very useful in developing an adaptive stick gain algorithm that was used to reduce the PIO tendencies of the orbiter (Ref. 7). It should be noted, however, that this technique is of significant value only for evaluating PIO characteristics that have already been observed in flight, because the flight-observed frequencies are required to tune the task.

3.0 F-8 DIGITAL FLY-BY-WIRE AIRCRAFT TESTS

One of the main causes of the pitch attitude PIO is the interaction of time-delay and high bandwidth requirements. In an effort to study this effect, flight tests were conducted using the F-8 digital fly-by-wire airplane (Ref. 6). The experiment consisted of several tasks. The two of most interest were the high-workload case in which the pilot was attempting to land precisely on a designated area of the runway, and the low-workload case where the pilot was attempting to land on the runway without any concern for the actual touchdown point.

The task was set up to simulate the low lift-to-drag ratio (L/D) approach and landing of the shuttle. Approaches were initiated at 260 KIAS, 1460 m (4800 ft) above ground level, about 10 km (6 mi) from touchdown point. A speed of 260 KIAS was maintained until 150 m (500 ft) above ground level. The outer glideslope was approximately 10°. Flare was initiated 150 m (500 ft) above ground level. A glideslope of approximately 1° was intercepted about 30 m (100 ft) above ground level. Aim touchdown speed was 190 KIAS; actual touchdown speeds were between 180 and 210 KIAS. The outer glideslope aim point was about 1.6 km (1 mi) from the runway threshold.

All landings were made on a concrete runway 4600 m (15,000 ft) long and 90 m (300 ft) wide. The evaluation terminated at touchdown, and a go-around initiated. Normal landings were made from straight-in approaches with no particular aim touchdown point. Because of the generous proportions of the runway, these landings caused relatively little workload for the pilot. The low L/D spot landings from the lateral offset consisted of an approach in line with the edge of the runway, followed by an offset maneuver initiated at 30 m (100 ft) above the ground to align with the runway centerline, and a touchdown at the 1500-m (5000-ft) marker. The lateral offset increased the pilot's workload and stress, providing a more demanding landing task.

After the ALT tests, the orbiter landing technique was changed to make the task easier. This was accomplished by relating the touchdown point to velocity rather than to a fixed point on the runway. This reduced the need for high bandwidth control and made the task more similar to the low-workload-task case evaluated in the F-8 DFBW tests. The results of the F-8 tests are shown in Fig. 8 along with the results from the TIFS evaluation of the orbiter. For the orbiter time-delay values of approximately 0.2 sec, the effect of task is significant; it appears that the current operational procedures for the orbiter produce a task that is between the low- and high-workload tasks of the F-8 tests. The results also indicate that the task plays a key role in any attempt to assess handling qualities during landing when there is a PIO tendency present.

In addition to the landing task, a formation tracking task was evaluated. It consisted of a simulated aerial refueling task with the airplane initially stabilized 5 to 12 m (15 to 40 ft) below the refueling position. The objective was to rapidly acquire the refueling position and then tightly maintain that position. A comparison of the formation tracking task results with the landing task results is shown in Fig. 9. The tracking task produced pilot ratings between those for the normal- and high-workload landings. In this case, unlike the shuttle TIFS results, the tracking task did not produce as much of a degradation due to time delay as the landing task. This could be partially due to the realistic landing task of the F-8 experiment. Because the F-8 is a single-seat aircraft with no reset button such as in the TIFS (the time delay could be removed by a push of a button, however), this experiment produced a real-world, high-workload task that cannot be duplicated in any other type of simulation. This produces very high quality results, but high-workload tasks near the ground have an associated high risk: The workload induced by the task is real.

4.0 CONCLUDING REMARKS

During the approach and landing tests of the space shuttle, a pilot-induced-oscillation (PIO) tendency was noted during the landing. As a result, several piloted simulations were used to evaluate the handling qualities of the orbiter during landing. The testing included simulation of the orbiter with fixed-base ground simulators, with moving-base ground simulations, and with in-flight simulation. The two moving-base ground facilities used were the flight simulator for advanced aircraft (FSAA) and the vertical motion simulator (VMS) at the NASA Ames Research Center, Moffett Field, California. The in-flight simulation was performed in the Calspan total in-flight simulator (TIFS). The F-8 digital fly-by-wire (DFBW) airplane at NASA Ames-Dryden was used for additional studies on the effect of time delay.

These tests have shown that the ability to assess the PIO characteristics of the shuttle during landing is significantly different for moving-base ground simulation as compared with in-flight simulation. The general conclusion from these tests is that flight simulation is the only reliable method of evaluating the landing characteristics of aircraft with PIO tendencies, and even then some type of artificial task must be introduced to produce pilot workload levels similar to those that can be encountered in

flight. A formation tracking task seemed to offer a better means of identifying PIO tendencies with ground simulation than the landing task did. This technique was used in the development of alternate control system concepts designed to reduce the PIO tendencies. The simulation of the landing task has always been difficult, but it has become more difficult because of the requirement to duplicate PIO characteristics. The simulation, no matter how realistic, does not produce the same sense of urgency as does the flight environment. The accurate representation of PIO-prone aircraft in the landing flight regime remains a challenge to the ground-based simulation facilities.

REFERENCES

1. Space Shuttle Orbiter Approach and Landing Tests — Final Evaluation Report, 1978, JSC-13864.

2. Powers, Bruce G.: Low-Speed Longitudinal Orbiter Flying Qualities, presented at "The Space Shuttle Program: From Challenge to Achievement," Johnson Space Center, Houston, Tex., June 28-30, 1983.

3. Zuccaro, J. J.: The Flight Simulator for Advanced Aircraft — A New Aeronautical Research Tool, 1970, AIAA Paper 70-359.

4. Jones, A. David: Operations Manual: Vertical Motion Simulator (VMS) S.08, 1980, NASA TM-81180.

5. Reynolds, Philip A.; Wasserman, Richard; Fabian, Gardner J.; and Motyka, Paul R.: In-Flight Simulation (TIPS), 1972, AFFDL-TR-72-39.

6. Berry, Donald T.; Powers, Bruce G.; Szalai, Kenneth J.; and Wilson, R. J.: In-Flight Evaluation of Control System Pure Time Delays, 1982, AIAA 80-1626R, J. Aircraft, vol. 19, no. 4, pp. 318-323.

7. Powers, Bruce G.: An Adaptive Stick-Gain to Reduce Pilot-Induced Oscillation Tendencies, 1982, AIAA 82-4078, J. Guidance and Control, vol. 5, no. 2, pp. 138-142.

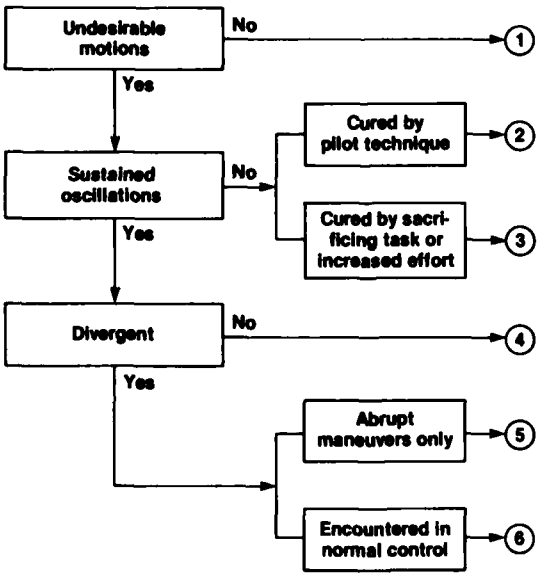

Figure 1. PIO rating scale.

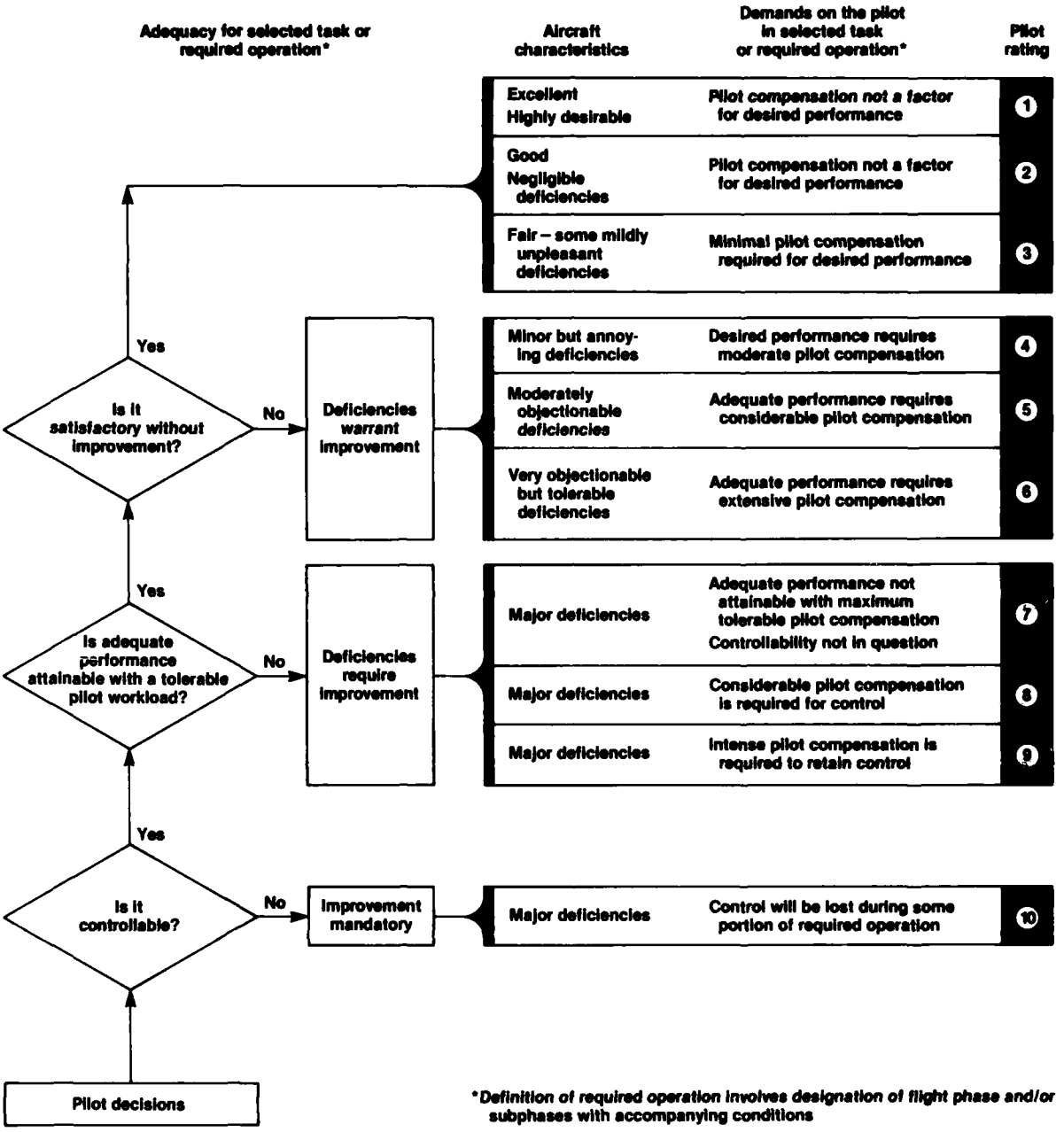

Figure 2. Handling qualities rating scale.

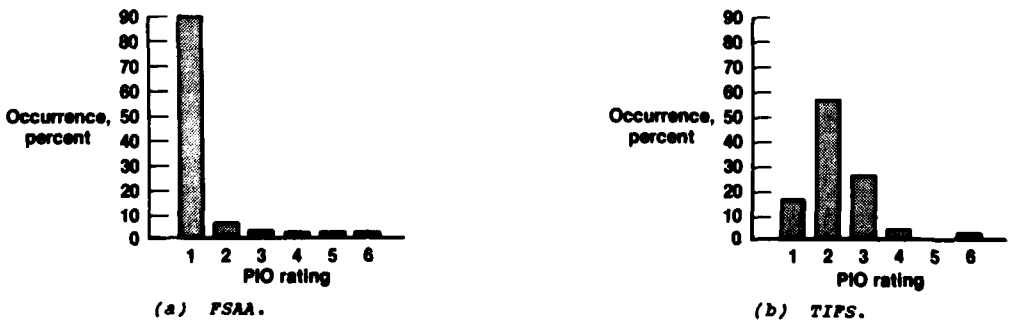

Figure 3. FSAA/TIPS landing task PIO rating comparison. Shuttle ALT configuration.

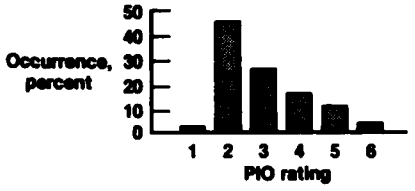

(a) FSAA.

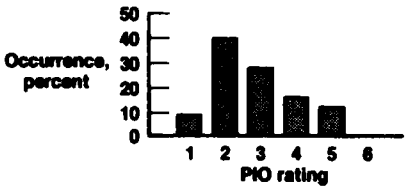

(b) TIFS.

Figure 4. FSAA/TIFS formation tracking task PIO rating comparison. Shuttle ALT configuration.

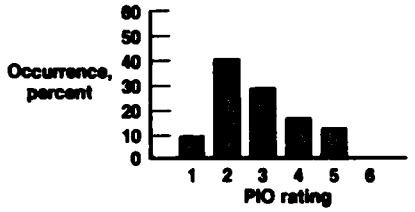

(a) Landing task.

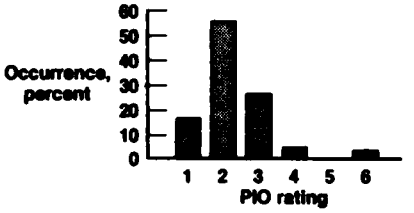

(b) Formation tracking task.

Figure 5. TIFS landing and formation tracking task PIO rating comparison. Shuttle ALT configuration.

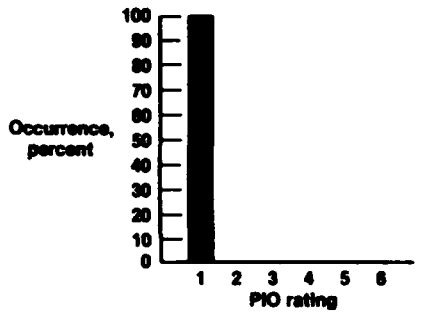

(a) VMS, configuration A.

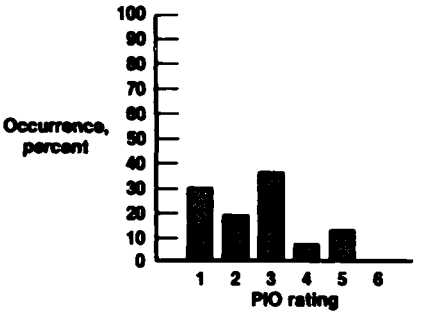

(b) TIFS, configuration A.

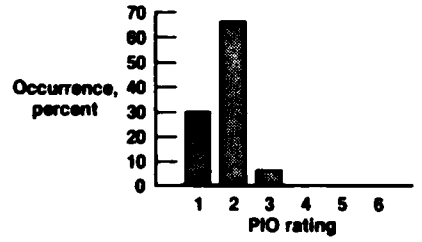

(c) VMS, configuration B.

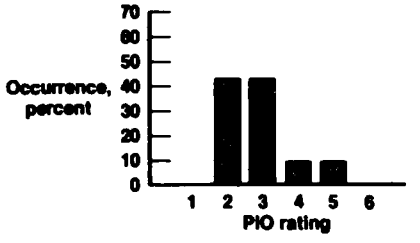

(d) TIFS, configuration B.

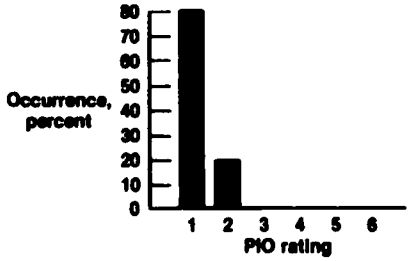

(e) VMS, configuration C.

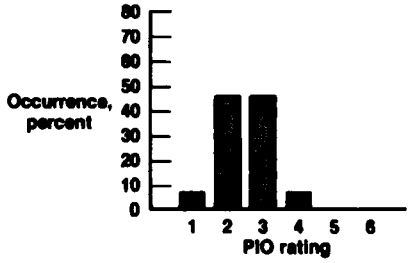

(f) TIFS, configuration C.

Figure 6. VMS/TIFS landing task PIO rating comparison.

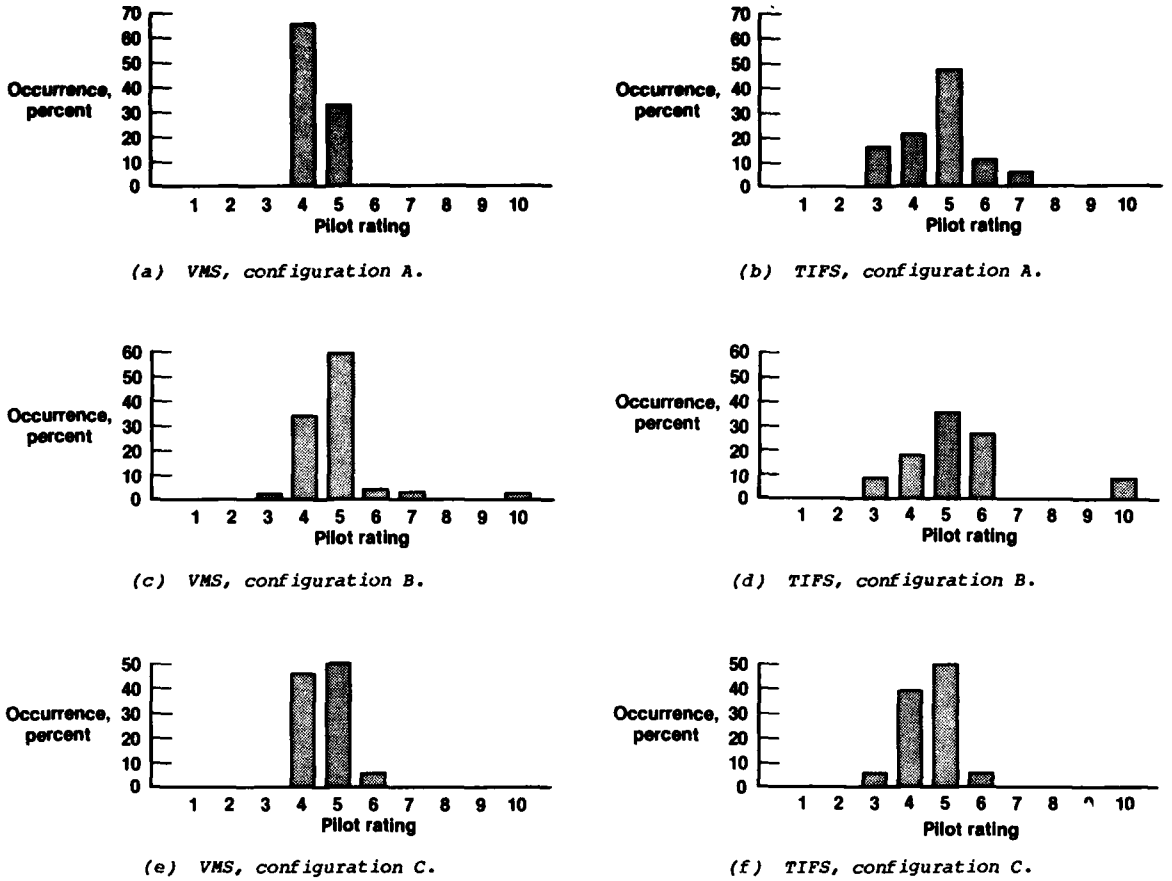

Figure 7. VMS/TIFS landing task pilot rating comparison.

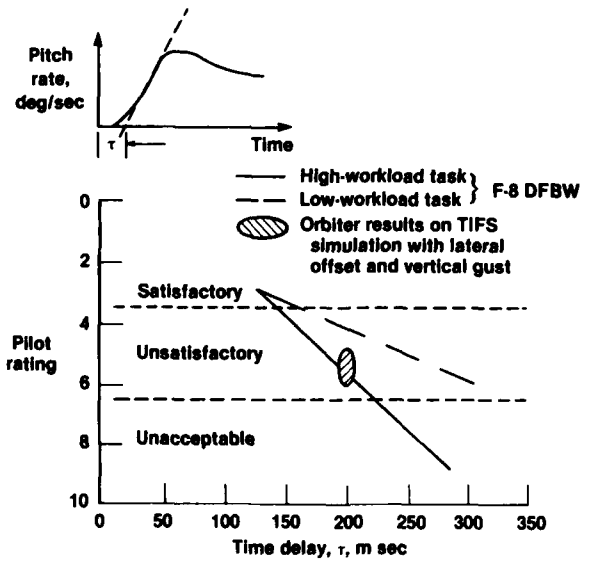

Figure 8. Results of the F-8 time-delay study for the landing task.

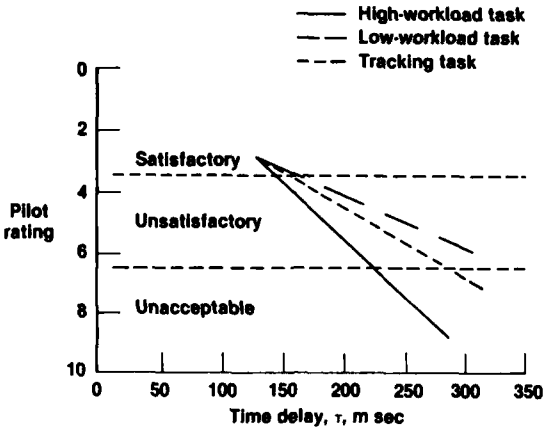

Figure 9. Comparison of the formation tracking task and the landing task for the F-8 time-delay study.

DYNAMIC WIND TUNNEL TESTING FOR ACTIVE CONTROLS RESEARCH

by

K. Wilhelm
B. Gmelin

Institut für Flugmechanik

Deutsche Forschungs- und Versuchsanstalt
für Luft- und Raumfahrt e.V. (DFVLR)
D 3300 Braunschweig-Flughafen, West Germany

SUMMARY

For the investigation of problems associated with the application of active control systems a technique has been developed, which allows a comprehensive treatment of flight mechanics problems including the effects of aerodynamics, aeroelastics and control systems. Since this technique, the dynamic wind tunnel test technique, is a synthesis of both computer simulation and wind tunnel test a variety of information on specific flight mechanical phenomena can be obtained.

At DFVLR two experimental devices have been developed:

the "Installation for Dynamic Simulation in Wind Tunnels" for investigation in the field of fixed-wing aircraft,

the "Rotor Test Stand" for investigation in the field of rotary-wing aircraft.

The paper deals with these test facilities. At first a brief description of the test facilities is given, further advantages and special problems associated with the application of this test technique are shown. In addition, test results of completed test programs are presented.

1. INTRODUCTION

The possible applications of active control systems cover a broad range, from low-frequency flight dynamics up to high-frequency structural dynamics vibration. However, the use of ACT will require a detailed understanding of the anticipated external disturbances, aerodynamic and structural characteristics, control system responses and compatibility problems and will require considerable advances in the ability to describe and model such phenomena. Due to the close interrelationship between aerodynamical, flight-mechanical, aeroelastic, and control engineering problems, the development and testing of ACT call for methods allowing a comprehensive treatment of the subjects concerned.

Analytical investigations using **computer simulation** can give good results concerning the physical relationship in the dynamics of a complex system. However, computer simulation is often not sufficient because the effects and phenomena to be investigated are unknown and therefore not open to mathematical modelling. The disadvantages of inadequate mathematical models for computer simulation require experimental investigations to check the results of computer simulation.

Experiments are possible with both full-scale aircraft and models. There is no question that **flight testing** with full-scale aircraft is necessary to test active control systems. However, the increase in the complexity, cost, and risks of flight tests of advanced control concepts requires other methods for obtaining more experimental results.

Consequently **dynamic wind tunnel tests** are improved as an effective way for fundamental research in the field of ACT. The main advantages of this kind of simulation are: it is more realistic than computer simulation, less risky and relatively inexpensive compared with flight tests, and allows systematic tests under reproducable conditions.

A number of recent papers [1, 2, 3, 4] have pointed out that this kind of wind tunnel test is required and that models can play an important role in the future development of control configured vehicles by providing data to verify analytical methods, thereby reducing the risks and cost of flight demonstration. Dynamic wind tunnel programs with free flying and controllable models at NASA Langley Research Center [5], IMFL and ONERA [6], and MBB München [7] have demonstrated the efforts undertaken to satisfy the need for more experimental results for ACT.

Transferability of wind tunnel to full-scale results is the fundamental condition for dynamic wind tunnel experiments. To ensure transferability similarity of forces and motion between model and full-scale aircraft must be guaranteed. This will be achieved if the interference effects of wind tunnel facility on the model motion are small, and especially if the laws of similarity are satisfied. The laws of similarity are non-dimensional ratios of forces which, if held constant when passing from aircraft to model, will ensure similitude of the dynamic behaviour.

Usually it is not possible to obtain exact similarity in wind tunnel experiments, i.e. to hold all the non-dimensional parameters constant when passing from aircraft to model. This is because of the inherent problem of capability in scaling for all parameters simultaneously (for example for Reynolds number, Mach number and Froude number).

For that reason one is forced to resort to approximate similarity. In that case the effect of the violation of a special scaling law on the experiment must be investigated. This leads to a choice of laws which are essential for validity of the experiment and which therefore must be satisfied.

In view of this two facilities for dynamic model testing in wind tunnels have been constructed at the DFVLR:

- the "Installation for Dynamic Simulation in Wind Tunnels" for investigations in the field of fixed-wing aircraft and
- the "Rotor Test Stand" for investigations in the field of rotary-wing aircraft.

This paper describes both wind tunnel facilities and discusses problems of transferability of measurement data from model to full-scale. Relevant results of completed tests are presented.

2. DYNAMIC MODEL TESTING FOR FIXED-WING AIRCRAFT

The design of future civil and military fixed-wing aircraft will be mainly influenced by the implementation of ACT in the design process. Some special applications of ACT which might be achieved in the next generation are [8]:

1. Active Gust Alleviation:
   - for improvement of pilot and/or passenger comfort
   - for increase of aircraft life by reducing structural loads
2. Active Lift Distribution:
   - for fatigue reduction (maneuver load control)
   - for improvement of maneuverability (direct lift control)
3. (Limited) Artificial Stability:
   - for weight/drag reduction
4. Envelope Limiting:
   - for "carefree maneuvering"
5. Active Flutter Control:
   - for suppression of wing-store flutter.

However, there is still a lack of knowledge of many aspects of the aerodynamic/aeroelastic/dynamic behaviour of the aircraft and consequently our ability to predict and improve aircraft characteristics by using ACT is limited at present. This applies particularly to flight mechanics, because it is the task of flight mechanics to investigate the interdisciplinary problems [9, 10].

DFVLR is working, in cooperation with other institutions, on the solution of problems associated with the above-mentioned research areas. For the investigations DFVLR uses the Installation for Dynamic Simulation in Wind Tunnels together with a reduced-scale rigid model of the ZKP experimental aircraft Do 28 TNT as a test bed [11, 12].

2.1 DFVLR-INSTALLATION FOR DYNAMIC SIMULATION IN WIND TUNNELS

The installation for the Dynamic Simulation in Wind Tunnels is an extension of a similar test technique, which is used for testing flutter-models but allows the simulation of a part of the rigid body motion. The main parts of the installation are (Figure 1, 2):

- the suspension frame for the model
- the central control station
- the gust generator system
- the weight compensation system
- the model.

Suspension Frame

The suspension frame consists of a large tubular frame in combination with a vertical rod, which allows freedom of motion in pitch, yaw, heave and to some extent in roll. The frame surrounds the open test section of the 3 m subsonic wind tunnel; the distance between frame and airflow is 0.5 m. The resonant frequency of the rod/frame

system is about 14 Hz. This value is high enough to allow measurements up to frequencies of 10 Hz. The maximum pitch motion is ± 10 degrees, the model can heave ± 0.4 m.

Central Control Station

The central control station is located in a container next to the test section. This container houses the model control devices, the measurement data processor, and various monitoring devices.

Gust Generator System

Two movable flaps are installed into the nozzle of the wind tunnel. They are driven by an electro-hydraulic actuator. This device allows a deflection of the airflow within the test section of up to 10 degrees. The gust generator can generate gusts in the frequency range from zero to 15 Hz. It is possible to generate various types of gust profiles, such as impulsive or stochastic gusts. The properties of the gust generator allow the simulation of a scaled stochastic gust field with a special characteristic (for example Dryden).

Weight Compensation System

A servo controlled vertical force generator can produce constant vertical forces independent of the model motion. This device is necessary due to the laws of similarity and in order to control the model in the airflow.

Model

The type of model depends on the actual problem to be investigated. The models may have inertial and elastic scaled properties. For the present purpose a 1 : 8 scaled model of a small transport aircraft is used. This model is built from carbon fiber material, which results in an almost rigid structure (Figure 3). It is equipped with control surfaces (inner flaps, outer flaps, elevator) which are driven by fast acting servo actuators. Sensors such as accelerometers, rate gyros, pressure transducers, potentiometers for the control surfaces, various angle of attack probes are installed at different locations of the model to measure the motion and the disturbances. Power supply, control signals and measured data are transmitted to and from the model via cables.

2.2 *TRANSFERABILITY OF WIND TUNNEL TEST DATA TO FULL SCALE FIXED-WING AIRCRAFT*

For a complete dynamic simulation the following set of parameters must be correct:

- Geometric Scaling
- Mach Number
- Reynolds Number
- Strouhal Number
- Relative Mass Parameter.

The other parameters, such as ratio of specific heats, body stiffness and material damping, are satisfied automatically because the dynamic simulation uses the same medium "air" as in real flight and the model is a rigid model.

The requirement for constant ratio of aerodynamic forces is fulfilled using the aerodynamic forces in non-dimensional form derived from static wind tunnel tests which correspond to the value of the full-scale aircraft.

In the case of experiments taking aeroelasticity of structure into account, the number of non-dimensional mode shapes, essential for the experiment must be approximated.

Geometric Scaling

In order to achieve the same aerodynamic characteristics on a model as exist on the full-scale aircraft it is necessary for the aerodynamically important portions of the aircraft to be geometrically scaled. The maximum size of the three-dimensional model is determined by the size of the wind tunnel test section. The test section of the DFVLR subsonic wind tunnel used for the experiments has a diameter of 3 m; this yields a length scaling ratio of 1 : 8, model to aircraft.

Mach Number

The Mach Number takes into account the compressibility effects of the airflow. In practice these effects can be neglected for Mach numbers below Ma ≈ 0.4, as in this case of dynamic simulation.

Reynolds Number

The use of a down scaled model makes it impossible to simulate the Reynolds number correctly in wind tunnels using air only. This is only possible by using very high velocities, which, however, leads to problems with Mach number again. It is important to have the Reynolds number in wind tunnel tests higher than the critical Reynolds number when the airflow becomes turbulent. The dynamic wind tunnel tests at DFVLR are conducted

with a Reynolds number of $0.53 \cdot 10^6$ which is close to the critical Reynolds number. However, static wind tunnel tests with different Reynolds numbers have shown that the Reynolds number has no important effect in the particular area being investigated. This is true especially as the dynamic tests only use an angle of attack of up to 5 degrees. Thus the high angle of attack region is avoided in which a reduction in maximum lift coefficient will occur and at which the moment curve will break if Reynolds number is reduced.

Mass and Mass Distribution

To ensure similar dynamic behaviour the relative mass parameter $\mu_L = 2\ m/\rho\ S\ l_\mu$ and the relative radius of inertia $k_y = (r_y/l_\mu)^2$ must be valid for both model and aircraft.

Strouhal Number

The Strouhal number, which corresponds to the reduced frequency $\omega\ l_\mu/V$, ensures equal dynamic angle of attack. Since the Strouhal number must be valid for both model and aircraft, the time scale factor can be determined for a given geometric scaling.

Froude Number

In dynamic processes gravity is of great importance, because the ratio between acceleration of motion and gravity acceleration must be constant. It is clear once the velocity and geometric scale factors have been established that it is often difficult to satisfy the requirements of the Froude number at the same time.

The significance of the Froude number as applied to airplanes is shown in [13]: the combination of the Froude number with the relative mass parameter μ_L yields $\mu_L/Fr = mg/\rho SV^2 = C_{L_o}/2$, where C_{L_o} is the lift coefficient in the initial steady flight condition. This shows that the Froude number determines the steady flight condition. In order to carry out similar wind tunnel tests it is often necessary to change the gravitational field. This can be done in the DFVLR test facility by a weight compensation system which produces a constant additional vertical force on the model independently of the model motion.

Thus two types of simulation are possible in the DFVLR installation [14]:

1. Froude scaled simulation
   The model flies without the vertical force generation in a state of natural gravity. All the lift has to be produced by the model itself.

2. Simulation with weight compensation
   The lift of the model is supported by a constant vertical force. This results in a reduction in the velocity needed to produce the required lift of the model.

Both types of simulation are conducted in the installation. For the investigations the simulation with weight compensation is preferred due to the better time scaling. In the special wind tunnel program with the Do 28 TNT model the weight compensation system has to create 28 % of the total lift to achieve the correct steady state conditions.

2.3 TEST SPECIFIC EFFECTS

The model suspension was chosen so as to allow the simulation of the longitudinal motion of an aircraft. Figure 4 shows that due to the vertical rod there are two additional forces K_x and K_z instead of thrust in the case of a free flying model. K_x respresents the horizontal rod-force which compensates for the drag of the model. K_z is the artificial constant vertical force on the model, obtained by using the weight-compensation system to model the correct Froude number.

The equation of the longitudinal motion of a suspended model in comparison with the equation of a free-flying model shows that due to the blockage of the x-degree of freedom the phugoid motion is fully suppressed. The short period mode, however, is not affected significantly because the corresponding terms in the equations are small. Figure 5 shows the Bode plot of the response of the suspended model and the free-flying model due to an elevator input. There is a good agreement between the motion of both models for frequencies equal or higher than the short period mode. In this frequency range good transferability of the results can be obtained. At frequencies lower than half the short period mode frequency the suppressed phugoid mode results in major differences.

The wind tunnel experiments conducted show that due to the special suspension technique some additional influences exist which affect the movement of the model:

1. The cables for data transmission to and from the model create small forces and moments which are dependent on the heave of the model [15] (Figure 6).

2. Although it is outside the test section the large suspension frame produces a contraction of the airflow in the plane of the suspension frame, but leads to an expansion of the airflow behind the frame. This results in a gradient $\partial\alpha/\partial z$, which varies according to the position in the test section [15] (Figure 7).

3. The two-dimensional gust field which is produced by the gust generator shows a nonlinear propagation dependent on frequency and position [12] (Figure 8).

Thus the wind tunnel investigations began with extensive experiments for the identification of the model motion and all disturbing effects. The goal was to obtain a mathematical description which models all effects. Difficulties arose in arriving at a mathematical model of the gust field. But despite some deficiencies a good agreement now exists between the results of measured and computed gust field within the frequency range from 0.8 Hz to 5 Hz.

2.4 WIND TUNNEL TEST PROGRAMS

The Installation for Dynamic Simulation in Wind Tunnels was used in two experimental programs, which were conducted in the DFVLR 3 m subsonic wind tunnel. In the first program ride smoothing systems and elastic mode suppression systems for wing and fuselage bending modes were evaluated. In this program, which showed the application potential of the installation, a flexible combat-type multipurpose aircraft was used [16]. In the second program the Installation for Dynamic Simulation in Wind Tunnels was used to develop and test a gust alleviation system. This gust alleviation system was designed for the small civil transport aeroplane Do 28 TNT, to improve the ride comfort of the passengers. The wind tunnel experiments helped to find a correct mathematical model of the aeroplane flying in a two-dimensional gust field. The wind tunnel experiments also showed the conditions, which are necessary for a good performance of the gust alleviation system. The experiments gave a profound insight into the interaction of the downwash with the gusts, which arrive at different moments at the position of the wing and the elevator. These results at least have given valuable data for the construction of the gust alleviation system for the full-scale aeroplane.

The aim of these experiments was a total compensation of the gust induced lift and pitching moment by an optimal adjustment of the parameters.

Figure 9 shows the block-diagram of the Open Loop Gust Alleviation system (OLGA). The disturbance signal is computed from the angle of attack and the aircraft motion parameters. The desired dynamic portion of the signal is obtained by filtering with a time delay filter and following subtraction from the gust signal. The gust compensation follows the following control law:

1. Compensation of the stationary portions:

   - symmetric aileron deflection for the compensation of the additional lift, which is given by the gust induced lift of the total aeroplane and by an elevator deflection.

   - simultaneous elevator deflection for the compensation of the pitching moment due to the gust and due to the symmetric aileron deflection.

2. Compensation of the dynamic portions:

   - elevator deflection for the compensation of the additional lift at the elevator due to the dynamic portions of the gust and aileron deflection.

3. Superposition of stationary and dynamic portions.

The optimal adjustment was found by observing the motion of the model and the vertical acceleration. The vertical acceleration was filtered by a special filter weighting those frequencies which are impleasant for the passengers (frequencies below 0.5 Hz). In [17] detailed information is given about these investigations.

In the wind tunnel test program specific experiments were performed to verify the motion parameters of the model and the accuracy of the sensors by application of parameter identification methods. Figure 10 shows as an example a comparison of measured and computed response to an impulsive elevator deflection.

The test program concentrated, however, on the investigation of the influence of constraints and deficiencies on the performance of the gust alleviation system by systematic parameter variations. These parameters are such as

- measuring accuracy, particularily the accuracy of the gust signal computation
- limitation of control surface deflection rates
- control surface saturation
- nonlinearities of the actuators
- sensor position and dynamic characteristics of the sensors
- filter design.

In the following some results of the test program are shown:

Control Surface Deflection Rate Limitation

Hydraulically or electrically operated control surface actuators only can produce a limited deflection rate. This has a profound effect on the performance of the gust alleviation system. Reasons of expense do not permit the installation of high performance electro-hydraulic actuators into the small transport aeroplane. Therefore the rate limitation severely influences the choice of the actuator. Simulations with different deflection rate limitations have shown, that for deflection rates higher than 60 °/s deteriorations only occur in the higher frequency domain. For deflection rates smaller than 60 °/s also the distinct minimum begins to disappear. This indicates, that under nonlinear conditions the simple phase relationship between time-delay and actuator phase-lag is no longer valid. Under these nonlinear conditions an adjustment of the gust alleviation system for one specific frequency is difficult. Figure 11 shows the effect of three different aileron deflection-rate-limitations.

The position of the minima is slightly different, because the gain-factors have been changed. The frequency response for $\dot{\delta}_{max}$ = 36 °/s clearly shows a deterioration of the gust alleviation throughout the whole frequency domain. The simulations have shown, that the deflection rates should not be reduced below values of 60 - 70 °/s. A rough estimation of the necessary maximum deflection rate is given by

$$\dot{\delta}_{max} \approx \omega \, \delta_{max}$$

ω is the upper boundary of the frequency domain, where good gust alleviation is demanded. δ_{max} is the maximum permissible control surface deflection for the gust alleviation.

Control surface deflection limitation

The block diagram of the gust alleviation system (Figure 9) shows a limiter for the α_G-signal. In the case the gust signal commands too large aileron deflections, these would reach the deflection limits (point of saturation). On the other hand, because the elevator deflections are smaller by a factor ten, they are far away from their deflection limits, so producing pitching motions. The limiter prevents the model getting out of balance if more than the maximum aileron deflection is commanded. Figure 12 (left side) shows the effect of the gust signal limitation for the case of a harmonically oscillating gust field of 1 Hz. The limitation affects the quality of the gust alleviation especially in the domain of higher frequencies.

Back-Lash

Another source for the deterioration of the gust alleviation is given by the back-lash within the aileron driving mechanism. Figure 12 (right side) shows the effect of aileron back-lash for a harmonically oscillating gust field of 1 Hz. For the purpose of investigation, the back-lash of the aileron was given a fairly large value. Despite of this large back-lash the gust alleviation is acceptable. This indicates, that some back-lash can be tolerated by the gust alleviation system. All attempts to improve the gust alleviation by adjusting the gain factors will result in a worse gust alleviation. If there is some back-lash, the parameters of the gust alleviation system may not be changed.

Dynamic Effects

The investigations in the Dynamic Simulation in Wind Tunnels have shown that the efficiency of such a system is influenced by the gust angle of attack measurement and, in particular, by the complicated interaction of downwashes, dead-times, actuator lags, sensor positions and unsteady aerodynamic transient effects. This means that an optimized realization is only possible if the dynamic effects are fully understood and if they can be modeled properly.

In the following example, the influence of the modeling of the dynamic effects on the efficiency of the open loop gust alleviation system (OLGA) is shown [18]. In Figure 13 the frequency response measurement of the vertical acceleration due to gust inputs are plotted without OLGA and with OLGA engaged but using various aerodynamic models.

Referring to the block diagram on Figure 9, in the first case the computed gust signal was fed directly to the control surface actuators. No time shift of the measured gust signal and its influence on the dynamic reaction was taken into account. It can be seen that the OLGA without considering a time shift leads to a 10 dB reduction of the acceleration amplitude for frequencies near the short period frequency. At higher gust frequencies, however, this type of OLGA begins to destabilize the model motion. The OLGA capability is rather limited because the phase conditions are not satisfied.

In the second case both the delayed interaction of the gust on the wing and the elevator and the delayed onset in change of the downwash on the elevator due to the quick acting flaps were taken into account. Figure 13 shows that in this case the efficiency of the OLGA can be improved significantly.

Figure 14 shows the response of the model flying in a scaled gust field. It can be seen that in the first case the plot shows a reduction of the vertical acceleration, while the pitching acceleration remains nearly unchanged. Using the model with time shift for the design of the OLGA the efficiency of the system is significantly better.

3. DYNAMIC MODEL TESTING FOR ROTARY-WING AIRCRAFT

In recent years theoretical work in the helicopter field has been intensified. It is necessary now more than ever before to verify and expand theoretical results with proper and sufficient testing in order to obtain improvements for the design of new helicopter systems.

One major advance in rotorcraft design will be the introduction of active control technology (ACT). For design application of this technology many questions remain to be answered. Extensive wind tunnel testing will contribute to finding the desired high-quality solutions.

3.1 ACTIVE CONTROL FOR HELICOPTERS

Before the application of ACT is discussed, some flight mechanical problems of helicopters will be reviewed shortly. This seems to be necessary because the extensive integration of control, lift generation and forward thrust generation into one system, the rotor, leads to substantial differences in comparison with fixed-wing aircraft [19].

Helicopter Control Problems

The pilot's control of forces and moments at the rotor is performed usually by varying the rotor blade pitch angles by means of a mechanical or hydraulic system.

The relatively simple realization of the normally used monocyclic rotor control and the basic fulfillment of helicopter trim and control requirements make the problems connected with this system appear less significant in the past.

In Figure 15 the basic flight mechanical deficiencies of helicopters using conventional control systems are shown:

- The basic helicopter is inherently unstable, longitudinally and laterally, particularly at high forward flight speed.
- To a greater or lesser extent, the helicopter's controls are coupled and the magnitude of these couplings varies with flight conditions.
- The vibration transferred from rotor to fuselage in specific speed ranges exceed the standard which is reasonable for passengers and jeopardize the mission performance.
- The maximum thrust levels obtainable and therefore the stationary load factors decrease as forward speed increases, which leads to the design of the rotor being determined essentially by high speed considerations and to the rotor having surplus capacity at low speed.

These flight mechanical problem areas are caused essentially by the aerodynamic and dynamic conditions at the rotor. For that reason major improvements in the helicopter dynamcis, including eigen-, disturbance-, and control-response, can only start at the rotor.

Objectives of Active Rotor Control

Even in normal flight conditions, but especially near the boundary of the flight envelope, the helicopter rotor must operate in a severe aerodynamic/dynamic environment. This includes

- stalled and reversed flow on the retreating blade,
- transient Mach number effects on the advancing blade,
- atmospheric turbulence,
- impulsive flow due to blade-vortex interaction,
- blade-fuselage interference flow,
- rotor instabilities,
- blade aerodynamic and/or dynamic mismatch.

The conventional monocyclic rotor control is unable to avoid these effects or to reduce the consequences, because the control angles of the individual rotor blades are completely determined by the flight condition and coupled with each other.

The solution consists in sensing instantaneous rotor behaviour and acting by means of additional or new controls to alleviate the disadvantageous effects caused by the above-mentioned rotor environment. The answer is active rotor control [20].

In several papers the objectives of the application of ACT principles for helicopters have been pointed out [20, 21, 22]; among these are

- reduction of rotor vibrations, blade stresses and control loads,
- improvement of performance, helicopter ride qualities and helicopter handling qualities.

In this way it seems possible to alleviate substantially the flight mechanical problems of helicopters and to expand the flight envelope considerably.

Realization of ACT

At least two conditions must be satisfied in order to implement active control for helicopters

- the limitation of the present swashplate that couples the blade pitch angles and provides only monocyclic pitch variation must be overcome,
- the conventional mechanical/hydraulic linkages between the pilot's control and the rotor blade must be supplemented or replaced by electrical/optical signalling, making possible the extensive application of feed-back techniques.

In order to realize all the benefits that active control can bring to helicopters, a concept involving individual blade control using extremely fast-response actuators combined with a full fly-by-wire/light system is envisaged. The technology for doing this is not yet available today.

3.2 TRANSFERABILITY OF MODEL TEST DATA TO FULL-SCALE HELICOPTERS, MODEL SIMILITUDE

The transferability of test data is dependent on the proper usage of the model scaling laws. Additionally other factors such as wind tunnel interference effects must be considered [23, 24].

For a complete simulation which takes into account a flexible rotor in a viscous, compressible flow in a gravity field, the following parameters must remain constant.

- Ratio of linear dimensions
- Mach number
- Reynolds number
- Froude number
- Density ratio
- Elasticity ratio.

Additionally it is supposed that only wind tunnels utilizing air at atmospheric pressure are available.

It is possible to define different sets of similarity parameters for a complete rotor simulation. The decision for this set was influenced by the specific problems which have to be investigated as well as by the clarity of these parameters [25].

Ratio of Linear Dimensions

The "geometrically scaling" approach is popular for rotors because of a number of factors, one of these being that, if everything is geometrically scaled, the material can be the same as in full scale and the stresses will be the same.

It is usually possible to reduce the external shape of a rotor by applying the same scale factor. Unfortunately the reduction of all full-scale dimensions by the same scale factor often brings fabrication and handling problems because of the decreased absolute thickness of many parts and the small absolute size of others. The geometrically scaling approach will be practicable for a large model rotor.

Mach Number

Compressibility effects on airfoil section characteristics are very extensive especially at the high subsonic Mach numbers encountered in the very important outboard regions of rotor blades.

As pointed out in the preceding sections, the effects of the unfavourable rotor characteristics which have to be reduced by active control are caused by aerodynamic influences to a great extent.

Thus correct simulation of Mach number is prerequisite for aerodynamic accuracy for rotor tests especially when active control technology is included. "Mach scaling" naturally implies a model tip speed the same as full-scale and a wind tunnel capable of covering the whole full-scale flight speed range.

Reynolds Number

The use of a Mach scaled model rotor makes impossible the correct simulation of Reynolds number in wind tunnels using air. For rotary-wing aerodynamics a number of papers [26, 27] have shown that the trends in $c_{L_{max}}$, Reynolds number, and Mach number produce a considerably more favourable model/full-scale relationship than for fixed-wing aircraft.

Although Reynolds number considerations are important, particularly for higher advance ratios (μ higher than 0.5), it is much more important to properly simulate the Mach number. Of course, this approach is a correct one for a large model rotor.

Froude Number

The Froude number also cannot be simulated correctly with a Mach scaled model rotor. Generally the Froude number is too large. For rotors with a substantially horizontal disc plane, the gravitational forces on a rotating blade have a constant value in the flapwise direction. Since the flapwise aerodynamic, centrifugal, and inertia forces are usually large compared to the blade weight, the gravitational forces can be ignored.

Density Ratio and Elasticity Ratio

In order to ensure similar dynamic characteristics with a Mach scaled model rotor, the structural density and the modulus of elasticity should be identical to the full-scale values. Geometrically scaling using the same materials is an obvious method of ensuring dynamic similarity. In this case the rotor blade natural frequency ratios and the stresses in the rotor system are the same as full-scale. For relatively large model rotors, this method of model fabrication is practicable.

The discussion of these conflicting model scaling laws results in the following demands with regard to ACT applications for model rotors:

- For a great many tests Mach scaled models are required,
- the rotor models have to be designed as large as possible, taking into consideration the wind tunnels available.

For future tests with large rotor models the German-Dutch Wind Tunnel DNW will be used, which is specially designed or at least very suitable for V/STOL, helicopter, and rotor testing. This new and most advanced low speed tunnel in Europe features four interchangable test sections up to 9.5 m by 9.5 m cross-section, and air speeds up to 150 m/s [28].

3.3 DFVLR-ROTOR TEST STAND

In the DFVLR Institute for Flight Mechanics a rotor test stand for testing in large wind tunnels has been assembled in a joint program with German aircraft industries under contract by the German Ministry of Defence. The test stand hardware is shown in Figures 16 and 17.

For the application of ACT a 4 m hingeless rotor model is used. In the design of the scaled rotor care was taken to model the MBB BO 105 main rotor accurately. The rotor control is realized by a conventional swashplate system. The non-rotating part of the swashplate is moved by three electro-hydraulic actuators, adjusting both collective and cyclic blade pitch angles and in addition moving the swashplate dynamically for active control.

The actuators are designed for high-frequency response up to more than 80 Hz, having a dynamic amplitude of ± 3 mm. The actuator's phase shift is roughly 1 degree/Hz, its performance is unaffected by the dynamic swashplate loads. So it is possible to vary the blade pitch up to six times the rotor rotational frequency Ω. Figure 18 shows the control processor configuration of the test stand as used for the wind tunnel tests [29]. In this way, higher harmonic rotor control as a first step of active rotor control can be realized.

The drive system of the rotor consists of a high power compact hydraulic motor which is installed in the test stand. In order to measure the forces and moments at the rotor hub a six-component strain gage balance has been installed. These balance measure the steady-state loads with good accuracy (error lower than 1 % of maximum load); it also provides dynamic load data up to 8 per revolution. Generally it is necessary to collect data from the rotor concerning blade motion, blade loads and other variables. Data from the rotor is transmitted to the stationary test stand by a PCM-system.

3.4 RESULTS OF COMPLETED TEST PROGRAMS

The Rotor Test Stand equipped with the four-bladed hingeless model rotor was used in several test programs which were conducted in the large low speed wind tunnels available in Germany. Out of these tests specific results will be presented in the areas of (1) rotor downwash, (2) dynamic model rotor loads, and (3) stability and control derivatives. Emphasis is laid on verification of the test data by flight test results and/or theoretical calculations. By this correlation the validity of the test data with respect to ACT will be shown.

Rotor Downwash

The ability to determine the effects of active control on the helicopter requires the ability, to predict the aerodynamic environment of the rotor including dynamic phenomena. In Figures 19 hot wire anemometer signals below the advancing rotor blades are presented. No applicable theory is available to predict the dynamic downwash, even the calculation of the averaged values exhibits relatively poor correlation with the measured flow field as shown in Figures 20 and 21 [30]. Therefore it seems to be absolutely necessary to conduct systematic and reliable measurements of the flow conditions near the rotor which can be realized only by wind tunnel test programs with Mach scaled rotor models. On the one hand the data will be used as a data base for the improvement of the analytical models and on the other hand more insight into the effectiveness of active control systems will be obtained.

Dynamic Rotor Loads

Rotor loads analysis generally provides acceptable results for 1/Rev. flapwise and lagwise loads at moderate level flight trim conditions [31]. For active control applications the higher frequency dynamic loads are of great interest because of the high frequency excitation of the rotor.

Figure 22 shows typical wind tunnel data compared with full-scale measurements [32]. The data showing the 4/Rev. pitching moment coefficient appear to differ widely especially in the low speed range. For the discussion of these differences the following points have to be considered:

- In-flight measurements are difficult at low speed,
- the high-frequency data have small absolute amplitudes,
- wind tunnel interference will be a limiting factor at low speeds, and
- Reynolds number effects at high speeds have to be taken into account.

As also shown in Figure 22, the correlation in the dynamic data is satisfactory in the medium speed range. Therefore increasing efforts have to be undertaken to solve the above mentioned problems in the low speed range in order to realize the promises of ACT in the entire flight envelope.

Stability and Control Derivatives [33]

Accurate stability and control analyses and handling qualities evaluations are of keen interest for the development of advanced rotorcraft including ACT. For the determination of reliable system parameters basically three approaches are applicable: (1) theoretical calculation methods, (2) wind tunnel test with scaled models, and (3) the extraction of system parameters from flight test data by parameter identification procedures. For rotary-wing aircraft the approaches (2) and (3) are seldom utilized due to some specific problems encountered in these configurations.

The main problem areas for wind tunnel tests in the field of handling qualities research are:

- It is not possible to achieve complete aerodynamic and dynamic similarity between model and full-scale helicopter.

- The rotor blades must be manufactured with extreme high accuracy.

- The rotor should be as large as possible, which means that tests must be conducted in large, costly wind tunnels.

Rotorcraft system identification is still a relatively complicated task because of three main difficulties:

- A large number of coupled degrees of freedom necessitates a high order mathematical model to adequately describe helicopter dynamics. However, successful application of system identification techniques is limited by the size of the model, the number of unknowns that have to be identified, and the information content of the data.

- Inherent rotorcraft instabilities limit the time length for a data run because increasing amplitudes quickly invalidate small perturbation assumptions used for linear models.

- Data measurement quality is affected by the high vibration level of helicopters. Furthermore, some variables (like speed components for low speed flight conditions and hover and, in particular, rotor blade dynamics) are difficult to measure.

In Figure 23 static stability and control derivatives are shown as obtained from theoretical calculations, measurements in two different wind tunnels, and system identifications of the helicopter BO 105.

The Z_u derivative represents the change of the vertical force due to a longitudinal speed change. Its primary contributor is the main rotor. Based on rotor inflow mass and angle of attack considerations it can be visualized that Z_u in general is negative in the low speed range and becomes positive for higher speed. It can be seen that a satisfactory agreement between calculated, measured, and identified values was obtained. Differences in the wind tunnel results are mainly due to the high sensitivity of Z_u to angle of attack changes and different rotor inflow angles in the wind tunnels. In contrast to flight tests the calculation and measurements were conducted for constant angle of attack. This certainly caused deviations from the identified values.

The velocity stability derivative M_u has a stabilizing influence when it is positive which means a nose up response of the helicopter with increasing speed. The rotor gives a positive contribution whereas the fuselage normally produces a destabilizing moment. The calculated and wind tunnel values agree almost perfectly up to a speed of about 30 m/s. Tests showed that differences in the higher speed regime could be significantly reduced by slightly varying the cyclic pitch and the angle of attack. It indicates that the deviations may result from wind tunnel induced effects. This assumption is confirmed by the DNW measurements. The identified derivatives are almost independent from speed. This is in good agreement with calculated and wind tunnel results. However, they are smaller which may be due to the influence of the fuselage.

The Z_w derivative is related to the slope of the lift curve (Z_α). It is often referred to as vertical damping and has a negative sign. Its main contribution arises from the rotor. In general, it slightly increases with speed because of a decreasing influence of the induced flow. The comparison of the results shows some discrepancies. Daimler Benz wind tunnel measurements are in good agreement with the calculation whereas the identified values show the same tendency as the DNW measurements.

The M_w derivative is related to the angle of attack stability M_α. A positive sign indicates static instability. Contributions to M_w arise from the rotor, the fuselage and the tail as well as from fuselage/rotor aerodynamic interferences. A destabilizing tendency is produced by the rotor and the fuselage, whereas the horizontal tail provides a negative (stable) value. The comparison of calculated and wind tunnel results shows some discrepancies especially in the low speed regime. The identified derivatives also increase with speed and show almost perfectly the same tendency as the calculated data. However, they are significantly smaller which results from the stabilizing influence of the horizontal tail and stabilizer. In addition, downwash interferences may also contribute to these differences.

The derivative $Z_{\theta s}$ characterizes changes in lift due to longitudinal cyclic pitch. It can be seen that the wind tunnel results and the calculated values agree satisfactorily. As the DNW measurements have a high confidence level it can be concluded that the deviations of the Daimler Benz wind tunnel measurements result from tunnel induced effects. As the $Z_{\theta s}$ derivative has only minor influence in the lift equation of the mathematical model it cannot be identified with sufficient accuracy.

The change in pitch moments due to longitudinal cyclic pitch is described by the $M_{\theta s}$ derivative. The comparison of calculated and wind tunnel results shows a satisfactory agreement although there are some deviations in the higher speed regime. Mainly for two reasons the identified derivatives are significantly smaller: (1) The BO 105 control inputs were measured at the stick. Influences of the dynamic characteristics of the helicopter hydraulic system were supposed to be negligible within the frequency range under consideration, and (2) the mathematical 6 DOF model is based on the assumption that there is an instantenous rotor tip path plane response due to control inputs and that the rotor reaches its new steady state immediately. It means that the influence of rotor dynamics is neglected which only can be justified by the high frequency response of the rotor in comparison to the relatively low rigid body frequencies.

The Z_{θ_0} derivative is the main collective control derivative. Wind Tunnel measurements and identified derivatives agree fairly well. The calculation yields slightly higher values which may be caused by inaccuracies in the rotor downwash model and uncertainties in the blade torsion modes used in the computation.

The change in pitch moments due to collective, the $M_{\theta o}$ derivative, increases with speed. There is a good agreement between measurements and calculation. The identified derivatives are smaller for the same reasons that were discussed above for the $M_{\theta s}$ derivative.

The advancement of rotorcraft mathematical modelling, wind tunnel testing, and system identification are major research goals in order to improve correlations and to evaluate the flight mechanical characteristics of future rotary-wing aircraft including active control systems.

4. CONCLUSION

In this paper the DFVLR technique of dynamic model testing for active controls research is presented. The follwing conclusions can be drawn:

- Dynamic model testing can play an important role in the future implementations of ACT.
- The DFVLR test facilities
  - "Installation for Dynamic Simulation in Wind Tunnels" for fixed-wing aircraft, and
  - "Rotor Test Stand" for rotary-wing aircraft

  have been proved to be suitable tools for the investigation of flight mechanical problems connected with ACT.
- A gust alleviation system was designed and optimized using the Installation for Dynamic Simulation in Wind Tunnels. The results of these dynamic model testing have given valuable data for the design of the gust alleviation system for the full-scale aircraft.
- A higher harmonic control system was checked out on the Rotor Test Stand and is prepared for investigation in the DNW.
- The investigation of specific flightmechanical phenomena associated with the development of ACT systems can benefit from the application of system identification technique to dynamic wind tunnel test data.
- Wind tunnel results show that the transferability of dynamic model data to full-scale data is feasible in areas which are of major interest in the development of ACT systems. This was demonstrated by flight test programs.

5. REFERENCES

1. Chalk, C.R., "Technical Evaluation Report on the Flight Mechanics Panel Symposium on Stability and Control", AGARD-AR-134 1979.
2. Thomas, H.H.B.M., "Technical Evaluation Report on the Fluid Dynamics Panel Symposium on Aerodynamic Characteristics of Controls", AGARD-AR-157, 1980.
3. Ham, N.D. (Editor), "Vertica", Vol. 4, No.1, 1980.
4. Rediess, H.A., "Impact of Advanced Control Concepts on Aircraft Design", 12. ICAS Congress , Preprint 80-0.4, Munich 1980.
5. Reed, W.H., "Comparison of Flight Measurements with Predictions from Aeroelastic Models in the NASA Langley Transonic Dynamic Tunnel", AGARD-CP-187, Paper No. 6, 1976
6. Gobeltz, J., "Simulation de Vol par Maquettes de Vol libre en Laboratories", AGARD-CP-187, Paper No. 14, 1976.
7. Hönlinger, H., Sensburg. O., "Dynamic Simulation in Wind Tunnels, Part I, Active Flutter Suppression", AGARD-CP-187, 1976.
8. Simpson, A., Hitch, H.P.Y., "Active Control Technology", Aeronautical Journal, June 1977.
9. Statler, I.C., "Flight Mechanics - A Review of the Activities of the AGARD Flight Mechanics Panel ", AGARD Highlights 78/1, 1978.
10. Anon., "Impact of Active Control Technology on Airplane Design", AGARD-CP-157, 1975.
11. Subke, H., Krag, B., "Dynamic Simulation in Wind Tunnels, Part II", AGARD-CP-187, 1976.
12. Krag, B., '"The Wind Tunnel Behaviour of a Scaled Model with a Gust Alleviation System in a Deterministic Gust Field", Symposium on Dynamic Analysis of Vehicle Ride and Manoeuvering Characteristics, London 1978.
13. Etkin, B., "Dynamics of Flight",John Wiley & Sons, 1958.

14. Subke, H., "Test Installation to Investigate the Dynamic Behaviour of Aircraft with Scaled Models in Wind Tunnels", Symposium on Dynamic Analysis of Vehicle Ride and Manoeuvering Characteristics, London 1978.

15. Rohlf, D., "Bewegungsgleichungen und modifiziertes Open-Loop-Böenabminderungssystem für das Do-28 TNT-Windkanalmodell", DFVLR Interner Bericht IB 154-79/17, 1979.

16. Hamel, P.G., Krag, B., "Dynamic Wind Tunnel Simulation of Active Control Systems", AGARD-CP-260, 1978.

17. Krag, B., Rohlf, D., Wünnenberg, H., "OLGA, a Gust Alleviation System for Improvement of Passenger Comfort of General Aviation Aircraft", Preprint 5.4, ICAS 1980.

18. Wilhelm, K., Verbrugge, R., "Correlation Aspects in the Identification of Dynamic Effects Using Complementary Techniques. Flight in Turbulence-Gust Alleviation." AGARD-CP-339, Paper No. 17 A, 1983.

19. Simons, I.A., "Advanced Control Systems for Helicopters", Vol. 1, pp. 17-29, Vertica 1976.

20. Kretz, M., Larche, M., "Future of Helicopter Rotor Control", Vol. 4, pp. 13-22, Vertica 1980.

21. Mc Cloud III, J.L., "The Promise of Multicyclic Control", Vol. 4, pp. 29-41, Vertica 1980.

22. Shaw, J., Albion, N., "Active Control of the Helicopter Rotor for Vibration Reduction", 36th Annunal Forum of the American Helicopter Society, Preprint No. 80-68, Washington D.C. 1980.

23. Zierep, J., "Ähnlichkeitsgesetze und Modellregeln der Strömungslehre", G. Braun, Karlsruhe 1972.

24. Carbonaro, M., "Review of Some Problems Related to the Design and Operation of Low Speed Wind Tunnels for V/STOL Testing", AGARD Report No. 601, 1973.

25. Simons, I.A., Derschmidt, H., "Wind Tunnel Requirements for Helicopters", AGARD Report No. 601, 1973.

26. Harris, F.D., "Aerodynamic and Dynamic Rotary Wing Model Testing in Wind Tunnels and other Facilities", AGARD-LS-63, 1973.

27. Hardy, W.G.S., "The Effects of Reynolds Number on Rotor Stall", AGARD-LS-63, 1973.

28. Seidel, M., Maarsingh, R.A., "Test Capabilities of the German-Dutch Wind Tunnel DNW for Rotors, Helicopters and V/STOL Aircraft", 5th European Rotorcraft and Powered Lift Aircraft Forum, Paper No. 17, Amsterdam 1979.

29. Lehmann, G., "A Digital System for Higher Harmonic Control of a Model Rotor", 8th European Rotorcraft Forum, Paper No. 10.1, Aix-en-Provence 1982.

30. Langer, H.-J., v. Grünhagen, W., Junker, B., "Comparison of Rotor Analysis Results with Aerodynamic Wind Tunnel Data", AGARD-CP-334, 1982.

31. White, W.F., Tomaine, R.L., "B.2.1 Rotors", AGARD-AG-292, 1983.

32. Langer, H.-J., Stricker, R., "Some Results of Dynamic Measurements with a Model Hingeless Rotor", 5th European Rotorcraft and Powered Lift Aircraft Forum, Paper No. 42, Amsterdam 1979.

33. Kaletka, J., Langer, H.-J., "Correlation Aspects of Analytical, Wind Tunnel and Flight Test Results for a Hingeless Rotor Helicopter", AGARD-CP-339, 1982.

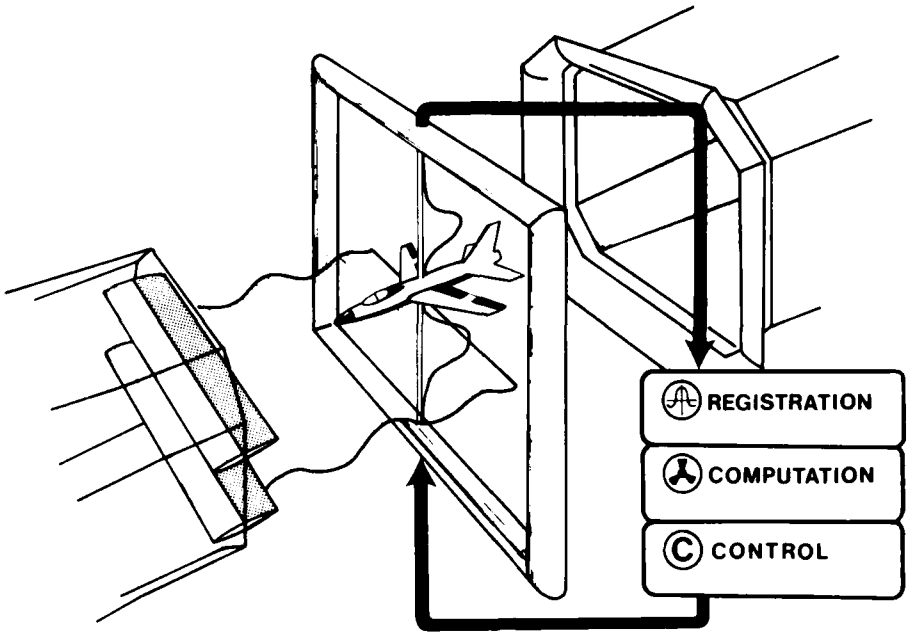

Figure 1 General View of the Installation for Dynamic Simulation in Wind Tunnels.

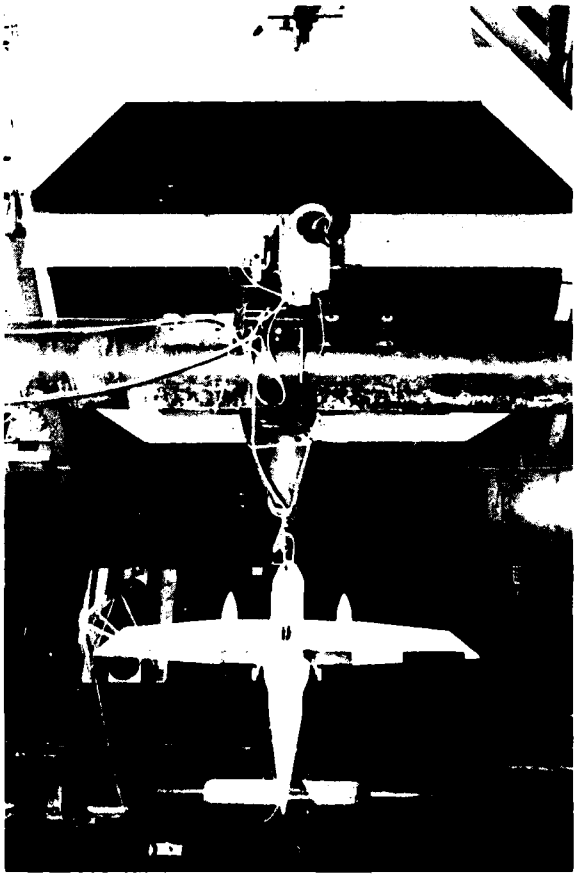

Figure 2 The Installation for Dynamic Simulation in the 3 m Subsonic Wind Tunnel.

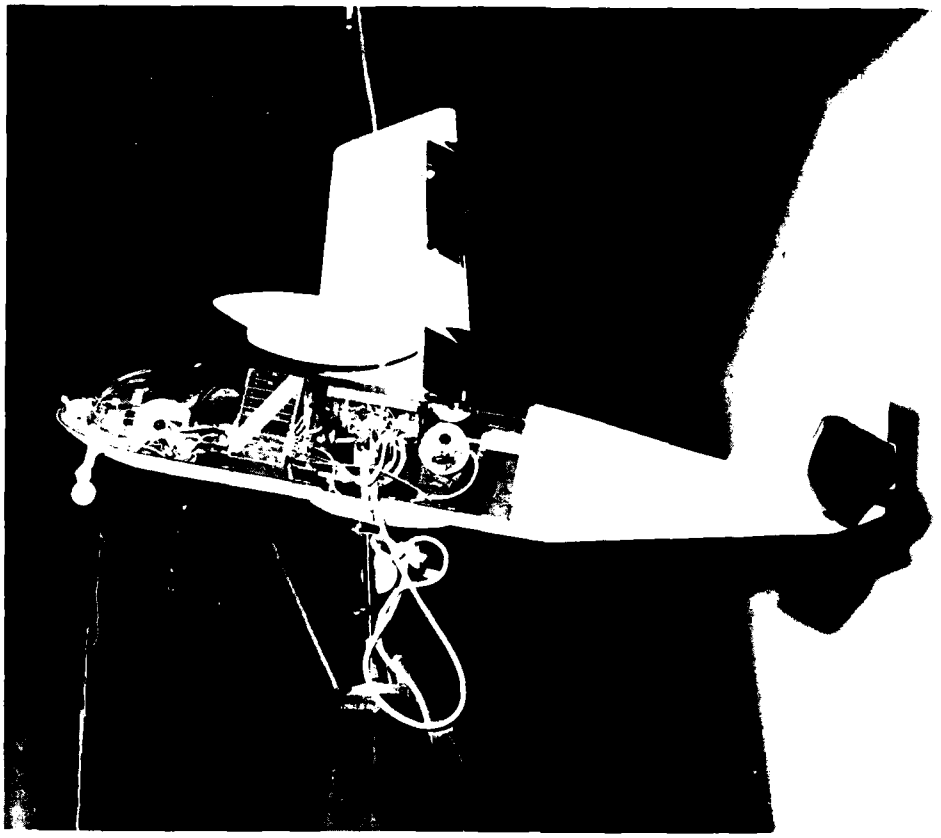

Figure 3. Remotely Controlled Wind Tunnel Model of the Do 28 TNT

	FREE FLYING MODEL	MODEL WITH ROD SUSPENSION
	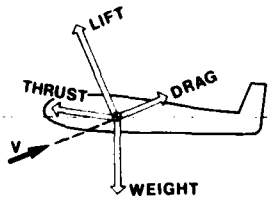	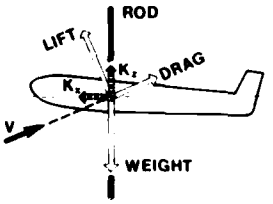
DEGREES OF FREEDOM (LONG. MOTION)	• PITCH MOTION • VERTICAL MOTION • HORIZONTAL MOTION	• PITCH MOTION • VERTICAL MOTION
MODES	• SHORT PERIOD MODE • PHUGOID MODE	• SHORT PERIOD MODE

Figure 4. Effect of Vertical Rod Suspension on Model Motion

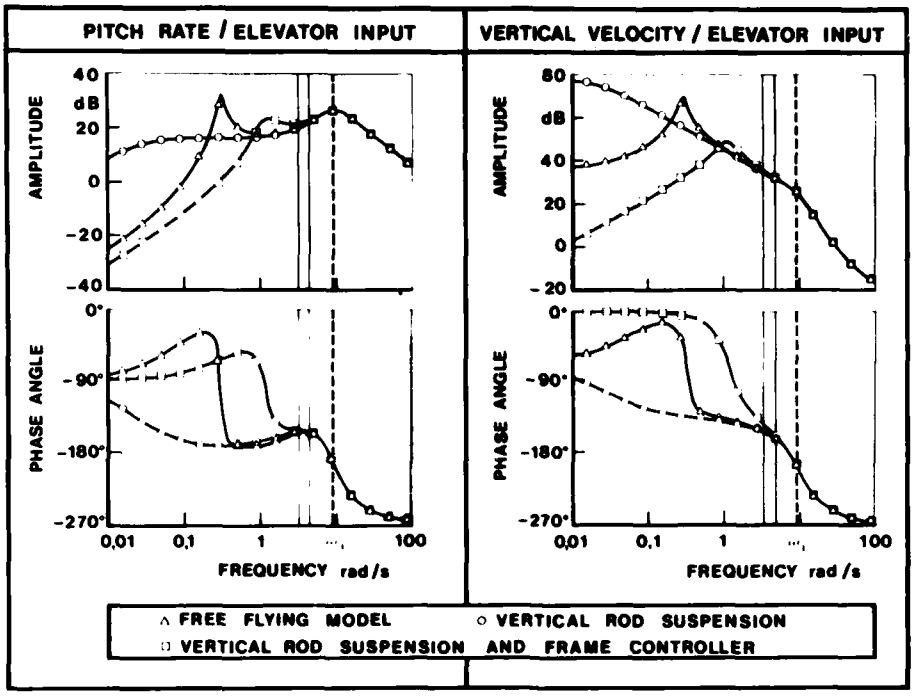

Figure 5. Frequency Response (Bode Plots) of Pitch Rate and Vertical Velocity to Elevator Input

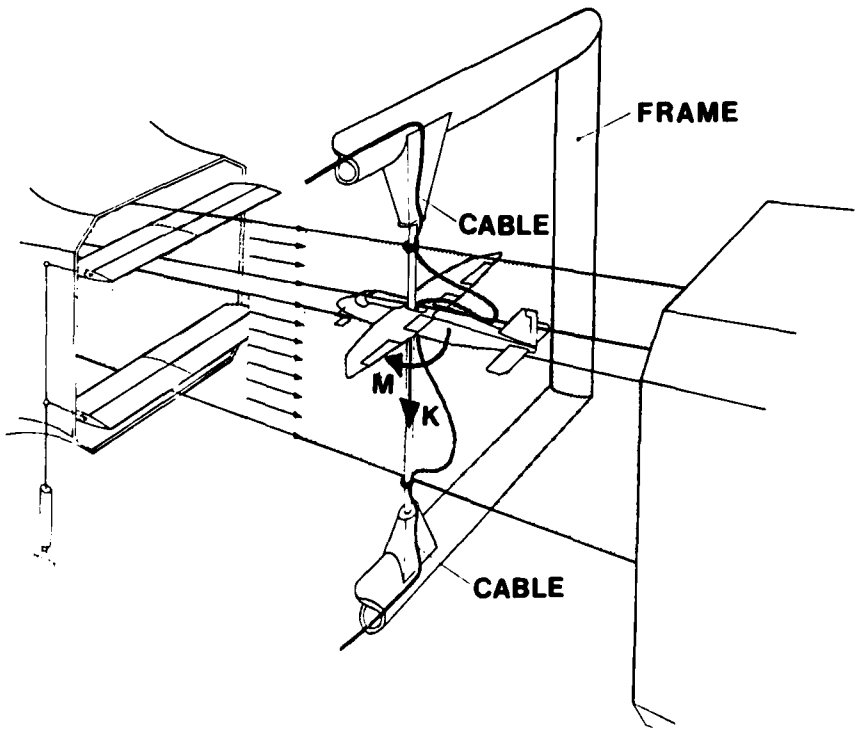

Figure 6. Disturbing Influence of Cables

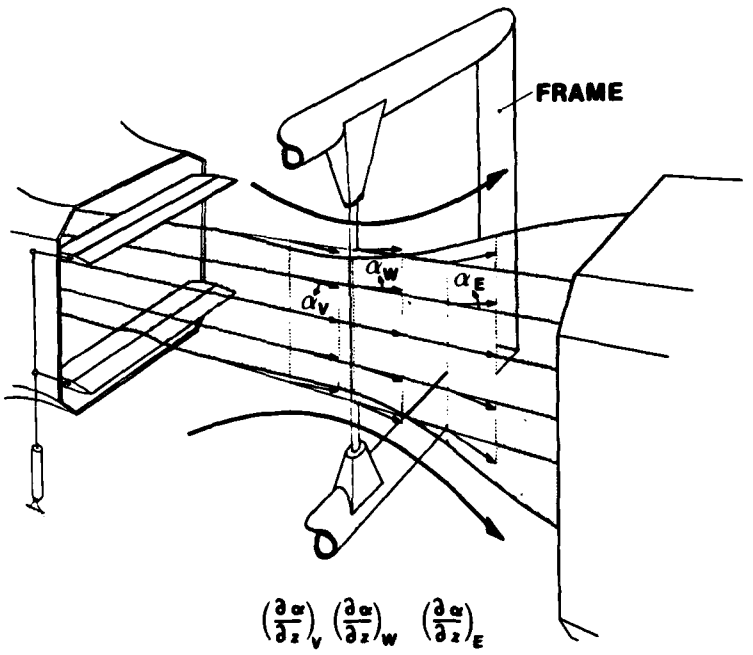

Figure 7. Suspension - Frame Interaction with Airflow

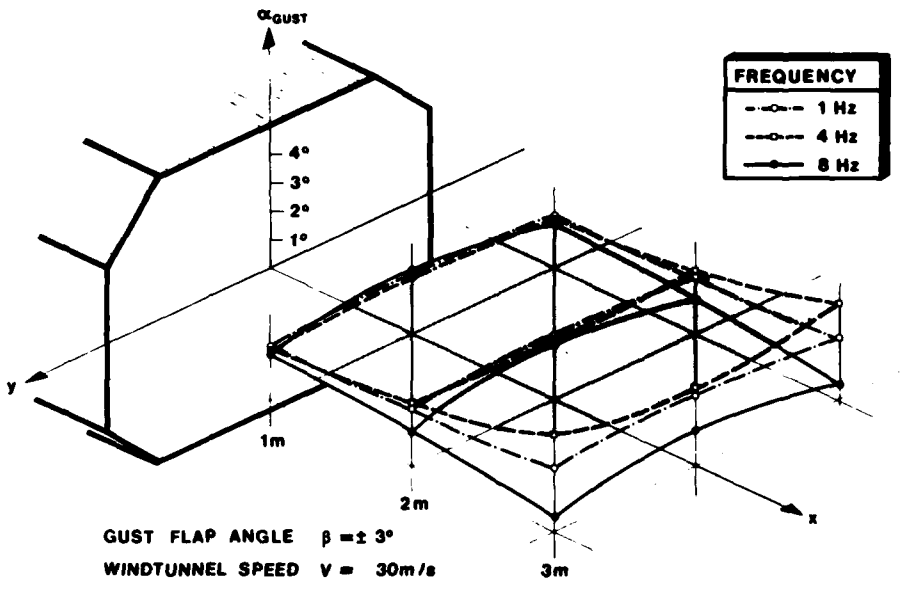

Figure 8. Gust Angle of Attack for Three Different Frequencies

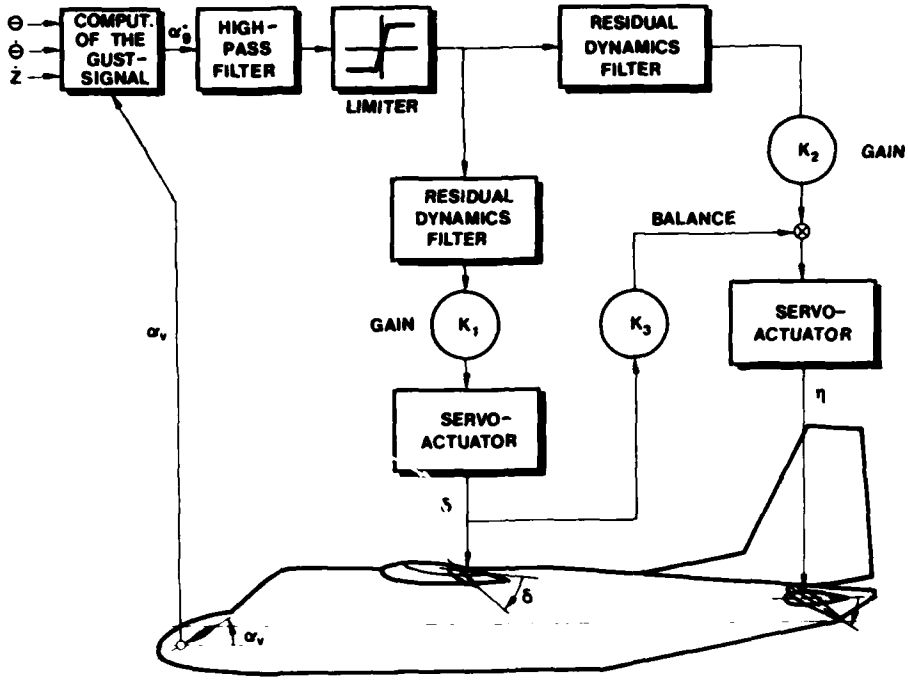

Figure 9. Block Diagram of the OLGA Gust Alleviation System

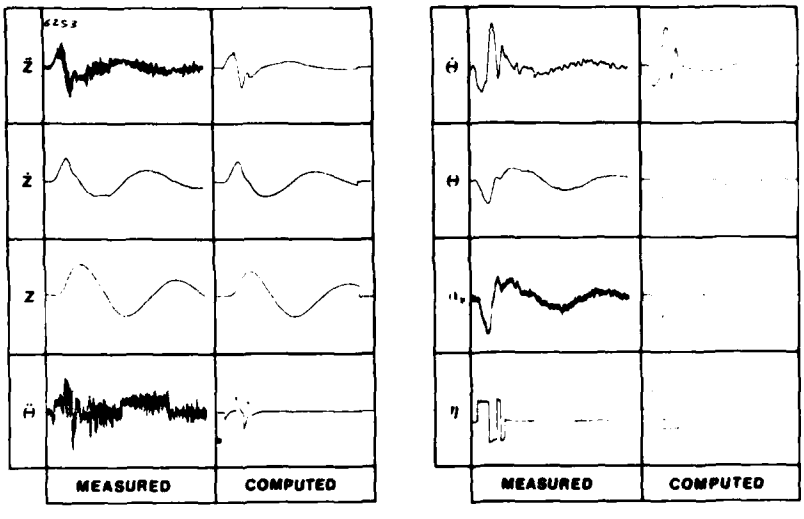

Figure 10. Comparison of Measured and Computed Response to an Impulsive Elevator Deflection

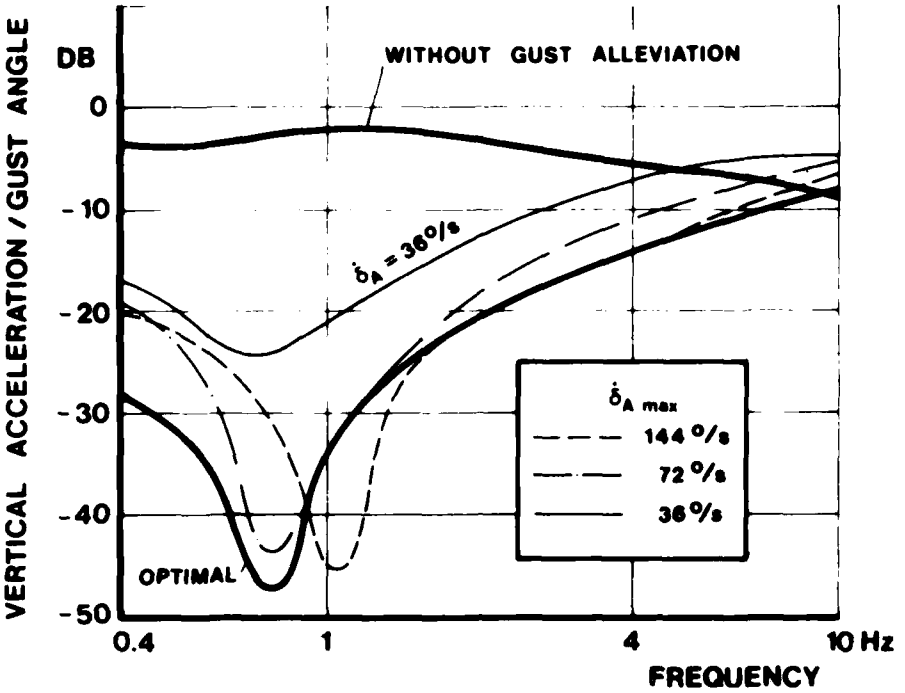

Figure 11. Effect of Aileron Rate Limitation on the Performance of the Gust Alleviation

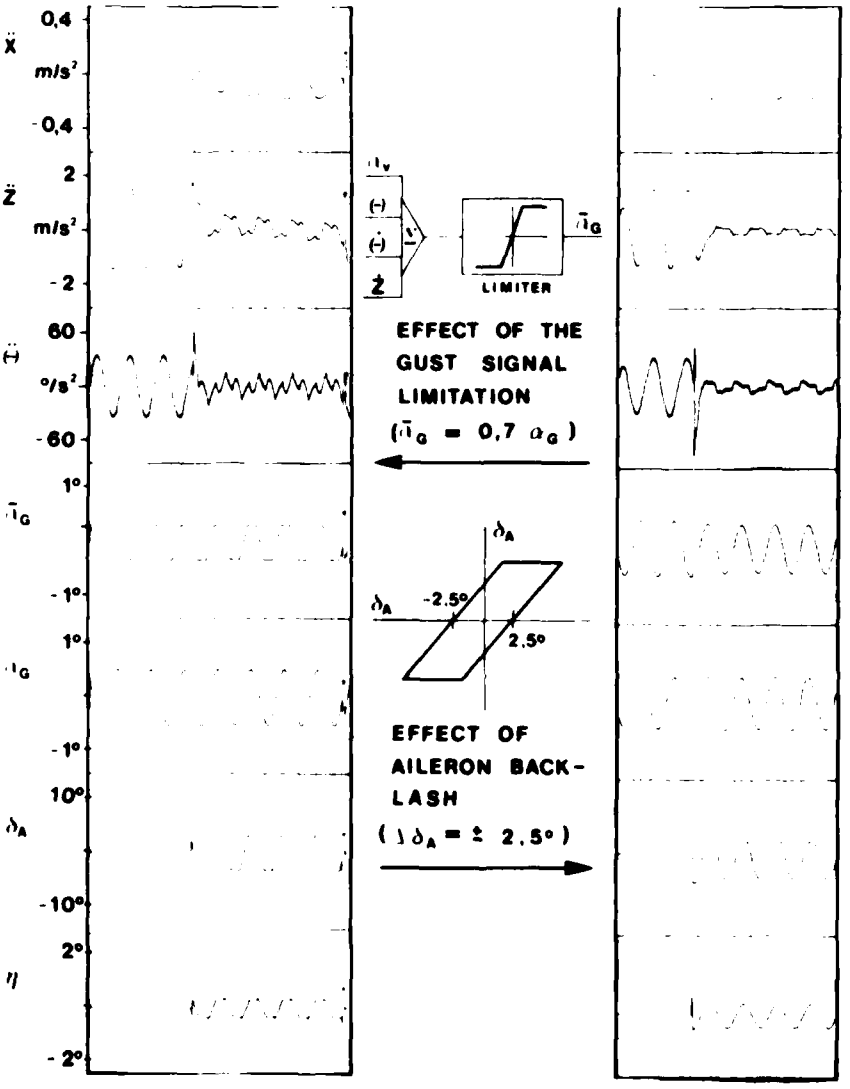

Figure 12. Effect of Nonlinearities on the Performance of the Gust Alleviation System

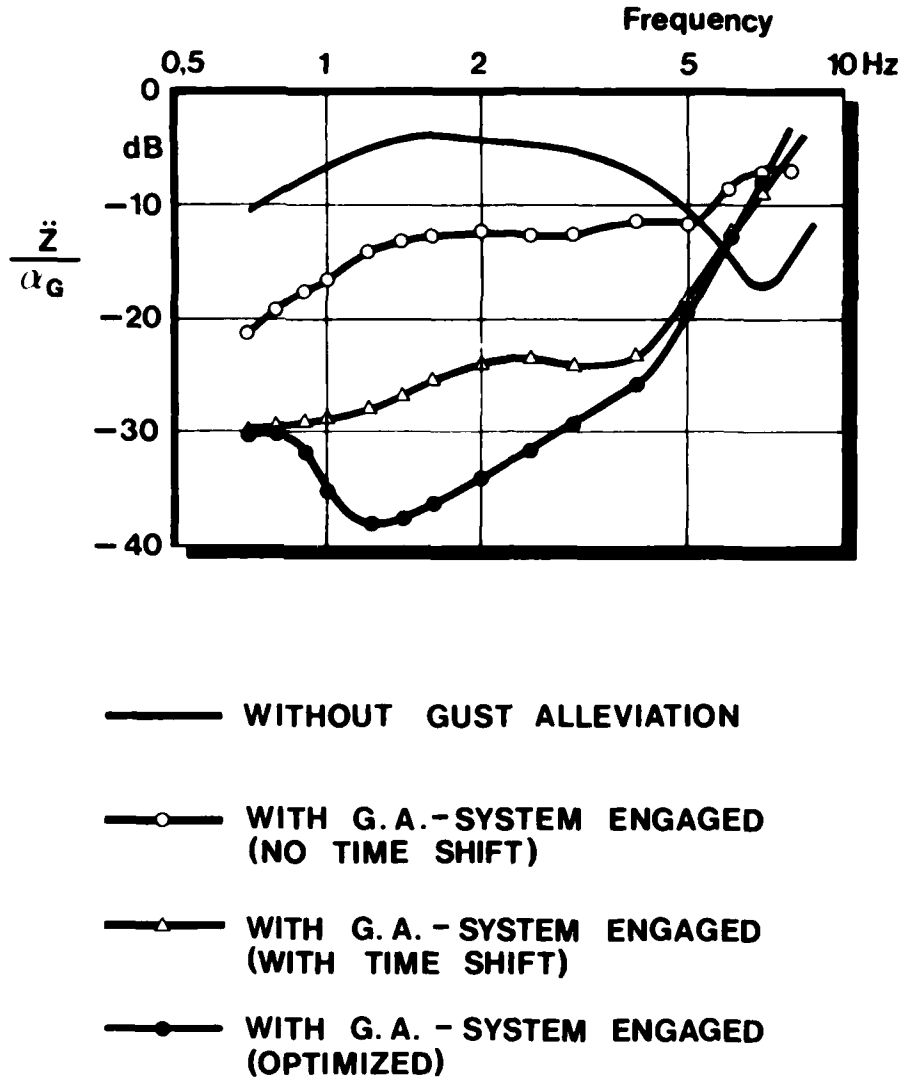

Figure 13. Frequency Response of the Vertical Acceleration. Effect of Gust Alleviation System

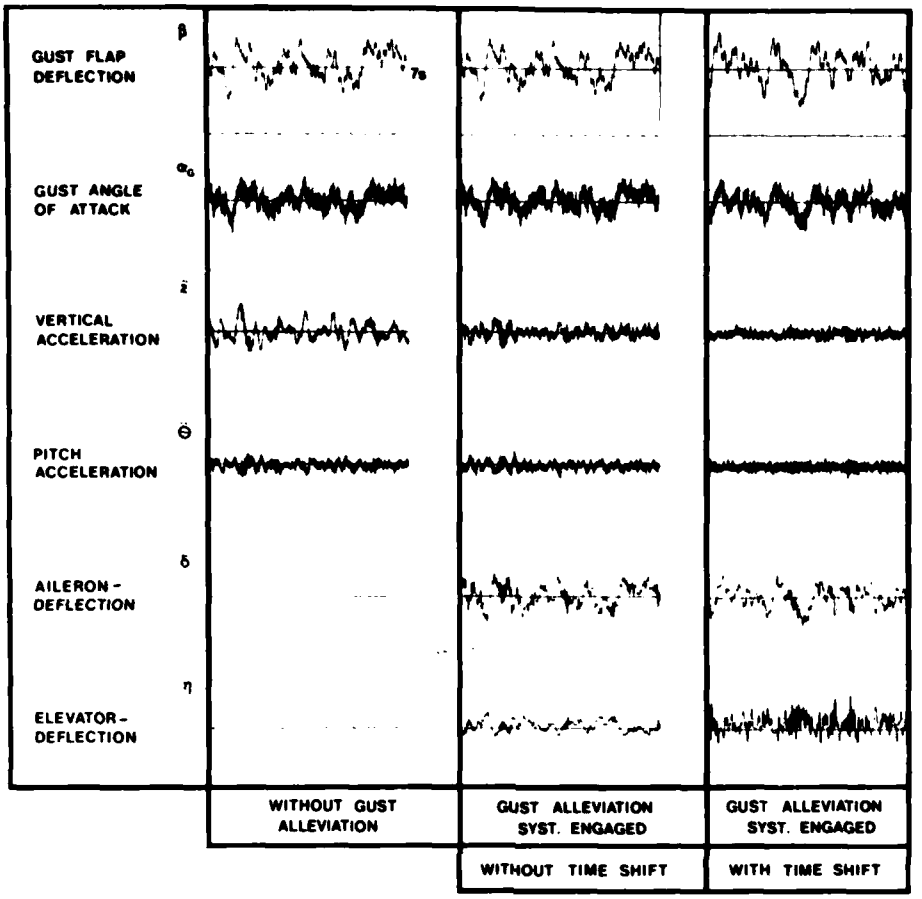

Figure 14. Time Histories of the Model response during Flight in a Scaled Turbulence Field

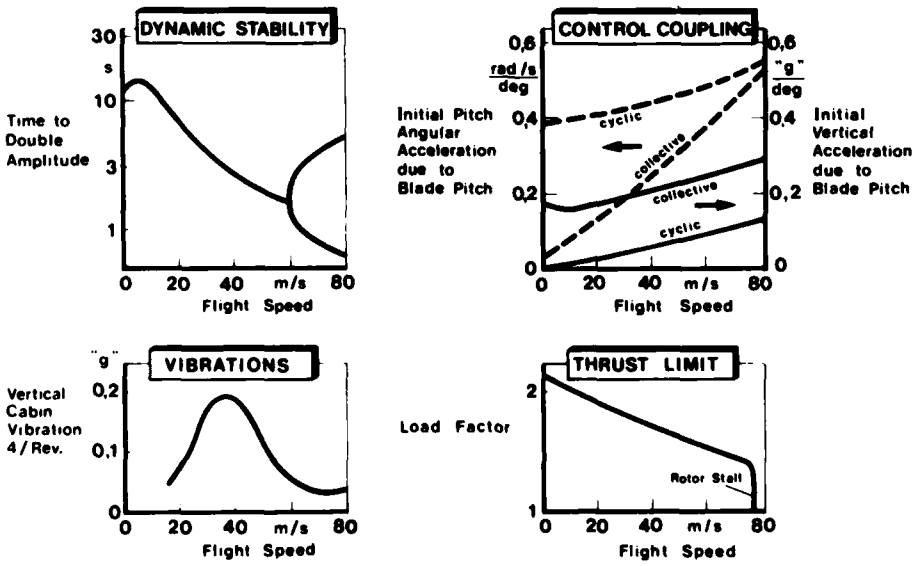

Figure 15. Problems of Helicopter Flight Mechanics

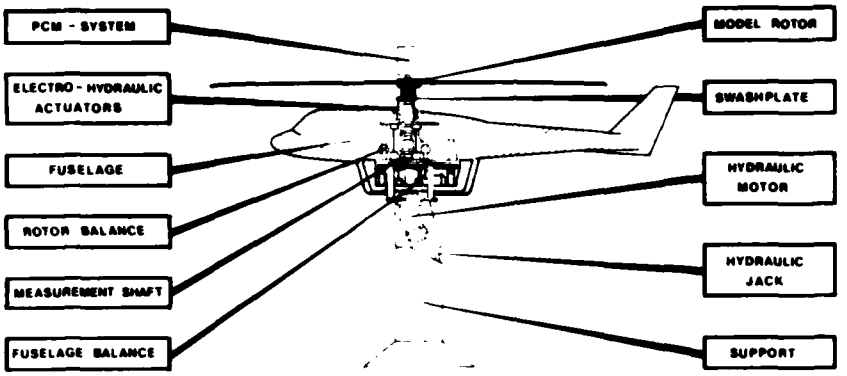

Figure 16. DFVLR-Rotor Test Stand

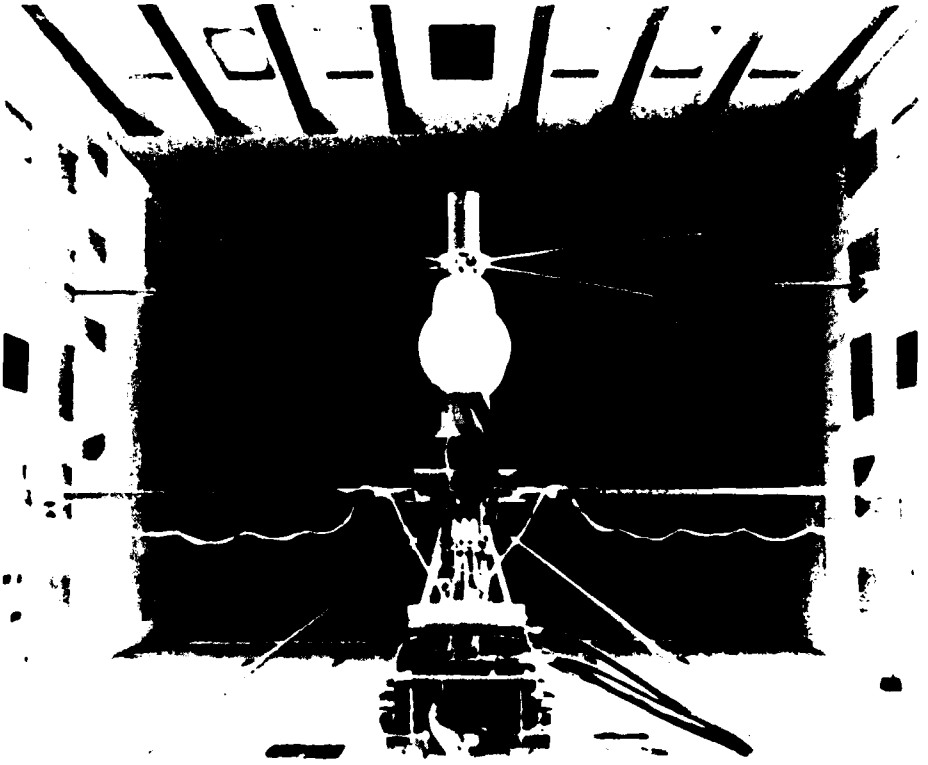

Figure 17. Rotor Test Stand in German-Dutch Wind Tunnel DNW

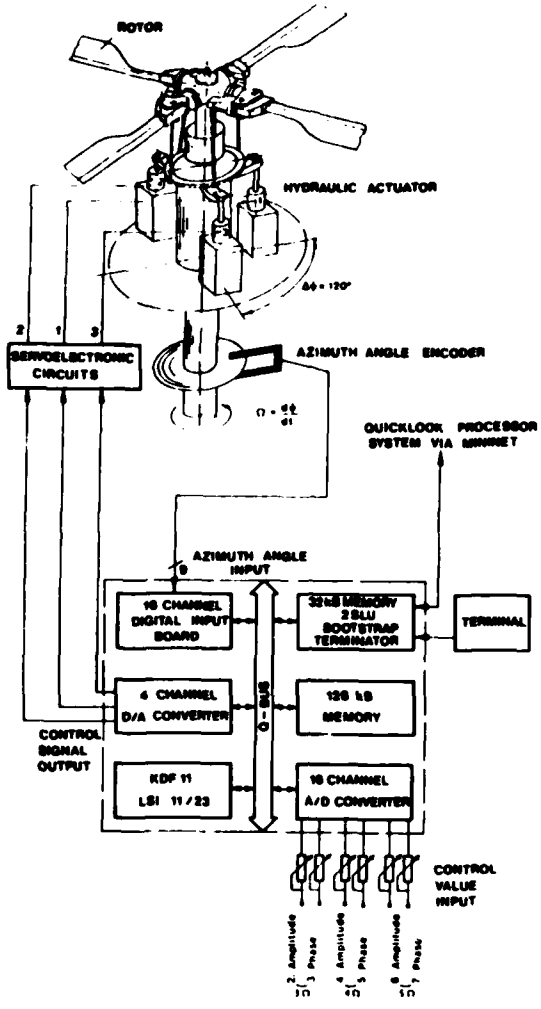

Figure 18. Control Processor Configuration

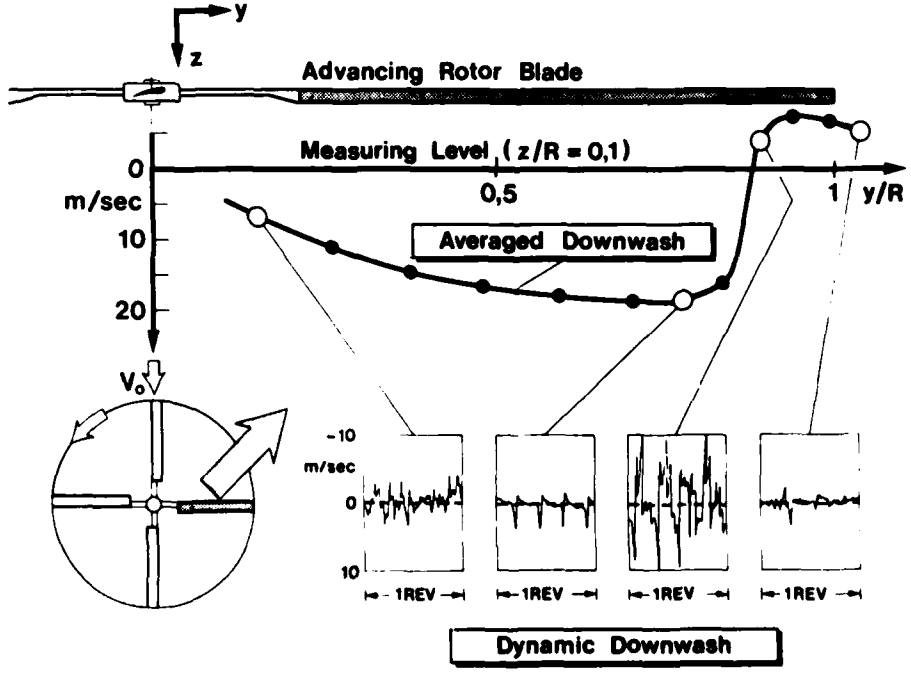

Figure 19. Rotor Downwash below the Advancing Blade

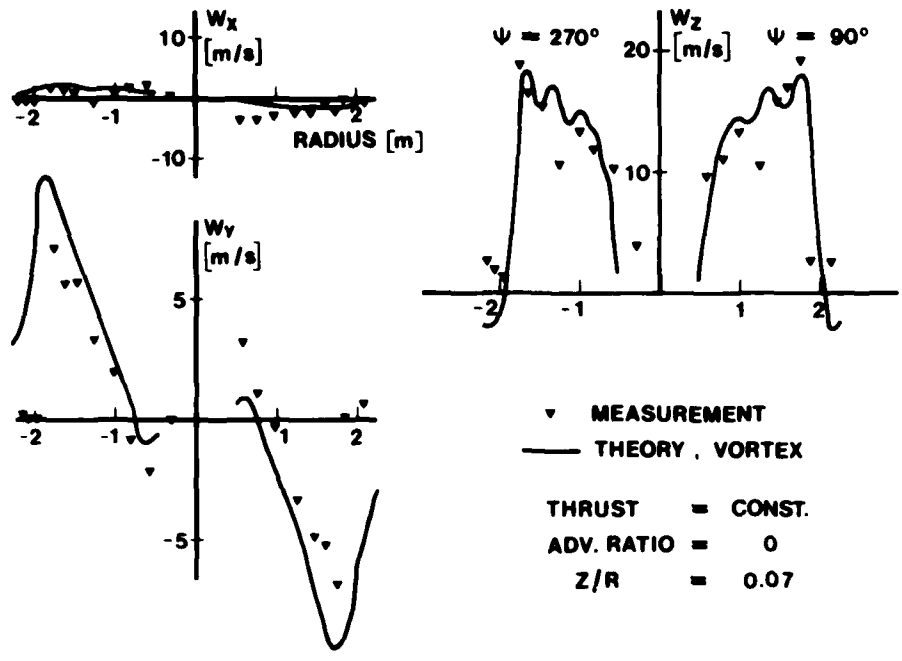

Figure 20. Downwash Velocities in X-, Y-, Z-Direction (rigid vortex theory, core radius variable)

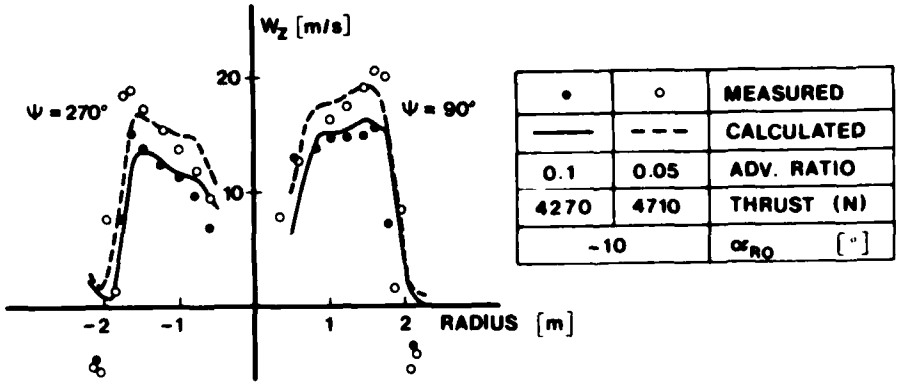

Figure 21. Downwash Velocities at Different Advance Ratios and Constant Angle of Attack ($\alpha_{RO} = -10^{O}$)

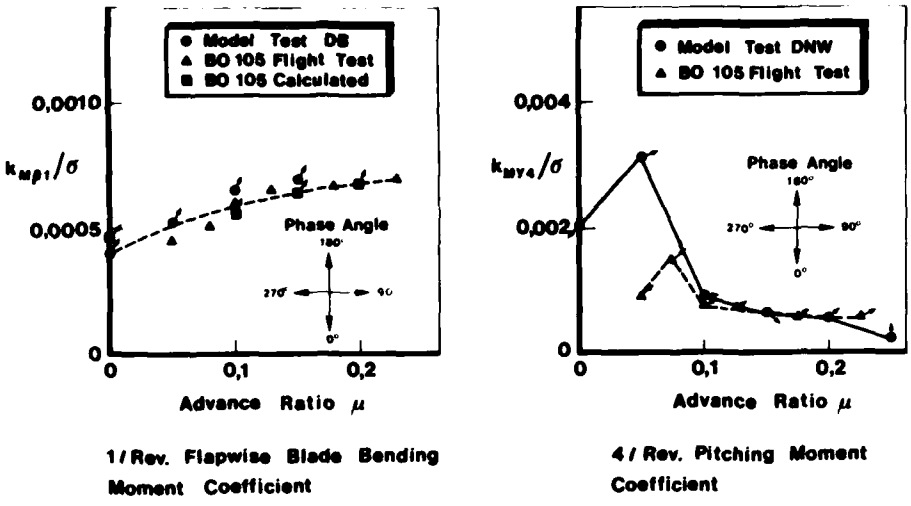

1/Rev. Flapwise Blade Bending Moment Coefficient

4/Rev. Pitching Moment Coefficient

Figure 22. Dynamic Test Data (Comparison Model/Full-Scale)

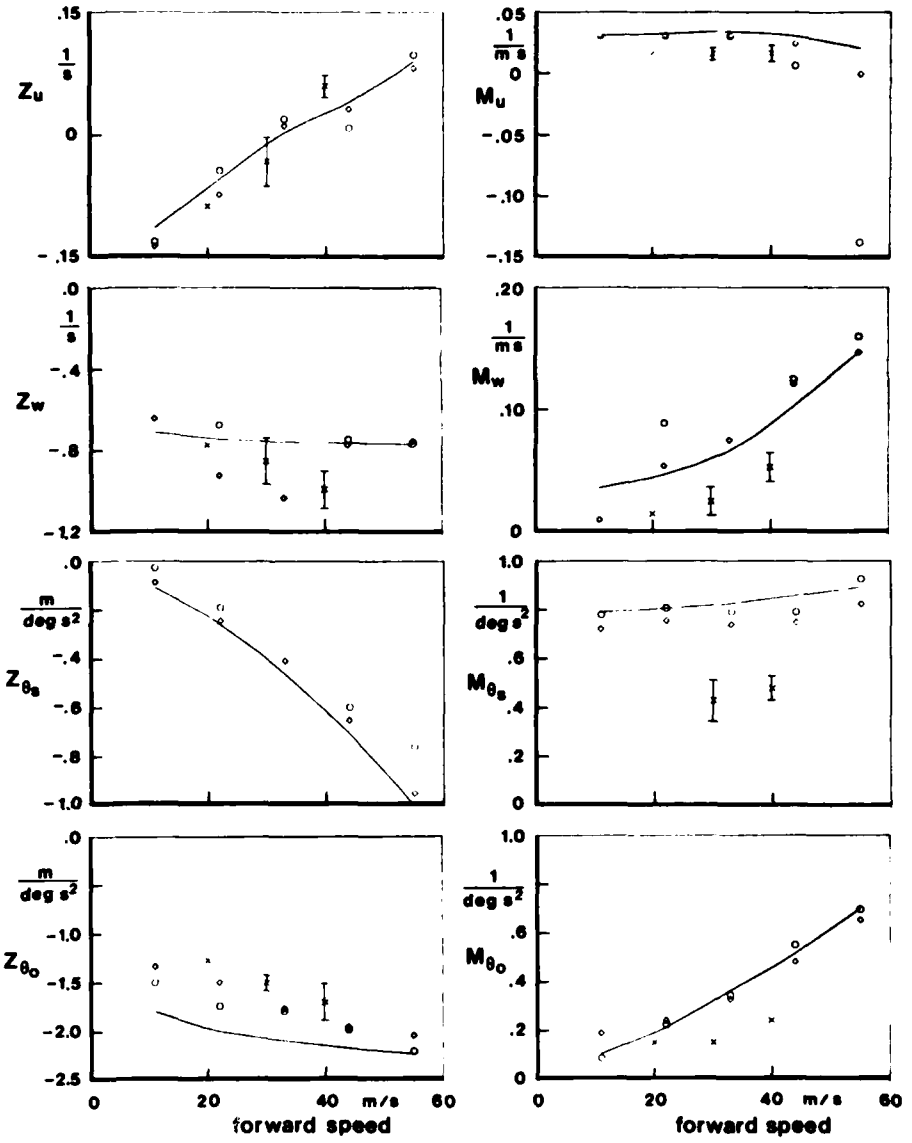

theoretically calculated

identified from flight test data (with standard deviation)

● measured in Daimler Benz wind tunnel

▲ measured in DNW wind tunnel

Figure 23. Comparison of Derivatives from Calculations, Measurements in Wind Tunnels, and Parameter Identification from Flight Tests (Bo 105, level flight, 2300 kg)

DYNAMIC WIND-TUNNEL TESTING OF ACTIVE CONTROLS BY THE NASA LANGLEY RESEARCH CENTER

By Irving Abel, Robert V. Doggett,
Jerry R. Newsom, and Maynard Sandford
Aerospace Engineers
NASA Langley Research Center
Hampton, Virginia 23665

SUMMARY

A review of dynamic wind-tunnel testing of active controls by the NASA Langley Research Center is presented. Seven experimental studies that have been accomplished to date are described. Six of the studies focus on active flutter suppression. The other study focuses on active load alleviation. In addition to presenting basic results for these experimental studies, topics including model design and construction, control law synthesis, active control system implementation, and wind-tunnel test techniques are discussed.

LIST OF SYMBOLS

a	control law gain parameter
a_1, a_2	control law gains, aerodynamic energy method
b	reference semichord
b_m	one-half mean geometric chord of wing
b_r	semichord length at spanwise location of inboard accelerometer
$[C], [G]$	real and imaginary control law matrix
c	wing streamwise chord
dB	decibel
$F(s)$	form of control law implemented on analog computer
$G(s)$	transfer function relating wing motion to control-surface deflection
g	gravitational constant
$H(s)$	transfer function relating control-surface deflection to wing motion
$\ddot{h}_{inbd}, \ddot{h}_{outbd}$	vertical acceleration at inboard and outboard accelerometer locations
h_1, h_2	vertical displacements at .3 and .7 of local delta wing chord, respectively
i	$\sqrt{-1}$
K_g	fraction of nominal gain
K_p	phase-control-filter gain
$K_{STAB}, K_{AIL}, K_{SAS}$	active load distribution control system gains
L	reference length
M	Mach number
m	mass of body
q	dynamic pressure
q_{max}	= 1.44 x calculated flutter dynamic pressure
q_{REF}	reference dynamic pressure

rms	root-mean-square
s	Laplace variable
V	free-stream velocity
V_f	velocity at flutter
$\ddot{Z}$	wing acceleration
α	local chord angle of attack
β	leading-edge control surface deflection
δ	trailing-edge control surface deflection
δ_a	control-surface deflection
$\delta_{a,c}$	aileron command deflection
δ_c	control-surface command to actuator
δ_c'	control-surface command from control law
$\delta_{c,c}$	canard command deflection
ζ	viscous damping coefficient
ζ_n	viscous damping coefficient (n = mode 1,2,...)
$\dot{\theta}$	pitch angle rate
μ	mass-density ratio
ρ_f	density of fluid
τ	phase-control-filter time constant
ϕ	phase angle, deg
ω	circular frequency, rad/sec
ω_n	natural frequency, rad/sec (n = mode 1,2 ...)

Dots over symbols denote derivatives with respect to time.

INTRODUCTION

Aeroelastic models have played important roles in the development of new technology for aircraft. In many cases model tests are the most timely and economical means for establishing proof of concept and for generating experimental data for comparison with analysis. Models also are used to obtain experimental results at conditions where analysis is known to be inaccurate, for example at transonic speeds.

Wind-tunnel testing of dynamically-scaled aeroelastic models equipped with active controls has become a widely used means of studying active control concepts. However, the addition of active controls to aeroelastic models has added a new complexity to modeling technology. Control surface and actuation systems must be miniaturized and be able to operate at high frequencies with relatively small phase and gain variations.

To accelerate technology development in active controls, research was begun by the NASA Langley Research Center in the late 1960's to advance this concept. Wind tunnel studies of aeroelastic models (primarily consisting of tests in the Langley Transonic Dynamics Tunnel) have been a cornerstone of the NASA active controls research program. This paper presents a review of seven experimental studies that have been accomplished to date. In addition to presenting basic results for these experimental studies, topics including model design and construction, control law synthesis, active control system implementation, and wind-tunnel test techniques will be discussed.

The first study to be presented involved flutter suppression on a delta-wing model (ref. 1). This model, which was a simplified version of a supersonic transport design, was used to develop basic flutter suppression modeling technology and to evaluate a control law synthesis approach developed by Nissim in ref. 2. The delta-wing study was the first successful experimental demonstration of active flutter suppression in the United States. The second study utilized a dynamically scaled aeroelastic model of the B-52 control configured vehicle (CCV). Both flutter suppression and ride quality control systems were implemented in this study which was done in

cooperation with the Air Force Flight Dynamics Laboratory (ref. 3). The third study was also done in cooperation with the Air Force and used an aeroelastic model of the C-5A. This study was performed in conjunction with the development of a proposed active lift distribution control system (ALDCS) for the full-scale airplane. The fourth model was a simplified aeroelastic model of a wing that was to be tested on a remotely piloted drone in the program called DAST (Drones for Aerodynamic and Structural Testing) which is described in ref. 4. The wind-tunnel model was used for a variety of flutter suppression studies including a limited evaluation of the control system that would be tested on the flight vehicle. Control laws were synthesized using classical, aerodynamic energy, and optimal methods and tested on the model (see ref. 5). The next two studies, which utilized the F-16 and YF-17 models respectively, were cooperative efforts with the Air Force, General Dynamics, Northrop, and NASA (refs. 6 and 7). Active flutter suppression is a promising method for preventing wing/external store flutter and is especially attractive for fighter aircraft because of the multitude of possible store configurations. The most recent study was a cooperative effort with the McDonnell Douglas Corporation on a derivative DC-10 wing. The purpose of this study (ref. 8) was to apply control law synthesis methods developed by NASA to a realistic transport configuration model with engines on the wing.

DELTA WING MODEL STUDY

The delta-wing model was tested in the first active flutter suppression study undertaken at the Langley Research Center. This program was initiated to develop the basic technology required to perform model studies and to demonstrate experimentally that flutter can be suppressed by using aerodynamic control surfaces. The flutter suppression concept chosen for implementation was the aerodynamic energy method proposed by Nissim (ref. 2).

A photograph of the delta-wing model mounted in the NASA-Langley Transonic Dynamics Tunnel (TDT) and the model geometry are presented in figure 1. The planform was a cropped delta with an aspect ratio of 1.28 and a leading-edge sweepback angle of 50.5 degrees, a taper ratio of 0.127, and a circular arc airfoil section with a thickness-to-chord ratio of 0.03. Two high-fineness ratio bodies were mounted on the wing lower surface to simulate engine nacelles. The model was cantilevered from a rigid mounting block that was bolted to the tunnel sidewall. The mounting block was enclosed in a simulated fuselage fairing. The model was equipped with leading- and trailing-edge aerodynamic control surfaces. The controls were actuated by an electrohydraulic system.

Design and Construction

The delta-wing model was considered representative of a proposed supersonic transport configuration. The design objective was to build a model that had similar flutter characteristics to those of a proposed supersonic transport configuration and which would flutter well within the operating limits of the TDT.

The construction of the model was relatively simple. The basic structure was an aluminum alloy insert which was tapered in thickness in the spanwise direction. Portions of the insert were chemically milled to simulate spars and ribs. The insert was then covered with balsa wood that was contoured to give the desired airfoil shape. The balsa wood was covered with a layer of fiber glass. The two engine nacelles were constructed of steel tubing with balsa wood nose and tail fairings. The nacelles were ballasted to provide the desired mass and inertia properties.

Both the leading- and trailing-edge control surfaces were constructed of balsa wood with streamwise hardwood stiffeners. The trailing-edge control surface was approximately 20 percent of the local wing chord, whereas the leading-edge control surface varied from about 15 percent of the wing local chord inboard to 20 percent of the wing chord outboard. Both controls were located approximately between 73 percent and 84 percent of the wing span.

Two special miniature hydraulic actuators were designed and fabricated as described in ref. 9. A photograph of the actuator installed in the delta-wing model is shown in fig. 2a. The actuator as shown in fig. 2b consisted of a closed cavity separated into two chambers by a self-sealing vane attached to a shaft and supported by two miniature precision ball bearings. Shaft rotation was obtained by applying a differential hydraulic pressure between the two chambers. The maximum angular displacement was approximately ±9 degrees. The development of these miniature actuators represents a significant contribution to active control modeling technology.

Flutter Suppression System

The flutter suppression system implemented on the model was synthesized using the aerodynamic energy method. The basic control law relates the control surface deflections β and δ to the wing motions h_1 and α through a set of coefficients.

The control law can be expressed as a matrix equation where β, δ, h_1, b, and α are shown in the following sketch.

$$\begin{Bmatrix} \beta \\ \delta \end{Bmatrix} = \begin{bmatrix} C_{11} & C_{12} \\ C_{21} & C_{22} \end{bmatrix} \begin{Bmatrix} \frac{h_1}{b} \\ \alpha \end{Bmatrix} + i \begin{bmatrix} G_{11} & G_{12} \\ G_{21} & G_{22} \end{bmatrix} \begin{Bmatrix} \frac{h_1}{b} \\ \alpha \end{Bmatrix} \tag{1}$$

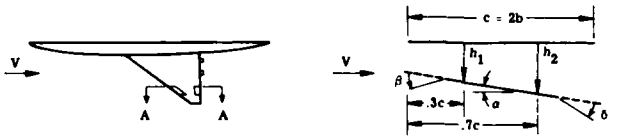

Section A-A

The elements of [C] and [G] are real numbers whose magnitudes are determined by using the aerodynamic energy method. Three variations of the basic control law were implemented and tested on the model (referred to as control laws A, B, and C in ref. 1). Control law A used values for the elements of [C] and [G] that were the same as those developed by Nissim using two dimensional unsteady aerodynamic theory (ref. 2). Control law B was similar to A except that three dimensional unsteady aerodynamics were used to determine the [C] and [G] elements. Control law C also used three dimensional unsteady aerodynamics but incorporated only a trailing edge control surface. When control laws B and C were implemented, the system was so sensitive that when the model was disturbed in still air an inertia coupling between the wing and control surfaces would drive the model unstable through the feedback loop. This instability was eliminated by experimentally varying the gains in [G] until the instability disappeared. A simplified block diagram of the delta-wing flutter-suppression system is given in figure 3. The values of the elements of [C] and [G] tested on the model are presented in figure 4. These values indicate the relative importance between vertical displacement and angular displacement in determining the control surface deflections.

The basic form of the control law was programmed on an analog computer. Each control law variation was implemented by simply changing potentiometer settings on the analog computer corresponding to the coefficients or gains for each control law. For the open-loop experimental studies the control surfaces were kept at zero degrees deflection by applying hydraulic pressure to the control-surface actuators. The pressurized system acted as a stiff spring to keep the rotational frequency of each control surface many times higher than the wing flutter frequency.

Results and Discussion

The flutter studies of the delta-wing model were conducted at Mach numbers of 0.6, 0.7, 0.8, and 0.9. Open-loop flutter tests of the model were conducted first to establish the basic-wing flutter boundary. Closed-loop tests then followed to evaluate the effect of active controls on raising the flutter boundary. The closed-loop tests included evaluation of control laws A, B, and C. Limited experimental studies of control laws A and B were conducted at a Mach number of 0.90 because of an unexplained high-frequency, large-amplitude oscillation of the leading-edge control surface. This phenomenon occurred with both open-loop and closed-loop operation of the controls and at a frequency of about 65 Hz, well above the flutter frequencies of 11 to 12.5 Hz, and therefore the problem is not believed to be a result of the control law. By the use of high-speed motion pictures and visual observation, it was determined that the flutter motion of the model for the open-loop operation and that for the closed-loop operation were similar.

Open-loop experimental results.- The experimental flutter characteristics for the delta-wing model are presented in figure 5 in terms of the variation of flutter-speed-index parameter with Mach number. The flutter boundary indicates a drop in the flutter-speed index (ref. 1) of about 15 percent from a Mach number of 0.60 to a Mach number of 0.90.

Closed-loop experimental results.- Each of the three control laws demonstrated increases in dynamic pressure above the open-loop flutter dynamic pressure at a Mach number of 0.90. For control law A the model fluttered at 12.5 percent increase in flutter dynamic pressure. Control law B demonstrated a 22-percent increase in flutter dynamic pressure. No flutter was encountered at this point; however, the test was terminated because of the leading-edge control surface instability discussed previously. Control law C demonstrated a 30-percent increase in dynamic pressure (no flutter encountered).

The effective operation of the flutter-suppression system is shown by the oscillograph trace of model response presented in figure 6. A typical time history of a bending strain gage with time increasing from left to right is shown in the figure. Open-loop flutter is shown on the left side, and closed-loop operation is shown on the

right side. Note the increase in oscillatory amplitude until flutter onset is observed. After about 4 seconds, (indicated by the dashed line) the flutter-suppression system (closed-loop) was turned on; its effect is seen almost immediately and the oscillatory motion was damped rapidly.

Comparison of analytical and experimental results.- A comparison of the calculated results for the three control laws with the aforementioned experimental results is presented in figure 7. The results are presented in terms of percent increase in dynamic pressure above the open-loop flutter dynamic pressure at a Mach number of 0.90. For control law A the calculated increase in flutter dynamic pressure shows very good agreement with the measured increase of 12.5 percent. For control law B the calculations predicted a 24-percent increase in flutter dynamic pressure as compared with a measured no-flutter increase of 22 percent. For control law C the calculations predicted a 34-percent increase in flutter dynamic pressure as compared with a measured no-flutter increase of 30 percent.

B-52 CCV MODEL STUDY

The objectives of the B-52 model wind-tunnel tests were to demonstrate the effectiveness of a flutter mode control (FMC) system and a ride quality control (RQC) system, and to obtain data for correlation with analysis and flight results. Some results from the B-52 model study are presented in references 3, 10 and 11. A photograph of the complete free-flying model mounted on the two-cable suspension system in the TDT is presented in figure 8. The flutter mode control portion of the model program was conducted by the NASA Langley Research Center in cooperation with the Air Force Flight Dynamics Laboratory with contractual support supplied by The Boeing Company, Wichita Division. The design of the model systems was based on the corresponding CCV aircraft systems. The B-52 CCV airplane program is discussed in references 12-14. The FMC system used actively controlled flaperons and outboard ailerons. A pair of fuselage-mounted horizontal canard surfaces (see fig. 8) were used for the RQC system. The locations of the control surfaces are also shown in figure 9. The feedback loops for both systems were implemented on an analog computer. The model control surfaces were actuated by using an electromechanical system.

Design and Construction

Scaling.- The B-52 model was a 1/30-size dynamically scaled aeroelastic model of the B-52 CCV airplane. The model weighed about 26 kg (57.75 lb) and had a wing span of 1.88 m (6.16 ft). The model was designed to match the dynamic similitude parameters of reduced wavelength (frequency), mass ratio, and Froude number. Some of the scaling relationships and corresponding model/airplane flight conditions are presented in figure 10. Because the airplane flight conditions were at relatively low Mach numbers where compressibility effects were small, it was not considered necessary to match the Mach number between the airplane and the model.

Construction.- The construction technique used for the B-52 model was one that has been used successfully for a number of years in building aeroelastic models. Some details of the model construction are shown in figure 11. Aluminum alloy spars and beams were used to provide the basic stiffness of the wings and fuselage, respectively. Segmented pods constructed of wood frames covered with thin plastic sheets were attached to the spars and beams to provide the proper aerodynamic contour. The empennage was not elastically scaled; but did have the proper total weight and center-of-gravity location. The engine nacelles were rigid streamlined bodies that had the proper inertia properties and were attached to the wing spars by flexible beams which simulated the pylon stiffnesses.

Mounting System.- The B-52 model was mounted in the wind tunnel by using a modified version of the two-cable suspension system described in reference 15. This mount system provided freedom for the model to translate laterally and vertically and to rotate about the pitch, roll, and yaw axes. The model was essentially flown in the tunnel test section on the mount system by a pilot located in the tunnel control room. Because the two-cable system introduces some spring restraints to the model that do not exist in free flight, the short-period mode is affected, and an additional rigid body mode (primarily a vertical translational mode) is added. In designing the B-52 model mount system, particular attention was given to properly simulating the airplane short-period mode and keeping the rigid body translational mode frequency as low as possible.

Active Control Systems

Active controlled outboard ailerons and flaperons were used for the FMC system. A pair of horizontal canards were used for the RQC system. The actuation systems for all of these surfaces were of the electromechanical type as opposed to the electrohydraulic system used on the airplane. The control surfaces were actuated by electric torque motors mounted in the model fuselage. The motors were mechanically connected to the control surfaces through a rather complex mechanism of linkages. The complexity of the system can be seen by examining the photograph shown in figure 11. A more detailed description of the actuation system is presented in reference 16. The control laws were

implemented on an analog computer located in the tunnel control room. Each control law was wired to a separate removable patch panel.

FMC System.- The design of the FMC system was based on the results of previous experience and analyses of the B-52 airplane. These results indicated that stabilizing aerodynamic forces were produced when the incremental lift generated by the control surfaces lagged the wing displacement by 90° over the entire flutter oscillation cycle. Thus, the FMC feedback system was designed to produce the required phase lag between lift and displacement at the flutter frequency. The airplane FMC system is described in reference 13. A simplified block diagram of the model FMC system is presented in fig. 12. The FMC system was redundant because there were two independent feedback loops. The first loop used the outboard ailerons as the active aerodynamic surfaces. Accelerometer signals from both the left and right wings were averaged and passed through a shaping filter to generate the aileron feedback command signal which was routed to a single actuator that drove both ailerons. The flaperon loop was similar to the aileron loop except that each flaperon had its own actuator. In concept, the model and B-52 CCV airplane systems were the same, the only difference was in the actuator dynamic characteristics. That is, a comparison of the two transfer functions would show a difference. However, over the frequency range of interest, the two actuators had similar dynamic characteristics. Note that a provision was made at summing junctions (see upper left of fig. 12) for introducing external command signals to the actuators. The external command signals were used to drive the control surfaces for model excitation. The command signals could be used when the FMC system was either operating (closed-loop) or not operating (open-loop).

RQC System.- The RQC system was designed to provide about a 30-percent reduction in the RMS vertical acceleration level at the pilot's station. A simplified block diagram of the RQC system is presented in fig. 13. Pilot station acceleration signals were fed back through a shaping filter to produce the required canard command signals. In the RQC system it was necessary to add compensation to account for the differences in dynamic characteristics between the model and airplane actuators. The design of the model RQC system is described in ref. 17.

B-52 Results

FMC system.- The primary objectives of the model FMC system studies were to establish the open-loop (FMC off) flutter velocity, to demonstrate the effectiveness of the closed-loop system (FMC on), and to obtain data for correlation with model analysis and the full-scale flight test program.

During the FMC studies the open-loop flutter velocity was determined, and both open- and closed-loop subcritical response measurements were made above and below the open-loop flutter velocity respectively. Several experimental techniques were used for determining the subcritical response characteristics. In general, the most useful results were from the forced response Co-Quad technique (ref. 18). Representative measurements of the in-phase and out-of-phase components of the wing acceleration $\ddot{Z}_{WBL\ 78.3}$ to aileron command displacement $\delta_{a,c}$ as a function of frequency are shown in fig. 14. These results were measured at a test point approximately 6 percent in velocity below the measured open-loop flutter point. The curves to the left on this figure are the frequency response of the open-loop system; the curves to the right represent the closed-loop response. The effectiveness of the FMC in reducing the forced response of the system is readily apparent by comparing the resonant response peaks of the open- and closed-loop systems.

The Randomdec technique (ref. 19) worked best as the flutter speed was closely approached and the damping in the flutter mode became very small. It was especially useful here because it was considered hazardous to apply external excitation. A typical response time history trace for the right wing accelerometer $\ddot{Z}_{WBL\ 47.8}$, and the associated Randomdec signature, taken approximately 3 percent in velocity below the flutter point, is shown in fig. 15.

A comparison of calculated and measured flutter mode damping versus airspeed for the model is presented in fig. 16. The measured values were obtained from the forced response technique while the calculated values were obtained from the characteristic roots of the equations of motion. The comparison shows the analysis to be conservative by about 10 percent in predicting the open-loop flutter velocity (damping = 0). This difference may be attributed in part to the fact that the measured structural damping of the model was somewhat higher than the damping used in the flutter analysis. Both experimental and analytical results show that the FMC system provides a substantial increase in damping near the open-loop flutter velocity. The measured closed-loop data show the system to be significantly less effective than analytically predicted. This difference is believed to be due to hysteresis in the outboard aileron actuator system combined with a reduced effectiveness of the control surfaces that was not accounted for in the analysis. The maximum velocity tested with the closed-loop system was 48.3 m/sec (158 ft/sec); however, no damping values were measured above 47.2 m/sec (155 ft/sec) (indicated by a dashed line in fig. 16).

A comparison of measured flutter mode damping versus airspeed for the model and full-scale airplane is shown in fig. 17 in terms of airplane velocity. The airplane damping values were obtained from transient response records. As indicated in this figure the model open-loop flutter speed is about 7.9 percent higher than the airplane

flutter speed. This difference is attributed to minor variations in model mass and stiffness from the required values combined with some cable-mount effects on the rigid body dynamics of the model. The calculated airplane flutter speed was about 8.3 percent below the measured point. Thus a consistency does exist between measured and calculated flutter velocities for both the model and airplane in that the analysis was conservative in both cases by about the same amount. The data in fig. 17 show that the model and airplane have the same closed-loop damping trends. In both cases the closed-loop system significantly increases the damping near the open-loop flutter velocity. Although some differences in damping level do exist, it is felt that the correlation between model and airplane was good.

RQC System.- The objectives of the RQC studies were to demonstrate the effectiveness of a ride control system in reducing the acceleration at the pilot's station due to atmospheric turbulence and to obtain data for correlation with analysis and full-scale flight. Part of the RQC tests were accomplished by using an airstream oscillator system to provide a symmetric sinusoidal gust input to the model. The oscillating vane system consists of a set of vanes in a biplane arrangement installed on each side wall in the entrance cone to the tunnel test section. The vane system is shown in fig. 18. The vanes are sinusoidally oscillated (either symmetrically or antisymmetrically) through mechanical linkages by a hydraulic motor and flywheel arrangement. A vertical velocity component is induced in the flow in the center portion of the test section by the trailing vortices from the vane tips. The installation and early use of the vane system is described in ref. 20. During the RQC studies the open-loop (RQC off) and closed-loop (RQC on) response of the model to external excitation was measured. The first series of tests that were performed involved measuring the response of the model to a sinusoidal gust field generated by the oscillating vanes. Sample results obtained from the in-phase and out-of-phase components of the pilot station acceleration $\ddot{z}_{nose}$ as a function of vane frequency are presented in fig. 19. The curves to the left are the open-loop response; the curves to the right, the closed-loop response. Attenuation of the closed-loop response around 2 Hz is apparent. However, the response in the 13 Hz mode is so low that the effect of the ride control system is not obvious. This is because the effectiveness of the oscillating vanes in generating the gust field falls off rapidly at the higher values of frequency. The canard surfaces were used to generate the excitation for the higher modes. The results shown in fig. 20 are at the same test condition, but obtained from a canard frequency sweep. The canard amplitude was ±2°. The data are presented for both the open- and closed-loop system in terms of the ratio of pilot station acceleration Z_{nose} to canard command signal $\delta_{c,c}$ as a function of canard frequency. The effect of the RQC system on the higher modes is now evident. It appears that some combination of testing techniques is required to accurately define the system response curves.

C-5A ALDCS MODEL STUDY

To reduce wing fatigue damage and thereby prolong the service life of the C-5A fleet, the U.S. Air Force contracted with the Lockheed-Georgia Company to develop and flight test a C-5A airplane with an active lift distribution control system (ALDCS). This system was designed to reduce the incremental inboard-wing stresses experienced during gusts and flight maneuver. The ALDCS uses existing controls on the airplane - ailerons to unload the wing tips and elevators to keep the airplane in trim. Specific design goals for the ALDCS were to reduce the symmetric flight incremental wing root bending moment by at least 30 percent while limiting any increase in torsional moment to less than 5 percent. Information concerning the C-5A ALDCS program is presented in refs. 21 through 26.

A wind-tunnel study of a dynamically scaled aeroelastic model equipped with the proposed ALDCS was undertaken to establish the following: (1) Determine the ALDCS effectiveness; (2) investigate the adverse coupling of structural modes due to the ALDCS, particularly wing flutter; and (3) obtain experimental data for correlation with analysis and to guide flight tests. A photograph of the 1/22-size model used in the study is presented in fig. 21. The model program study was a joint effort of the Air Force, the Lockheed-Georgia Company, and the NASA Langley Research Center. The model study was performed concurrently with the development of the airplane ALDCS and was completed within a 9-month period prior to the beginning of airplane flight tests. Basically, the model program involved the modification of an existing 1/22-size flutter model to match Froude number scaling, the incorporation of the ALDCS in the model, and wind-tunnel tests in the TDT. Some unique features of the C-5A model study were that it was the first scaled model of a lift distribution control system, and the model had an onboard hydraulic system for driving the actuators.

Model

Scaling.- Although a 1/22-size flutter model of the complete C-5A airplane was available from earlier flutter clearance studies in the TDT, the decision was made to modify the model to match airplane Froude number. This allowed a closer simulation of the aerodynamic loading and dynamic characteristics of the airplane, thus, a better evaluation of the ALDCS could be made. For a Froude number scaled model, the mass ratio and reduced wavelength are also matched at the selected design test conditions. The model scaling factors were derived so that Froude number was matched for the model at a Mach number of 0.263 and a dynamic pressure 2.394 kN/m^2 (50 lb/ft^2) in the wind

tunnel. The corresponding airplane flight conditions were a Mach number of 0.58 and a dynamic pressure of 19.87 kN/m^2 (415 lb/ft^2) which corresponded to an altitude of 1524 m (5000 ft). It was assumed that at these relatively low subsonic Mach numbers the compressibility effects were not important and that there would not be any significant differences between the aerodynamic characteristics of the model and the airplane.

Design and construction.- The C-5A ALDCS model was designed to scale two airplane mass configurations - wing fuel loadings of 0 and 33 percent with approximately 113,400 kg (250,000 lb) of cargo for both cases. The 1/22-size model had a wing span of 3.037 m (9.96 ft). The 0-percent fuel configuration weighed 65.1 kg (143.5 lb), and the 33-percent fuel configuration weighed 77.2 kg (170.2 lb). To minimize costs, components of an existing flutter model were used as much as possible for the ALDCS model. A spar and segmented pod type of construction was used. Some of the construction details are shown in figs. 22 and 23. The ALDCS model required close simulation of the wing properties. Therefore, new wing spars, engine-pylon spars, and fuselage spars were constructed. Some new wing and fuselage pods were also constructed. The existing flutter model empennage was used in the ALDCS model; consequently, the empennage stiffness was not properly scaled. In reworking the empennage to incorporate the horizontal tail active control mechanism, an attempt was made to simulate the required scaled mass properties of the overall empennage; however, the final empennage was considerably under weight. The ailerons were scaled and consisted of a metal spar covered with balsa wood which was faired to give the proper scaled aerodynamic shape. The aileron-wing gap was not sealed on the model, although the gap was kept as small as practical.

With the exception of the empennage, the model simulated the mass and stiffness of the airplane quite well, including the important wing structural frequencies and mode shapes. It was concluded that the model adequately represented the airplane for the purposes of the ALDCS study.

Control systems.- The aerodynamic surfaces used for active controls on the C-5A airplane consisted of the ailerons and the elevators. However, for practical model design considerations, the all-movable horizontal tail was used to provide active pitch control instead of the elevators. An appropriate compensation was made in the control law to account for this difference. All active control surfaces on the model were actuated by an onboard hydraulic system. The aileron actuators were of the same design as those used for the delta-wing research model described previously. The aileron also could be remotely controlled (by the model pilot) to permit static roll trim control.

Mounting system.- The free-flying mount system used for the C-5A model was essentially the same as that previously described for the B-52 model.

In the static aerodynamic studies, the simulated lift device shown in figure 24 was employed. Briefly, this device consisted of a single cable attached to the fuselage at the model center of gravity which would exert a down force to the model as needed. This was accomplished by attaching the cable to a piston essentially floating in an air cylinder which was located in the plenum outside of the test section. By varying the pressure on the top side of the piston, a down load could be transmitted to the model. In operation, as the model angle of attack was varied, the air pressure to the cylinder was adjusted to compensate for the additional model lift and to maintain the model at its normal flying position near the center of the tunnel. By measuring the tension in the cable, the additional lift on the model could be determined.

Control Law

A simplified diagram of the active control systems used in the C-5A ALDCS model is presented in figure 25. There were two active control systems operating on the model, the basic aircraft pitch stability augmentation system (pitch SAS) and the ALDCS. Both commanded symmetric actuation of the control surfaces. The pitch SAS employed a feedback from the pitch rate gyro at the fuselage center of gravity to actuate the horizontal tail. The ALDCS employed feedbacks from both the pitch rate gyro and the fuselage center-of-gravity accelerometer to actuate the horizontal tail and feedbacks from the wing tip accelerometers to actuate the ailerons. Note that the acceleration signals from the two wings were summed to filter out unsymmetrical motions. The capability of supplying external command signals to the control surfaces was included. The gains K_{STAB}, K_{AIL}, and K_{SAS} were manually set according to a predetermined Mach number/dynamic pressure schedule.

Results

The major objectives of the C-5A ALDCS model study were successfully accomplished. The model and the active control systems appeared reasonably representative of the airplane, and the model ALDCS achieved its design goal in reducing wing dynamic bending moment. However, because the model suspension system significantly distorted the rigid body modes, the effect of the ALDCS on these modes was not determined. The ALDCS effect on the model wing flutter characteristics appeared to be negligible, probably because the wing flutter mode was antisymmetric, whereas the ALDCS was designed to attenuate symmetric loads only. Some typical results are presented in figures 26 through 29.

The model appeared to simulate reasonably well the overall static aerodynamic characteristics of the airplane including wing load distribution. However, the ailerons were not as effective as those of the airplane. A given model aileron deflection produced less (ranging from about 15 to 35 percent less) of a load change than was produced on the airplane for the same deflection. Aileron gains of 1.6 times nominal were therefore included in the test parameters. The dynamic effects on the model loads due to the control surface oscillations compared favorably with analysis.

The ALDCS effectiveness was best established from the aileron frequency sweeps. The aileron sweeps excited higher frequency modes better than either the stabilizer sweeps or the sinusoidal gust sweeps. The response of the model wing to a typical aileron sweep at the scaled flight condition is shown in figure 26. For these sweeps, the model scaled the 33-percent wing fuel configuration, the aileron amplitude was set for ±5°, the ALDCS was at nominal aileron gain, and the pitch SAS was on. The normalized wing bending moment at the wing root station is shown on the left plot; the normalized wing torsional moment is shown on the right. The frequency of the wing first bending mode was about 4 Hz and the torsional mode had a frequency of about 11 Hz. It can be seen that the major effect of the ALDCS is to reduce the incremental bending moments by about 50 percent at the 4 Hz mode; the incremental torsional moments were also reduced by the ALDCS. The distribution of the bending and torsional moments along the wing span is shown for the same conditions in figures 27 and 28. In figure 27 the bending moments pertain to the 4 Hz mode. The torsional moment in figure 28 is for the 11 Hz mode where the torsional moments are greatest. It can be seen that the load reduction experienced at the root is in nearly the same proportion over the entire span.

In the flutter tests, the 33-percent wing fuel configuration did not flutter within the scaled flight envelope. The 0-percent fuel configuration experienced antisymmetric wing flutter at the two points shown in figure 29. The data in this figure are presented in the form of airplane equivalent airspeed. In each instance, the ALDCS had no effect on the flutter. The model flutter occurred at a frequency of about 13 Hz and appeared to consist of a combined higher wing bending and torsional mode with most of the motion on the outboard portion of the wing. A similar type of wing flutter occurred during earlier flutter model tests.

DAST AEROELASTIC RESEARCH WING NUMBER ONE MODEL STUDY

The aeroelastic model used for this study was originally built to support the DAST (Drones for Aerodynamic and Structural Testing) flight program (ref. 4). The model is a dynamically scaled representation of a research wing that was tested on the drone flight vehicle. The model was scaled to flutter within the operational limits of the TDT. A photograph of the model in the wind tunnel is presented in figure 30. Model geometry along with the location of accelerometers is shown in figure 31. The model has an aspect ratio of 6.38 and a leading-edge sweep of 44.32 degrees.

Design and Construction

The model was of conventional spar and segmented pod construction. It was equipped with a hydraulically actuated trailing-edge control surface which was 20 percent of the local wing chord and was located between the 76.3 percent and 89.3 percent semispan stations. The control surface was driven by an electrohydraulic servo-actuator system which was similar to the system developed for the delta-wing model study. Maximum control surface displacement and rate were approximately ±14° and 820°/sec., respectively.

Flutter Suppression System

Two control laws were synthesized for the wind-tunnel model. The synthesis techniques used were the relaxed aerodynamic energy method and optimal control theory. The basic objective was to design control laws and to demonstrate experimentally their capability of providing at least a 44 percent increase in flutter dynamic pressure at Mach numbers from 0.6 to 0.9. In demonstrating the required increase in flutter dynamic pressure, flutter suppression systems must be capable of maintaining stability in the presence of turbulence. For wind tunnel tests, a concern is that the response of the control surface to tunnel turbulence must be within the limits of the actuator. In this study, calculated rms control surface deflection to tunnel turbulence was required to be less than 6° rms for dynamic pressures up to q_{max}. In addition, a minimum ±6 dB gain margin was required up to q_{max}.

Aerodynamic energy control law.- The relaxed aerodynamic energy method is described in ref. 27. It allows "free parameters" to be introduced into the synthesis procedure which tailors the control law to the specific problem. The form of the control law is

$$\delta_c(s) = \frac{a_1 s^2}{(s^2 + 2\zeta_1\omega_1 s + \omega_1^2)} + \frac{a_2 s^2}{(s^2 + 2\zeta_2\omega_2 s + \omega_2^2)} \frac{4h_{inbd}}{b_r} \qquad (2)$$

The control law used is referred to in ref. 27 as a localized damping-type transfer function. For this application, the constant term given in the reference 27 definition was deleted. With the free parameters, optimization procedures were used in the synthesis process to determine a control law that minimizes control surface response to turbulence while maintaining stability. Classical techniques were used to both adjust the parameters of the control law and determine additional compensation to achieve the ±6 db gain margins. The final form of the control law tested on the model was

$$\frac{\delta_a}{\ddot{h}_{inbd}} = \frac{\delta_a}{\delta_c} \quad \frac{s\,(s + 78)}{s + 10} \times \frac{151.92}{(s^2 + 2(1)\ 5.9s + 5.9^2)} \quad \frac{deg}{g} \tag{3}$$

where δ_a/δ_c is the actuator transfer function.

Optimal control theory control law.- The method used to synthesize the optimal control law is the one described in ref. 28. This method uses the results of a full-state feedback optimal control law to synthesize a feedback filter. The filter was synthesized by requiring the filtered open-loop frequency response to match that of the desired optimal open-loop frequency response over a finite frequency range. This matching was accomplished by employing a nonlinear programming algorithm to search for the coefficients of a feedback filter that minimizes the error between the optimal frequency response and the filtered frequency response. Detailed discussion of the synthesis results can be found in ref. 5. The final form of the control law tested on the model was

$$\frac{\delta_a}{\ddot{h}_{outbd}} = \frac{\delta_a}{\delta_c} \quad \frac{2214}{s + 10} \quad \frac{s}{s + 1} \times \frac{(s^2 + 2(.127)(121.21)\ s + 121.21^2)}{(s^2 + 2(.962)(297.62)\ s + 297.62^2)}$$

$$\times \frac{(s^2 + 2\ (.088)(269.14)\ s + 269.19^2)\ deg}{(s^2 + 2(.964)(294.91)\ s + 294.91^2)\ g} \tag{4}$$

Implementaton.- A simplified block diagram of the flutter suppression system is presented in figure 32. Both control laws were programmed on an analog computer. Acccelerometer output signals were processed by the analog computer and the control law used determined the appropriate actuator command signal. The command signal was then passed to the hydraulic servovalves which control the hydraulic fluid to the actuator.

Results and Discussion

Experimental flutter studies were conducted in the TDT at Mach numbers of 0.6, 0.7, 0.8, 0.9, and 0.95. System-off tests were performed at each Mach number to establish the basic wing flutter boundary. The system-off flutter characteristics are shown in figure 33. The system-off tests were followed by closed-loop tests with both control laws to evaluate their effect on raising the flutter dynamic pressure.

During closed-loop tests, unexpectedly large amplitude peak deflections of the control surface due to tunnel turbulence were encountered. Because of these peak deflections (which at times approached ±14°) the objective of experimentally demonstrating a 44 percent increase in flutter dynamic pressure from M = 0.6 to 0.9 could not be achieved. Tests at M = 0.95 were successful in demonstrating this increase because of a decrease in turbulence intensity.

A summary of the increases in dynamic pressure (above that for the system off tests) to which the model was tested is presented in figure 34. At M = 0.95 both control laws demonstrated a 44 percent increase in flutter dynamic pressure. At M = 0.9 increases of 33 percent and 27 percent were demonstrated by the optimal control law and the energy control law respectively before control surface saturation occurred. At saturation, the control surface was forced to one side against its mechanical stop and there was an overload of the analog computer amplifiers, thus, resulting in a violent instability. At M = .6 and .8 modest increases in dynamic pressure were demonstrated with both control laws. These tests were terminated when it was determined that the 44 percent increase could not be achieved with the available control authority.

The effectiveness of the flutter suppression system is illustrated by the oscillograph record of outboard wing acceleration presented in figure 35. (The record shown is for the energy control law but similar results were obtained with the optimal control law.) The model was being tested slightly above the system-off flutter boundary at approximately M = 0.95. The flutter suppression system was initially on, then it was turned off for about 4.5 seconds; and then turned on once again. When the flutter suppression system was turned off, the unstable oscillations built up rapidly. Turning the system on again eliminated the instability almost immediately.

Another illustration of flutter suppression performance is presented in figure 36. The spectrum of outboard peak accelerations for the wing with system off is compared to that for the two control laws. The model was being excited by tunnel turbulence. The data were measured at a dynamic pressure just below the system-off flutter boundary at

M = 0.9. The decrease in amplitude and shift in the maximum response frequency resulting from the control laws are evident.

WING-STORE ACTIVE FLUTTER SUPPRESSION

The varied missions of modern fighter/attack aircraft require the ability to carry many combinations of wing-mounted external stores. It is quite common that certain store combinations will cause reductions in flutter speeds, thus causing restrictions to be placed on the airplane operating envelope. Frequently, new store requirements are added after the airplane has become operational. The new store combinations may cause adverse effects on airplane flutter characteristics that cannot be corrected easily or economically by conventional methods. Because active flutter suppression appears to offer a means of maintaining satisfactory flutter characteristics for different store loadings, it has been the subject of considerable research. Two combined analytical and experimental studies of significance are the F-16 study (refs. 6, 29-31) and the YF-17 study (refs. 7, 32-34). Brief discussions, with highlight results from both of these studies, are presented in this section.

F-16 Study

The F-16 flutter model with an active flutter suppression system (FSS) was tested in the TDT in a joint USAF/NASA test. The model was designed and fabricated by General Dynamics-Ft. Worth. A photograph of the full span, cable-mounted model is shown in figure 37. The results of flutter tests on two store configurations, one having a symmetric flutter mode and one having an antisymmetric flutter mode, are shown in figures 38 and 39, respectively. Initially, the flutter boundary of the F-16 with stores and with FSS off were determined, and an appropriate control law was developed by General Dynamics engineers for each configuration.

A symmetric FSS was developed for the store configuration with the symmetric flutter mode. With this FSS engaged, the model was tested above the unaugmented flutter boundary. As shown by the data in figure 38, a 45-percent increase in dynamic pressure at Mach number 0.95 was demonstrated before flutter was encountered with the FSS operating.

Three significant achievements were demonstrated during tests of the antisymmetric flutter suppression system which was developed for the stores configuration with the antisymmetric flutter mode. First, with the FSS engaged, the model was tested at conditions well above the unaugmented flutter boundary without encountering flutter (see figure 39). While no attempt was made to determine a maximum increase in velocity or dynamic pressure obtainable, increases in dynamic pressure in excess of 100 percent at M = 0.8 were demonstrated. Second, the model was flown at the same test conditions above the flutter boundary with the control surface disabled on one wing, simulating a failed actuator. Although the damping was reduced, indicating that stability margins were less for this failed actuator case, the original control law was still effective in preventing flutter up to flight conditions tested for the fully effective actuator case. Third, frequency response methods were used to estimate FSS gain and phase margins for the basic system. These estimated margins were verified experimentally by changing the control law until flutter occurred. In general, the gain and phase margins exceeded the desired ±6 db gain margin and ±45 degrees phase margin.

YF-17 Study

The YF-17 is the most recently completed study in a series of NASA/Air Force cooperative research programs on wing/store active flutter suppression conducted in the TDT. The semi-span, Northrop-built YF-17 model mounted in the wind-tunnel is shown in figure 40. This model was mounted on a special suspension system that provided rigid body pitch and vertical translation degrees of freedom. In one series of tests, control laws that previously were implemented using an analog computer were implemented with a digital computer. This was done because on aircraft it is desirable to use the more versatile digital computer.

Data which were obtained at a constant Mach number are shown in figure 41. These data show how damping in the flutter mode decreased as dynamic pressure was increased for the cases of inactive flutter suppression system (open-loop) and closed-loop with the same control law implemented first by an analog computer and then by a digital computer. It can be seen that the digital data agree very well with the analog data and that in both cases the projected flutter dynamic pressure is about twice the value projected for the open-loop condition.

An additional achievement was the development of a method for capturing a tip missile when it was ejected from the model. In the photograph (figure 40) it can be seen that two steel cables were threaded through the tip missile--one at each end. Each cable was attached to the ceiling and floor of the test section. When the missile was ejected, it slid down the cables to shock absorbers which prevented the missile from striking the floor. This ejection/capture system was developed for use in studying the effectiveness of adaptive active control systems in suppressing flutter when the model

transitions from a stable configuration (with tip missile) to an unstable one (tip missile ejected).

The use of adaptive flutter suppression was demonstrated by ejecting a wing tip missile at a tunnel flow condition that was above the flutter boundary for the wing without the tip missile. The data shown in figure 42 are oscillograph records which show oscillations of the wing and control surface. Before the missile was ejected, neither the wing nor control surface was moving significantly. When the missile was ejected, the wing began to flutter. The digital computer first sensed that the wing oscillatory motion had become unstable (i.e. damping less than zero) then activated a control law and stabilized the motion, producing a no-flutter situation as indicated by the decayed oscillations of the wing bending response.

DC-10 DERIVATIVE WING STUDY

In order to accelerate energy efficiency technology in future commercial transports, NASA has sponsored an Aircraft Energy Efficiency Program (ACEE). As a participant in this program, the Douglas Aircraft Co. built and tested an aeroelastic model of a DC-10 derivative equipped with an active control system for flutter suppression (ref. 35). Cooperative studies were initiated to study alternate flutter suppression control laws to be tested on this model. The scope of this cooperative study was to apply control law design methods developed at NASA to the model and to test their performance in the wind tunnel. The objective was to design control laws that would be capable of demonstrating at least a 20% increase in flutter speed over that of the passive wing.

The aeroelastic model was representative of a wing which has a 4.27 m span increase over the standard DC-10 wing. A plan view drawing and photograph of the model installed in the Douglas Long Beach Low Speed Wind Tunnel is presentedin figure 43. The model was cantilevered from the tunnel wall and had an outboard aileron which was used as the active control surface.

Design and Construction

The model was of conventional spar and pod construction. The engine was represented by a flow thru nacelle which was attached to the wing spar with a beam that provided the nacelle-pylon with the desired degrees of freedom. The model was equipped with a trailing-edge control surface which was located between the 66.2 percent and 95.5 percent semi-span stations and was approximately 25 percent of the local wing chord. The control surface was driven by an electrohydraulic servo-actuator system which was quite similar in principle to the system developed for the delta-wing model study. Maximum control surface rotation was approximately ±15 degrees.

Flutter Suppression System

Two control laws, one patterned after the aerodynamic energy method (ref. 27) and the other after optimal control methods (ref. 5) were designed and implemented. For the sake of brevity only the results for the energy method (hereafter called control law #1) will be presented. Further details for both of these control laws are presented in reference 8.

Control Law #1.- The equation used during the design process was as follows:

$$\frac{\delta_a}{\ddot{Z}} = \left(\frac{\delta_c}{\ddot{Z}}\right) \times \left(\frac{\delta_a}{\delta_c}\right) \quad \frac{deg}{g} \tag{5}$$

where δ_a/δ_c is the actuator transfer function and the control law is defined by

$$\frac{\delta_c}{\ddot{Z}} = \frac{a}{(s^2 + 2\zeta_n\omega_n s + \omega_n^2)} \times \frac{s}{(s+5)} \tag{6}$$

and $s/(s+5)$ is a "washout filter" used to eliminate any static deflection of the control surface.

The design process, using the aerodynamic energy method, involved determining the values of a, ζ_n, and ω_n which minimized the control surface response to turbulence. Because a spectrum of turbulence for the wind tunnel during the flutter testing was not available, the design process was modified to determine the values of a, ζ_n, ω_n which provided the required increase in flutter velocity with acceptable gain and phase margins across the velocity range. Gain margins of ±6 db and phase margins of ±30 degrees were arbitrarily selected. The values of a, ζ_n, ω_n which satisfied these requirements were determined by trial and error. The following transfer function represents control law #1 that was implemented on the model:

$$\frac{\delta_c}{\ddot{z}} = \frac{8.449 \times 10^3}{(s^2 + 50s + 625)} \times \frac{s}{(s + 5)} \quad \frac{deg}{g} \tag{7}$$

Implementation.- A simplified block diagram of the active control system is presented in figure 44. Both control laws (shown in fig. 44) were programmed on an analog computer. A phase control filter of the form

$$K_p \frac{(1 - \tau s)}{(1 + \tau s)} \tag{8}$$

where

$K_p = 1$ for phase lag

$K_p = -1$ for phase lead

was included in the analog computer. By properly choosing the quantities τ and K_p, a phase lead or lag of known amount ϕ was introduced at a given frequency ω without changing the system gain.

Results and Discussion

Open-loop results.- A comparison of measured and predicted flutter mode damping is presented in figure 45. For analysis purposes the structure, the control surface actuator transfer function (for closed-loop analysis), and the unsteady aerodynamics are combined by approximating the variation in frequency of the unsteady aerodynamics with a rational polynomial in the variable s. A description of this analysis method is presented in reference 36. The damping at subcritical speeds was measured experimentally by determining the time to half amplitude of the response of the wing to a pulsed input. Estimates of subcritical damping and the flutter velocity are quite reasonable.

Closed-loop results.- Calculated flutter boundaries in terms of flutter velocity versus system gain for six values of phase are presented in figure 46. Three or four distinct flutter modes are exhibited, depending on phase angle. For all phase angles analyzed, a decrease in flutter speed is shown for mode 3 at low values of gain. At negative values of phase angle the reduction in flutter velocity is more pronounced. The velocity at which mode 8 goes unstable is nearly independent of system gain and phase. The mode 4 instability is aggravated by negative phase angles and stays relatively fixed for positive phase angles. At phase angles of +20 degrees and above a new flutter mode resulting from a coupling between the feedback filter mode and the first wing bending mode becomes critical. (It should be noted that the phase angles referred to in figure 46 correspond to equation 8 evaluated at ω = 78 rad/sec. The phase angles produced by the phase control filter at other frequencies is significantly different.)

Also presented in figure 46 is the experimental data measured during the test. A correction factor has been applied to the experimental data. It was stated in reference 35 that computed aileron forces were typically 40 percent higher (i.e. a factor of 1.4 greater) than measured quantities. When a correction factor was used to account for this difference, the response of the wing due to control surface motions was predicted with much better accuracy. Therefore, this correction factor was also used in the present analysis. Since system gain is directly proportional to control surface effectiveness, a correction factor of 0.714 (1/1.4) was used for the experimental data before comparing it to analytical data. With this correction factor applied to the experimental data, the comparison of experimental results and predictions are quite good as indicated by the following:

(1) The tendency of mode 3 to be destabilized below the passive flutter speed for all phase angles at low values of gain. This effect is more pronounced at negative phase angles;

(2) the tendency of phase lead to improve the mode 3 flutter characteristics at low velocities and to have the opposite effect at higher velocities;

(3) the existence of a mode 4 instability at ϕ = -10 degrees; and

(4) the existence of a coupled filter first wing bending mode at ϕ = +30 degrees.

From the data presented in figure 46, it can be shown that increases in flutter speed in excess of 25 percent were demonstrated at phase angles of 0°, +10°, +20°, and +30°.

CONCLUDING REMARKS

In this paper seven active control research studies have been described. All of these studies involved wind-tunnel model tests, and but for one exception, all of the tests were conducted in the NASA Langley TDT. Highlights of the experimental results

have been presented and discussed for each study. For most of the studies such topics as model design and construction, control law synthesis, control system implementation, test techniques, and experiment/analysis correlation have been discussed as well.

The seven model studies were a simple delta-wing active flutter suppression model, a 1/30-size dynamically scaled aeroelastic model of the B-52 CCV that was used to study active flutter suppression and ride quality control, a 1/22-dynamically scaled aeroelastic model of the C-5A aircraft that was used to study active load alleviation, a semi-span active flutter suppression model that was a dynamically scaled representation of the initial DAST (Drones for Aerodynamic and Structural Testing research wing), full span F-16 and semi-span YF-17 models that were used for active flutter suppression studies of wings with external stores, and finally a semi-span active flutter suppression model that was a dynamic representation of a DC-10 derivative wing. In all of these studies the active control systems were successfully implemented on the models and were effective in achieving the desired benefits. In general, the experimental results compared favorably with corresponding analytical results. Where flight data were available (e.g. B-52 CCV flutter suppression) there was good correlation between model and full-scale results. Experiences with these model studies have indicated that active control systems can be effective in alleviating unwanted aeroelastic response and that much useful data can be obtained from wind-tunnel model studies.

REFERENCES

1. Sandford, M. C.; Abel, I.; and Gray, D. L.: Development and Demonstration of a Flutter Suppression System Using Active Controls. NASA TR-450, December 1975.

2. Nissim, E.: Flutter Suppression Using Active Controls Based on the Concept of Aerodynamic Energy. NASA TN D-6199, 1971.

3. Redd, L. T.; Gilman, J. Jr.; Cooley, D. E.; and Sevart, F. D.: Wind Tunnel Investigation of a B-52 Model Flutter Suppression System. Journal of Aircraft, Vol. 11, No. 11, November 1974.

4. Murrow, H. N.; and Eckstrom, C. V.: Drones for Aerodynamic and Structural Testing (DAST)--A Status Report. J. Aircraft, Vol. 16, No. 8, August 1979, pp. 521-526.

5. Newsom, J. R.; Abel, I.; and Dunn, H. J.: Application of Two Design Methods for Active Flutter Suppression and Wind Tunnel Test Results. NASA TP-1653, May 1980.

6. Peloubet, R. P., Jr.; Haller, R. L.; and Bolding, R. M.: F-16 Flutter Suppression System Investigation. AIAA Paper No. 80-0768, May 1980.

7. Hwang, C.; Johnson, E. H.; and Pi, W. S.: Recent Developments of the YF-17 Active Flutter Suppression System. AIAA Paper No. 80-0769, May 1980.

8. Abel, Irving; Perry, Boyd III; and Newsom, Jerry R.: Comparison of Analytical and Wind-Tunnel Results for Flutter and Gust Response of a Transport Wing with Active Controls. NASA TP-2010, June 1982.

9. Bergmann, Gerald E.; and Sevart, Francis D.: Design and Evaluation of Miniature Control Surface Actuation Systems for Aeroelastic Models. J. Aircraft, Vol. 12, No. 3, March 1975, pp. 129-134.

10. Doggett, Robert V., Jr.; Abel, Irving; and Ruhlin, Charles L.: Some Experiences Using Wind-Tunnel Models in Active Control Studies. Proceedings of NASA Sponsored Symposium on Advanced Control Technology and Its Potential for Future Transport Aircraft, NASA TM X-3409, August 1976.

11. Thompson, G. O.; and Sevart, F. D.: Wind Tunnel Investigation of Control Configured Vehicle Systems. Presented at AGARD Structures and Materials Panel Specialists Meeting on Flutter Suppression and Structural Load Alleviation, Brussels, Belgium, April 15, 1975.

12. Johannes, R. P.; and Thompson, G. O.: B-52 Control Configured Vehicles Program, Advances in Control Systems. AGARD CP-137, 1973.

13. Hodges, Garold G.: Active Flutter Suppression - B-52 Controls Configured Vehicle. AIAA Preprint 73-322, March 1973.

14. Arnold, J. I.; and Murphy, F. B.: B-52 CCV Flight Test Results. Proceedings of NASA Sponsored Symposium on Advanced Control Technology and Its Potential for Future Transport Aircraft, NASA TM X-3409, August 1976.

15. Reed, Wilmer H. III; and Abbott, Frank T., Jr.: A New "Free-Flight" Mount System for High Speed Wind-Tunnel Flutter Models. Proceedings of Symposium on Aeroelastic and Dynamic Modeling Technology, RTD-TDR-63-4197, Part I, March 1964.

16. Severt, F. D.; Patel, S. M.; and Watlman, W. J.: Analysis and Testing of Stability Augmentation Systems. NASA CR-132349, 1973.

17. Sevart, Francis F.; and Patel, S.: Analysis and Testing of Aeroelastic Model Stability Augmentation Systems. NASA CR-132345, 1973.

18. Keller, Anton C.: Vector Component Techniques: A Modern Way to Measure Modes. Sound and Vibration, Vol. 3, No. 3, March 1969, pp. 18-26.

19. Cole, Henry A., Jr.: On-Line Failure Detection and Damping Measurement of Aerospace Structures by Random Decrement Signatures, NASA CR-2205, 1973.

20. Gilman, Jean, Jr.; and Bennett, Robert M.: A Wind-Tunnel Technique for Measuring Frequency-Response Functions for Gust Load Analysis. Journal of Aircraft, Vol. 3, No. 6, December 1966.

21. Disney, T. E.; and Eckholdt, D. C.: Historical Review of C-5A Lift Distribution Control Systems. Proceedings of NASA Sponsored Symposium on Advanced Control Technology and Its Potential for Future Transport Aircraft, NASA TM X-3409, July 1976.

22. Hargrove, W. J.: The C5A Active Lift Distribution Control System. Proceedings of NASA Sponsored Symposium on Advanced Control Technology and Its Potential for Future Transport Aircraft, NASA TM X-3409, August 1976.

23. Grosser, W. F.; Hollenbeck, W. W.; and Eckholdt, D. C.: The C5A Active Lift Distribution Control System. AGARD Joint FMP/GC Symposium--Impact of Active Control Technology on Airplane Design, Paper 24, Paris, France, October 1974.

24. Disney, T. E.: C5A Active Load Alleviation System. AIAA 1975 Aircraft and Systems Technology Meeting, Paper 75-991, August 4-7, 1975.

25. Disney, T. E.: C5A Active Load Alleviation System. Journal of Spacecraft and Rockets, Vol. 14, No. 2, February 1977.

26. Disney, T. E.: C5A Load Alleviation, Active Controls in Aircraft Design. AGARDograph No. 234, November 1978.

27. Nissim, E.: Recent Advances in Aerodynamic Energy Concept for Flutter Suppression and Gust Alleviation Using Active Controls. NASA TN D-8519, 1977.

28. Newsom, J. R.: A Method for Obtaining Practical Flutter Suppression Control Laws Using Results of Optimal Control Theory. NASA TP-1471, 1979.

29. Peloubet, R. P., Jr.; Haller, R. L.; and Bolding, R. M.: F-16 Flutter Suppression System Investigation Feasibility Study and Wind Tunnel Tests. AIAA Journal of Aircraft, February 1982.

30. Peloubet, R. P., Jr.; Haller, R. L.; and Bolding, R. M.: F-16 Active Flutter Suppression Program. DGLR International Symposium, Nuremberg, West Germany, October 1981.

31. Peloubet, R. P., Jr.; Haller, R. C.; and Bolding, R. M.: Recent Developments in the F-16 Flutter Suppression with Active Control Program. AIAA/ASME/ASCE/AHS 23rd Meeting, May 1983.

32. Hwang, C.; Winther, B. A.; Noll, T. E.; and Farmer, M. G.: Demonstration of Active Wing/Store Flutter Suppression System. AGARD R-668, July 1978.

33. Hwang, C.; Johnson, E. H.; Mills, G. R.; Noll, T. E.; and Farmer, M. G.: Wind Tunnel Test of a Fighter Aircraft Wing/Store Flutter Suppression System - An International Effort. AGARD R-689, August 1980.

34. Johnson, E. H.; Hwang, C.; Joshi, D. S.; Kesler, P. F.; and Harvey, C. A.: Test Demonstration of Digital Control of Wing/Store Flutter. AIAA CP 82-0645, May 1982.

35. Winther, B. A.; Shirley, W. A.; and Heimbaugh, R. M.: Wind Tunnel Investigation of Active Controls Technology Applied to a DC-10 Derivative. AIAA-80-0771, May 1980.

36. Abel, I.: An Analytical Technique for Predicting the Characteristics of a Flexible Wing Equipped with an Active Flutter Suppression System and Comparison with Wind-Tunnel Data. NASA TP-1367, 1979.

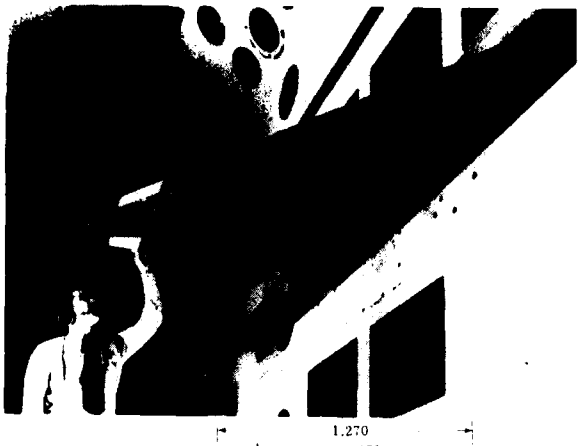

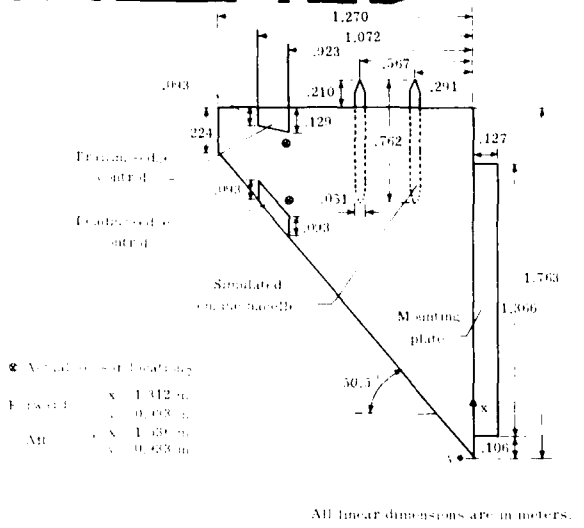

All linear dimensions are in meters.

Figure 1.- Delta-wing flutter-suppression model.

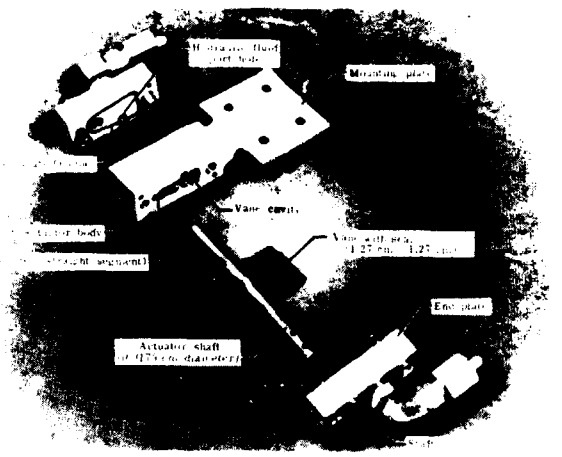

(b).- Actuator components.

Figure 2.- Miniaturized hydraulic actuator.

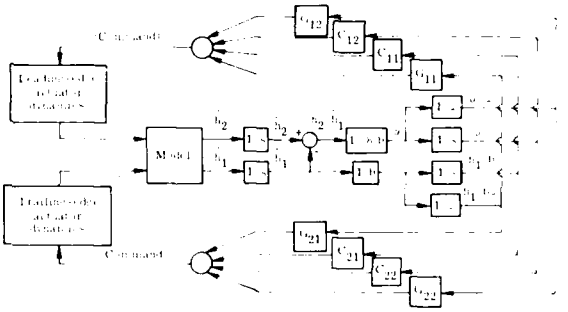

Figure 3.- Simplified block diagram of delta-wing flutter suppression system.

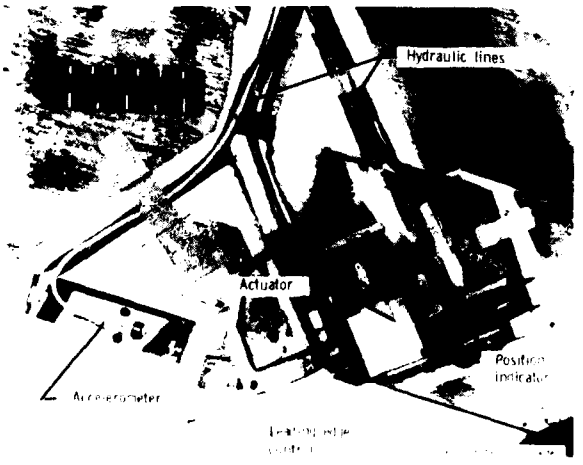

(a).- Installed in model.

CONTROL LAW A

$$\begin{Bmatrix} \beta \\ \delta \end{Bmatrix} = \begin{bmatrix} 0 & 5.6 \\ 0 & -1.4 \end{bmatrix} \begin{Bmatrix} h_1/b \\ \alpha \end{Bmatrix} + i \begin{bmatrix} 0 & 1.5 \\ 0.4 & 0.1 \end{bmatrix} \begin{Bmatrix} h_1/b \\ \alpha \end{Bmatrix}$$

CONTROL LAW B

$$\begin{Bmatrix} \beta \\ \delta \end{Bmatrix} = \begin{bmatrix} 0 & 0 \\ 2.7 & -5.3 \end{bmatrix} \begin{Bmatrix} h_1/b \\ \alpha \end{Bmatrix} + i \begin{bmatrix} 0 & 2.5 \\ 1.0 & 0.75 \end{bmatrix} \begin{Bmatrix} h_1/b \\ \alpha \end{Bmatrix}$$

CONTROL LAW C

$$\begin{Bmatrix} \beta \\ \delta \end{Bmatrix} = \begin{bmatrix} 0 & 0 \\ 2.7 & -5.3 \end{bmatrix} \begin{Bmatrix} h_1/b \\ \alpha \end{Bmatrix} + i \begin{bmatrix} 0 & 0 \\ 2.5 & 0.75 \end{bmatrix} \begin{Bmatrix} h_1/b \\ \alpha \end{Bmatrix}$$

Figure 4.- Values of [C] and [G] matrices tested on model.

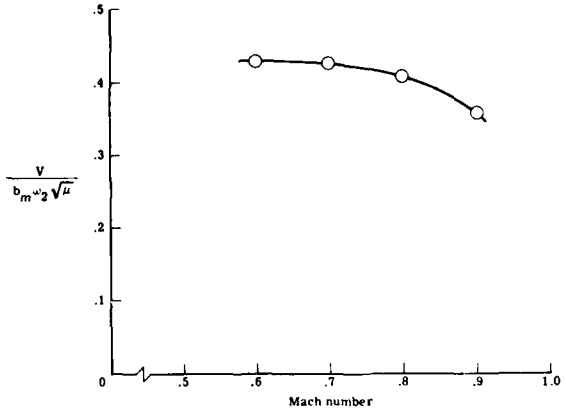

Figure 5.- Open-loop flutter characteristics of delta-wing model.

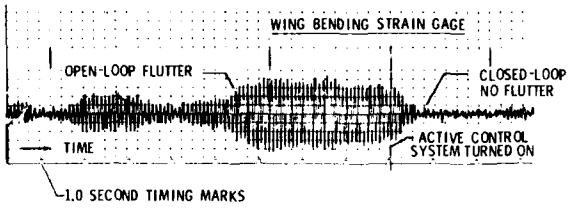

Figure 6.- Typical time history trace showing effective operation of delta-wing flutter-suppression system.

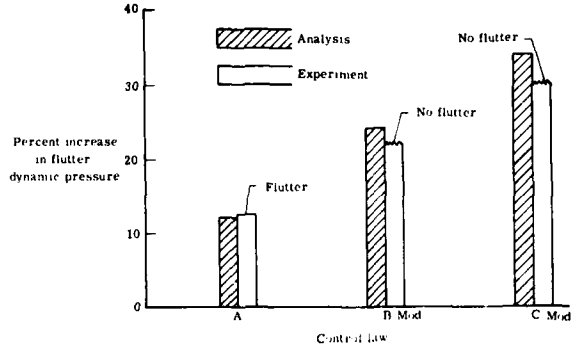

Figure 7.- Effect of different control laws on flutter dynamic pressure at M = 0.9.

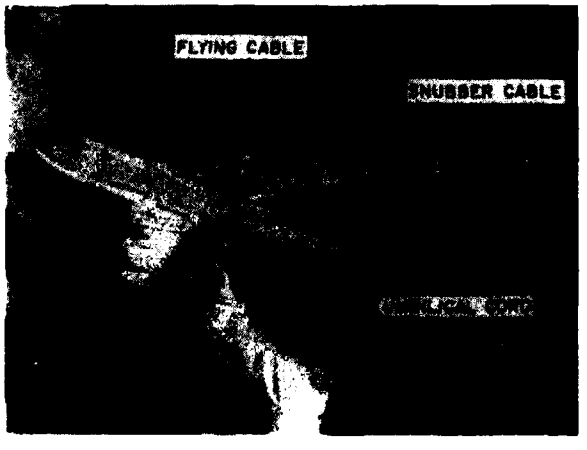

Figure 8.- B-52 Model in Transonic Dynamics Tunnel.

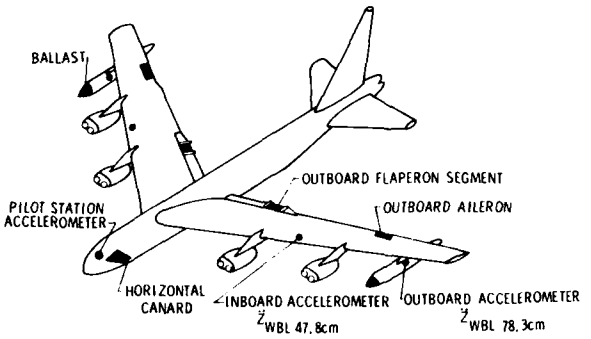

Figure 9.- B-52 control surface and sensor locations.

MATCHED DYNAMIC SIMULITUDE PARAMETERS

- FROUDE NUMBER, $\frac{\text{INERTIA FORCE}}{\text{GRAVITY FORCE}} \cdot \frac{V^2}{Lg}$
- REDUCED WAVELENGTH, $\frac{\text{FLUID VELOCITY}}{\text{VIBRATION VELOCITY}} \cdot \frac{V}{\omega L}$
- MASS RATIO, $\frac{\text{MASS OF BODY}}{\text{APPARENT MASS OF FLUID}} \cdot \frac{m}{\rho_f L^3}$

MODEL / AIRPLANE DESIGN CONDITIONS

	AIRPLANE	MODEL
GROSS WEIGHT	170 097 Kgm	25.67 Kgm
ALTITUDE	6 400 m (FMC) 1 646 m (RQC)	———
DENSITY	.631 Kg/m^3 (FMC) 1.041 Kg/m^3 (RQC)	2.572 Kg/m^3 4.123 Kg/m^3
MEDIUM	AIR	FREON (95%)

Figure 10.- B-52 model scaling parameters.

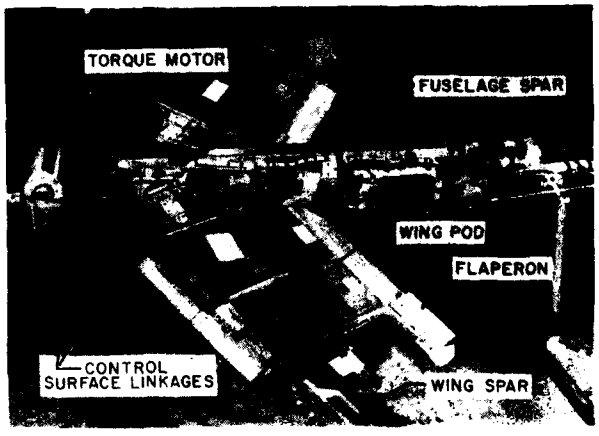

Figure 11.- B-52 model construction.

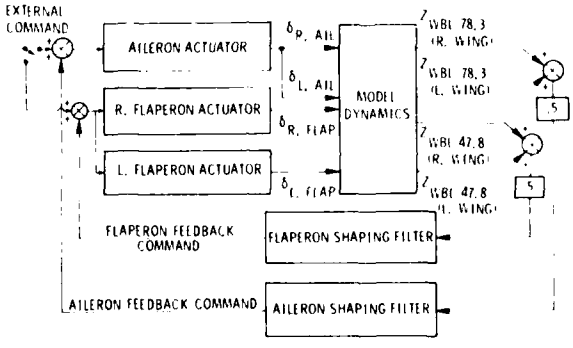

Figure 12.- Block diagram of FMC system.

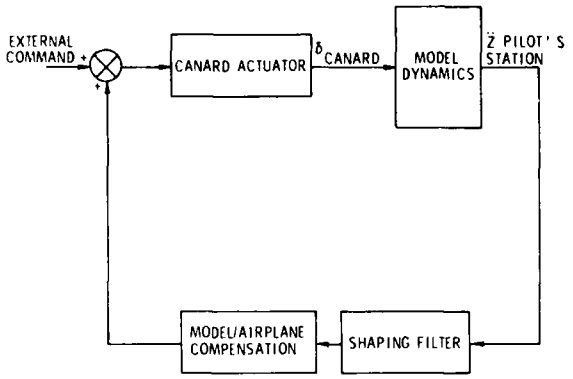

Figure 13.- Block diagram of RQC system.

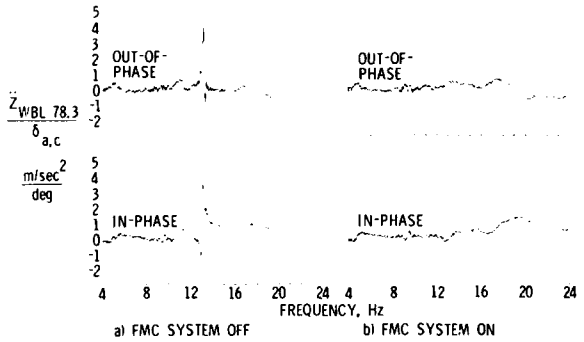

Figure 14.- Frequency response to aileron excitation.

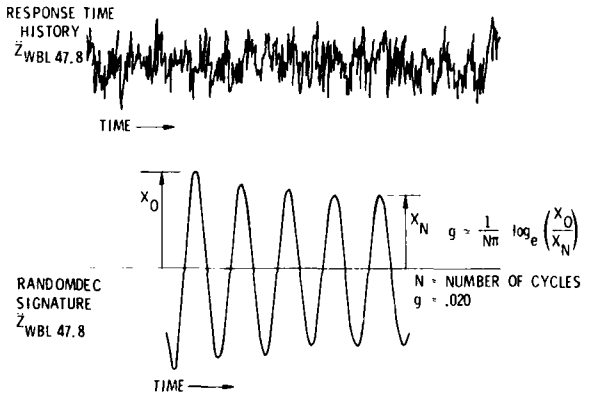

Figure 15.- Randomdec damping measurement.

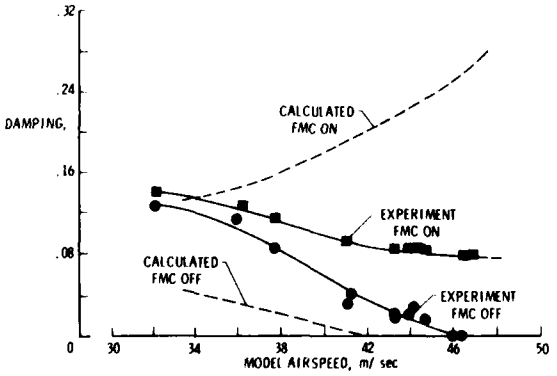

Figure 16.- Variation of B-52 model damping with airspeed.

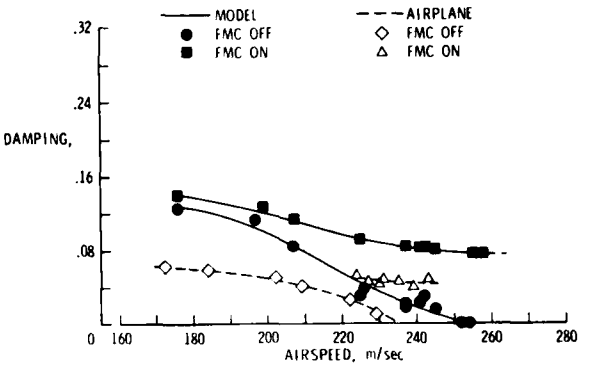

Figure 17.- Comparison of B-52 model and airplane damping.

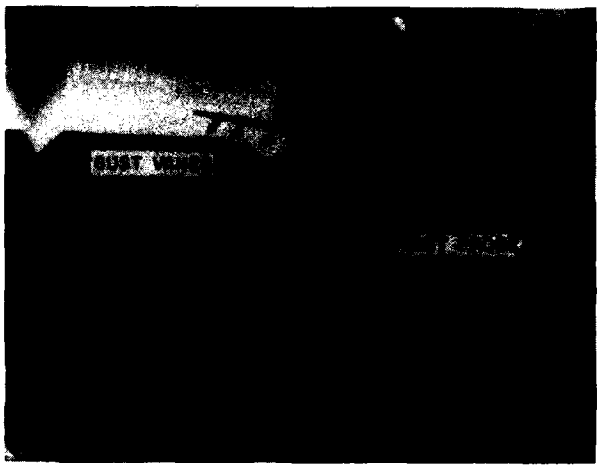

Figure 18.- B-52 model showing wind-tunnel gust vanes.

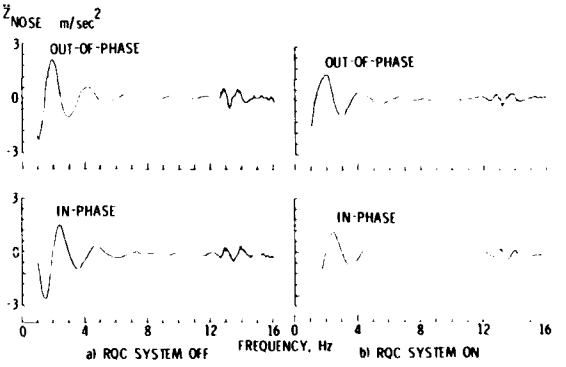

Figure 19.- Frequency response to gust vane excitation.

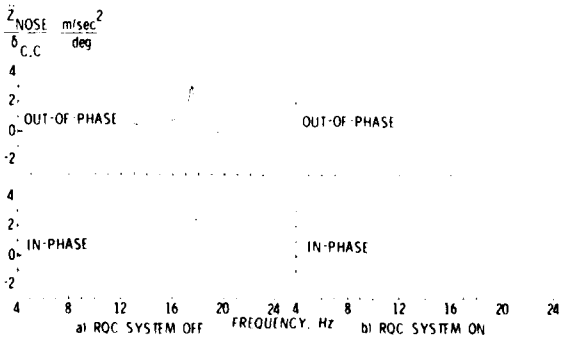

Figure 20.- Frequency response to canard excitation.

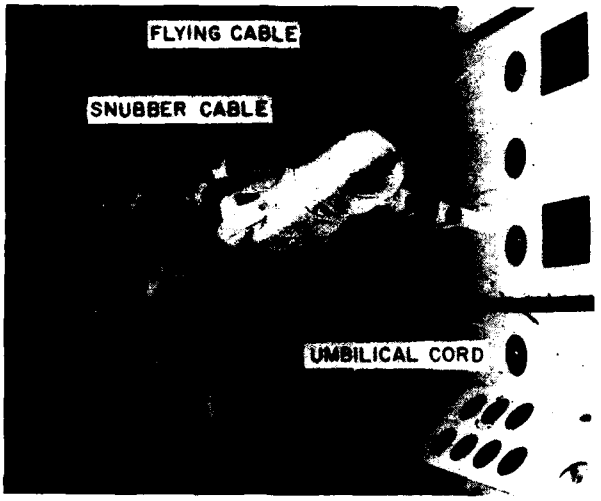

Figure 21.- C-5A model mounted in Transonic Dynamics Tunnel.

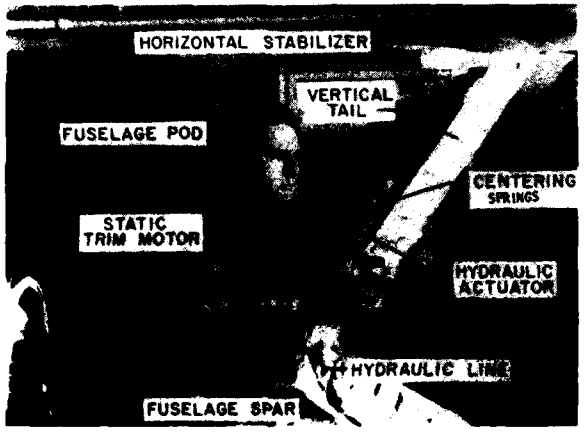

Figure 22.- Exposed view of rear portion of C-5A model fuselage.

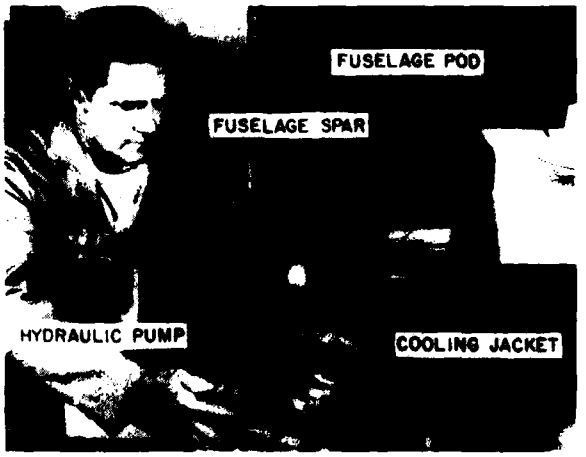

Figure 23.- Exposed view of forward portion of C-5A model fuselage.

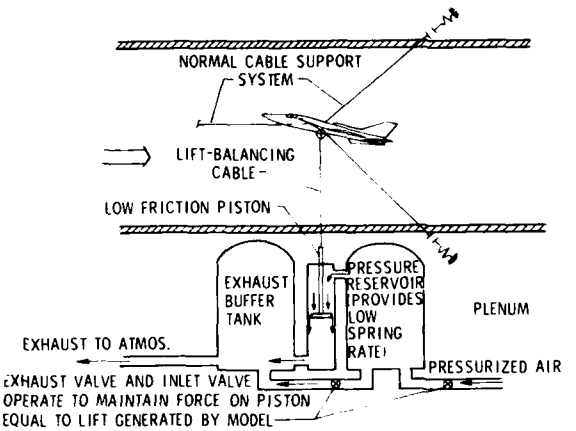

Figure 24.- Wind tunnel model lift control device.

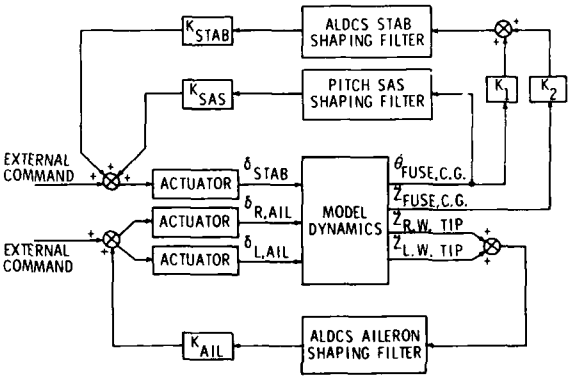

Figure 25.- Block diagram of ALDCS.

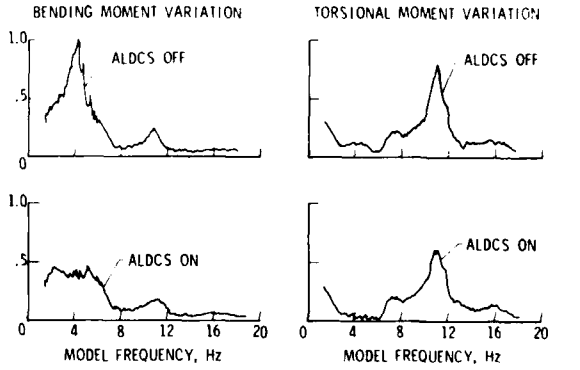

Figure 26.- Variation of normalized wing moments with aileron frequency.

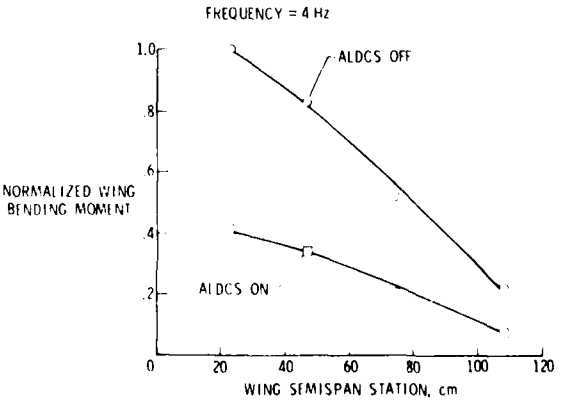

Figure 27.- Spanwise distribution of wing bending moment.

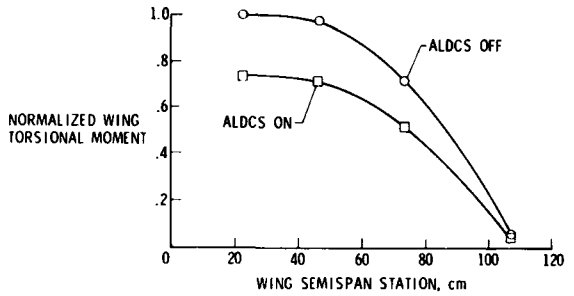

Figure 28.- Spanwise distribution of wing torsional moment.

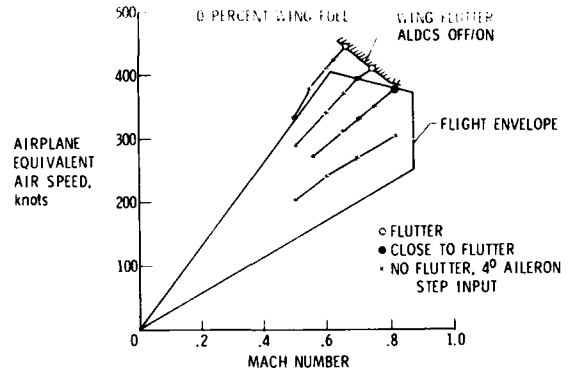

Figure 29.- Effect of ALDCS on C5-A model wing flutter.

Figure 30.- Flutter-suppression model in Langley Transonic Dynamics Tunnel.

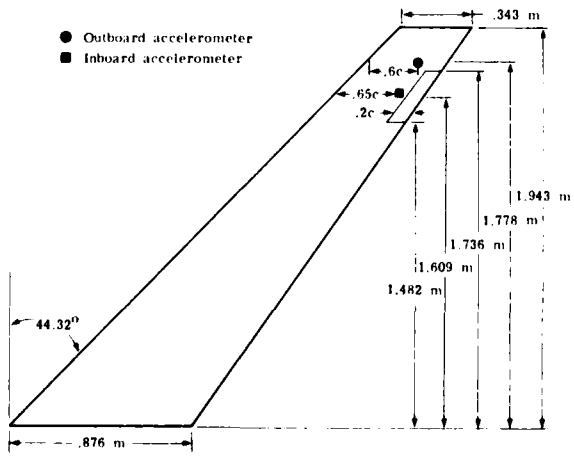

Figure 31.- Model geometry.

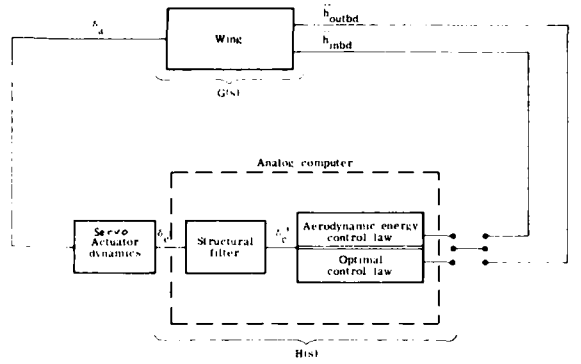

Figure 32.- Simplified block diagram of flutter-suppression system.

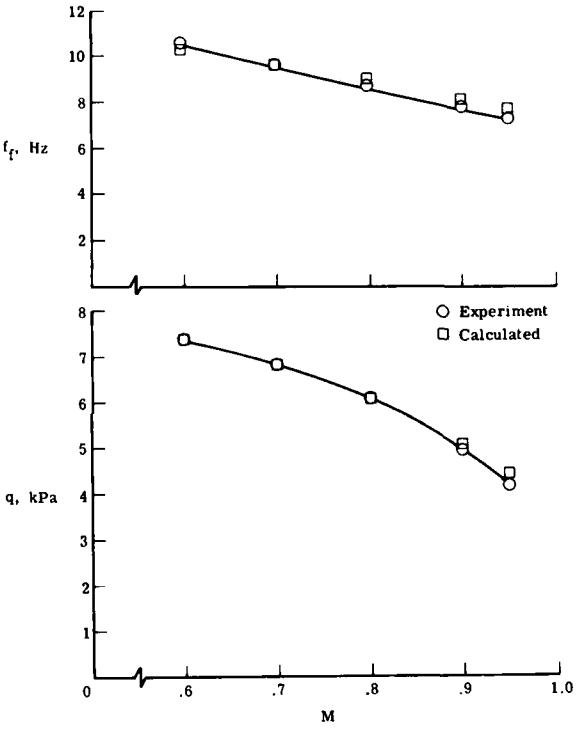

Figure 33.- Comparison of calculated and measured flutter characteristics (system off).

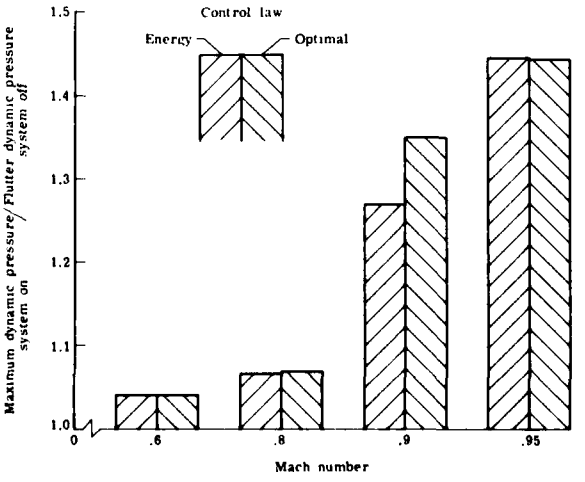

Figure 34.- Maximum dynamic pressures achieved during wind-tunnel tests.

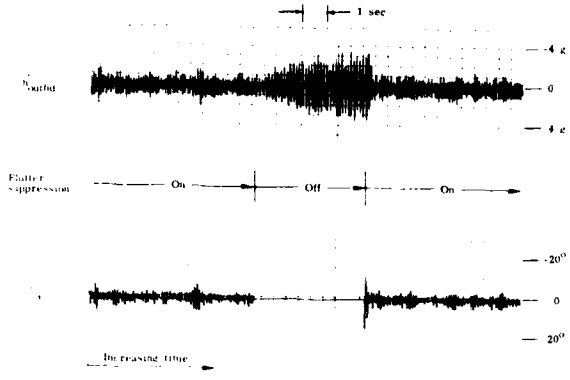

Figure 35.- Time history of acceleration at outboard accelerometer and control-surface deflecion.

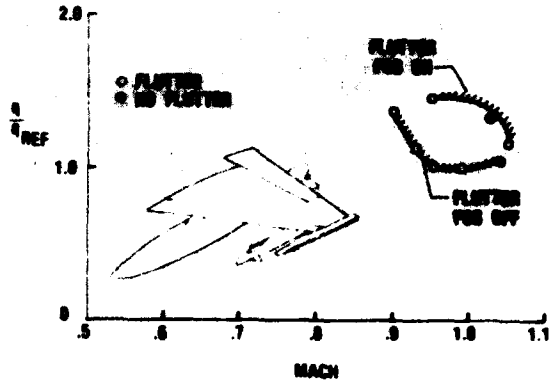

Figure 38.- F-16 symmetric normalized flutter dynamic pressure.

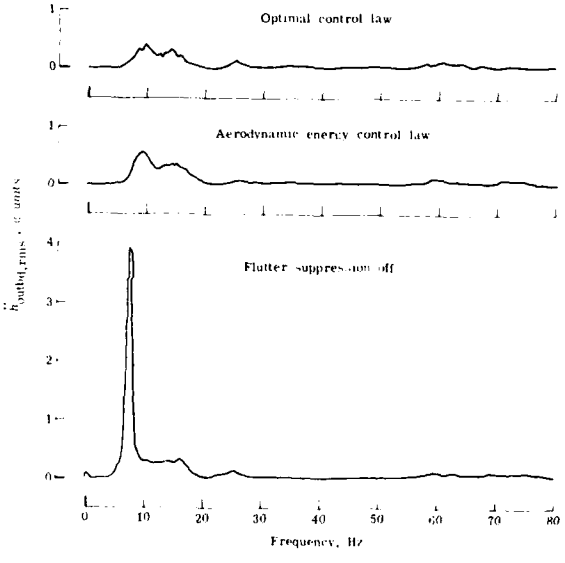

Figure 36.- Comparison of rms acceleration at outboard accelerometer with flutter-suppression system turned on and off. M = 0.9; q = 4.92 kPa.

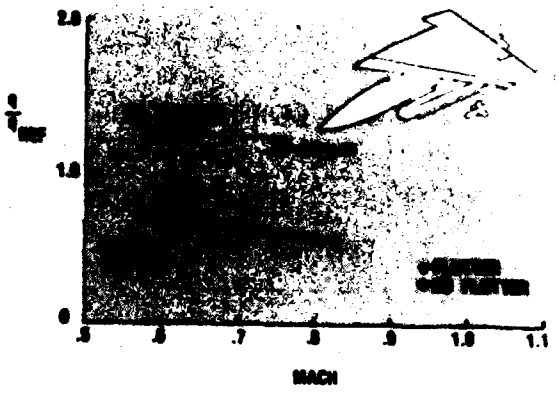

Figure 39.- F-16 antisymmetric normalized flutter dynamic pressure.

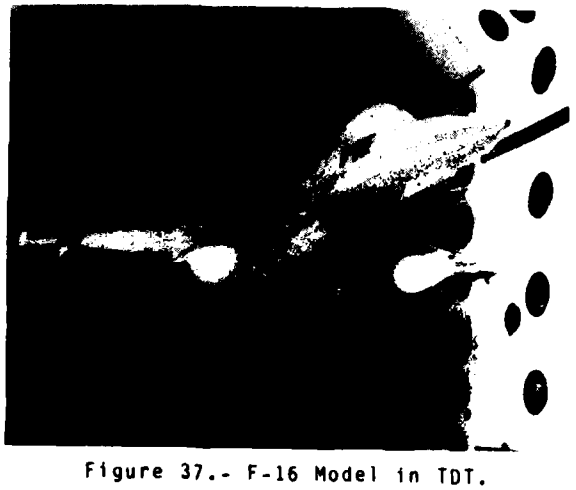

Figure 37.- F-16 Model in TDT.

Figure 40.- YF-17 Model in TDT.

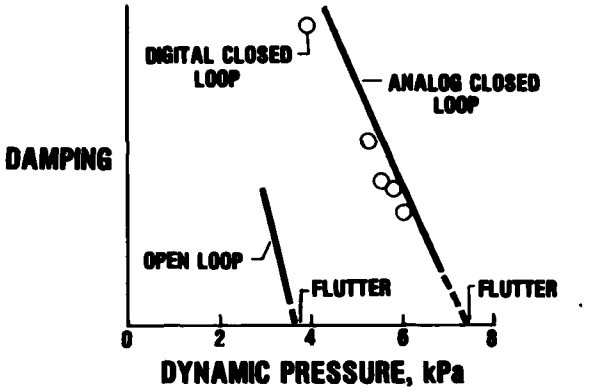

Figure 41.- YF-17 damping as a function of dynamic pressure.

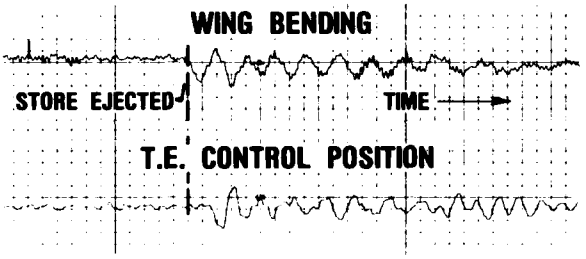

Figure 42.- Time history of wing bending moment and trailing edge control surface position during store ejection.

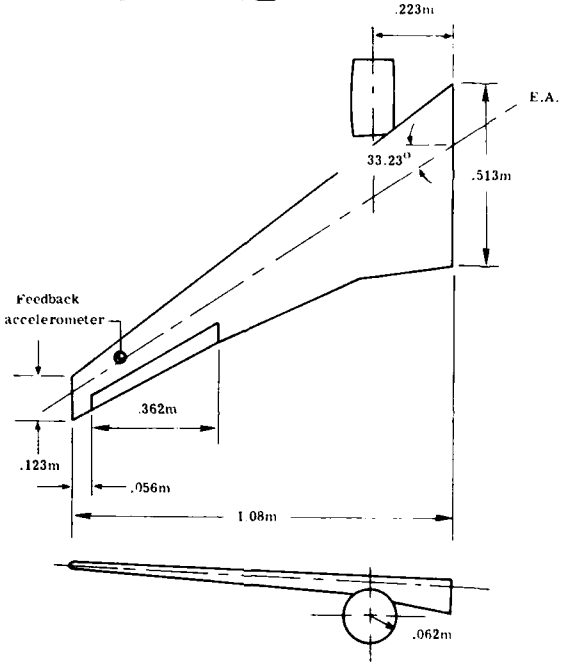

Figure 43.- DC-10 derivative aeroelastic wing.

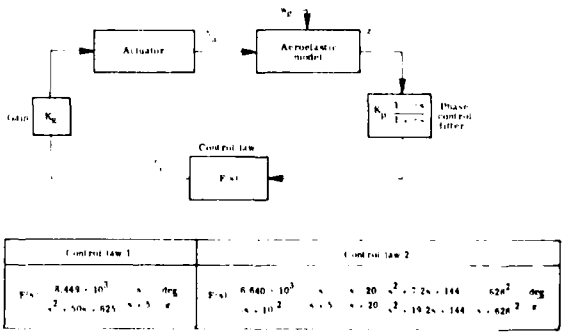

Figure 44.- Block diagram of active control system.

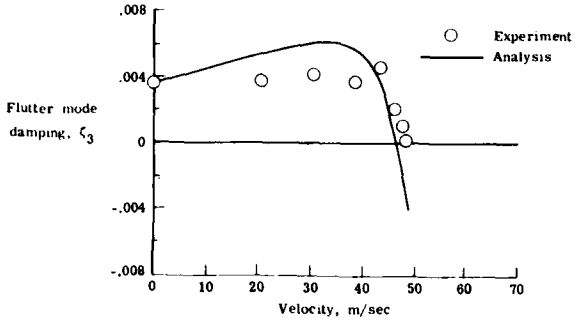

Figure 45.- Comparison of measured and predicted flutter mode damping for passive wing.

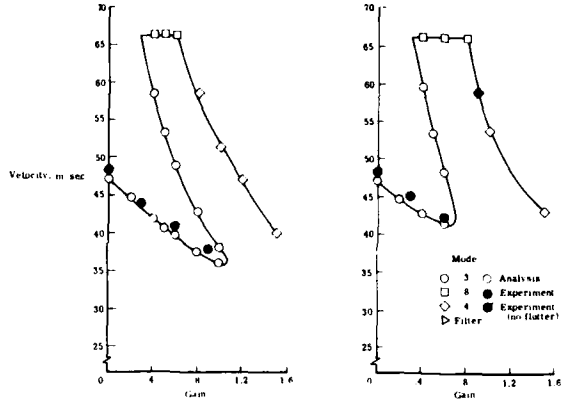

(c) ϕ = -20° (d) ϕ = -10°

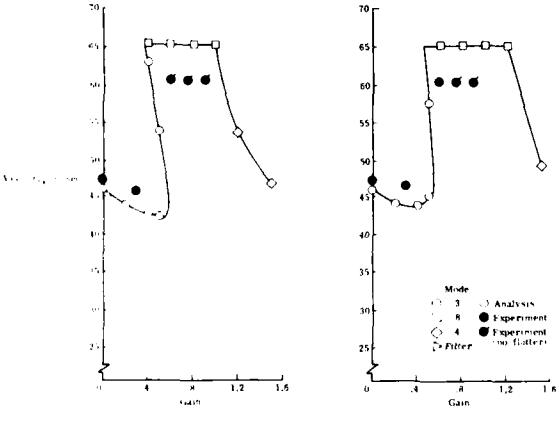

(a) ϕ = 0° (b) ϕ = 10°

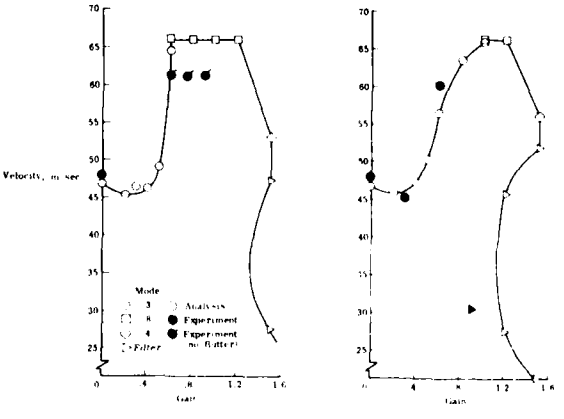

(e) ϕ = 20° (f) ϕ = 30°

Figure 46.- Measured and predicted flutter boundaries as function of gain and phase for control law 1.

CIVIL AVIONICS FLIGHT TESTING WITH THE RAE(B) BAC1-11

by

R R Newbery and P England

from reports and papers by staff of

Operational Systems Division, Flight Systems (Bedford) Department

Royal Aircraft Establishment, Bedford, UK

1 SCOPE OF THE PROGRAMME

RAE Flight Systems (Bedford) Department, in collaboration with British Industry and under the sponsorship of the Department of Trade and Industry, conducts research into the application of avionic systems to civil aircraft. The trials aircraft is a BAC 1-11 which has been equipped with the necessary facilities for research into navigation, flight control, electronic displays and advanced interfacing techniques between the crew, the aircraft systems, and the ground. The programme is studying both the individual component systems and how these can be integrated into an effective total system. First, the environment and the future trends in the use of these developing systems will be discussed.

To have a maximum effectiveness, the major part of the programme is aimed at the areas of greatest change. It can be argued that, with the rise in fuel prices, this must mean energy management. Fuel costs are an increasingly large proportion of direct operating costs and many airlines have rightly emphasised the efforts that are being made to minimise their fuel bills. There are a number of constraints or uncertainties that militate against fuel saving and one of these is the air traffic control requirements which are themselves constrained by the capabilities of the aircraft. It is quite clear that any departure from the optimum profile and route will increase the direct operating costs, and an Air Traffic Management system that can minimise the route length and delays will not only reduce the fuel burnt but should also lead to a better utilisation of airspace. This is now recognised by the authorities and work by the Civil Aviation Authority and the Royal Signals and Radar Establishment is looking at ways in which better use can be made of the airspace, both to reduce delays and to increase capacity in order to cope with the predicted traffic increase. In order to make optimum use of the airspace available, some improvements are necessary in the aircraft. For example, captains have referred to the high workload in computing the correct descent path - a task which lends itself to automation. They have also emphasised the problems of using automatic systems in a tactical situation.

It was concluded, therefore, that there are a number of areas where changes could be made which would contribute towards the desired improvements. These are, improved navigation, both in the terminal area as well as en-route, the integration of this with flight management requirements, the automatic flight system and advanced interfacing techniques including electronic displays. The Flight Management System should provide the capability to optimise the flight profile within the constraints (in four-dimensions) imposed by Air Traffic Control. Conversely, Air Traffic Control should be aware of the capabilities of these systems to provide accurate performance and improve the predictability of aircraft. This must reduce the Air Traffic Control workload and so allow better sequencing to be carried out with a resulting reduction in delays.

There are a number of problems to be overcome before advantage can be taken of these potential gains and these lie firmly in the areas of communication. These must include not only the communication between the pilot and the ground controller but also between the pilot and his Flight Management System. Another area that must be resolved in order to optimise Air Traffic Management is the communication between the various Air Traffic Authorities to allow the earliest possible prediction of arrival times to be made and slot times allocated. This will involve international cooperation.

The purpose of this contribution is to describe the flight test facility that is available at RAE Bedford, to give a brief outline of the current research programme and to discuss how the continuation is planned for the future.

2 THE TEST FACILITY AT RAE BEDFORD

The main flight test aircraft for the Civil Research Programme at RAE Bedford is a BAC 1-11 200 Series aircraft (Fig 1). This is a short range commercial jet aircraft with a maximum take-off weight of 35834 kg (78835 lb). The power plants are two Rolls Royce Spey 506-14a 2-spool turbo fans. The facilities provided in this aircraft have been assembled over a number of years in order to make it into a versatile research aircraft suitable for work on flight control, navigation, displays and flight management.

The equipment has been installed in the aircraft cabin to provide ready access, and extensive use has been made of junction boxes and trunk routes to enable changes to be made as simply as possible. The general cabin layout is shown in Fig 2. A Smiths Industries SEP 5 duplex autopilot provides a full autoland capability. In addition, a microprocessor and a digital computer provide, in conjunction with the SEP 5 servo

systems, a 'versatile' autopilot. The aircraft has been modified to provide a direct lift facility, using the spoilers, and a series actuator has been provided in the elevator control to provide pitch compensation. Both the spoilers and this actuator can be operated by the versatile autopilot (Fig 3).

The navigation installation includes two VOR receivers to ARINC 579, three DME receivers to ARINC 568, an inertial navigation system with ISS outputs to ARINC 581 and an R Nav system to ARINC 582 which was supplied by Flight Navigation Ltd, a joint Smiths Industries, Racal Decca Company. The navigation computer has additional store capacity for experimental use and, in conjunction with a general purpose digital computer, provides a Flight Management capability.

Two electronic displays manufactured by Smiths Industries Ltd to ARINC 725 format D (8" x 8") have been installed in the first pilot's position (Fig 8). These provide a dedicated display for normal flight use but also have a flexible capability for research purposes. These displays are linked with the R Nav system via the general purpose computer to enable the investigation of interactive display techniques (Fig 9).

Recent additions to investigate new interfacing techniques have included:

a. An experimental data link based on a VHF channel, linking computer interface modems in the aircraft and on the ground;

b. two advanced speech recognisers, one interfacing with the displays and flight management system and the other controlling;

c. a Radio Management Control and Displays system.

Two observers' stations, each with seating for two, are provided in the aircraft cabin. These have a full set of flight instruments and displays for monitoring purposes.

Comprehensive instrumentation facilities are provided together with a large number of signal conditioning units. The primary aircraft recording system uses a Plessey PV 1512 Digital Recording System. This is supported by an FM recorder and an 8-channel analogue pen recorder. A radio clock is provided for real time synchronisation with ground tracking systems. In addition to the normal aircraft supplies, 4 kW of power at 240 V 50 cycles is provided.

In order to support the facilities in the aircraft, a ground-based simulation rig has been developed. This is used during development studies. It simulates the whole Flight Management System and aircraft aerodynamics together with a fully representative simulation of radio aids. It is also used to test the aircraft Flight Management and display systems hardware and software in real-time on the ground.

3 THE FLIGHT PROGRAMME

A summary of the RAE/FSB2 Civil Avionics Programme is given in Table 1. As well as the flight programme, the Table includes some of the relevant study work undertaken by Industry. The programme's ultimate objective is to demonstrate an aircraft system compatible with the requirements of an Air Traffic Control System of the future designed to make optimum use of the available airspace, reduce delays and, as far as practicable, allow the aircraft to fly optimum profiles.

The initial part of the programme was designed to establish the 'tools' that are likely to be available in the future and was therefore aimed at improvements in flight control, the measurement of the performance of navigation aids, the development of automatic navigation systems working in two-, three- and four-dimensions, and the development of electronic displays, which, apart from providing an alternative to the conventional instruments, make other forms of display possible. This part of the programme provides data that could be used by civil aviation authorities in their assessment of changes in separation standards that might be possible in the future and also in studying Air Traffic Management Systems for the future. A number of interfacing techniques are also being researched; these include speech recognition, data link, data bus and radio management systems.

The second half of the programme is aimed at the integration of these 'tools' into a total system which includes both the aircraft and Air Traffic Control Systems. The main flight programme activities and results are summarised in the following paragraphs.

4 FLIGHT CONTROL

The early part of the flight control programme was concerned with an examination in flight of the performance gains that could be obtained using Direct Lift Control (DLC). Both manual and automatic control systems were evaluated using laws based on Industry studies[1,2]. Although the authority of the Direct Lift Control is small (0.15 g) the trials showed that significant performance benefits were achieved without increased elevator, throttle or pitch activity. Some of the results obtained are given in Table 2 and Fig 10.

Flight trials were also undertaken to examine the handling characteristics of the aircraft with reduced stability margins. Studies undertaken by British Aerospace had shown that a reduction in the stability margin, which was nevertheless still within the

constraint of the pilot being able to control the aircraft, would provide a significant improvement in trim drag and also in tailplane size and weight. These would all lead to a reduction in fuel usage. For normal use, good handling qualities would be restored to the aircraft by artificial means but, because of the constraint stated above, there would not be the formidable certification problems that would arise from the use of full-time full authority active control.

The purpose of the flight trials was to confirm the reduction in stability that could be reasonably controlled by the pilot, to evaluate a control augmentation system and to assess the effects of failures. Because the BAC 1-11 had been fitted with the series actuator in the elevator control run to allow pitch compensation to be applied when using manual Direct Lift Control, it was possible to use this facility to de-stabilise the aircraft and simulate, in flight, the effects of a reduction in the stability margin without the safety and other problems associated with moving the cg[3]. Fig 11 shows a comparison between the theoretical response of the aircraft at various cg positions and the response of the artificially de-stabilised aircraft. The short flight experiment was successful and gave British Aerospace the confidence to fly their own aircraft with the cg considerably behind the normal limit.

After completion of this work, trials were directed onto other items in the programme and flight control work has been concentrated on studies both within the RAE and in Industry, into non-linear control laws. A small portion of the flight time available is now being devoted to an investigation of these laws. One system under consideration should provide improved speed control with reduced throttle activity, whilst another should enable a relaxation to be made to the operating limits of the automatic landing system.

5 NAVIGATION

5.1 TRIALS PROGRAMME

This part of the programme was aimed at assessing the accuracy and characteristics of the currently available navigation aids and, in cooperation with Flight Navigation Ltd (a joint Smiths Industries - Racal Decca company) to establish in flight, the automatic navigation performance that could be obtained using various combinations of radio aids augmented by on-board sensors.

First the measurement of the performance of radio aids was carried out in order to provide a basis for theoretical studies. The results were obtained using the Airborne Digital Recording System synchronised with recordings made on the ground using either the Kinetheodolite tracking system at Bedford or the FPS 16 C Band Tracking Radar at RAE Aberporth. The results obtained using DME equipment are given in Ref 4.

Using the same tracking facilities, the automatic navigation performance was established when using VOR/DME or DME/DME as the radio aids, augmented either by air data or an inertial sensing system. The results of these trials are reproduced in some detail in the following sections from Ref 5.

5.2 TRIALS PROCEDURE

5.2.1 RNAV SYSTEM PERFORMANCE

All the assessment flights were made with the RNAV system controlling the aircraft through the autopilot roll and pitch channels. The required airspeeds were selected by the pilot and maintained by the autothrottle system. The route to be flown was selected from the data base before take-off and the required altitude at each waypoint was entered using the CDU keyboard. The particular navigation mode to be assessed was selected by the pilot, while the ground navigation aids were automatically selected and tuned by the RNAV computer to obtain optimum radio guidance information throughout the flight. For comparison purposes, some of the flights were conducted using manual station selection, but still with automatic tuning of the VOR/DME receivers.

Two modes of vertical control were available. Path mode controlled the aircraft onto the straight line between the altitude selected at the previous waypoint and the desired altitude at the next waypoint, while rate mode gave a facility for immediately climbing (at a rate matched to the aircraft's normal climb performance) or descending (at 2000 ft/min) until reaching the required flight level, which was then maintained until reaching the next waypoint.

5.2.2 ASSESSMENT ROUTES

The flight trials were conducted in the area covered by the FPS16 tracking radars at RAE Aberporth on the Welsh coast. Fig 12 shows the 'figure-of-eight' pattern followed on the majority of the en route flights. The route was designed to keep the aircraft within good radar tracking coverage, to keep clear of controlled airspace, to provide a variety of turn angles, and to maintain a reasonably good navigational aid environment. The mean distance between waypoints was approximately 40 n mile, with the route being flown at altitudes varying between 16000 ft and 24000 ft, both to assess the vertical performance and to increase the chances of meeting windshear conditions. A further en route flight plan enabled much longer distances between waypoints to be used (up to 164 n mile).

Fig 13 shows the routes provided for simulating terminal area operations. The runs were started at an altitude of 10000 ft, descending to 8000 ft approaching the holding pattern, with a further descent to 7000 ft while in the hold. A typical approach sequencing path was then flown from exiting the hold on to final approach, maintaining a continuous 3 degree descent until reaching 2000 ft at the end of the run. The tracks followed are representative of the published standard arrival route at Heathrow for westerly landings, but the navigational aids available in the trials area were very limited compared with those available in most major European TMAs.

5.3 DATA ANALYSIS

Data was collected throughout the two hours of tracking radar coverage obtained on each of 28 flights made in an en route environment. In addition, a total of 30 runs (each having approximately 20 minutes of tracking radar coverage) were made with the aircraft following typical TMA arrival routings.

The total lateral aircraft navigation error was determined by computing the difference between the aircraft's actual position (as determined from tracking radar data) and the desired position (as defined by the route selected from the RNAV system data base). This total navigation error is made up of two components; the first being the difference between the RNAV system's estimate of aircraft position and the aircraft's true position, while the second is the error in controlling the aircraft's path to make the estimated position coincide with the desired position. This second error is generally referred to as flight technical error (FTE). The lateral error components described above are shown diagrammatically in Fig 14.

To allow ready comparisons with performance achieved by other types of navigation systems, circular position error (CPE) was used to define the error in estimated position. CPE is the horizontal distance between the aircraft's actual position and the RNAV system's estimate of position, and includes the radio guidance ground station and airborne receiver errors as well as the RNAV computer calculation errors.

When considering the possible effects of improved navigational accuracies on present airways separation standards, the total crosstrack error is probably of more use than CPE and therefore the total system error (position estimate error + FTE) has been resolved into total crosstrack and total along track components. However, because of the 'figure-of-eight' type of route used during the assessment flying, these two error components were often being interchanged (an error in one component converts to an error in the other component when the aircraft turn through 90 degrees) and therefore care must be taken in reading these results across to more representative en route airways situations, where an aircraft proceeds in the same general direction throughout a flight.

5.4 RESULTS

5.4.1 LATERAL PERFORMANCE

Fig 15 shows the mean and standard deviation of CPE for all flights using each of the navigation modes tested in both en route and TMA environments. The en route results clearly show the substantial improvement in accuracy of position estimation when using DME/DME guidance compared with using VOR/DME guidance, irrespective of whether air data or inertial velocity information was used for smoothing the guidance data. With air data smoothing, the mean error using DME/DME guidance was 0.3 n mile (standard deviation 0.16 n mile) compared with a mean of 0.76 n mile (sd 0.58 n mile) when using VOR/DME guidance. Similarly, with inertial smoothing, DME/DME guidance gave a mean error of 0.26 n mile (sd 0.12 n mile) compared with the mean of 0.56 n mile (sd 0.44 n mile) achieved using VOR/DME guidance.

Performance in a TMA environment also showed that DME/DME guidance gave more accurate position estimation than VOR/DME guidance, although the improvement was less marked than in the en route case because of the rather poor DME/DME environment at low altitude in the trials areas, which is unrepresentative of a major TMA.

The improved performance using DME/DME position fixing was obviously achieved as a result of the DME system errors being much less than the VOR system errors. Earlier flight trials carried out by FS2, RAE Bedford[4] to determine DME system accuracy gave a mean bias error of 0.2 n mile (sd 0.14 n mile) over all the ground stations used. Noise, when using modern digital DME receivers, was found to be less than the system resolution of 0.01 n mile. The VOR overall system accuracy is often quoted as ± 4.5 degrees (95% probability) and can therefore give rise to large position errors compared with DME accuracy, particularly at long ranges from the ground station.

The use of inertial velocity data for smoothing the VOR/DME derived position estimate, improved the accuracy in both en route and TMA conditions, giving a mean CPE of 0.56 (sd 0.44 n mile) compared with the mean error of 0.76 n mile (sd 0.58 n mile) when using air data smoothing in the en route phase, and a mean of 0.56 n mile (sd 0.34 n mile) compared with 0.70 n mile (sd 0.34 n mile) in the TMA environment. This improvement was largely caused by the quicker response to wind changes along the route made possible by the use of inertial velocity information, which avoids the very long time constant on wind learning demanded in VOR/DME/air data mode to overcome radio guidance noise and bias variations.

Inertial velocity smoothing showed much less improvement compared with air data smoothing when applied to DME/DME guidance in the en route phase, because when using DME/DME with air data smoothing, the wind learning is already relatively rapid owing to the fairly short time constant allowable because of the low DME noise level, and therefore only a small improvement was achieved using inertial smoothing. In the TMA situation, inertial smoothing helped to overcome some of the effects of the poor DME environment experienced in the trials area, and gave a similar performance improvement to that achieved when applying inertial smoothing to VOR/DME guidance.

Fig 16 shows the mean and standard deviation of total crossstrack error for all flights in each navigation mode. These crosstrack errors include both the position estimate error and FTE. Also shown are the crosstrack errors measured when auto-coupled to VOR radials using the autopilot alone. This is representative of the performance achieved by non-RNAV fitted aircraft flying conventional airway routes but does not include the often large errors encountered when turning from one radial to another. The standard deviation of crosstrack error was 1.25 n mile (compared with the standard deviation of 0.7 n mile obtained when using RNAV in VOR/DME mode) and included FTE.

Fig 17 shows the mean and standard deviation of lateral FTE for each of the navigation modes tested. A noticeable reduction in error occurred when the RNAV computer was using DME/DME information for position estimation, indicating that the autopilot/aircraft response was not sufficiently rapid to null the larger and faster changes in estimated position experienced when using VOR/DME guidance.

During the en route flying a limited sample was obtained of the errors which can occur during periods of operating an RNAV system in the dead reckoning mode (ie with no guidance information to update the position estimate). The maximum position error experienced after 20 minutes of D/R operation was 6.5 n mile and was caused by a combination of an incorrect wind estimate at the time of losing radio guidance, a significant wind change along the route, and errors in the heading input from the magnetic compass. Although in much of European airspace it is unlikely that radio guidance information would be lost for significant lengths of time, this type of problem is largely overcome if inertial velocity information is available to the RNAV computer. Inertial equipment also provides a more accurate heading reference than magnetic compass systems.

5.4.2 WIND EFFECTS

The assessment flying took place over a total period of 16 months, with a wide variety of weather conditions being experienced. Wind information for the trials area over the duration of each flight was reported from the Meteorological Office at RAE Aberporth and wind data as computed by the inertial navigation system was recorded continuously on the airborne digital recorder. Reported winds at 20000 ft altitude covered the range from 5 knots up to 100 knots during the en route flying, with the direction being predominantly westerly. During the TMA flying, wind strengths from 4 knots to 41 knots were reported at 6000 ft altitude, again mainly from a westerly direction. Considerable windshear and turbulence were experienced on some of the flights, but the spread of wind conditions was fairly equal for each of the navigation modes assessed, and therefore the performance differences between navigation modes was not caused by differing weather conditions.

Wind conditions clearly affected the performance achieved from one flight to another when using VOR/DME guidance with air data smoothing. TMA flights in fairly calm wind conditions, gave a mean CPE of 0.5 n mile (sd 0.25 n mile) while flights in strong wind conditions, with windshear present, gave a mean CPE of 1.1. n mile (sd 0.48 n mile). Using DME/DME guidance with air data smoothing, no significant difference occurred between the performance achieved on flights in light winds and that achieved in strong winds with windshear present. Similarly no noticeable difference occurred with changes in wind conditions when using inertial position smoothing instead of air data smoothing.

5.4.3 NAVIGATIONAL AID PERFORMANCE

The quality of the navigational signals from the various ground stations obviously has a major effect on the accuracy of the RNAV estimate of aircraft position, and some examples of the guidance variations and characterisitics affecting RNAV performance during these flight trials are given in references 4 & 5.

5.5. NAVIGATION PROGRAMME APPLICATION AND CONTINUATION

The trials summarised above took place during 1978/79 and as well as providing a sound basis for the establishment of Minimum Navigation System Performance Specifications (EUROCAE Working Group 13) spearheaded the rapid development in the UK of Flight Management Systems, the supporting trials for which are described in more detail in paragraphs 6 and 8. Ever since the beginning of these trials which established accuracies and initial operating procedures there has been a continuing evolutionary development of the detailed features, algorithms and capability of the RNAV system in the BAC 1-11. Extensive experience has been obtained during trials throughout Europe and the United States affording the opportunity to identify and overcome deficiencies in the original system which were largely those of interfacing, ie data input, clarity of presentation or ease of mode changing. Lessons have also extended to the development of the flight test facilities in the BAC 1-11. One major step forward has been the introduction of a general purpose mini-computer which allows for on-line development of systems software in flight greatly reducing the duration of the flight development programmes. From these RNAV

trials the programme has progressed to address 3D and 4D aspects which are described in later paragraphs.

6 DISPLAYS

6.1 THE UK PROGRAMME

The application of electronic displays to the flight decks of transport aircraft began seriously in the mid 1970s. The main research activity in the UK was based at British Aerospace in Weybridge, Surrey, on the advanced flight deck (AFD) simulator. The initial work involved monochrome CRT displays[7], which helped to identify the benefits which could be obtained through the use of suitable electronic displays to present flight deck information. This was followed by work on colour coding[8]. Encouraged by these results a decision was taken to install two large format (ARINC type D, with a case size of 203 x 203 mm) colour CRT displays, to be developed by Smiths Industries[9], in the left-hand instrument panel of the BAC 1-11.

Full colour displays were installed in June 1981 preceded by monochrome units fitted in 1980 for debugging and system interfacing. This process allowed a useful comparison to be made between the standard instruments, monochrome CRTs and the use of colour.

A smaller but parallel exercise was mounted to gain experience with a compact, easily retrofitted head up display, the 'MONOHUD' manufactured by Marconi Avionics. This proved extremely useful during the low visibility flight programme which will not be described further in this paper.

The main programme on displays concentrated on the development and integration of the colour head down instruments with the rapidly evolving Flight Management System[10].

6.2 SYSTEM ARCHITECTURE

The architecture of the installation and the interface with other experimental equipment have been designed to achieve a high level of flexibility in the content and format of displays that can be presented using the system. Figure 9 illustrates the major components.

The symbol generator units receive data to be displayed from ARINC 429 serial digital highways, and generate the waveforms for the cursively written symbols. These, together with digitally coded colour commands, are fed to the pilot display units. Since the aircraft is not equipped with sensors producing serial digital outputs directly, a 'front end' interface unit is required to take in analogue signals and output them in the required digital format; such interfacing would not be needed in a more modern aircraft and will be removed in a future installation.

The two Pilot Display Units (PDUs) on the flight deck are installed side by side, in contrast to the one up, one down configuration more commonly used with smaller CRTs. The left-hand PDU is situated in front of the pilot, and normally displays the primary information required to fly the aircraft (the Primary Flight Display (PFD)). The second PDU presents navigational information (the Navigational Display (ND)). However, the system is configured so that each Symbol Generator Unit (SGU) can produce any of the possible formats, and also that each PDU may display the output of either SGU. Consequently, even in the event of the failure of one SGU and one PDU, all the information available with the full system would still be available, though not all simultaneously.

An important contribution to the flexibility of this experimental system is provided by the general purpose minicomputer. The primary role of this machine is the generation of experimental display formats through the output of commands to the SGUs to draw symbols from a 'symbol library', at given screen positions. By this means, changes in format can be implemented and evaluated quickly and easily without the need to modify the software of the SGUs themselves. However, should the need arise to make more far-reaching changes that do necessitate new SGU software, the computer is also equipped to down-load this as an alternative to the standard SGU programs.

6.3 PRIMARY FLIGHT DISPLAY

There are many potential advantages of using CRT displays to provide primary flight information. Most notable is that they can be readily programmed to display information relevant to the current flight situation and to remove unnecessary information, thereby reducing clutter, and thus making the best use of a given display area. The use of colour provides additional information coding which can reduce visual clutter still further.

The format of the colour PFD in use in the BAC 1-11 is illustrated in Fig 4, and contains only minor changes from that which evolved during the advanced flight deck study. The mixtures of primary red, green and blue needed to produce each of the 15 possible colours of which the system is capable, are stored in programmable memory (PROM) within the pilot display units. Consequently, the colour set may be redefined to suit particular applications, merely by fitting a new PROM containing the appropriate data. Table 3 included in the colour plate describes the colour set which evolved from the subjective opinions of a number of pilots, and which was used for the displays illustrated. All achieve a discrimination index greater than unity when viewed in 80000 lx of illumination.

The colour format provides all the information, presented in the same relative positions, that is available from the familiar T pattern of conventional instrumentation. However, the flexibility of the display medium has been used to enhance the presentation. On the airspeed indicator (top left) an expanded scale is used to give an analogue indication of ± 50 knots from present speed (the scale changeover point being always located opposite the pointer). Additionally, critical speeds for current phase of flight are automatically 'bugged' on the airspeed scale. Attitude director, barometric altitude and vertical speed presentations (centre, top right and bottom right respectively) differ little from their conventional counterparts with the exception that radio altitude information is also shown on the barometric altitude scale, when appropriate, by means of a small labelled bug on the inside of the scale. Along the bottom of the display, a strip heading scale is provided; areas at the sides and top are used to show autopilot mode and command annunciations.

In that this PFD provides a complete source of primary flight data on one CRT, it differs significantly from the combination of electronic and electromechanical displays being fitted to airliners now entering service.

The relatively conventional approach to the initial format design has been useful in this application since it provides information in a fashion essentially familiar to pilots trained on conventional instruments, enabling them more readily to assess the concept of using CRTs for display of primary flight data.

6.4 NAVIGATION DISPLAY

Perhaps the simplest way of providing navigational information on a CRT display is to reproduce the conventional horizontal situation indicator presentation. However, it is becoming increasingly common for transport aircraft to be equipped with some form of area navigation (RNAV) capability, and it is when used in conjunction with these more sophisticated types of equipment that a CRT display has the most to offer.

Paragraph 5 has illustrated the superior lateral navigational accuracy offered by RNAV systems, and has also pointed to the possibility of improved airspace utilization through a reduction in lateral separation between aircraft so equipped. However, the workload associated with programming such equipment to fly the required route and monitor its performance, particularly during operation in TMAs, has been found to be excessive, resulting in a high incidence of operating errors. Without reduction of both workload and error occurrence to a very low level, it is unlikely that the measures proposed could be effectively implemented.

It is in order to overcome these problems that the development of a colour map format for the ND has been pursued. The basic facility is illustrated in Fig 5 and shows aircraft position and orientation, relative to the waypoints, track lines and any holding patterns that comprise the programmed RNAV route. (Additional navigational information is provided in the side frames). The display of danger areas and prohibited airspace on the map, suitably colour-coded, has also been demonstrated.

The pilot is offered a number of switchable functions to tailor the map presentation to suit different phases of flight and also personal taste. As well as a choice of various range scales, a number of orientations are provided: heading up, track up and north up are all possible. Also offered is the display of radio aids and/or waypoints in the RNAV database, serving either to complete the pilot's mental picture of his position, or as an aid to implementing route changes. Assistance with the latter is also provided by a so-called 'look ahead' facility, which enables a small section of the route, possibly a great distance from present aircraft position, to be examined in fine detail.

Extension of the Flight Management system to perform automatic control in 3 and 4 dimensions, to be discussed in paragraph 8, requires effective communication between FMS and crew. The CRT flight deck displays are an essential feature of these systems.

6.5 THE FUTURE DISPLAYS PROGRAMME

The lessons learned during the development and trial of the experimental display system fitted to the RAE's BAC 1-11[10] (Fig 8) are being applied to the design of equipment for commercial application. An improved generation of flight deck displays is undergoing development by Smiths Industries to offer, in addition to improved performance, reductions in weight, volume and power consumption.

The development of alternative primary display formats is continuing on the British Aerospace Advanced Flight Deck Simulator with a view to subsequent testing in flight. The colour displays development is now an integral part of the future programme which will deal with advanced techniques in Flight and Air Traffic Management.

7 WORKLOAD AND DATA INPUT DEVICES

7.1 THE NEED AND THE PROGRAMME

Experience with the advanced RNAV and FMS systems have established their superior capability for the precise control of the flight path; also large colour displays enable a satisfactory presentation of complex situation information to be given to the pilot. The use of these systems for flight planning and the control of the resulting flight

trajectories is generally very satisfactory. However, there are peak periods of activity particularly in the Terminal Movement Areas when configuration and mode changes coincide with heavy radio traffic and system checking requirements. The very success of flight management systems is also leading to progressively more complex applications with the associated demand for more detailed instructions or input data. Improved techniques for handling system selection, mode changes and data input are clearly required to meet this demand.

With its now mainly elderly and cramped flight deck, the BAC 1-11 is not really suitable for experiments concerning ergonomic improvements so this work, together with format developments for flight instrument, flight checks and engineering displays are being addressed by the Advanced Flight Deck Simulator at BAe Weybridge with other UK industry involvement. However, some techniques for better system integration can be pursued effectively on the aircraft. One such example in current development is the integration of all the radio and navigation aids. New technology is also being examined in flight where a representative airborne environment is important. The main example in current trials is the application of speech recognition equipment or 'Direct Voice Input' (DVI).

7.2 DIRECT VOICE INPUT - PHASE II

Studies into the potential application of Automatic Speech Recognition (ASR) on the transport flight deck began in 1981. It became clear that early equipment on the commercial market (Phase I) fell far short of the recognition accuracy required in the relatively noisy environment of a flight deck. However, Marconi Space and Defence Systems were engaged in the development of an advanced system known as the SR128 which is based on spectrum matching and dynamic programming algorithms and one of these machines was procured under combined MOD/DTI/Industry funding in 1982. Coupling of the SR128 to the BAC 1-11 avionics system was achieved and successfully demonstrated by September 1982. In parallel with this development and installation, studies were progressing on the subjects of syntax structure, suitable applications, and test methods which involved the use of a range of head-set microphones and standard issue aircraft intercom equipment. The results of noise level measurements and the SR128 recognition tests are summarised in Table 4.

The first application to be chosen for investigation involved the interface with the navigation display. Prior to this work the pilot had a choice of 16 switches of the push, lever or rotary variety, enabling him to change map scales, orientation, add or remove route information and look ahead along the preprogrammed flight plan. These controlling switches were positioned both on the centre pedestal and the glare shield coaming. The general schematic of the system with voice control is shown in Fig 8. The microprocessor downstream from the ASR interprets the words or word numbers that have been recognised and sets the correct bits at the flag interface card within the digital computer. As expansion was envisaged for DVI to control other systems, the introduction of a microprocessor, as opposed to modifying the software of the navigation display programme, was the most appropriate approach. Also in Fig 8 a microphone control unit is shown, this comprises a pre-amplifier, microphone gain control, microphone input and output sockets and the DVI activation switch. The pilot on activating this switch and speaking to the ASR could change the navigation display to the desired format. Although the position of the DVI control was not ideal (a better position would be on the aircraft's control column with the intercom and RT selectors) the pilot did not find using a switch for this task a problem.

DVI control duplicated the manual selectors but additional features were included to show, to a limited degree the advantages of DVI and software based controls. One example of this is of interest. If the pilot required to inspect the airfields, reporting points or other known positions and navigational aids in the area, he previously had to select two switches labelled WAYPOINTS or NAVAIDS. By voice he could either say WAYPOINTS NAVAIDS or NAVAIDS WAYPOINTS or ROUTEDATA. The Word ROUTEDATA shows that under software control one word can have many actions associated with it. Furthermore a repeat of this word would remove the display data, yet again this was controlled by software. As a result of these additions, the vocabulary size for map control was 37 words. Each pilot could control the map, but as the ASR is speaker dependant the very first utterance was his name. This allowed the correct voice templates to be selected and used in the matching process.

DVI control of the electronic navigation display has now been tested on 42 flights covering 50 hours of flying and been evaluated by two pilots using a variety of microphones [11]. A summary of the results obtained is shown in Table 4.

Although it could be considered that the extent of DVI control so far investigated has been almost trivial, it has been most useful in providing an early pilot reaction. In fact, the scientific staff have been almost embarrassed at the enthusiasm with which DVI has been received and the speed at which the pilots would like its control extended. Particular findings are:

a. Vocabulary was easy to recall.

b. Training of the ASR produced no problems.

c. Freedom to use other words during training was appealing.

d. System activation by switch is acceptable.

e. A maximum speech rate of approximately 3 words/sec is acceptable.

f. Recognition accuracy results were very encouraging.

7.3 RADIO MANAGEMENT, DVI PHASE III AND THE FUTURE

The 10 separate radio and navigation controllers have been integrated by a 'Radio Management System' based upon a 'smart' Integrated Control and Display Unit (ICDU) manufactured by Marconi Avionics, Basildon. This unit has greatly simplified the task of monitoring and selecting the radio and navigation aids. It is now proposed to couple this system to a new speech recognition equipment developed by Marconi Flight Automation Research Laboratories which uses the NPL feature matching technique as well as dynamic programming.

By emulating the keyboard's actions by the use of speech recognisers and microprocessors, the pilot will be able to carry out all functions by voice. Laboratory investigations before flight trials commence have been successful but the size of vocabulary needed is large (102 words) and it is wondered if the human memory may be under some strain in remembering what exactly the correct commands should be. It is intended to explore the possible use of place names, for example, the pilot would like to select his aid by saying 'VOR 2 Daventry' or 'Bedford Approach'.

The results achieved by the Phase II equipment which are already equivalent to the accuracy of keyboard operation, and the enthusiastic acceptance by the flight crews give considerable promise for a successful continuation of this flight test work.

8 ADVANCED FLIGHT MANAGEMENT SYSTEMS

Systems to perform automatic control in three and four dimensions have been developed at RAE and are undergoing flight trial in the BAC 1-11. Effective communications with the crew by means of the CRT flight deck displays is an essential feature of these systems. Figure 6 shows a simple attempt to illustrate on the map display the vertical profile programmed by the crew. The waypoints are annotated by the flight levels corresponding to them, and further reinforcement is added by the colour coding of the track lines - climb, cruise and descent segments are shown in blue, white and brown respectively. Figure 7 shows the display format appropriate to four-dimensional navigation. The pilot has nominated a particular waypoint, and also programmed a target time, airspeed and altitude at which the aircraft must arrive at that point. In addition to these inputs, a small chevron is displayed which illustrates the position currently required for the aircraft to remain on the time schedule. The chevron is dimensioned so that when exactly on schedule it overlays the nose and wings of the aircraft symbol. Also shown are the system estimates of arrival time at the remaining waypoints as well as at the top of en route descent point which is (illustrated by a small arc).

Trials to establish '4D' performance so far, have proved very encouraging. After a period of development during the first half of 1983, operation of the system has revealed that in moderately well behaved atmospheric conditions, terminal time errors of less than 5 seconds are consistently achievable. Liaison is being established with the Meteorological Office at Bracknell in an attempt to incorporate some prediction of the atmospheric conditions, namely wind and temperature, that are to be encountered during the descent. This is particularly important when the aircraft has to fly through some form of atmospheric discontinuity such as frontal activity or inversion. Inability to predict these phenomena can result in very large airspeed changes being required during descent, resulting in poor fuel efficiency, or even inability to meet the requested constraints. Suitable algorithms are being developed and flight tested.

Some refinement of the autopilot demand and throttle laws is also desirable. Inevitably there is a conflict between the achievement of terminal constraints with high precision and the maintenance of an acceptable level of control and particularly throttle activity. Present laws, while providing satisfactory performance, possibly do not represent the most effective compromise.

Following attention to these areas, a period of evaluation is anticipated, during which such aspects of performance as terminal time, speed and height errors, control activity, and precision of atmospheric predictions will be assessed. Such data will be valuable when the design of air traffic management procedures, which can effectively use the capabilities of time controlled aircraft, is considered.

4D speed control can only achieve large time delays when the requirement for delay is known well in advance. Because of the problems of international communication this may not be possible and so other means of time control may be needed. Holding patterns for delay have been programmed and in order to provide delays corresponding to less than one orbit of holding pattern, (about 3 to 6 minutes) 'U'-shaped delay patterns that would be compatible with dual tracked airways have been studied and flight tested. The aim of these holding patterns is to achieve an accurate exit time which would then be followed by the cruise descent with 4D control, all of the holding patterns being at high level for most efficient fuel utilisation. Accuracies of exit times have been of the order of ±5 secs.

It is likely that the most profitable use of automatic time control would require an aircraft to be equipped to manoeuvre itself through not one but several time/speed/altitude constraints during the course of its flight, with the final one being

situated at the destination runway threshold. The airborne system would probably need to use a combination of speed control and path stretching to plan the optimum route through these windows in space and time. The longer term aims of the work on time control are to develop the present system to offer these facilities.

9 AIR TRAFFIC MANAGEMENT - THE AIR/GROUND INTERFACE

The individual constituents are now available that make possible accurate control in three dimensions and time, and if accurate wind information can be made available then the time control can also be made fuel efficient. It is now necessary to develop means by which these facilities can be used to improve the overall Air Traffic Management operation and in order to do this it is obviously essential that there is close collaboration between air traffic control research and the avionics research programmes[12,13,14,15].

ATC research in the UK is studying a type of computer assistance that will be needed by a controller to plan departure and arrival flows. Most of this research has, until now, assumed aircraft whose timing predictability and accuracy of navigation is no better than at present. It is necessary to study how to use predictable and precise flight path control to improve traffic flow and how to inform the controller of what the system requirements are. There is the problem of how to convey this requirement to the pilot so that the data can be input to the flight management system of the aircraft with a low probability of insertion errors. For this reason studies need to take place on whether voice links can be used or whether data links are essential. There is also the question of how the overall plan is made. Should the aircraft request time at critical waypoints that would enable a fuel optimal profile (knowing in advance the wind profile that it will experience) or should the ground computer have a complete knowledge of all aircraft performance and plan everything on the ground? Upon this decision depends the type of data interchange required and hence the data link formats and message structures.

10 CONCLUSION

This contribution has described the BAC 1-11 research aircraft of RAE Bedford and its installation. The research programme is funded by the UK Department of Trade and Industry and has been run with the assistance and co-operation of the UK Avionics Industry. Significant results have been achieved in the fields of automatic control, inproved accuracy of navigation, the use of CRT flight deck displays, the development of time control manoeuvres and the use of Direct Voice Input. The programme is continuing to develop the experimental installation to address the role of avionics systems in the total Air Traffic Management system. The development of flight path and time control algorithms will be extended to deal with multiple constraints. Further attention will be paid to the interfaces between the aircraft systems, the crew and air traffic control. In co-operation with other research groups, particularly RSRE studying ATC developments, the problems of organisation, control and data distribution will be addressed.

REFERENCES

1	K F Goddard N Cooke	Flight trials of an Automatic Control Law for a BAC 1-11 aircraft utilising the wing spoilers for direct lift control. RAE Technical Report 80003 (1980).
2	G Ingle	Flight optimisation of a manual direct lift control facility on a BAC 1-11 aircraft. RAE Technical Report 79036 (1979).
3	G Ingle	Trials on Flight Systems' BAC 1-11 aircraft operating with artificially relaxed longitudinal stability and a command augmentation system. Unpublished MOD(PE) Technical Report (1980).
4	R C Rawlings R A Harlow	Flight trials to determine the overall system performance of distance measuring equipment. RAE Technical Report 79140 (1979).
5	R A Harlow	Flight measurement of area navigation system performance using various combinations of ground aids and airborne sensors. Presented at the IEEE Position Location and Navigation Symposium, Atlantic City, NJ, December 1980.
6	R C Rawlings	Flight Assessment and Operation of Navigation Systems. Proceedings, Royal Institute of Navigation, London, March 1980.
7	J W Wilson R E Hillman	The Advanced Flight Deck. Royal Aeronautical Society's Spring Convention "Aerospace Electronics in the Next Two Decades", London, May 1979.
8	J W Wilson L F Bateman	Human Factors and the Advanced Flight Deck. 32nd International Air Safety Seminar, London, October 1979.
9	R A Chorley	Electronic Flight Deck displays for military transport aircraft. AGARD CP312 "The impact of new guidance and control systems on military aircraft cockpit design", May 1981.
10	N W Witt E Strongman	Application and experience of Colour CRT Flight Deck Displays. Displays Journal, April 1983.
11	N Cooke	The Flight Testing and System Integration of Direct Voice Input Devices in the Civil Flight Deck. Institute of Electrical Engineers colloquium, "Digital Processing of Speech", London, April 1983.
12	R R Newbery R W Jones	UK Research on the Modern Transport Flight Deck and the interaction with Air Traffic Control. American Institute of Aeronautics and Astronautics, International Air Transportation Meeting, Cincinnati, May 1980.
13	R W Jones R C Rawlings	The FS(B)2 RAE Bedford, Civil Flight Research Programme. Royal Aeronautical Society Spring Symposium, "Energy Management and its impact on Avionics" London, March 1981.
14	N W Witt	The potential impact of electronic flight deck displays on future Air Traffic Management. Institute of Electrical and Radio Engineers, Colloquium, London, October 1982.
15	R R Newbery	The capability and potential role of airborne avionic systems in Air Traffic Management. Royal Aeronautical Society Spring Symposium, "Air Traffic Management - Current Problems and Future Concepts" London, May 1982.
16	R C Rawlings	The role of Advanced Navigation in future Air Traffic Management. International Congress of Institutes of Navigation, Paris, September 1982.

Flight Control	
DLC and relaxed stability trials	completed January 1978
Non-Linear and Total Energy concepts	in progress 1983
Navigation Systems	
Area Navigation equipment installed	1977
Phase I and II of Industry studies Measurement of radio aids performance	completed Autumn 1978
Trials of VOR/DME, DME/DME with or without ISS	completed Autumn 1979
Vertical profile navigation trials	Autumn 1980 - Spring 1982
Displays	
MONOHUD Flight Tests	Autumn 1979
BAe Weybridge Flight Deck experiments	Commenced 1975
Installation of Monochrome electronic displays	Completed August 1980
Installation of Full Colour electronic displays	June 1981
Navigation Display development	1981 - 1983
Pilot Interfacing Techniques	
Direct Voice Input - initial evaluation	Spring/Summer 1981
Phase II DVI. Installation and Trials	August 1982 - in progress
Radio Management System Installation and Trials	Spring 1983 - in progress
Flight Management	
Phase III Industry Studies	Autumn 1979 - Spring 1983
Four-dimension control	Autumn 1981 - Spring 1983
Holding and time delay control	Autumn 1982 - Summer 1983
Wind correction techniques	in progress
Air Traffic Management	
Data Link installation and coverage trials	Autumn 1982
Experiments with data links	Commenced 1983
Link with S E England ATC simulation	1985/6

TABLE 1. RAE(B)/FS(B)2 CIVIL AVIONICS FLIGHT PROGRAMME SUMMARY

Parameter	Height Hold	Glidepath hold	Touchdown
Range	-	-	0.70*
Glidepath error	-	0.63	-
Height	0.76	-	-
Height rate	-	0.74	0.49
Vertical acceleration	0.83	0.86	-
Pitch attitude	0.78	0.69	0.78*
Pitch rate	0.48	0.47	-
Air speed	0.93*	0.85*	0.75*
Elevator	0.77	0.85*	-
Elevator rate	0.88*	0.95*	-
Throttle	0.96*	0.81	-
Throttle rate	0.87*	0.89*	-

*Not significant at the 5% level

TABLE 2. RATIOS OF STANDARD DEVIATIONS IN AUTOMATIC LANDINGS WITH/WITHOUT DLC

COCKPIT SOUND PRESSURE LEVELS			
RAE/BAC 1-11	On ground (equipment on) During flight	 130K IAS 210K IAS 300K IAS	72 dbA 73 dbA 78 dbA 85 dbA
WESSEX	On ground (equipment on) During flight	 85K IAS	90 dbA 105 dbA

PHASE II RECOGNITION TESTS - ALPHANUMERICS		
Conditions	Microphone used	% error rate
Laboratory	Shure SM10 Airlite 62 Boom Throat Amplivex Oxygen mask V2	0.64 0.91 0.67 1.35
Flight	Shure SM10 Airlite 62 Boom	0.65 2.1

PHASE II RECOGNITION TESTS - DISPLAYS OPERATION IN FLIGHT				
Microphone used	PILOT A		PILOT B	
	% error rate	sample	% error rate	sample
Airlite 62 Boom	1.76	1251	1.96	1073
Oxygen Mask	0.78	128	2.88	417
Throat Amplivox	3.77	265	3.31	242

TABLE 4. SPEECH RECOGNITION RESULTS

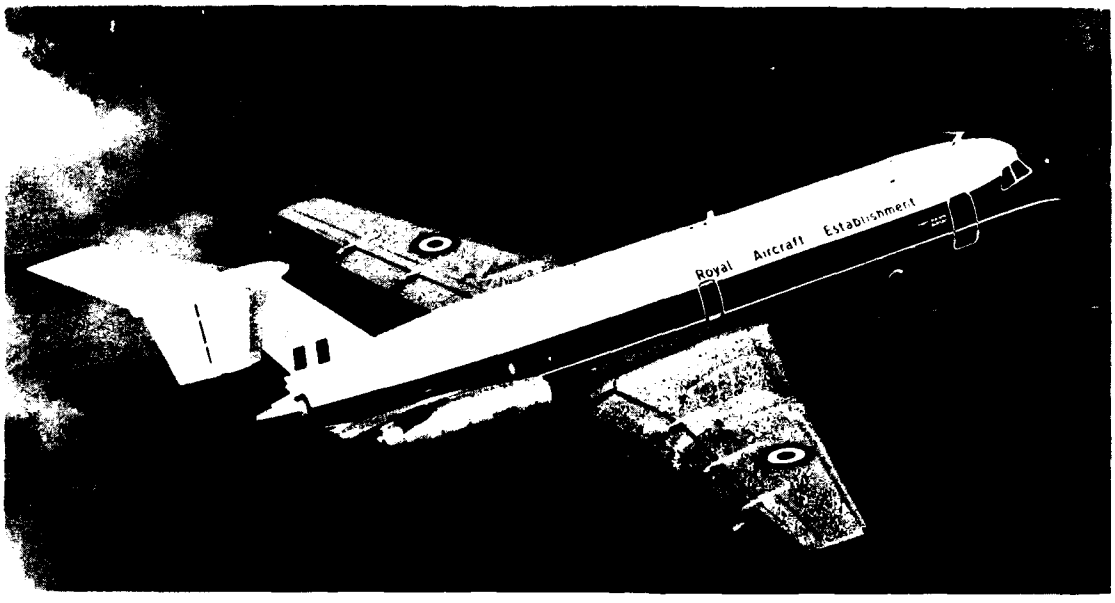

FIG 1. RAE(B) BAC 1-11

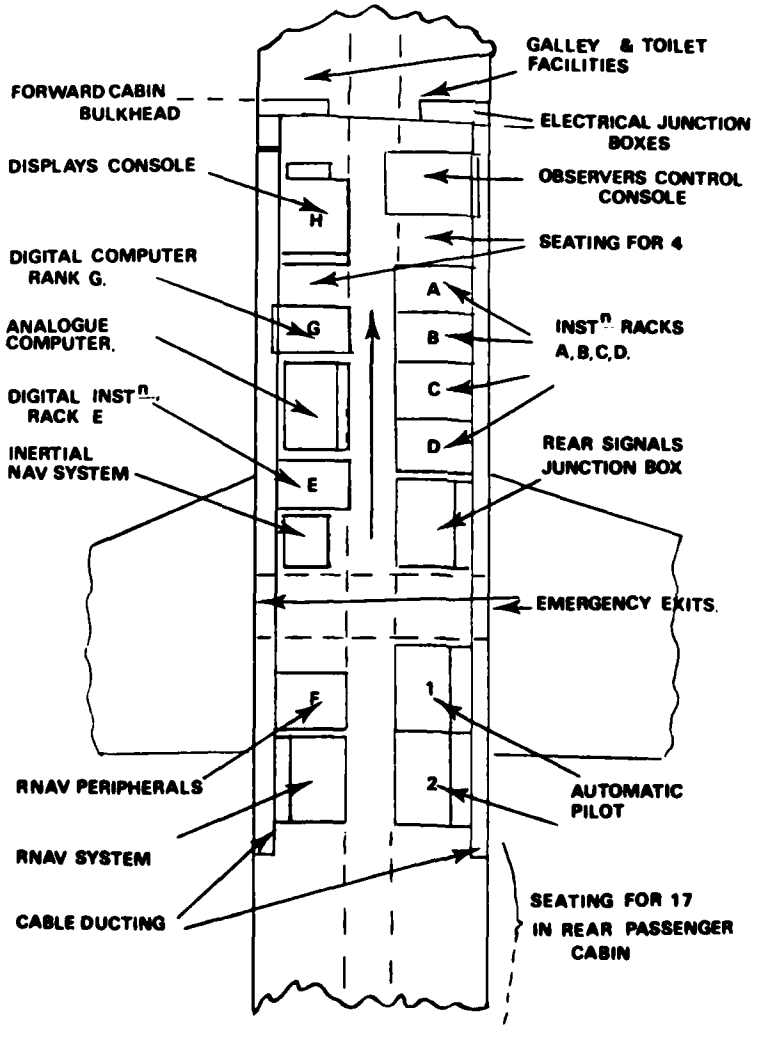

FIG 2. CABIN LAYOUT

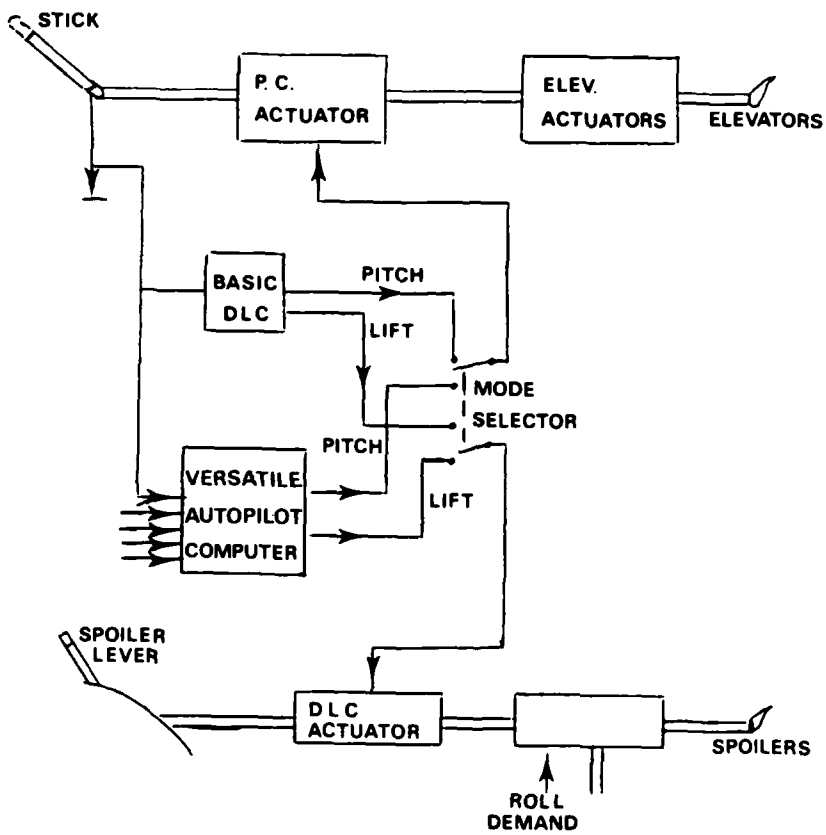

FIG 3 IMPLEMENTATION OF DIRECT LIFT CONTROL IN BAC 1-11

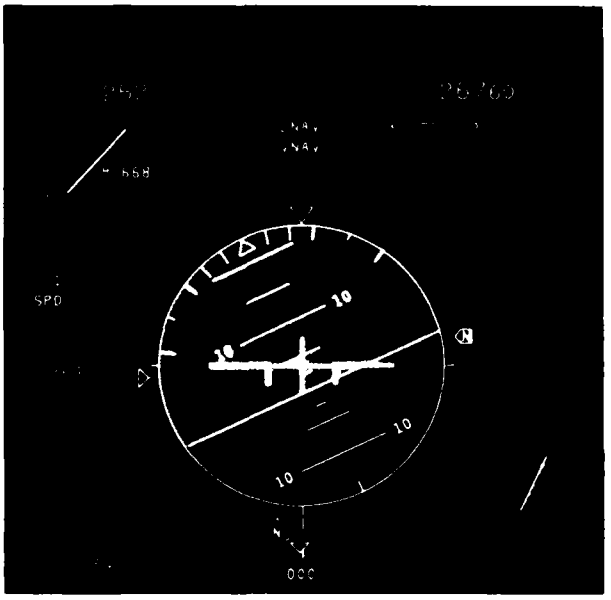

Fig. 4 Colour primary flight display format

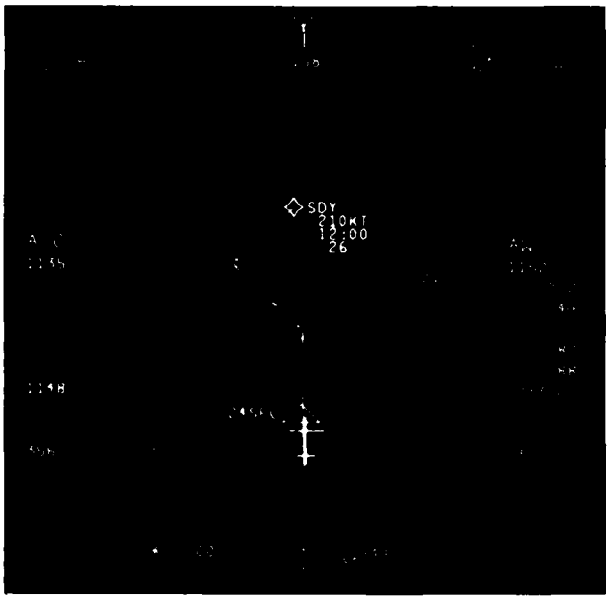

Fig. 7 Map display including four-dimensional navigation data

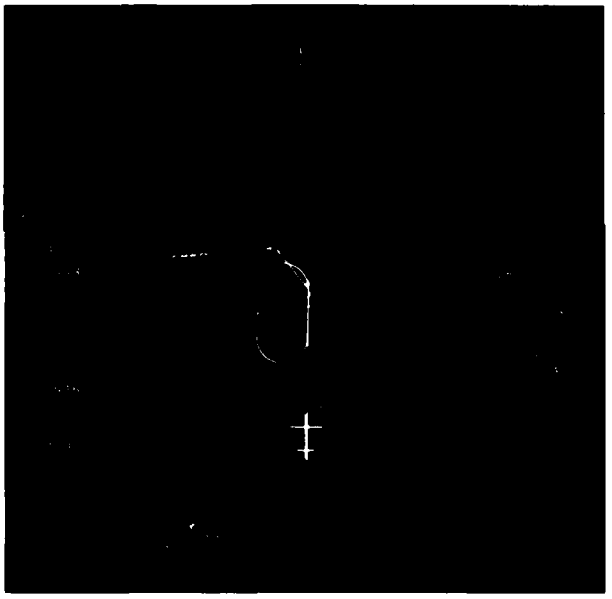

Fig. 5 Basic colour map display

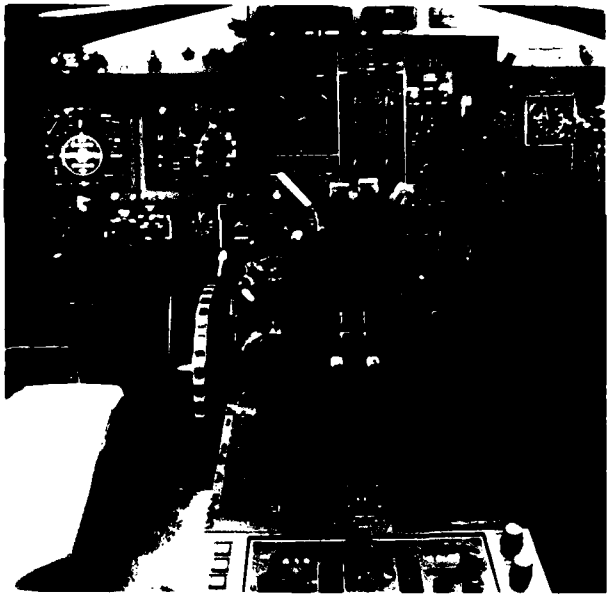

Fig. 8 Colour EFIS displays on the flight deck of the RAE BAC 1-11

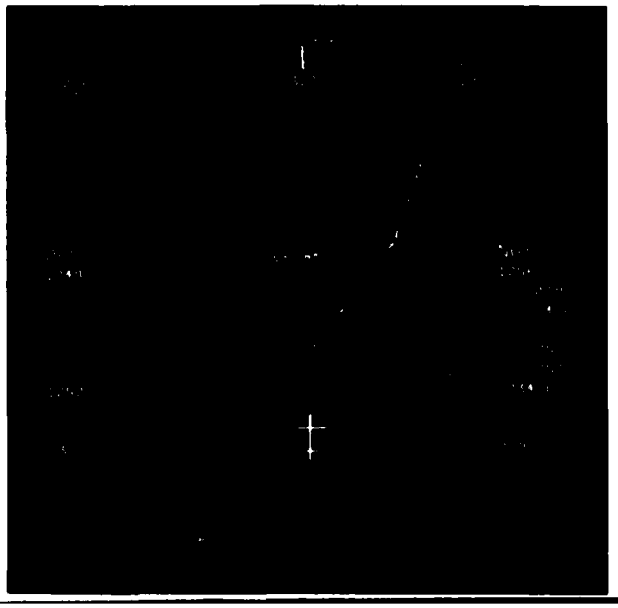

Colours used for the cursively written symbology are described by the CIE coordinates

	x	y
Red	0.659	0.322
Green	0.290	0.588
Blue (Mixture of blue and green primaries)	0.178	0.166
Cyan	0.190	0.238
Yellow	0.490	0.439
Magenta	0.282	0.172
White	0.333	0.333

The shading used for the sky and ground segments of the attitude indicator on the PFD are written at lower intensity and have CIE coordinates

	x	y
Sky shading	0.256	0.276
Ground shading	0.256	0.276

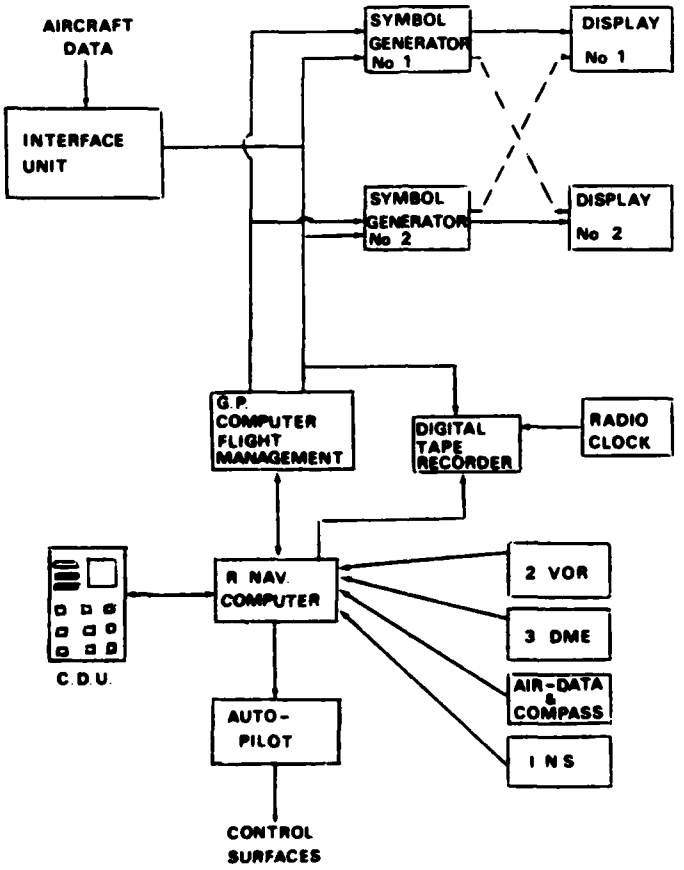

FIG 9. R NAV/DISPLAY SYSTEM

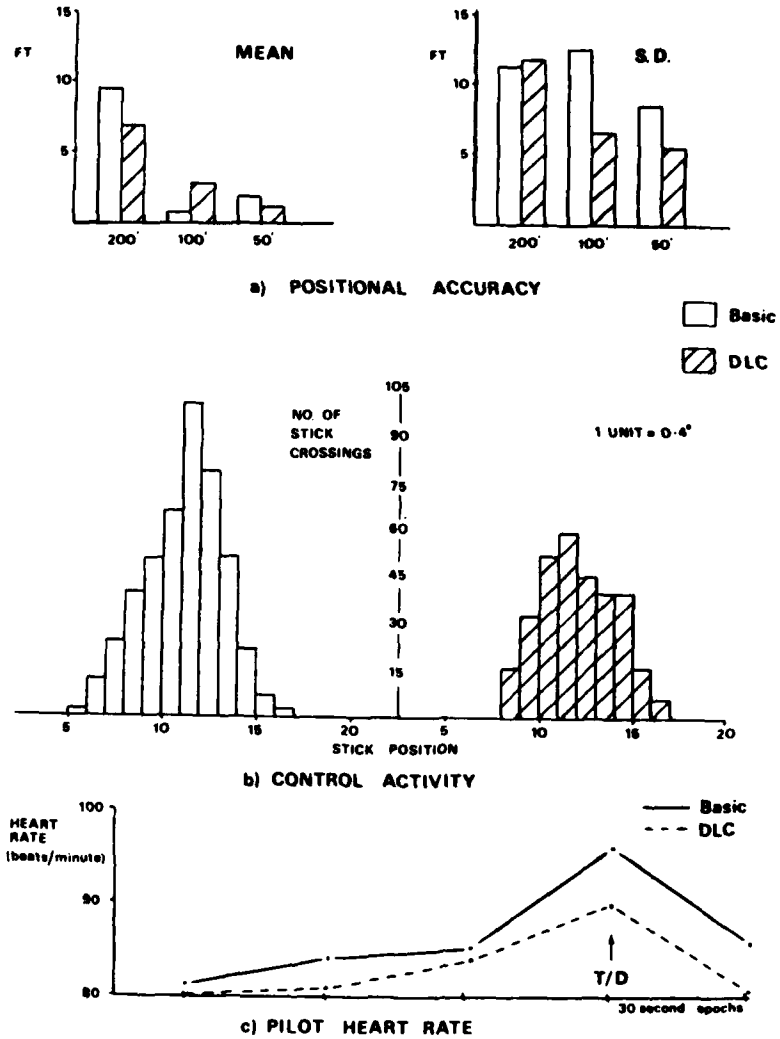

FIG 10. MANUAL DLC RESULTS

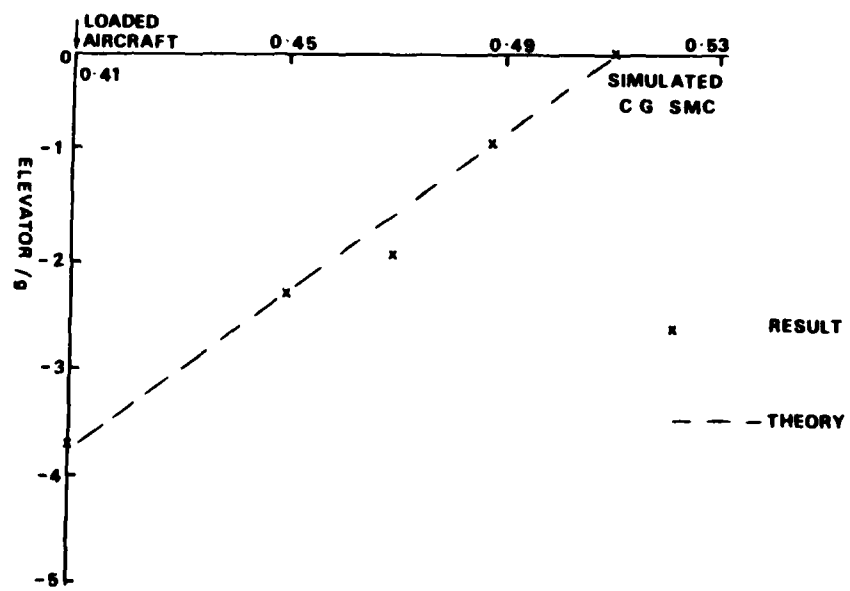

FIG 11. AFT Cg STABILITY TRIALS

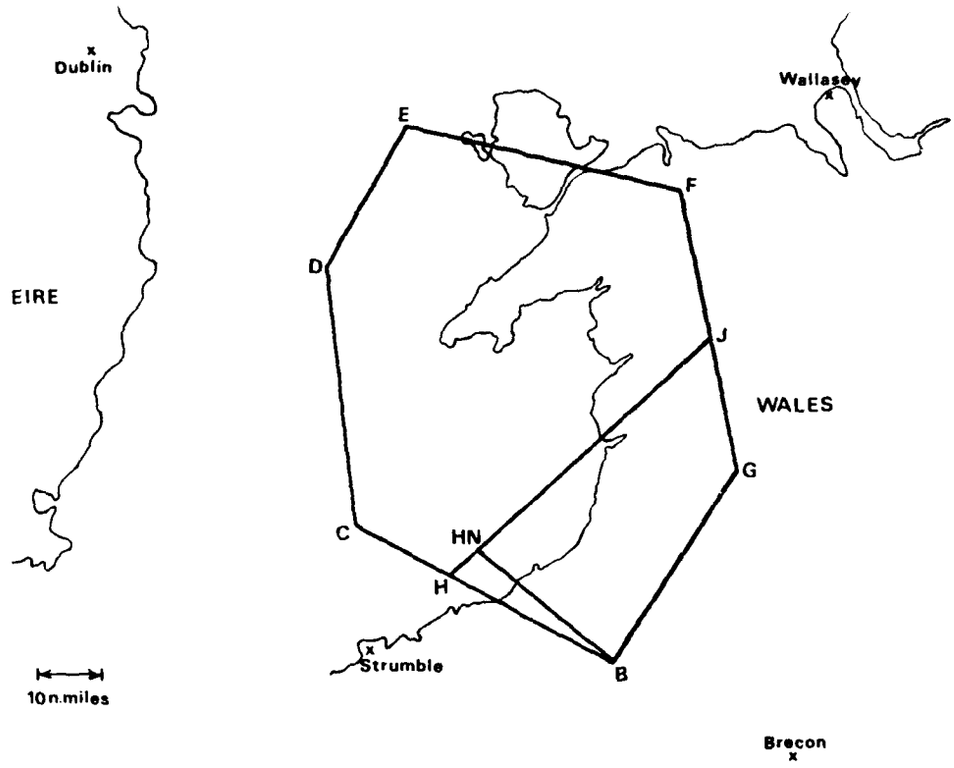

EN-ROUTE ASSESSMENT TRACKS

FIG 12. EN-ROUTE ASSESSMENT TRACKS

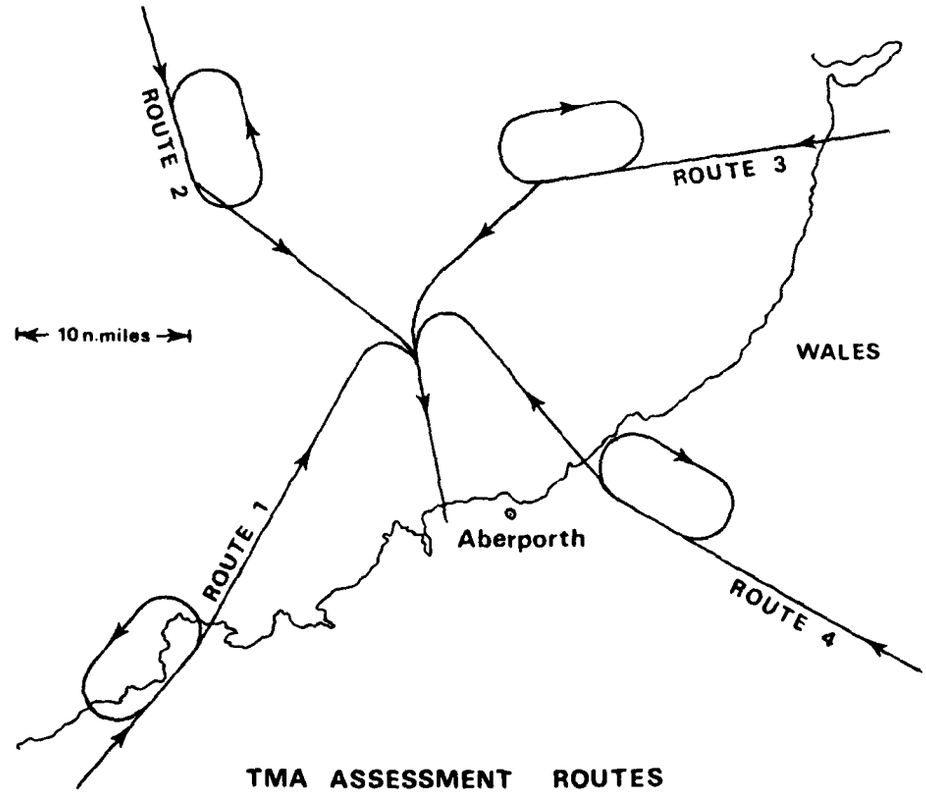

TMA ASSESSMENT ROUTES

FIG 13. TMA ASSESSMENT ROUTES

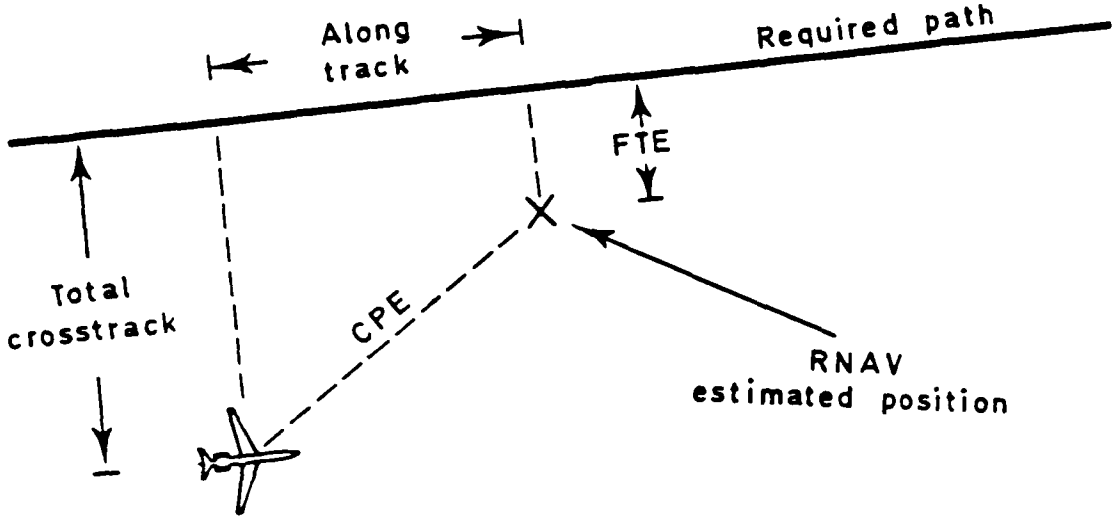

FIG 14. LATERAL ERROR COMPONENTS

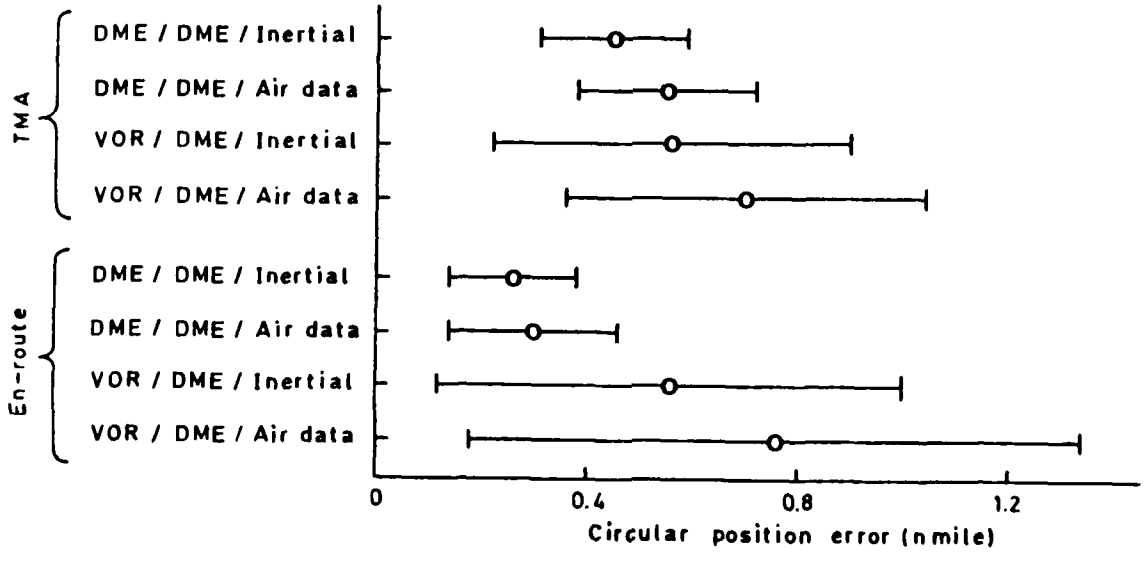

FIG 15. MEAN & SD OF CIRCULAR POSITION ERROR

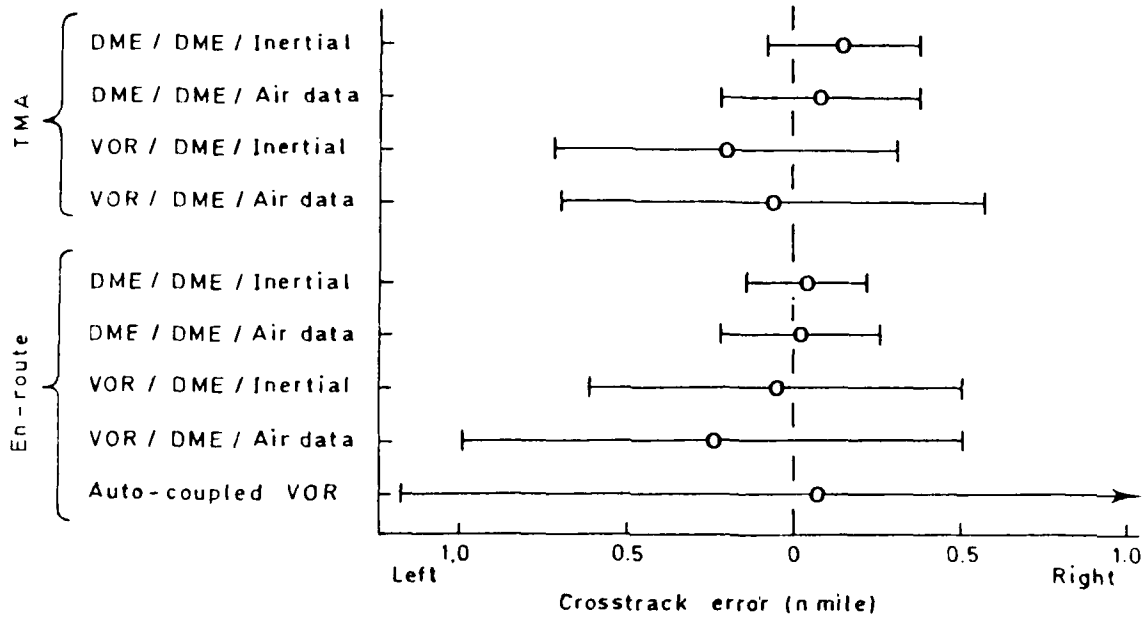

FIG 16. MEAN & SD OF TOTAL CROSSTRACK ERROR

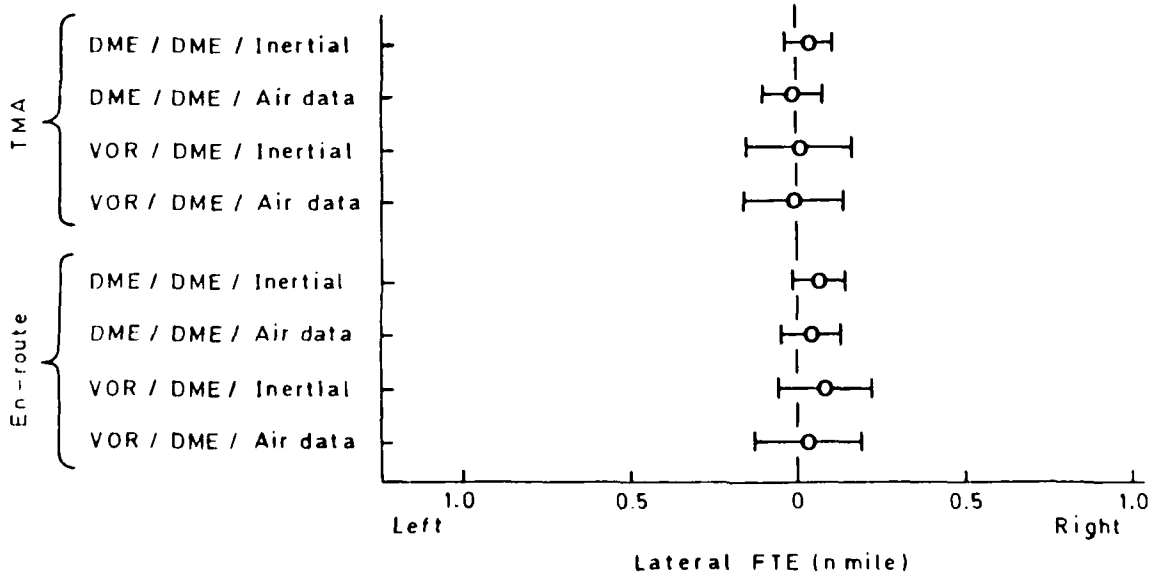

FIG 17. MEAN & SD OF LATERAL FLIGHT TECHNICAL ERROR

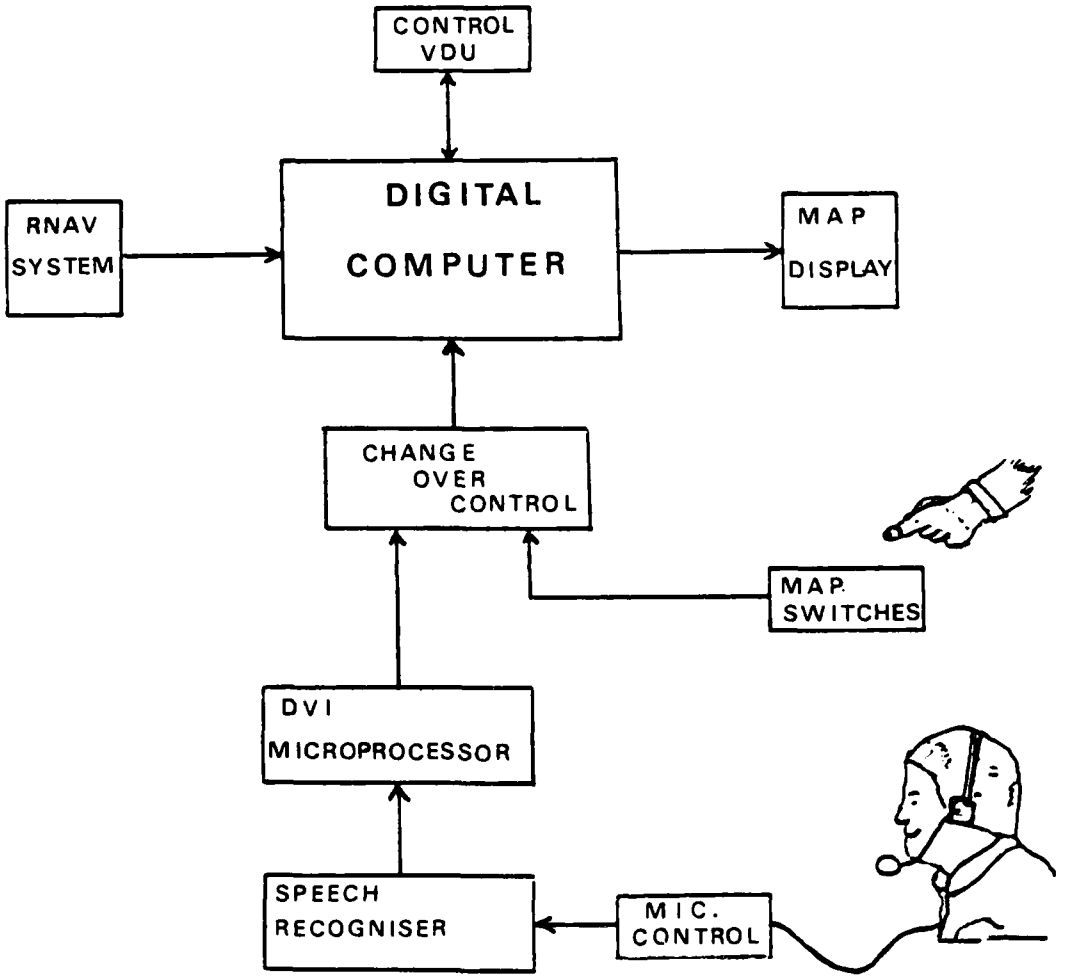

FIG 18. VOICE CONTROL OF ELECTRONIC MAP DISPLAY

Guidance and Control Research Flight Testing with HFB 320 Test Aircraft

by
V. Adam, W. Lechner
Deutsche Forschungs- und Versuchsanstalt
für Luft- und Raumfahrt e.V.
Flughafen
D-3300 Braunschweig
Federal Republic of Germany

1. INTRODUCTION

Flight testing is the last and decisive phase in the development process of new aircraft guidance and control methods, procedures and equipment to give evidence of the expected functional performance. No highly elaborated ground-based simulation can replace this phase unless there is complete knowledge of the aircraft system characteristics and no restriction on expenditure. On the other hand there is no doubt that simulation including most of the real system hardware is a necessary phase to pass before flight testing can be started. This is the means for step by step system validation on the ground under reproducible conditions.

The objective of this article is to report on some of the test activities with utilization of the test aircraft HFB 320 of the DFVLR (Fig. 1). There is a great number of test programs conducted by two institutes of the DFVLR through the past with this aicraft, including in-flight simulation, direct lift control, side stick control, fly-by-wire and integrated navigation [1,2,3,4,5]. This article will be focussed on experiments recently accomplished to investigate automatic control of transport aircraft for which the HFB 320 test aircraft can be considered as representative.

In the following the ground-based experimental system and the flight test equipment will be briefly described as well as some examples of test programs in order to illustrate the process and what makes testing worthwile.

2. GROUND-BASED TESTING ENVIRONMENT

The preparation of flight tests can be divided into a number of working phases as shown in Fig. 2. Depending on the volume and complexity of the experimental task there can be an overlap between subsequent phases. Insufficient specifications or upcoming unexpected results may lead to reconsider or restart the preceding phase or to go even further backward in the development process. This underscores the necessity of verification and validation to be executed along with all phases. Typical sources of errors as for initial design phase and design improvement are incomplete specifications, changes in interfacing characteristics because of hardware modifications or discrepancies between the characteristics of the simulated system compared to those of the real system.

The flight experiment is, in general, not carried out as a closed-shop operation at the DFVLR. The engineers who are responsible for the experiment are involved in about all working phases mentioned. These are according to Fig. 2:

a) Task definition, i.e.

- Description of test subject, experimental objective, methods and techniques to be applied.
- Definition of parameters to be evaluated and corresponding measurements.
- Indication of possible difficulties and risks.
- Definition of necessary test site support requirements such as data link and radar tracking etc.

With respect to the operational limits of the aircraft and restrictions in air space Air Traffic Control and the test pilots must be consulted for the planning of the flight tests.

b) Concept of realization, i.e.

- Overall structure of the experimental system in the airplane and on the ground.
- Modifications to the baseline system.
  (instrumentation, interfaces, software)
- Validation and certification procedures.
  (laboratory tests, ground-based simulation runs, first flight test, preflight test, flight test)
- Documentation requirements.

c) Development and composition of experimental system, including

- Functional tests of subsystems.
- Integration of subsystems.

d) Ground-based simulation, i.e.

- Simulation including real experimental system hardware.
- Simulation of complete test sequences, including pilot inputs, parameter variations.
- Checking for violations of operational limits.
- Functional test concerning the derivation of status and error messages.
- System ground tests of the experimental system onboard the aircraft using a simplified dynamic model of the aircraft (first flight test).

The ground-based experimental system used for simulation and software development is shown in its main features in Fig. 3. It includes a copy of the main experimental system components of the airplane in order to deal with the same interface peculiarities on the ground as they are valid for the on-board system.

3. ON-BOARD SYSTEM

The basic aircraft HFB 320 has got a purely mechanical control system for the primary control axes without any hydraulic boosters. Only landing flaps and spoilers are driven by hydraulic actuators. The requirements for the investigation of experimental digital fly-by-wire systems and in-flight simulation have led to the experimental outfit with fly-by-wire control by means of electrohydraulic actuators for the primary control surfaces and electromechanical actuators for engines, flaps and spoilers. This yields the potential for driving primary and secondary controls by electrical signals as shown in Fig. 4. The experimental control system actuators are linked to the basic control system by clutches and shear elements in order to provide the means for deliberate disconnecting in the case of emergency or control force overloading.

The control wheel in front of the seat on the right hand side of the cockpit is dedicated to the test pilot. It is disengaged from the basic mechanical control system and is equipped with transducers for the pilot control inputs. The transducer signals are fed into the experimental system computer and the computer outputs in turn are driving the actuators. Both the conventional control column and the three-axes side-grip controller can alternatively be used as pilot inputs (Fig. 5). Conventional control by means of the basic mechanical control system is available from the left hand pilot seat, where the safety pilot is seated. He can disengage the fly-by-wire control inputs at any time in case of events interfering with safety requirements, for instance in case of fly-by-wire malfunction. The fly-by-wire control system should not be engaged close to the ground and under IMC because of lacking system redundancy.

In addition to the fly-by-wire system, the complete on-board experimental equipment comprises the necessary components for digital computation, pilot interfacing devices and a comprehensive sensor system including signal conditioning and filtering units as well as a telemetry transmitter (Fig. 6). Fig. 7 demonstrates the signal flow between the on-board devices and the telemetry ground station via radio link. Computer 1 (Honeywell H316) in Fig. 7 constitutes the central data-processing component on-board the airplane. It controls the entire data flow between all experimental system devices. It reads the sensor signals, calculates the filter and control algorithms of the experimental automatic flight control system including certain fail-safe routines, processes the status words of the mode control panel of the automatic flight control system and drives the instruments on the test pilot's experimental instrument panel. Computers 2 and 3 do not belong to the permanent experimental equipment. They are utilized to expand the computational capabilities in the airplane for flight trials on four-dimensional (4-D) guidance that will be described in detail later. Computer 2 (Norden 11/34 M) carries out the 4-D flight path planning calculations and communicates with computer 1 and computer 3 via DMA. Computer 3 (LSI 11/23) functions as a symbol generator for the 4-D map display. As part of the on-board experimental system an IBM-compatible tape recorder is installed for computer program transfer between ground-based and on-board computers and for the recording of flight data. By this means the data can be fed into post flight evaluation routines running on DFVLR main computer facilities. There is sufficient capacity to record 120 signals sampled with 10 Hz for about 90 minutes.

The sensor system (Fig. 8) consists of a digital air data computer (DADC), an inertial navigation system (INS), DME-, VOR/ILS-receivers, rate gyros, accelerometers, displacement transducers and a front boom mounted flight log.

4. EXPERIMENTS WITH AN INTEGRATED DIGITAL FLIGHT CONTROL SYSTEM FOR TRANSPORT AIRCRAFT

As a result of a cooperative venture with german industry an integrated digital guidance and control system for transport aircraft has been developed. The DFVLR was mainly responsible for the development and experimental testing of the flight control modes based on a commonly agreed control system operational concept and mode structure. The objective was to effectively relieve the pilot by use of improved automatic control modes as well as increased guidance accuracy. A great number of modes were newly developed, in particular for the low speed flight regime with landing flaps extended. Table 1 gives the particulars of the hierarchically structured control modes, from semi-automatic control wheel steering modes to fully automatic control of certain flight phases designated as functions. The experiments had to provide evidence of the performance of both each single control mode and all available combinations of compatible modes. The envelope was confined to airspeeds between 130 and 290 knots and altitudes from 2000 feet at the lowest up to flight level 130.

For the first phases of flight testing it had to be taken into account that stability problems could occur. Hence some means for varying control law parameters during flight had been provided for. Besides the need of varying parameters modifications to the computer programs could be foreseen to happen rather frequently in the course of the entire development process including the flight tests. Therefore a higher order language (FORTRAN IV) was used for coding. This facilitated software design and documentation of software changes. The complete software package is modularly structured in order to ease transparency as well as step by step design and system extension. For illustration Fig. 9 shows the modular structure in its correspondence to the functional segments of the control system. It is shown for instance which guidance commands, control loops and actuator commands are calculated by which module (shaded blocks) in case of the 4-D NAV mode being engaged. The software modules are activated by two 16-bit mode control words NBW1 and NBW2 of the mode control logic. This logic is driven through depressing push buttons on the mode control panel installed in the glareshield, the deflection of the control column and some additional sensor data. It is taking care of compatibility for modes being engaged.

The control system development and testing was sequentially carried out for different sets of control modes (Table 1). The flight test trials were scheduled accordingly (Table 2).

CONTROL WHEEL STEERING MODES		CONTROL MODE	PHASE OF FLIGHT TEST 1	2	3	4
CWS $\dot{\theta}$	pitch rate	CWS $\dot{\theta}$	x	x		
CWS $\dot{H}$	vertical acceleration/vertical speed hold	CWS $\dot{H}$	x	x		
CWS $\dot{\Phi}$	roll rate/bank angle hold	CWS Φ	x	x		
AUTOMATIC MODES						
ALT HOLD	ALTITUDE HOLD	ALT HOLD	x	x		
ALT ACQ	ALTITUDE ACQUIRE	ALT ACQ	x	x		
HDG HOLD	HEADING HOLD	HDG HOLD	x	x		
HDG ACQ	HEADING ACQUIRE	HDG ACQ	x	x		
NAV	VOR NAVIGATION	NAV		x	x	
VC	CAS SELECT	VC	x	x	x	
VS	MULTIPLE OF STALLING SPEED	VS			x	
VX	STEEPEST CLIMB	VX			x	
VY	FASTEST CLIMB	VY			x	
FUNCTIONS						
AUTOLAND	AUTOMATIC LANDING APPROACH	AUTOLAND		x	x	
GO AROUND	GO AROUND	GO AROUND			x	
3-D NAV	3-D NAVIGATION	3-D NAV				x
4-D NAV	4-D NAVIGATION	4-D NAV				x

Table 1: Control modes

Table 2: Planning of flight test schedule

Specific maneuvers and flight path profiles were selected for the flight experiments extending the experimental flight envelope step by step (Fig. 10).

The flight test program started in stationary horizontal flight conditions at FL 100 and 170 knots airspeed. The objective for the first flight tests was to verify the control law parameters of pitch, roll and yaw control with respect to stability. The following maneuvers were flown during this phase:

- Climbs and descents utilizing the control wheel steering mode CWS $\dot{\theta}$ and transition to ALT HOLD.
- Heading changes utilizing control wheel steering mode CWS $\dot{\Phi}$ and transition to HDG HOLD.
- Climbs and descents by ALT ACQ and commanding different climb and descent rates.
- Heading changes by HDG ACQ.
- Engaging and disengaging of the ALT ACQ mode during level flight, climb and descent.
- Engaging and disengaging of the HDG ACQ mode during straight and curved flight.
- Climbs and descents by control wheel steering mode CWS $\dot{H}$ and transition to ALT HOLD or ALT ACQ and vice versa.
- Speed change in level flight.

During the second test phase additional modes were incorporated:

- VOR NAV, i.e. automatic inbound tracking of preselected VOR radials.
- AUTOLAND, i.e. automatic landing approach using the microwave landing system capability of DLS. Fig. 11 shows a typical test flight pattern. The approach flight on steep and curved approach profiles were performed at higher altitudes for safety reasons. Their "touchdown point" was supposed to be at an altitude of 2000 ft or above.

The third test phase was focussed on the extension of the flight regime in airspeed and altitude (see Fig. 10). The interaction between airspeed and altitude control during continuously changing airplane configurations (i.e. flap setting) were investigated in more detail. Also new automatic modes for the control of aerodynamic state variables such as angle of attack rather than airspeed were tested. Fig. 12 shows a typical sequence of climb and descent profiles and pilot input actions during tests of a Go Around (GA) mode with automatic flap retraction.

The last test phase was dedicated to the 3-D NAV and 4-D NAV functions. These functions are working on the automatic control modes tested before. While automizing entire flight phases they reduce pilot inputs to a minimum.

In the following some flight test results are discussed:

Fig. 13: Control wheel steering CWS $\dot{H}$ and CAS select mode VC

A descent flight phase is shown. The upper time history illustrates the pulse type pilot inputs on the control column over short time intervals to set the command value for the descent rate which entailed execution by the automatic control system. The engine pressure ratio reflects the effect of commanded descent rate on engine thrust in order to avoid speed deviations. Airspeed did not deviate beyond 1 knot from the commanded value.

Fig. 14: ALT ACQ, CAS select mode VC and flap setting

By use of the ALT ACQ mode pilot handling of flight level changes is enhanced. The pilot inserts the desired flight level via the keyboard of the Mode Control Panel and adjusts the commanded vertical speed (climb or descent rate) by a toggle switch. As long as the switch is pushed down from neutral the descent rate command is increased and the aircraft is parabolically transitioning into the descent. As soon as the selected new flight level is approached, the descent rate command is automatically reduced. This reduction in descent rate will be started at suitable time in advance depending on the descent rate command and the preprogrammed vertical acceleration limit. The interception of the new flight level becomes parabolic, too, i.e. the vertical acceleration remains constant during this phase. Therefore, the overshoot of the new flight level is independent of the selected vertical speed as is evident from the comparison between the descent and climb sections in Fig. 14. In the lower time history in Fig. 14 the flap setting is plotted indicating retraction from 40° to 20°. Resulting speed or altitude deviations are insignificant. The maximum deviations in altitude of about 20 ft occur during the instationary transition phases when departing from a flight level and approaching a new one.

Fig. 15: AUTOLAND with CAS select mode VC

An AUTOLAND approach and virtual "landing" is shown. For safety reasons the virtual "landing" took place at 3000 ft of altitude. Therefore speed was not reduced during virtual "flare". The descent to "landing" was performed along a precalculated flight path with a flight path angle of 4° and parabolic transition off and into level flight. The landing flaps were set to 40° and the commanded airspeed was 140 knots.
In AUTOLAND the aircraft intercepted the runway centerline radial of the microwave landing system DLS. During this trial the aircraft started the approach in level flight and on a track perpendicular to the centerline radial. When the airplane arrived a lateral distance of about 1.6 NM from the centerline the intercept angle was reduced to 25°. Interception speed adjustment was carried out by use of the ground speed signal from the inertial navigation system. The maximum lateral deviation from the centerline was about 75 ft when windshear was encountered. Besides that the lateral deviation was less than 20 ft. The vertical profile of the interception path into descent is calculated when the AUTOLAND mode is engaged.

Fig. 16: 4-D NAV

In the 4-dimensional guidance mode the digital flight control system guides the aircraft automatically on a pre-calculated flight path with high precision is space and time. The aim was to attain a time-of-arrival (TOA) error at the merge gate of less than + 5 s. Such accuracy level is necessary in order to allow for the precise control of minimum separation margins and thus efficient use of the available approach capacity in high density TMA's.

When the HFB 320 test aircraft is entering the TMA the airborne 4-D navigation computer calculates a 4-D approach flight path taking into account specific speed and altitude profiles and the actual wind situation of the respective area. The altitude profile is composed of level flight sections and descent sections at constant vertical speed. Speed reduction takes places at a constant deceleration rate, using a higher rate in level flight than in descent. The wind is measured by the evaluation of the vector difference of ground speed and true airspeed. The corresponding signals are provided by an inertial navigation system and a digital air data computer. Wind modelling and prediction along the planned 3-dimensional flight path is carried out by application of Kalman filtering techniques.

TOA control can be realized by speed control or altering the flight path. Speed control is not applied, because speed command is determined by fuel efficiency aspects. A typical 4-D flight path is shown in Fig. 16.

When the 4-D approach was started the aircraft turned towards the fan waypoint (FP). The fan area to be entered from FP allows for limited heading changes for the purpose of time control. The suitable heading towards the centerline is calculated. Shifting the centerline intercept waypoint (CP) along the extended centerline results in a corresponding TOA error compensation. During this test flight a first flight path update was performed at waypoint UP_1. A second and last TOA error compensation took place at waypoint UP_2.

The compensation of the time error becomes necessary, if the time error exceeds the predefined upper or lower error bound, as shown in Fig. 17. Fifty automatic 4-D approaches were performed with different airspeed and altitude profiles. Several types of windmodelling and prediction techniques have been tested, resulting in verifying a TOA lo-error of less than $\pm$ 5 s.

On the basis of the integrated digital guidance and control system as discussed in the foregoing paragraphs, a flight test program on a sensor redundancy management concept was conducted, too. This experiment will be described in the following.

The concept investigated features sensor duplication instead of triplication for meeting the requirement of keeping the system fully operative in case of one sensor failure (1 fail-op), a typical requirement for CAT III automatic landing. The lacking third sensor is compensated for by analytical means (Fig. 18). Each of the duplicated channels of sensor output signals are feeding observers, i.e. mathematical models of the aircraft motion, which are driven by the same control signals (u) as the real aircraft. The observer output constitutes estimates of the aircraft motion state variables which are measured by the sensors. In case of a sensor failure, a discrepancy will show up between measured value and the sensor signal estimate, which in turn activates the failure detection logic in order to disconnect the defective sensor from the feedback control loop.

The objective of the flight experiment was to validate the concept under real conditions after extensive foregoing simulation tests. Three major types of flight test items were planned.

a) Test flights for establishing the thresholds of the failure detection logic. The thresholds have to be set dependent on the discrepancy between modelled and real airplane behaviour also taking into account the noise level due to air turbulence representative for the respective aircraft and the specific automatic control system. Different maneuvers utilizing semiautomatic and fully automatic control modes were performed.

b) In-Flight simulation of two different types of failures

   - slow or swift signal drift and

   - step input in each of the singal paths of one of the duplicated sensor packages without activating the switching from the defective sensor to the healthy one.

c) In-Flight simulation of failures as carried out under the foregoing paragraph, but with switching over from the faulty signal to the healthy signal.

During the ground tests it became evident that the step function failure type could lead to extreme control commands possibly causing breakage of the shear elements which mechanically link the experimental system to the basic aircraft control system. In order not to jeopardize the overall goals of the experiment within the limited number of test flights at disposal the second failure type was relinquished.

The computation of the algorithms for both observers and the failure detection logic was carried out in computer 2 (see Fig. 3 and Fig. 7) whereas the failure simulation and the sensor switching algorithm were implemented in computer 1, in addition to the algorithms for the integrated guidance and control system as described earlier (Fig. 19).

The observers provide estimates of the following sensor signals:

Θ	pitch angle	a_y	lateral acceleration
Φ	bank angle	CAS	calibrated airspeed
p	roll rate	TAS	true airspeed
q	pitch rate	$\dot{H}$	vertical speed
r	yaw rate	H	altitude

There are no duplicated sensors available on the aircraft. Therefore, computer 1 simulates the second sensor package by feeding the signals of the simplex sensor sources into both observer channels. An additional error signal can be fed into one of the observer input channels for failure simulation purposes.

Fig. 20 shows the time history of the drifting error signal being applied. The absolute error signal for each sensor is derived in the course of the ground-based simulation tests by allocating a multiplicative coefficient.

The ground-based simulation tests have demonstrated that the experimental hardware and software functions as required. All simulated errors were detected and the disabled sensors were disengaged. Since the experimental failure detection system including the failure simulation could effect the basic aircraft controls only through the same unchanged interfacing between fly-by-wire system and basic controls as used for earlier experiments, no additional certification effort was necessary. Fig. 21 presents a typical result obtained from the flight tests. In this case an airspeed sensor failure is detected through the increasing difference between measured and modelled pitch angle.

5. CONCLUSION

The evidence for functional fulfillment of the requirements of new designs and developments in guidance and control systems, hardware and software, has to be pursued through all phases of the development process concluded by the flight tests. The DFVLR-HFB 320 test aircraft is well suited for the flight testing task because of its comprehensive sensor system, the computer outfit and the fly-by-wire capability. Some examples of flight experiments have been briefly described to illustrate the aircraft's flexible utilization for a great variety of experimental tasks within the schemes commonly considered as necessary for modern guidance and control equipment test and validation.

However, it became obvious that experiments of highly complex experimental system including redundancy will exceed the potential of this airplane. Therefore, a new test aircraft (called ATTAS - Advanced Technologies Testing Aircraft System) allowing for more comprehensive aircraft guidance and control experiments is being developed on the basis of the VFW 614 airplane.

6. REFERENCES

|1| Lange, H.-H., Flight Test Results of the Model Simulation Controller for the HFB 320 for In-Flight-Simulation of the A 310 Airbus, Techn. Transl. ESA-TT-660 (1981), Translation of DFVLR-Mitt. 79-13.

|2| Hanke, D., In-Flight Handling Qualities Investigation of A 310 Airbus DLC-Configurations on Landing Approach Using the DFVLR-HFB 320 Variable Stability Aircraft. Techn. Transl. ESA-TT-630 (1980), Translation of DFVLR-FB 79-18.

|3| Wilhelm, K., Schafranek, D., In-Flight Investigation of the Influence of Pitch Damping and Pitch Control Effectiveness on Landing Approach Flying Qualities of Statically Unstable Transport Aircraft, DFVLR-FB 84-12, 1984.

|4| Onken, R., Joenck, H.-P., Tacke, L., Gottschlich, M., Digital Fly-By-Wire Control System with Self-Diagnosing Failure Detection, AGARD Conference Proceedings No. 137 on Advances in Control System, Geilo, Norway, 1973.

|5| Stieler, B., Winter, H., Advanced Instrumentation and Data Evaluation Techniques for Flight Tests. Proceedings of the 11th ICAS Congress, Vol. 2., 1978.

|6| Adam, V., Lechner, W., Investigations on Four-Dimensional Guidance in the TMA. AGARD Conference Proceedings No. 340, Lisbon, Portugal, 1982.

|7| Adam, V., Leyendecker, H., Control Law Design for Transport Aircraft Flight Tasks, AGARDograph No. 251, Theory and Application of Optimal Control in Aerospace Systems, 1981.

|8| Lechner, W., Adam, V., A Concept for 4-D Guidance of Transport Aircraft in the TMA; 13th ICAS Congress, Seattle, USA, 1982.

|9| Adam, V., Flight Control Modes for Control of Aerodynamic State Parameters, 12th ICAS Congress, Munich, Germany, 1980.

|10| Stuckenberg, N., An Observer Approach to the Identification and Isolation of Sensor Failures in Flight Control Systems, ESA TT 738, 1982.

|11| Stuckenberg, N., A diagnosis scheme for sensors of a flight control system using analytic redundancy, AGARD Conference Proceedings No. 349, Toulouse, France, 1983.

WINGSPAN	14.49 M	ENGINES	GE CJ 610-5
LENGTH	16.61 M	TAKE OFF THRUST	2680 KP
WING AREA	30.0 M^2	SPEC. FUEL CONSUMPTION	0.96 KP/KP/H
EMPTY WEIGHT	5600 KP	MAX. SPEEDS V_{MO}	320 KIAS
OPER. EMPTY WEIGHT	6500 KP	M_{MO}	0.76
MAX. TAKE OFF WEIGHT	9200 KP	APPROACH SPEED 1.3 V_{SO}	120 KIAS
		MAX. ALTITUDE	*38000 FT*

Figure 1: Technical data of the HFB 320 test aircraft

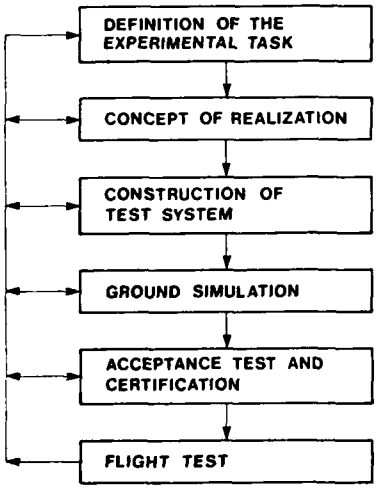

Figure 2: Working phases of flight test preparation

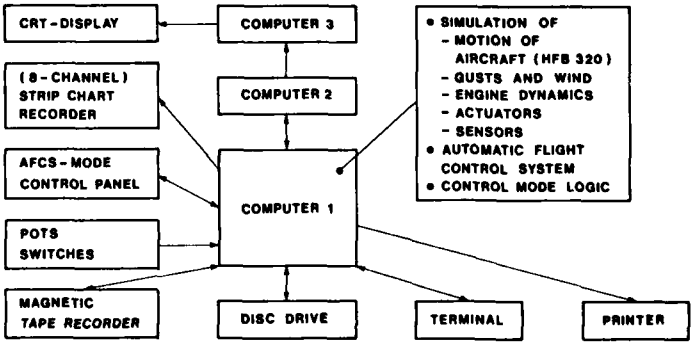

Figure 3: Ground-based experimental system for simulation and software development

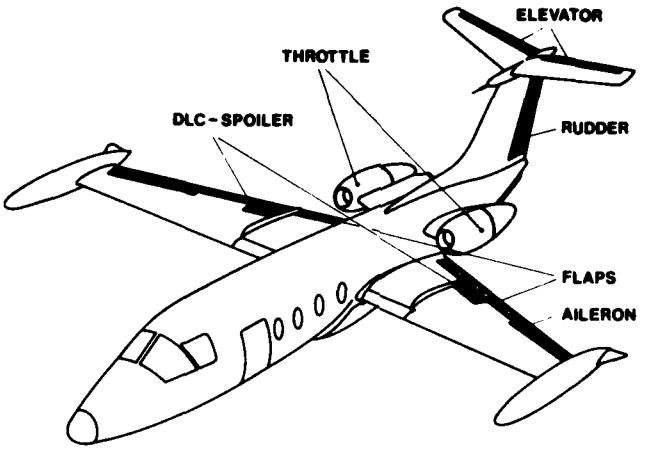

Figure 4: Electrically driven controls of the test aircraft HFB 320

Figure 5: Test pilot's seat with doubled side-grip controllers

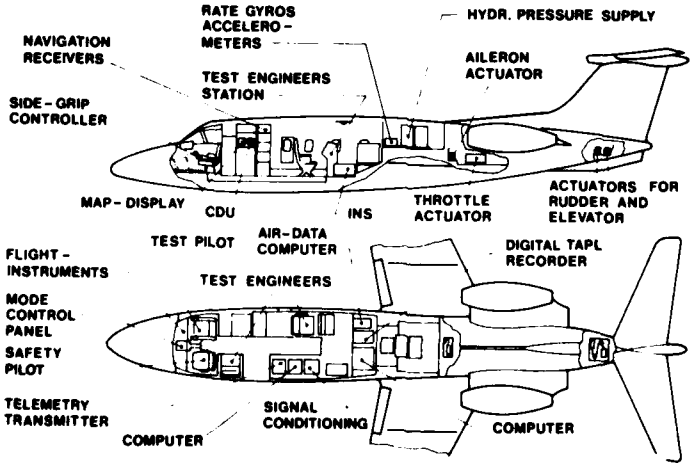

Figure 6: Airborne experimental equipment

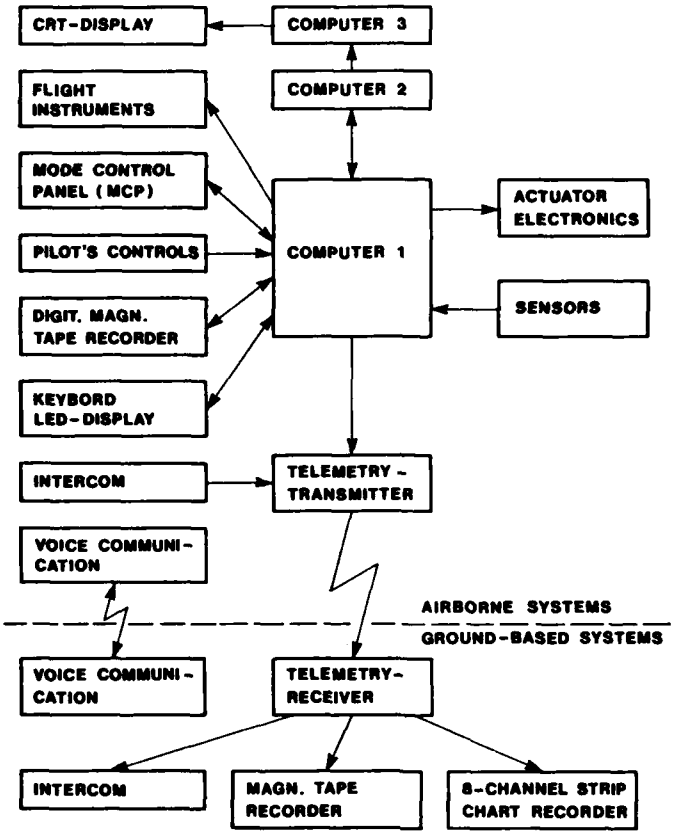

Figure 7: Signal flow between system components in the airplane and on the ground

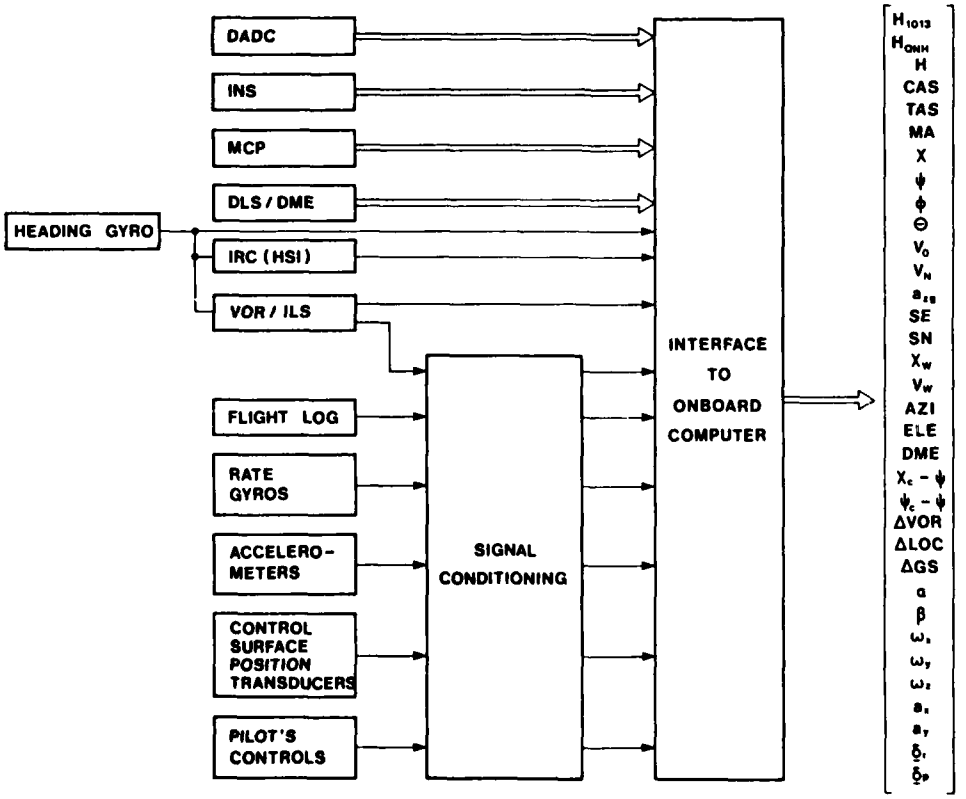

Figure 8: Sensor system of the HFB 320 test aircraft

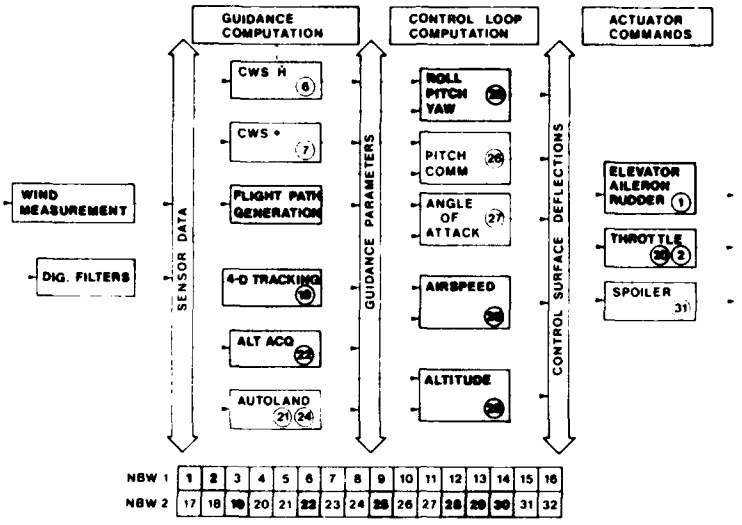

Figure 9: Modular structure of the control system software

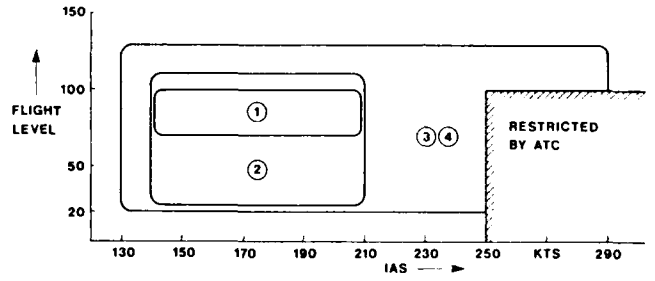

Figure 10: Stages of extension of the experimental flight envelope

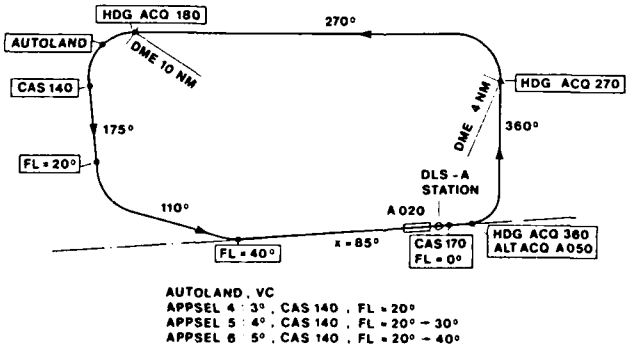

Figure 11: Typical ground track pattern for testing a sequence of different AFCS modes, e.g. HDG, ACQ, ALT ACQ, AUTOLAND and CAS select mode

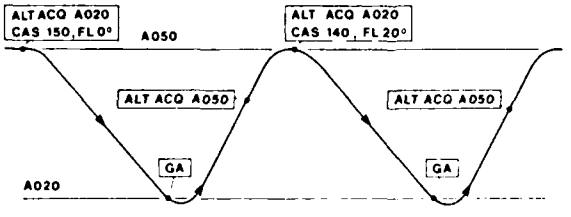

Figure 12: Test sequence for testing the Altitude Acquire and Go Around mode

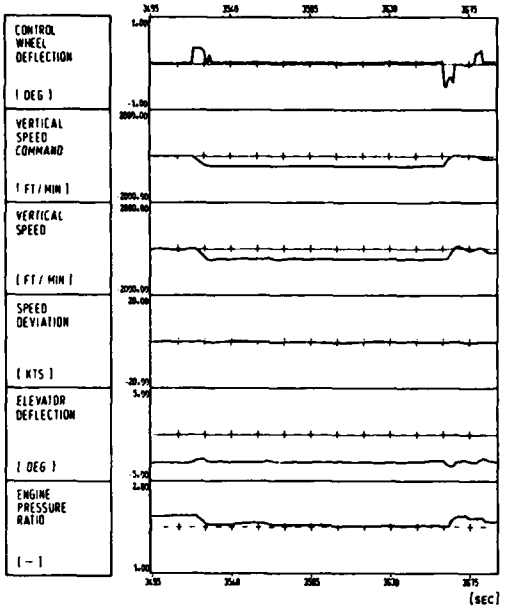

Figure 13: Control wheel steering CWS $\dot{H}$ combined with CAS select mode

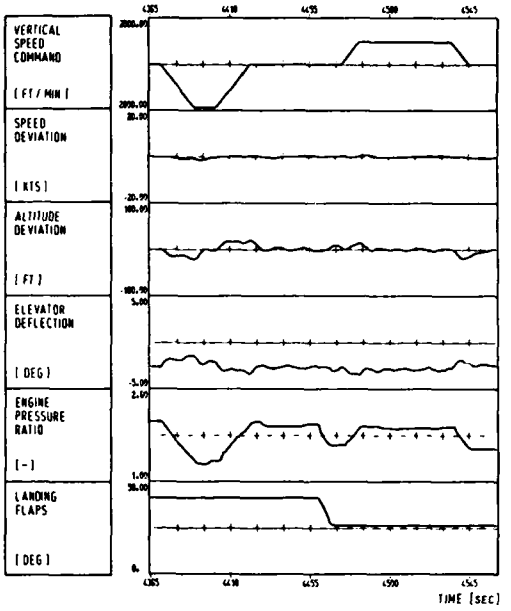

Figure 14: Test of the Altitude Acquire mode with CAS select mode engaged and manual flap setting

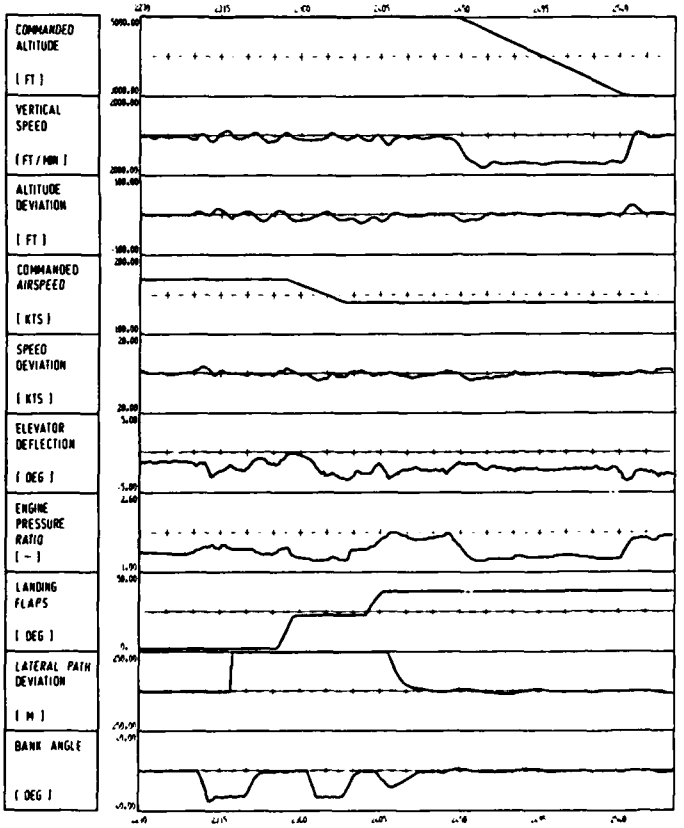

Figure 15: Test of AUTOLAND mode with CAS select mode engaged and manual flap setting

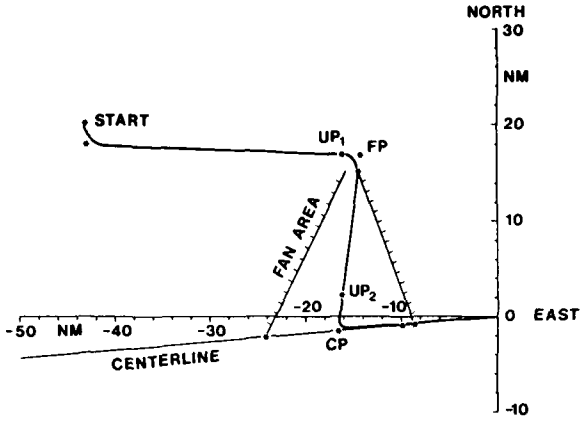

Figure 16: Typical flight path of an automatic 4-D approach

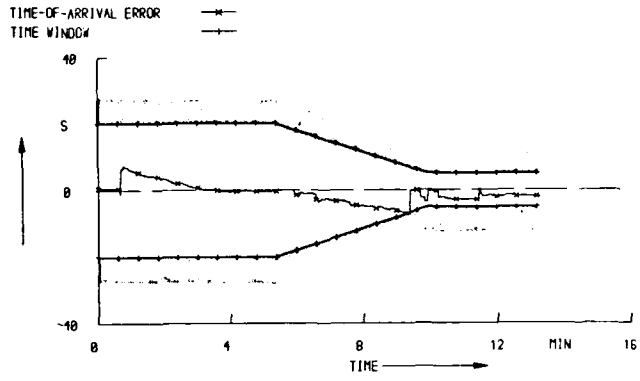

Figure 17: Time history of the time-of-arrival error estimate

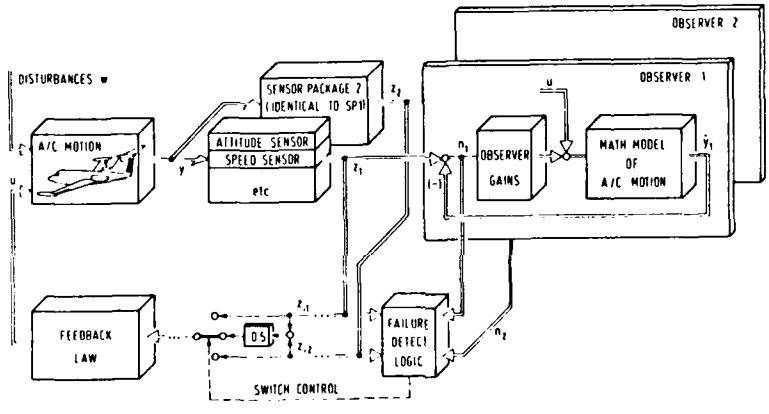

Figure 18: Duplex sensor system featuring 1 fail-op

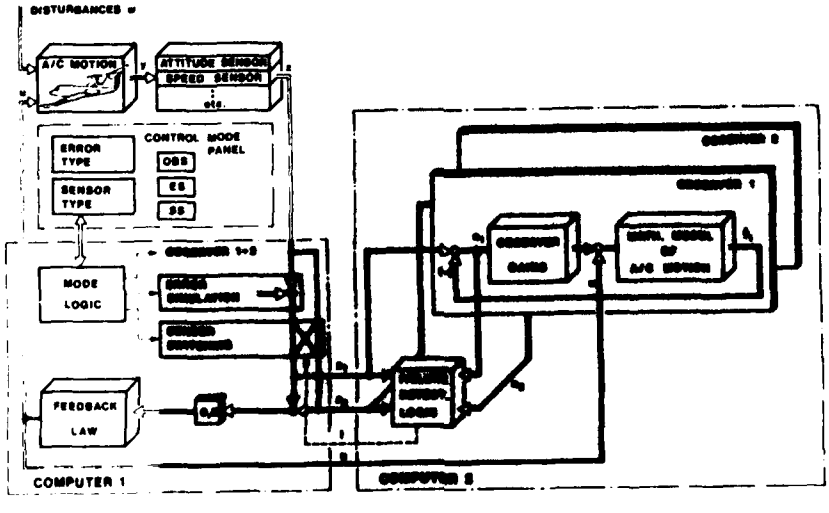

Figure 19: Experimental system for the flight test evaluation of the analytical redundancy concept

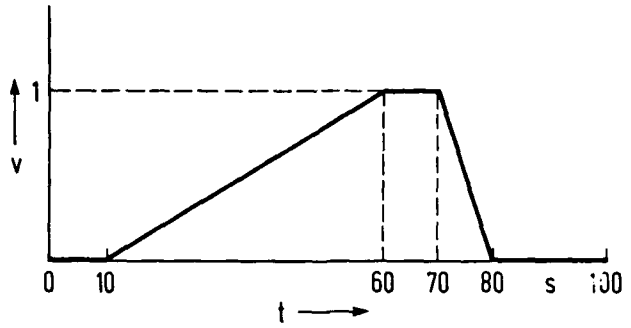

Figure 20: Time history of a simulated error signal

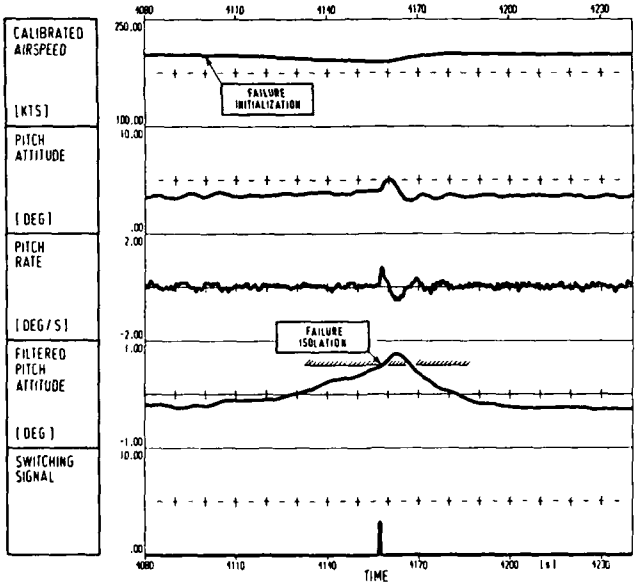

Figure 21: Example of a typical failure detection test during actual flight

AD-A153 254 GROUND AND FLIGHT TESTING FOR AIRCRAFT GUIDANCE AND CONTROL(U) ADVISORY GROUP FOR AEROSPACE RESEARCH AND DEVELOPMENT NEUILLY-SUR-SEINE (FRANCE) R ONKEN ET AL. 2/3

UNCLASSIFIED DEC 84 AGARD-AG-262 F/G 1/4 NL

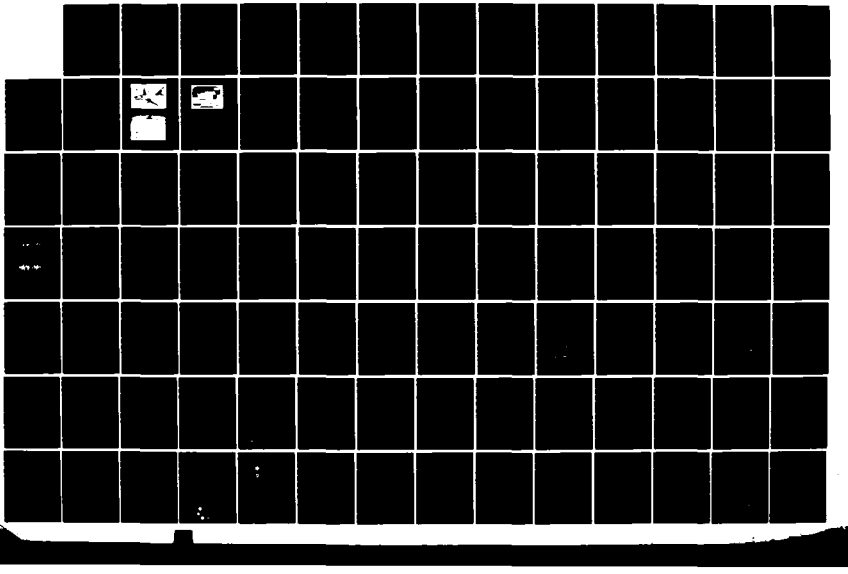

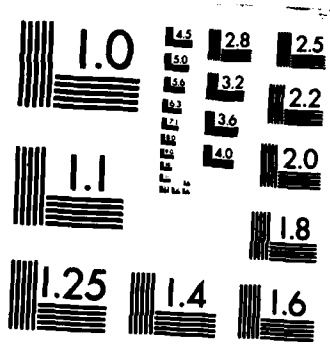

A FLIGHT MANAGEMENT ALGORITHM AND GUIDANCE FOR FUEL-CONSERVATIVE DESCENTS IN A TIME-BASED METERED AIR TRAFFIC ENVIRONMENT: DEVELOPMENT AND FLIGHT TEST RESULTS

by
Charles E. Knox
Aero-Space Technologist
NASA Langley Research Center
Flight Control Systems Division
MS 156A
Hampton, Virginia 23665

SUMMARY

The Federal Aviation Administration has developed an automated time-based metering form of air traffic control for arrivals into the terminal area. The local flow management/profile descent (LFM/PD) concept provides fuel savings by matching the airplane arrival flow to the airport acceptance rate through time control computations and by allowing the pilot to descend at his discretion from cruise altitude to the metering fix in an idle-thrust, clean configuration (landing gear up, flaps zero, and speed brakes retracted). Substantial fuel savings have resulted from LFM/PD, but air traffic control workload is high because the radar controller maintains time management for each airplane through either speed control or path stretching with radar vectors. Pilot workload is also high since the pilot must plan for an idle-thrust descent to the metering fix using various rules of thumb.

The National Aeronautics and Space Administration has designed in its simulation facilities and flight tested in its Transport Systems Research Vehicle (TSRV) Boeing-737 airplane a flight management descent algorithm designed to improve the accuracy with which an airplane can be delivered to a metering fix at a time designated by air traffic control. This algorithm provides a three-dimensional path plus terminal time constraints (fourth dimension), for an airplane to make an idle-thrust, clean-configured descent to arrive at the metering fix at a predetermined time, altitude, and airspeed. The descent path is calculated for a constant Mach/airspeed schedule by using linear approximations of airplane performance to account for gross weight, wind, and nonstandard pressure and temperature effects.

Flight test data were obtained on 19 flight test runs to the metering fix. The standard deviation of metering fix arrival time error was 12 sec, with no arrival time error greater than 29 sec. Comparable statistics for time error accumulated between the top of descent and the metering fix (approximately 40 n.mi.) give a 6.9-sec standard deviation, with no error greater than 15 sec. The calibrated airspeed and altitude errors at the metering fix have standard deviations of 6.5 knots and 23.7 m (77.8 ft), respectively, and the maximum errors were less than 12.9 knots and 51.5 m (169 ft).

SYMBOLS

ACLT	actual computed landing time
ARTCC	air route traffic control center
ATC	air traffic control
CAS	calibrated airspeed
CAS_d	descent calibrated airspeed, knots
CRT	cathode ray tube
EADI	electronic attitude director indicator
EASILY	Experimental Avionics Systems Integration Laboratory
EHSI	electronic horizontal situation indicator
ETA	estimated time of arrival
FLnnn	flight level
LFM/PD	local flow management/profile descent
M_d	descent Mach number
M_c	cruise Mach number
MSL	mean sea level
NCDU	navigation control and display unit
NCU	navigation computer unit
TAS	true airspeed
$(\dot{h})_{CAS_d}$	descent rate as a function of descent airspeed, m/sec
$\left(\frac{d\dot{h}}{dh}\right)_{M_d}$	change in descent rate with respect to altitude as a function of Mach number, (m/sec)/m
$\frac{dTAS}{dt}$	change in true airspeed as a function of time, m/sec/sec

INTRODUCTION

Rising fuel costs combined with other economic pressures have resulted in industry requirements for more efficient air traffic control and aircraft operations. The Federal Aviation Administration (FAA) has developed an automated form of air traffic control (ATC) for arrivals into the airport terminal area. This concept, called local flow management/profile descent (LFM/PD), provides for increased airport capacity and fuel savings by combining time-based metering with profile descent procedures. Time-based metering procedures provide for the sequencing of arrivals to the airport through time control of airplanes at metering fixes located 30 to 40 n.mi. from the airport. Time metering of airplanes at these fixes reduces the low-altitude vectoring (and associated fuel consumption) required to position the airplanes into a final queue for landing. In addition, delays due to terminal area sequencing may be absorbed at higher altitudes which further minimizes fuel usage (refs. 1 and 2).

Profile descent procedures permit the initiation of the airplane descent at the pilot's discretion so that the airplane passes the metering fix at a specified altitude and airspeed. This procedure allows the pilot to plan the descent in a fuel-conservative manner while accounting for the performance characteristics of his particular airplane.

In the original operational concept of the time-based metering LFM/PD program, the flight crew was responsible for both the descent and time navigation to the metering fix. However, the pilots had little or no computed guidance to aid them with this highly constrained four-dimensional (4-D) navigation problem (fuel-conservative descent with a fixed time objective). Flight crews were forced to rely on past experience and various rules of thumb to plan descents. This practice resulted in unacceptably high cockpit workloads and the full potential of fuel savings from a planned descent not being obtained (ref. 3).

In an effort to reduce the cockpit workload, the responsibility of delivering the airplane to the metering fix at an assigned time was transferred to the ATC controller. The ATC controller directs the pilots with path-stretching radar vectors and/or speed control commands as required so that each airplane crosses the metering fix at its assigned time. These operations have resulted in airplane arrival time accuracy at the metering fix of between 1 and 2 minutes (ref. 4). Improved arrival time accuracy and resulting increased fuel savings could be obtained at the cost of a significant increase in the ATC controller's workload.

Splitting the navigation responsibilities between the flight crew and ATC controller reduced the pilot's workload. However, when the ATC controller must apply path stretching or speed control for time management purposes, the pilot is forced to deviate from his planned descent profile; thus, more than the minimum fuel required is used.

The NASA has used its Transport Systems Research Vehicle (TSRV, formerly known as the Terminal Configured Vehicle) Boeing-737 research airplane to flight test a flight management descent algorithm designed to increase fuel savings by reducing the time dispersion of airplanes crossing the metering fix at an ATC-designated time through transfer of the responsibility of time navigation from the radar controller to the flight crew. The algorithm computes a profile descent from cruise altitude to the metering fix based on airplane performance at idle thrust and in a clean configuration (landing gear up, flaps zero, and speed brakes retracted). Time and path guidance are provided to the pilot for a constant-Mach descent, followed by a constant airspeed descent, to arrive at the metering fix at a predetermined (ATC specified) time, altitude, and airspeed.

The flight management descent algorithm concept, pilot interface, and flight guidance were initially developed in the TSRV piloted simulation facilities. Implementation and initial testing of the software and pilot interface in the flight computers used in the TSRV airplane were completed in the Langley Experimental Avionics Systems Integration Laboratory (EASILY). Flight tests were conducted in the Denver, Colorado, LFM/PD ATC environment to quantify the accuracy of the descent algorithm and to investigate the compatibility and pilot acceptability of an airplane equipped with a 4-D area navigation system in an actual ATC environment. This report describes the algorithm and facilities used in its development and presents the results of the flight tests.

ARTCC AUTOMATED LOCAL FLOW MANAGEMENT/PROFILE DESCENT DESCRIPTION

The ATC concept of automated local flow management/profile descents utilizing time-based metering is designed to permit operators of high-performance, turbine-powered airplanes to descend in a clean configuration at idle thrust to a point within the airport terminal area. Significant fuel savings are achieved on a fleet-wide (all users) basis by matching the airplane arrival rate into the terminal area to the airport's arrival acceptance rate, thus reducing the need for holding and low-altitude vectoring for sequencing. Fuel savings are also achieved on an individual airplane basis by permitting the pilot to descend in a fuel-efficient manner at his discretion. In addition to arrival fuel savings, safety, noise abatement, and standardization of arrival procedures are all enhanced (ref. 5).

The Denver ARTCC's automated version of LFM/PD employs four metering fixes located around the Stapleton International Airport. Each arriving high-performance airplane is time-based metered to one of these four metering fixes. Metering is accomplished by using the ARTCC computer, with consideration given to the following parameters:

(1) Airport acceptance rate (number of arrivals per unit time) specified by the Stapleton International Airport tower personnel

(2) Nominal path and airspeed profiles associated with each of the four metering fixes to the runway

(3) True airspeed filed on the airplane's flight plan

(4) Airplane position detected by ATC radar

(5) Forecast winds-aloft data from several stations in the Denver ARTCC area and/or measured winds from pilot reports

These parameters are processed by the ARTCC computer to determine an estimated time for each metered airplane to land on the runway, assuming no conflicts. The ETA's for all metered airplanes are chronologically ordered and compared to determine whether any of the airplanes are in conflict. Landing times are reassigned by the computer to resolve any time conflicts. The adjusted landing time is referred to as the actual computed landing time. If the ACLT and the ETA are different, the difference indicates the delay that an airplane must accommodate prior to reaching the metering fix through holding, speed control, or path stretching. The ACLT is always greater than or equal to the ETA. The metering fix arrival time assigned to each airplane is computed by subtracting a nominal transition time (from the metering fix to the runway) from the ACLT.

SIMULATION FACILITIES

The TSRV airplane simulation facilities were used to implement software for the descent profile computations, to design guidance for the pilot and the automatic flight control system, to develop data input/output formats for the NCDU, and to train the guest subject pilots for operations in the TSRV research flight deck. The TSRV simulation facilities consist of a fixed-base cockpit identical to the research flight deck in the TSRV B-737 airplane, a general-purpose scientific mainframe computer, and a calligraphic graphics computer.

The program residing in the mainframe computer is a sophisticated, six-degree-of-freedom digital representation of the airplane, its subsystems, and the experimental research systems (flight control, electronic displays, navigation and guidance). Nonlinear effects such as engine response, varying stability functions, and control servo models represent the airplane with a high degree of realism. Automatic and control-wheel-steering flight control modes and navigation control functions have also been simulated, allowing research requiring flight crew interactions with the systems to be conducted over the full operational envelope of the airplane and its experimental systems.

Data distribution between the research cockpit, the mainframe computer, and the graphics computer allows appropriate data transfer during the real-time simulation. Man-machine interaction capability in the fixed-base simulation is equivalent to that obtained in the TSRV airplane.

LOCAL FLOW MANAGEMENT/PROFILE DESCENT AIRBORNE ALGORITHM

General Description

The airborne flight management descent algorithm computes the parameters required to describe a seven-segment cruise and descent profile between an arbitrarily located entry fix and an ATC-defined metering fix (Fig. 1). These parameters are then used by the navigation and display systems to present guidance to the pilot and/or autopilot. The descent profile is based on linear approximations of airplane performance for an idle-thrust, clean-configured descent. Airplane gross weight, wind, and nonstandard temperature and pressure effects are also considered in these calculations.

Figure 1 shows the vertical-plane geometry of the path between the entry fix and the metering fix. Each path segment from the entry fix to the metering fix is numbered according to the order in which it is calculated by the algorithm. To be compatible with standard airline operating practices, the path is calculated assuming the descent will be flown at a constant Mach number with transition to a constant calibrated airspeed and with speed changes being flown at constant altitude. The path is flown starting at the entry fix and proceeding to the metering fix.

Segment 7 begins at the entry fix and is flown at a constant cruise altitude and a constant cruise Mach number. Segment 6 is a relatively short path segment in which the speed of the airplane may be changed from the cruise Mach number to the descent Mach number. Segment 6 is eliminated if the descent and the cruise Mach numbers are the same. The descent to the metering fix altitude is started on segment 5. This segment is flown at a constant Mach number. As altitude is decreased along this path segment,

the calibrated airspeed increases. The desired descent calibrated airspeed is obtained at the beginning of segment 4. The descent is continued along this path segment at a constant calibrated airspeed. If the metering fix altitude is below 10 000 ft MSL and the descent airspeed is greater than 250 knots, segments 2 and 3 are computed so that the pilot may comply with the ATC-imposed 250-knot airspeed limit. Segment 2 is a level-flight segment at 10 000 ft MSL so that the descent airspeed may be slowed to 250 knots. The descent is then continued at 250 knots along segment 2.* When the metering fix altitude has been obtained, the airplane is flown at a constant altitude along segment 1 and is slowed from the descent airspeed to the designated metering fix calibrated airspeed. This path segment is eliminated if the descent and metering fix airspeeds are the same.

The flight management descent algorithm may be used in either of two modes. In the first mode, the pilot may input the Mach/airspeed descent schedule to be flown. The descent profile will be computed based on this descent speed schedule with no consideration given for metering fix arrival time constraints.

The second mode was designed for time-metered operations. In this mode, pilot inputs include the entry fix ETA and the ATC-specified metering fix arrival time. The descent profile is then calculated based on a Mach/CAS descent schedule computed through an iterative process which will closely satisfy the crossing times for both of these waypoints.

The logic flow for the flight management descent algorithm in the time-metered mode starts with the computation of an initial Mach/CAS descent schedule that is proportional to the desired time (the difference in arrival times specified for the entry fix and metering fix) and the times required to fly between these fixes at the maximum and the minimum Mach/airspeed operational limits (0.78/340 knots and 0.62/210 knots, respectively, for the TSRV B-737 airplane).

Once the values for the initial Mach/CAS descent speed schedule are selected, an iterative process is begun to arrive at the final descent speed schedule. After completing the first iteration of the profile descent algorithm computations, a convergence test is made to determine whether a satisfactory Mach/CAS descent speed schedule was used. The test consists of checking that the predicted time to fly the profile descent using the selected Mach/CAS descent speed schedule is within 5 sec of the required time to fly the descent.

If the convergence test is not satisfied, additional iterations are required with appropriate changes to the descent airspeed. The descent Mach number is not changed unless the descent CAS has reached its maximum or minimum boundary. This time convergence criterion is usually satisfied in less than five iterations with an allowable time error of 5 sec.

Checks are made to ensure that the final Mach/airspeed schedule selected is within the operational speed limit range. If a selected metering fix time requires a speed which violates one of these speed limits, the descent parameters are computed using the exceeded speed limit and the resultant difference in desired time and programmed time of arrival at the metering fix is displayed to the pilot.

Empirical Representation of TSRV Airplane Aerodynamic and Performance Characteristics

Computer memory considerations precluded the use of detailed aerodynamic and performance tables to represent the TSRV airplane for profile descent calculations. Instead, an empirical model of airplane performance was developed for a nominal gross weight and standard atmospheric conditions. Gradient techniques were used to modify predicted performance for deviations from the nominal conditions of the empirical model.

The form of the equations needed to develop the empirical model was determined from simulator data of a Boeing 737 airplane executing idle-thrust, clean-configured, constant-Mach and constant-CAS descents. Actual flight test data were then used to determine the specific numerical constants and parameters that were used in the empirical model of the TSRV airplane.

The constant-Mach and constant-airspeed descent computations require that the vertical speed of the airplane be known so that time to descent from one altitude to another may be computed. Figure 2 shows altitude rate as a function of altitude derived from a simulation program of a Boeing 737 airplane making 0.73/320 knots and 0.68/250 knots idle-thrust, clean-configured descents. These traces illustrate that during the constant-Mach portion of the descent, altitude rate decreases almost linearly with decreasing altitude. However, the slopes $(d\dot{h}/dh)_{M_d}$ of a family of these linearized constant-Mach descent lines decrease as Mach number is reduced. The slope of these

*The software required to compute segments 2 and 3 was not implemented for the flight tests at Denver since the descents were discontinued at altitudes greater than 10 000 ft. Subsequent versions of the descent management software include the computations to calculate segments 2 and 3.

lines as a function of Mach number was then modeled in the form of a quadratic equation, as shown in Figure 3.

A similar derivation was used to obtain a function for altitude rate for the constant calibrated airspeed portion of the descent. It was found that vertical speed was approximately constant at all altitudes for a given calibrated airspeed but decreased for an increased airspeed.

Figure 4 shows the idle-thrust descent flight performance data of the TSRV airplane for the variation of altitude rate as a function of calibrated airspeed. The straight line represents the vertical speed of the airplane as a function of airspeed and was derived through a linear regression analysis of the illustrated data.

Acceleration performance data were required for speed changes at cruise and metering fix altitudes. Figure 5 illustrates the level-flight, clean-configured, idle-thrust deceleration capability as a function of true airspeed of the TSRV airplane based on flight test data at typical metering fix altitudes. A linear expression was derived through a regression analysis so that an average acceleration, in terms of knots per seconds, could be calculated given the average true airspeed along a path segment.

Flight test data also showed that the level-flight, clean-configured, idle-thrust speed changes at cruise altitudes of approximately FL330 to FL350 resulted in a computed constant acceleration of approximately -1.15 knot/sec.

Wind Modeling Technique

A two-segment (upper and lower altitude) linear wind model was used to describe the wind speed and direction between the cruise altitude and the ground. Two gradients for each segment, one showing the variation of wind speed and the other showing the variation of wind direction with changes in altitude, were stored in the computer. A complete wind model for the upper altitude segment (metering fix floor altitude, approximately 5200 m (17,000 ft) to cruise altitude) was derived by applying the upper altitude gradients to the inertially measured winds at cruise altitude. The lower altitude model (surface to the metering fix floor altitude) was derived by applying the lower altitude gradients to the surface winds measured at the airport.

The magnitude of each gradient was derived from the winds-aloft forecast for the test area and stored in the computer before each flight. The surface wind at the airport was inserted by the pilot through the NCDU prior to each descent. The magnitude of the wind velocity at cruise altitude was the value measured by the inertial system at the time of the initial profile descent calculation.

Descent Path Computations

The cruise and descent path between the entry fix and the metering fix was defined by computing the relative location and altitude of the necessary intermediate waypoints. The altitude of each waypoint was computed first. Ground speed at which the airplane was to cross each waypoint was determined by summing the result of the Mach-number- or CAS-to-true-airspeed conversions with the headwind component derived from the wind model. The relative locations of the waypoints were then determined by computing the lengths of the path segments between the waypoints. On the level-flight path segments, the assigned waypoint ground speeds and the airplane deceleration capability were used. On the descent path segments, the average rate of descent and the required altitude change were used to determine the time to travel between the waypoints. This path segment time was combined with the average segment ground speed to determine the segment length. The specific equations for these computations may be found in reference 6.

Input/Output Requirements

Data required for profile descent calculations are obtained from the NCU navigation data base, from pilot inputs through the NCDU, and from real-time sensor inputs through a data bus to the NCU. Parameters contained in the NCU navigation data base include:

(1) Arrival path waypoints: location (latitude and longitude), programmed altitude, and programmed speed

(2) Metering fix: location (latitude and longitude), maximum and minimum programmed altitudes, and programmed airspeed

(3) Maximum and minimum airplane operational descent Mach number and airspeed

(4) Wind speed and direction gradients

Inputs required for the profile descent calculations inserted through the NCDU by the pilot include:

(1) Entry fix description: location, programmed altitude, programmed ground speed, and programmed crossing time (the entry fix is the last waypoint the pilot has defined on his path before using the LFM/PD algorithm)

(2) Descent Mach/CAS schedule (not required if both the metering fix and entry fix times are specified)

(3) Metering fix time (not required if the pilot selects the descent Mach/CAS schedule)

(4) Surface winds

(5) Airport altimeter setting

(6) Airplane gross weight

(7) Total air temperature

Information required for the profile descent calculations that are input to the navigation computer automatically through a data bus include winds-aloft speed and direction, cruise Mach number, and cruise altitude (Magnitudes measured at time of profile descent calculation).

The flight management descent algorithm calculates and outputs the following parameters to be used by the guidance and display system:

(1) All descent waypoint distances relative to the metering fix, programmed altitudes, and programmed ground speeds

(2) The magnetic direction of the entry fix relative to the metering fix (all waypoints used to describe the descent profile lie in the vertical plane defined between the metering fix and entry fix)

(3) Mach/CAS descent schedule

EXPERIMENTAL AVIONICS SYSTEM INTEGRATION LABORATORY

The initial step of the flight evaluation tests was to program the airborne flight management algorithm and necessary flight guidance which were developed in FORTRAN langugage in the TSRV real-time piloted simulation facilities, into assembly-level software appropriate for the navigation computer onboard the airplane. A facility called the Langley Experimental Avionics System Integration Laboratory (EASILY) was used to debug and validate the software for these flight tests. The laboratory environment provided by these facilities significantly reduces the time required to implement the flight software and also allows the airplane to be used for other tests.

The Experimental Avionics Systems Integration Laboratory is a special-purpose test facility utilized for the development and integration of the advanced TSRV experimental flight avionics hardware and software systems. A block diagram of the EASILY is shown in figure 6. The EASILY was established recognizing that the sophisticated TSRV avionics required a high level of integrated tests. EASILY tests, which are in essence a ground-based extension of flight tests, integrate actual flight hardware and software with a mathematical simulation of the TSRV aircraft in real time. Prototype flight profiles through touchdown and turnoff are debugged and verified, thereby authenticating the hardware integrity and hardware-software compatibility of the flight systems.

An on-site digital computer is used to model the TSRV aircraft. The six-degree-of-freedom linearized small-perturbation aircraft model simulation iterates its mathematical solution every 50 msec to 12-place accuracy. The computer's digital output channels provide simulated air data, inertial and body-referenced attitudes and rates, flight path accelerations, and terminal guidance parameters to dedicated signal-conditioning equipment. The signal-conditioning equipment reformats the computer digital signals to make them compatible with the experimental flight systems.

Real-time analysis of the aircraft system performance during the simulated flights is provided by six multichannel strip chart recorders and two cathode ray tube (CRT) repeater displays of the aircraft ground track and flight attitude. The CRT's are laboratory counterparts of the pilots' flight displays and are used by the laboratory engineers during simulation runs in a manner analogous to the research pilots' use of the flight displays. The strip chart recorders provide 78 data channels for quick-look analysis. Real-time CRT display of 20 variables in predetermined engineering units augmets the permanent strip chart records. Two nine-track digital tape recorders are used to record system variables for off-line analysis. A remotely located Langley Research Center central computer complex provides a nonlinear digital simulation capability to augment the on-site systems. Duplicate analog sensor and command signals are transmitted between the sites over buried telephone lines. A master control switch in EASILY selects either the remote or on-site simulation. The EASILY equipment dedicated to the backup mode is controlled through the master control switch.

DESCRIPTION OF AIRPLANE AND EXPERIMENTAL SYSTEMS

The test airplane is the TSRV B-737 research airplane (a twin-engine subsonic commercial jet transport). The experimental systems consist of a triplex digital flight control system, a digital navigation and guidance system, and an electronic CRT display system that is integrated into a separate research flight deck (ref. 7). The full-scale

research flight deck is located in the airplane cabin just forward of the wing, as shown in figure 7. Figure 8 shows the instrument panel of the research flight deck.

The triply redundant digital flight control system provides both automatic and fly-by-wire control wheel steering options. The velocity vector control wheel steering mode (ref. 7) was utilized during these flight tests. In this control mode, the flight control computers vary pitch attitude and heading to maintain flight path angle and track angle, respectively.

The navigation computer is a general-purpose digital computer designed for airborne computations and data processing tasks. It utilizes a 24-bit word length and has a 32 000-word directly addressable core memory. Major software routines (refs. 8 and 9) in the navigation computer include navigation position estimate, flight route definition, guidance commands to the flight control computer system, piloting display system computations, and flight data storage for navigation purposes. The flight management descent algorithm software was also included in the navigation computer.

The captain and the first officer each have three CRT displays and conventional airspeed and altimeter instrumentation for guidance. The three CRT displays include the EADI, the EHSI, and the NCDU, which is a digital display of various navigation information stored in the NCU.

The EADI display is formatted much like a conventional attitude indicator but has additional symbology to help the pilot navigate and control the airplane. A detailed explanation of the EADI display may be found in reference 8. Two options of the EADI display used for lateral and vertical path navigation on these flight tests are the vertical and lateral course deviation indicators and the waypoint indicator used with flight path angle wedges, as shown in figure 9.

The vertical and lateral course deviation indicators are presented in a conventional needle and tape format. The vertical tape on the right-hand side of the EADI shows the vertical path error. A standard "fly-to" deviation convention is employed in which the needle represents the desired path and the center of the tape represents the airplane (i.e., if the airplane is below the desired path the needle will be displaced above the center of the tape). The indicated range of the tape scale is ±152 m (±500 ft). The lateral course deviation indicator is displayed on the bottom of the EADI. The fly-to deviation convention is utilized and the indicated range of the horizontal tape is ±1829 m (±6000 ft).

The second EADI navigation option used during this test was the waypoint indicator used with flight path angle wedges, as shown in figure 9. This star-shaped symbol represents the next waypoint on the programmed route. The symbol's vertical displacement on the EADI pitch grid represents the flight path angle at which the airplane must be flown to arrive at the programmed altitude at the next waypoint. The waypoint indicator is also displaced laterally to provide lateral path tracking guidance.

The flight path angle wedges used with the waypoint indicator symbol represent the inertially referenced flight path of the airplane. If the airplane flight path angle and track angle are adjusted so that the flight path angle wedges center directly on the waypoint indicator, the airplane will be flying directly to the waypoint.

Figure 10 is a drawing of the EHSI display operated in a track-up mode. This display is a plan view of the desired route and optionally displayed features such as radio fixes, navigation aids, airports, and terrain drawn relative to the airplane's position (indicated by a triangular airplane symbol). A trend vector is displayed in front of the airplane symbol to aid the pilot in route capture and tracking and in time guidance utilization. The trend vector is composed of three consecutive lines which predict where the airplane will be in the next 30, 60, and 90 sec based on the airplane's current ground speed and bank angle. The EHSI display also provides the pilot with time guidance and an altitude predictive arc to aid the pilot during altitude changes.

Time guidance is provided on the EHSI by a box symbol that moves along the programmed path. The time box represents the desired position of the airplane along the route based on the programmed ground speeds and the time profile. The pilot nulls the time error by maneuvering the airplane so that the airplane symbol is contained within the time box.

During climbs and descents, the pilot may opt for the range/altitude arc symbol to be drawn on the EHSI, as shown in figure 10. This symbol depicts the range in front of the airplane within which a pilot-selected reference altitude will be achieved based on the airplane's current altitude and flight path angle and the desired reference altitude.

The range/altitude arc was used on the descent profile during these tests by setting the magnitude of the reference altitude to the programmed altitude of the next waypoint. Then the pilot could adjust the flight path angle of the airplane so that the arc would lie on top of the next waypoint displayed on the EHSI. This resulted in the airplane crossing the next waypoint at the programmed altitude.

The NCDU display contains numerous navigational data for the pilot to select, including programmed route information, tracking and navigational error information, and systems status checks. This information is presented in alphanumeric form. A complete description of the NCDU and its operations may be found in reference 8.

DATA ACQUISITION

Data were recorded onboard the airplane by a wide-band magnetic tape recorder at 40 samples/sec. These data included 93 parameters describing the airplane configuration, attitude, and control surface activity, and 32 selectable parameters from the navigation computer. Airborne video recordings of the EADI and EHSI displays were made throughout each flight. In addition, audio records of test crew conversations and air-ground communications were recorded.

On the ground, the ATC radar controller's scope presentation and the Air Route Traffic Control Center computer-generated time-based metering update list were video recorded.

FLIGHT TEST OBJECTIVES

The objectives of the flight tests were to document the descent path parameters determined by the descent flight management algorithm, including wind modeling effects; to determine the compatibility of the airborne flight management descent concept with time control in the cockpit while operating in the time-based metered LFM/PD air traffic control environment; to determine pilot acceptance of the cockpit procedures to program and fly a fuel-conservative, time-controlled descent; and to obtain data for estimates of fuel usage. These objectives were achieved by using qualitative data in the form of pilot and ARTCC radar controller comments; audio recordings of controller, cockpit, and air-to-ground conversations; and video recordings from the ARTCC radar scope, and by using quantitative data in the form of speed, altitude, and time error recorded onboard the airplane.

FLIGHT TEST CREW

The flight test crew consisted of a captain and a first officer. The captain was responsible for flying the airplane in the velocity vector control wheel-steering mode and for operation of the thrust levers. The first officer was responsible for making program inputs to the navigation computer, selecting appropriate display guidance, and assisting the captain as requested. In addition, the first officer recorded flight notes of various parameters describing the profile descent for postflight analysis.

Two NASA test pilots and four management and line airline pilots served as captain during the flight tests. Both NASA pilots had extensive previous flight and simulation experience with the TSRV airplane and its experimental flight control and display systems. The four airline pilots each had approximately 6 hours of simulator training prior to the flight tests. One of the airline pilots had 4 hours of flight time in the TSRV airplane which was acquired during unrelated flight tests 9 months earlier.

A NASA engineer served as first officer on all flights. He had previous flight crew experience in simulation and flight tests with the TSRV airplane and its experimental systems.

EXPERIMENT TASK

Other than requiring the time navigation responsibility to be in the cockpit, the experiment task required the flight crew to operate the airplane as a normal arrival flight to the Denver airport participating in the time-based metered LFM/PD air traffic control system. Each test run was started with the airplane at cruise altitude and speed on a 4-D programmed path to an entry fix 110 n.mi. from Denver. Prior to passing the entry fix, the flight crew received a profile descent clearance and an assigned metering fix time from the Denver ARTCC. The flight crew then keyed the appropriate parameters into the NCDU so that an idle-thrust descent path to the metering fix would be generated and displayed. Then the crew flew to the metering fix using 4-D path guidance presented on the EADI and EHSI displays. Each test run was terminated at the metering fix and the airplane was repositioned for another test run (or flown back to the airport after the final test of the day).

The flight crew was expected to null lateral and vertical path errors throughout the test and to null the time error prior to the top-of-descent waypoint. The pilot was instructed to null small time errors (less than 20 sec) through speed control and larger time errors through path stretching maneuvers (with ATC concurrence). However, the pilot was to have attained the programmed ground speed and altitude at the top-of-descent waypoint regardless of the time error. During the descent to the metering fix, thrust was retained at flight idle, and speed brakes were not used regardless of any time error so that the effects of wind modeling on the predicted descent path could be observed. Path deviations for air traffic control purposes or due to weather were accepted and accommodated during the test runs.

The captain would anticipate leveling the airplane for the programmed altitude at the bottom-of-descent waypoint with reference to a conventional barometric altimeter and

then would proceed to the metering fix. After passing the metering fix, the test run was complete and the captain would turn the airplane to reposition for another test run.

RESULTS AND DISCUSSION

Airborne Algorithm Flight Performance

The prime indicator of performance of the flight management descent algorithm and the concept of time control in the cockpit was the accuracy in terms of time, airspeed, and altitude with which the airplane passed the metering fix. This accuracy was quantified through the calculation of the mean and standard deviation of the altitude error, airspeed error, and time error for 19 test runs.

The mean, standard deviation, and maximum value for the altitude, airspeed, and time errors are summarized in the following table:

Parameter	Altitude error, m (ft)	CAS error, knots	Absolute time error, sec
Mean	10.2 (33.6) high	0.3 slow	6.6 late
Standard deviation	23.7 (77.8)	6.5	12.0
Maximum error	51.5 (169) high	12.9 fast	29.0 late

The values of these errors were judged by the pilots to be very good for this flight environment. These data demonstrated that highly accurate fuel-efficient descent profiles that satisfy terminal time boundary constraints can be generated and flown using a relatively simple and straightforward empirical model for the aerodynamic and performance characteristics of the airplane. Because of the simplicity of modeling these characteristics, this algorithm could be applied to various flight management/planning systems that are much less sophisticated than the NASA TSRV B-737 experimental system.

The standard deviation and the maximum value of the altitude error were slightly higher than expected. This was attributed to the fact that the pilots had been instructed not to make minor altitude corrections after the initial level-off at the bottom-of-descent waypoint so that the difference between the actual and predicted airspeed changes between the bottom-of-descent and metering fix waypoints could be accurately assessed.

The absolute time error of the airplane crossing the metering fix resulted in a significant error reduction with time control in the cockpit. The pilots felt that they could have reduced the time error even further had they been allowed to modulate thrust and speed brakes during the descent. Since the thrust was at flight idle and the speed brakes were not employed during the descent, the absolute time error was a function of the initial time error at the top of descent and of the flight management descent algorithms (which included wind modeling).

The time error accumulated between the top-of-descent and metering fix waypoints more appropriately reflects the accuracy with which the performance of the airplane and the winds had been modeled in the flight management descent algorithm. The mean and standard deviation of the accumulated time error for the 19 test runs were 2.5 sec and 6.9 sec, respectively. The maximum accumulated time error was 15 sec but typically was less than 9 sec.

The mean and standard deviation of the time errors associated with crossing the metering fix may have been influenced by the time error in the Mach-CAS descent speed schedule convergence test. During these flights, the descent speed schedule was computed based on a 5-sec error convergence criterion. This time was chosen because the descent speed schedule could then be computed in less than six iterations and because it would result in a reasonable bound upon the time error with the resulting descent speed schedule. However, if more computational iterations to compute the descent speed schedule are permissible, then the convergence criterion could be reduced and a corresponding reduction of time error in crossing the metering fix would be expected.

Wind Modeling

The two-segment linear wind model was designed to provide a simple representation of the winds which would minimize the time error of the airplane crossing the metering fix. This was accomplished by using forecasted wind information to define the speed and direction of the wind model line gradients and by using wind velocities measured at the airport (surface winds for the lower wind segment) and at cruise altitude (inertially measured winds for the upper wind segment) to position these line gradients and complete the wind model. This type of representation minimized the impact of wind modeling

errors since most of the flying time between entry fix and metering fix was at cruise altitude where wind modeling was most accurate. Wind modeling errors that occurred during the descent were attenuated by the relatively short exposure time to improperly modeled winds.

The direction and speed gradients of the two-segment linear wind model were entered into the descent flight management software each day prior to flight. The gradients for the wind model were based on the winds-aloft forecast for the Denver area for the time period of the test flights. Since the winds-aloft forecast was made 6 to 8 hours before the flight tests, actual winds aloft were measured and recorded onboard during the climb to cruise altitude on the first test run of the day. This wind information was plotted and compared to the forecast to determine if the wind model gradients should be modified. The gradients could be changed in flight for succeeding test runs, if required. The wind speed gradient was changed on only two of the test runs.

Airborne and Ground System Compatibility

The profile descent calculated by the flight management descent algorithm, the pilot's guidance, and the cockpit procedures were designed to be compatible with current time-based metering LFM/PD ATC procedures and with other traffic participating in the ATC system. The test airplane was treated by the automated time-based metering LFM/PD computer program in the same manner as other airplanes inbound to the Denver airport. The only ATC procedural difference during the flight tests was that the test airplane pilots were given the assigned metering fix time since they were responsible for time management. As a result, no path-stretching radar vectors or speed control commands were required for sequencing purposes. Controller comments indicated that this difference reduced their workload due to less required ground-to-air radio transmissions.

Pilot comments indicated that the task of flying profile descents with time control with the electronic displays was very easily accomplished. The descent algorithm and the path guidance substantially reduced the pilot's workload, no cockpit calculations were required to determine the top-of-descent waypoint, and guidance presented to the pilot made it easy to maintain accurate time control. Computer inputs prior to descent were direct and simple.

Video tape recordings of the ATC controller's radar scope have shown that the test airplane operated compatibly with other traffic. The TSRV airplane merged with, and remained in, a queue of other airplanes bound for the metering fix. This compatibility resulted because of the Mach/airspeed descent schedule and resulting time profile calculated with the descent management algorithm based on the assigned metering fix time. This assigned metering fix time was based upon the position and metering fix time assigned to the airplanes landing prior to the TSRV airplane. Proper spacing between these airplanes and the test airplane would result if the time profile were followed.

Fuel Savings

Fuel savings are achieved on both a fleet-wide basis and an individual-airplane basis. Time-based metering procedures produce fleet-wide fuel savings by reducing extra vectoring and holding of airplanes at low altitude for sequencing into an approach queue. Profile descent procedures produce individual-airplane fuel savings by allowing the pilot to plan for a fuel-efficient descent to the metering fix.

No attempt was made to quantify the increased fleet-wide fuel savings realized due to the reduction of time dispersion in crossing the metering fix since the TSRV airplane was the only airplane that utilized onboard-generated four-dimensional guidance during these tests. It is apparent, however, that a reduction in time dispersion between airplanes being merged into an approach queue can produce an increase in fuel savings by reducing extra maneuvering for longitudinal spacing and can produce an increase in runway utilization by reducing excessively large time separation between airplanes.

Fuel savings at the Denver airport as a result of conventional profile descent operations have been estimated to be as high as $3.25 million per year (ref. 5). Additional fuel savings as a result of the flight-tested airborne algorithms were quantified through an analytical comparison of a descent calculated by the flight management descent algorithm and a conventional descent typical of those airplanes observed on the ARTCC radar display. Fuel use for each descent was based on fuel flow for a B-737 airplane.

Figure 11 shows the vertical profile of both the calculated and conventional descents. Identical initial and final boundary conditions (location, altitude, speeds, and transition time) were used for both descents so that a valid comparison of fuel use could be made. Both descents begin at the entry fix, 76 n.mi. from the metering fix, at an altitude of FL350, and a cruise Mach number of 0.78. The descents end at the metering fix at an altitude of FL195 and a calibrated airspeed of 250 knots. Flying time for both descents is 11.7 min.

The conventional descent is based on idle thrust at a Mach number of 0.78 with a transition to a CAS of 340 knots. The descent from cruise altitude is started at a point 60 n.mi. from the metering fix, which is consistent with various pilot rules of

thumb for descent planning. At the bottom of descent, the airplane is slowed until it reaches a calibrated airspeed of 250 knots. Thrust is then added as required to maintain the airspeed at 250 knots.

The descent calculated by the flight management descent algorithm is based upon an 11.7-min time constraint. The calculated Mach/CAS descent schedule for this profile is 0.62/250 knots. Thrust is set to flight idle approximately 7 n.mi. prior to the descent so that the airplane may slow from the cruise to the descent Mach number. A descent segment at a constant Mach number of 0.62 is started 40.6 n.mi. from the metering fix with transition to a descent segment at a constant CAS of 250 knots until the metering fix is crossed.

Both descents, by definition of the comparison, require the same amount of time to fly between the entry fix and the metering fix. This time objective is achieved with similar ground speeds on both descents. Even though the calculated descent is flown at a slower indicated Mach/CAS descent schedule, similar ground speeds result since the airplane stays at altitudes higher than on the conventional descent.

Fuel usage on these two descents is substantially different, however. The descent calculated by the flight management descent algorithm required approximately 28 percent less fuel to fly between the entry fix and the metering fix [2989 N (672 lb) on the conventional descent and 2148 N (483 lb) on the calculated descent]. Approximately two-thirds of this fuel savings was attributed to the lower indicated airspeeds and one-third to flight at higher altitudes.

CONCLUDING REMARKS

A simple airborne flight management descent algorithm designed to define a flight profile subject to the constraints of using idle thrust, a clean airplane configuration (landing gear up, flaps zero, and speed brakes retracted), and fixed-time end conditions was developed and flight tested in the NASA TSRV B-737 research airplane. The research test flights, conducted in the Denver ARTCC automated time-based metering LFM/PD ATC environment, demonstrated that time guidance and control in the cockpit was acceptable to the pilots and ATC controllers and resulted in arrival of the airplane over the metering fix with standard deviations in airspeed error of 6.5 knots, in altitude error of 23.7 m (77.8 ft), and in arrival time accuracy of 12 sec. These accuracies indicated a good representation of airplane performance and wind modeling. Fuel savings will be obtained on a fleet-wide basis through a reduction of the time error dispersions at the metering fix and on a single-airplane basis by presenting the pilot with guidance for a fuel-efficient descent. Pilot workload was reduced by eliminating the need for rules of thumb and/or extensive experience to achieve a solution to a complex four-dimensional (4-D) navigation problem and by providing steering guidance for 4-D path following. ATC controller workload was reduced through a reduction of required ground-to-air communications and through the transfer of time navigation responsibilities to the cockpit.

REFERENCES

1. Stein, Kenneth J.: New Procedures Key to Fuel Savings. Aviation Week and Space Technology, Vol. 111, No. 9, Aug. 27, 1979, pp. 105-111.

2. Stein, Kenneth J.: Advanced Systems Aid Profile Descents. Aviation Week and Space Technology, Vol. 111, No. 8, Aug. 20, 1979, pp. 57-62.

3. Ames Research Center and Aviation Safety Reporting System Office: NASA Aviation Safety Reporting System: Fifth Quarterly Report April 1 - June 30, 1977. NASA TM-78476, 1978.

4. Heimbold, R. L.; Lee, H. P.; and Leffler, M. F.: Development of Advanced Avionics Systems Applicable to Terminal-Configured Vehicles. NASA CR-3280, 1980.

5. Cunningham, F. L.: The Profile Descent. AIAA Paper 77-1251, Aug. 1977.

6. Knox, Charles E.; and Cannon, Dennis G.: Development and Test Results of a Flight Management Algorithm for Fuel-Conservative Descents in a Time-Based Metered Traffic Environment. NASA TP-1717, October 1980.

7. Terminal Configured Vehicle Program - Test Facilities Guide. NASA SP-435, 1980.

8. Cosley, D.; and Martin, A. J.: ADEDS Functional/Software Requirements. SST Technology Follow-On Program - Phase II. Rep. No. FAA-SS-73-19, Dec. 1973 (Available from DTIC as AD B000 287).

9. McKinstry, R. Gill: Guidance Algorithms and Non-Critical Control Laws for ADEDS and the AGCS. Doc. D6-41565, Boeing Company, 1974.

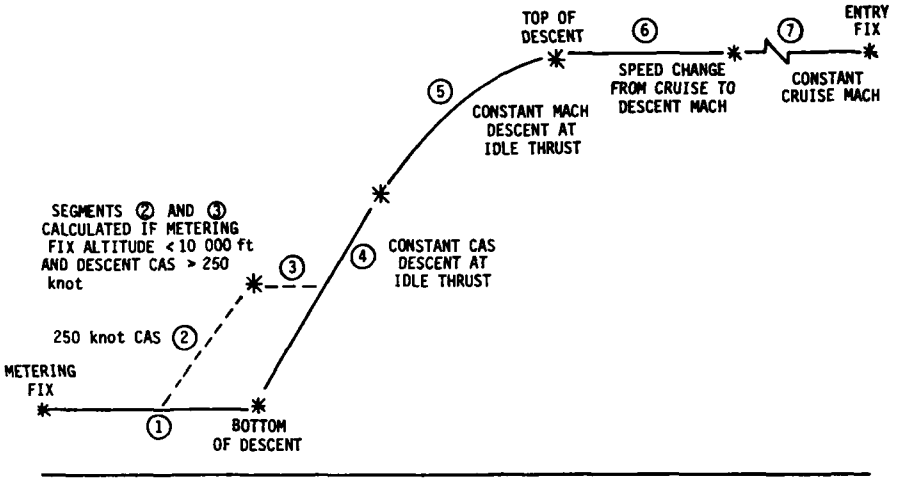

Figure 1.- LFM/PD vertical-plane geometry.

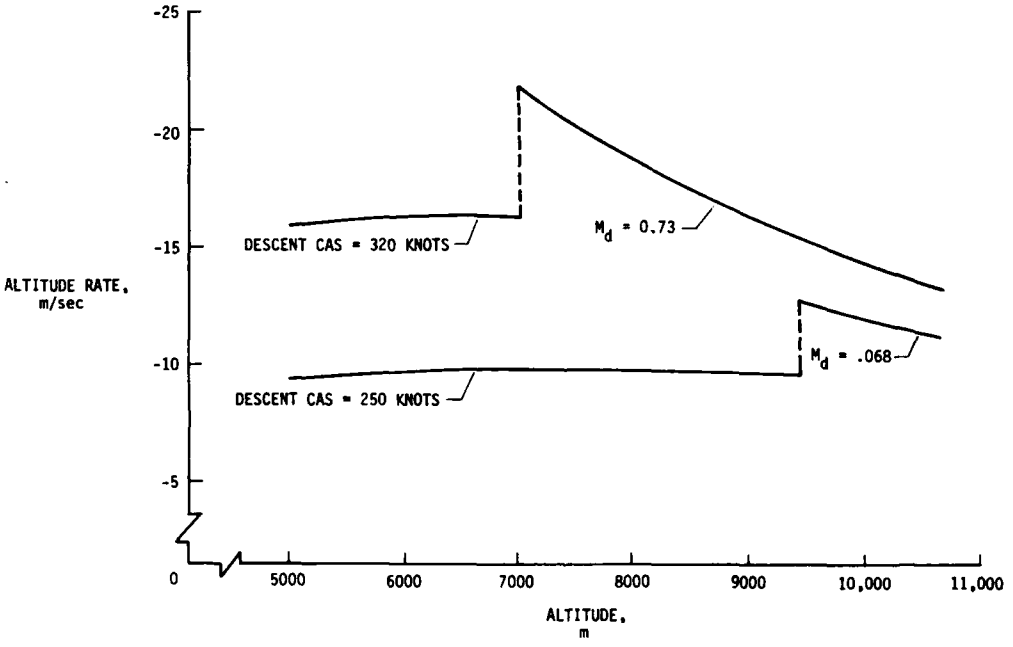

Figure 2.- Altitude rate flight performance data from initial altitude of 10 700 m for B-737 airplane. Gross Weight = 378 080 N; idle thrust.

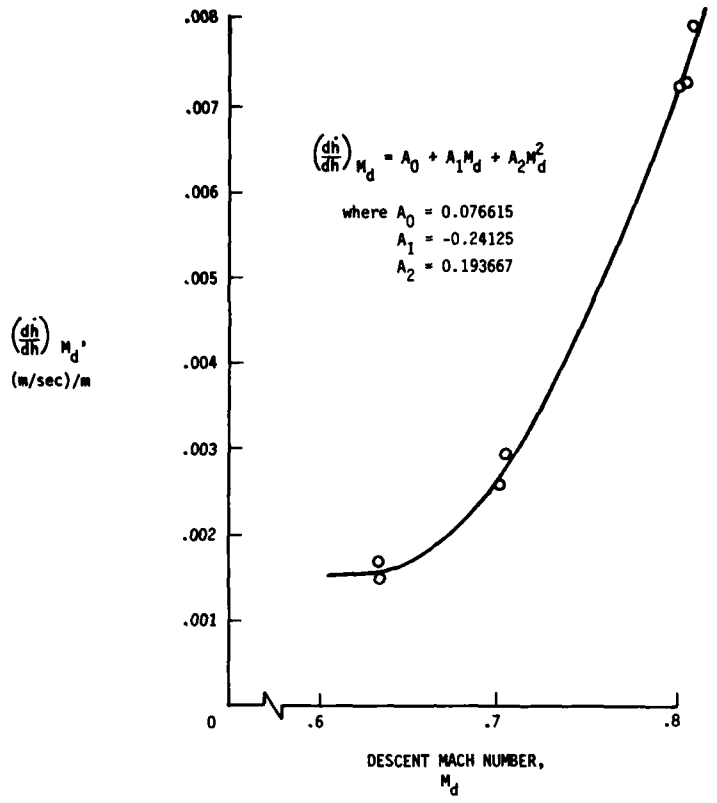

Figure 3.- Variation of $\left(\frac{dh}{dh}\right)_{M_d}$ as a function of descent Mach number for NASA TSRV B-737 airplane. Gross Weight = 378 080 N; idle thrust.

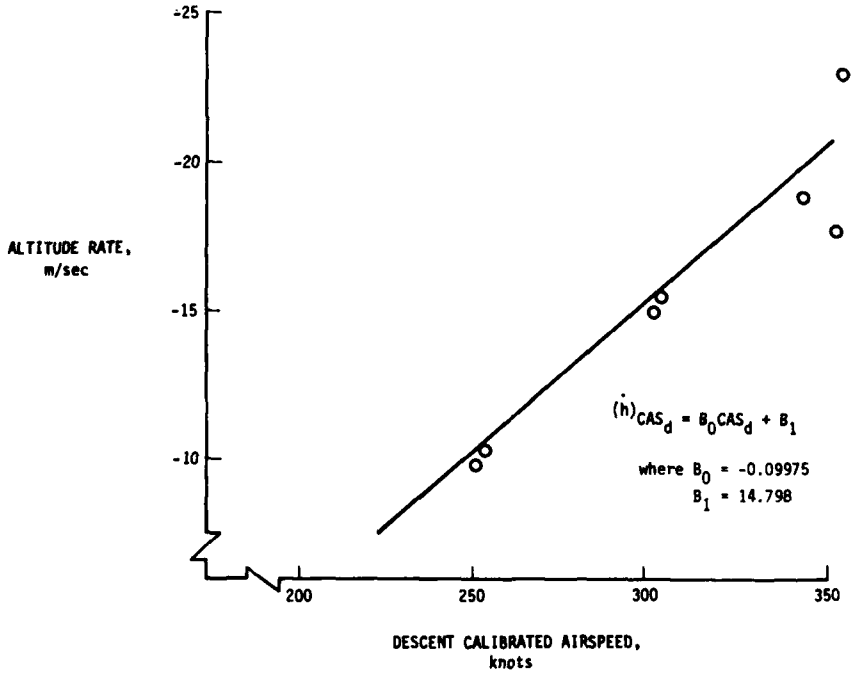

Figure 4.- Variation of altitude rate and descent CAS flight performance data for NASA TSRV B-737 airplane. Gross Weight = 378 080 N; idle thrust.

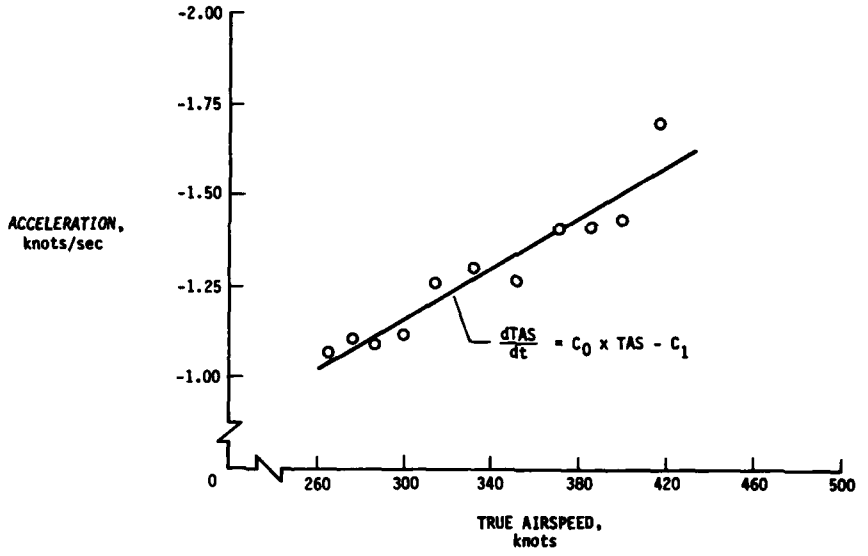

Figure 5.- Acceleration flight performance data for NASA TSRV B-737 airplane.

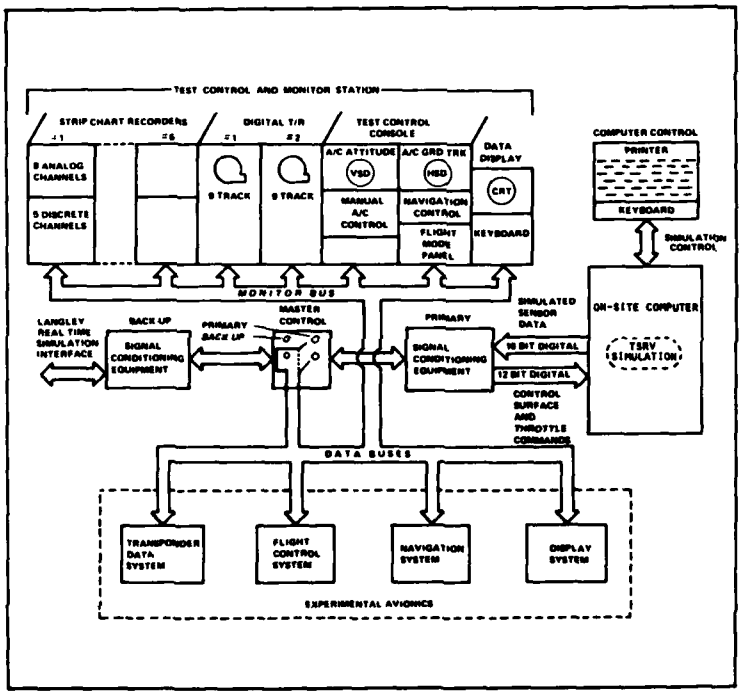

Figure 6.- Block diagram of Experimetal Avionics Systems Integration Laboratory (EASILY).

Figure 7.- Cutaway view of NASA TSRV B-737 airplane.

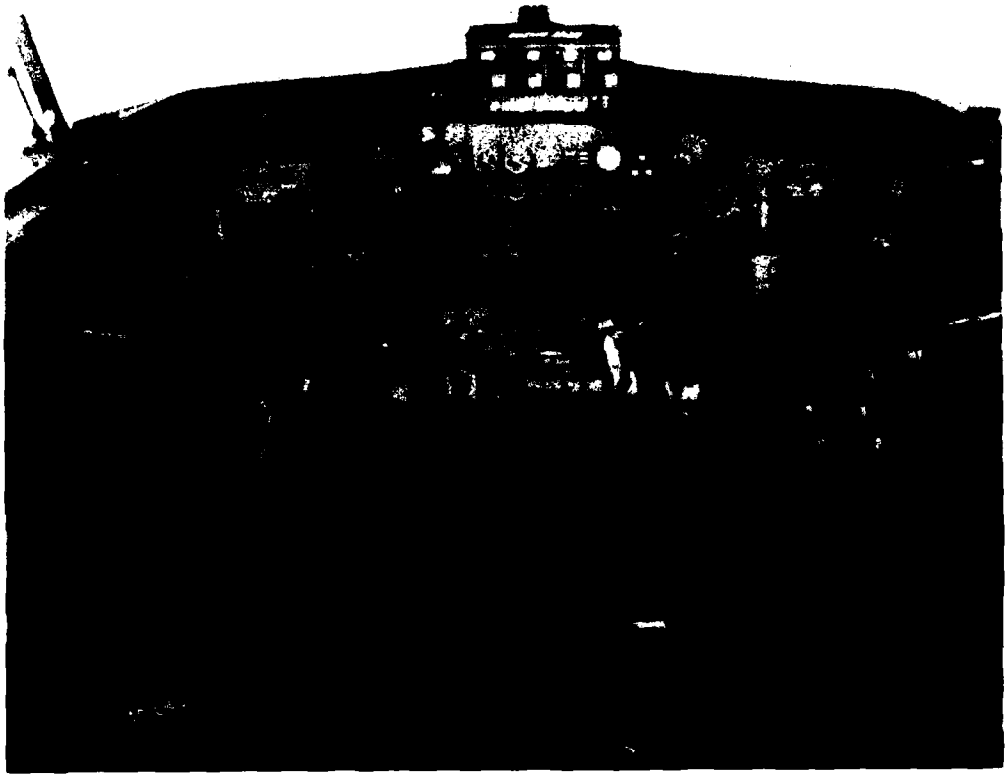

Figure 8.- Instrument panel of research flight deck.

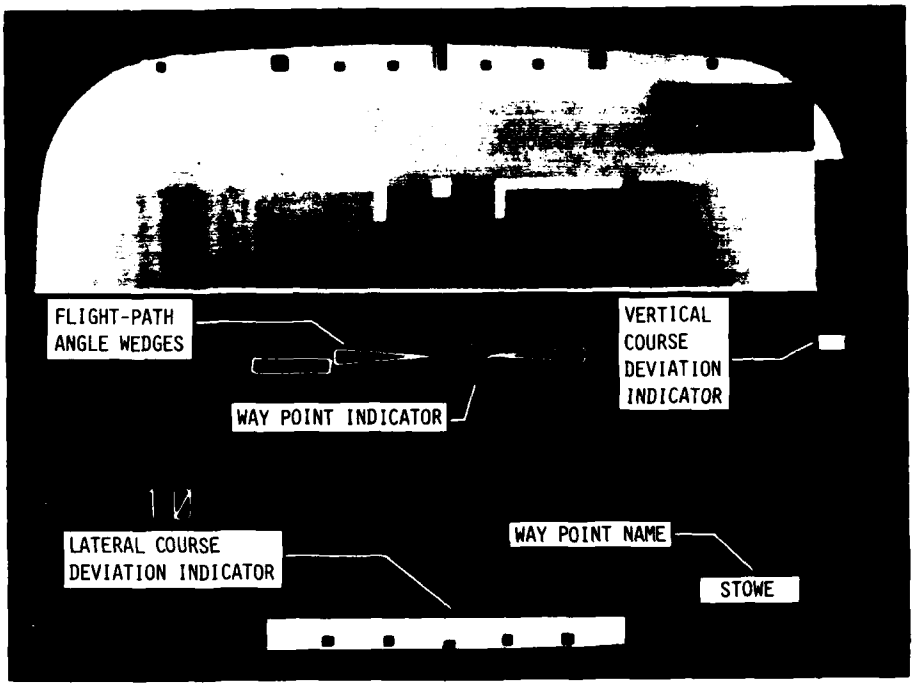

Figure 9.- EADI display with course deviation indicators, waypoint indicator, and flight path angle wedges guidance symbology.

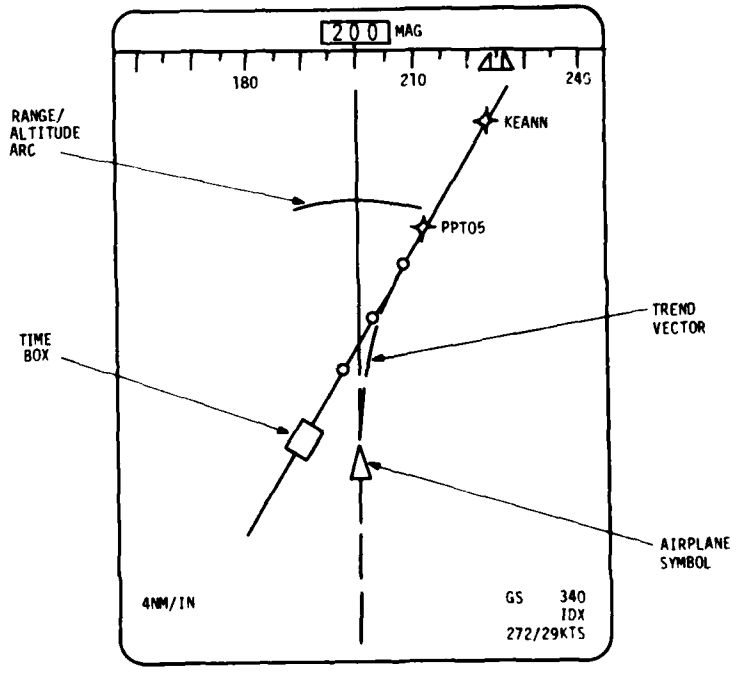

Figure 10.- EHSI display with trend vector, range/altitude arc, and time guidance symbology.

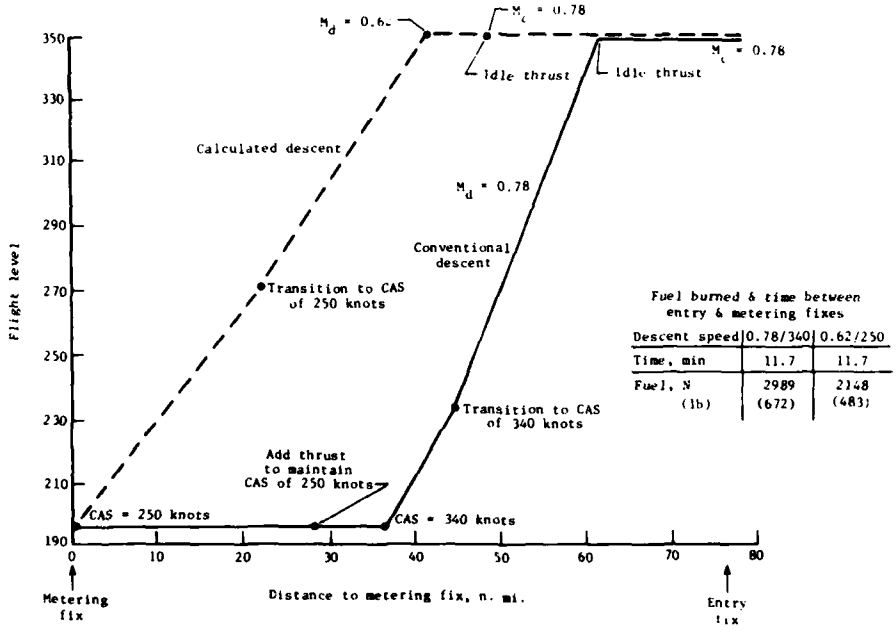

Fuel burned & time between entry & metering fixes

Descent speed	0.78/340	0.62/250
Time, min	11.7	11.7
Fuel, N (lb)	2989 (672)	2148 (483)

Figure 11.- Comparison of descent profile typically flown and descent profile calculated by flight management descent algorithm.

AVIONICS FLIGHT EVALUATION SYSTEM (AFES)

Karlheinz Hurraß
Deutsche Forschungs- und Versuchsanstalt
für Luft- und Raumfahrt e. V. (DFVLR)
Institut für Flugführung
3300 Braunschweig, Germany

ABSTRACT

New avionic systems require thorough testing. Particularly as far as navigation systems are concerned, very accurate reference trajectories have to be established.

For this purpose, DFVLR has developed an Avionics Flight Evaluation System (AFES). A tracking radar, a laser tracker, and an inertial navigation system (INS) on board the test aircraft are used in order to measure flight trajectories. The data of all these sensors are combined by optimal filters.

In order to be able to evaluate in real time, computers are used at different locations. All elements of this measurement system are linked together by an efficient data transfer system.

Besides the reference system, AFES contains subsystems for artificial traffic loading and measuring multipath effects.

1. INTRODUCTION

New avionic systems have to undergo careful tests, before they can be introduced. Particularly as far as navigation systems are concerned, the results of such test programs must show clearly the advantages and disadvantages of the navigation system which is tested. In addition, the tests have to show that certain demands are met. In this connection, the navigation accuracy of a navigation system is an important factor. Therefore, the determination of reference trajectories is an essential means of testing navigation systems.

The first test system which was used by DFVLR for such purposes mainly consisted of cinetheodolites, a tracking-radar, and an inertial navigation system on board the test aircraft (Fig. 1). Due to the use of cinetheodolites, on-line computation was not possible. Normally, it took one to two weeks to evaluate the films from the cinetheodolites, and to get a reference flight path. Therefore, the new test system, i. e. the Avionics Flight Evaluation System (AFES), uses a laser tracker instead of cinetheodolites.

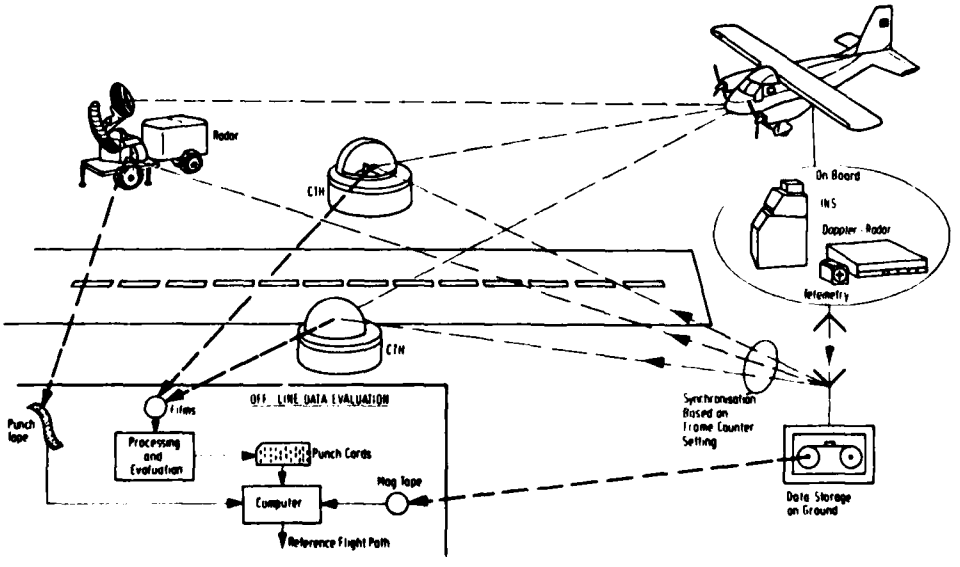

Fig. 1 Reference System using Cinetheodolites.

As far as testing radio navigation systems is concerned, the following is necessary:

- study of coverage and precision,
- study of influence of multi-path and traffic load,
- study of operational suitability,
- presentation to experts.

When testing autonomous on-board systems, e. g. INS, it is very important to determine the error behaviour.

In order to do all the above mentioned work with the aid of AFES, the following sub-systems are necessary:

- reference system,
- telemetry and data system,
- multi-path system,
- traffic load system.

The most important sub-system is the reference system which provides reference trajectories having a high degree of accuracy. Thus this report mainly describes that system.

2. SENSORS OF THE REFERENCE SYSTEM

The main components of the reference system are:

a tracking radar and a laser tracker on the ground,
an inertial navigation system, and a DME interrogator
on board the aircraft.

Figure 2 shows a sketch of the tracking radar. This radar is able to measure automatically and simultaneously range, azimuth, and elevation. The radar was built by Radio Corporation of America (RCA). Angle tracking is achieved by electronically scanning the radar beam. The most important values characterizing this radar are:

pulse power	250	kW
pulse duration	1,5	µs
maximum range	234	km
accuracy (1σ)		
angle	0.03°	
range	5	m

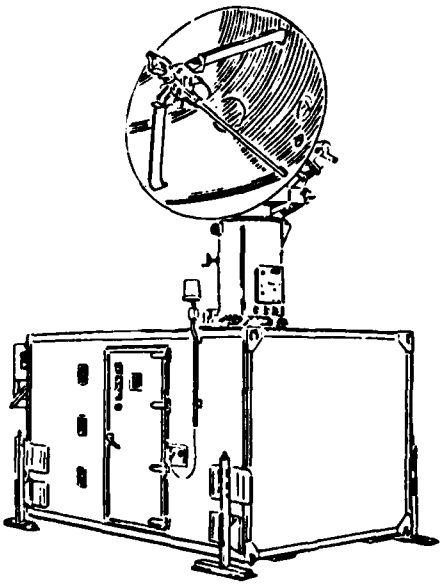

Fig. 2 Tracking Radar DIR.

The radar is built around a digital computer having complete control of all radar functions, e. g. all servo-loops are controlled by the computer. No mechanical indicators are provided, but all essential information is displayed on a video monitor. The radar can transmit the radar data (status, range, azimuth, elevation) to external equipment with a maximum rate of 20 Hz. The interrogation of the radar data can be synchronized by an external clock.

As already mentioned before, no on-line evaluation with cinetheodolites is possible. For this reason, a laser tracker was developed by the DFVLR Institute for Flight Guidance. The same accuracy will be reached with the aid of this tracker, as in the case of the cinetheodolites.

The principle of the laser tracker is similar to a micro-wave tracking radar (Fig. 3). The laser transmitter contains a gallium arsenid diode and generates short laser pulses. The pulses are directed to the target via two mirrors. The target is equipped with a set of retro-reflectors. Thus the laser pulses are re-transmitted to the receiver of the laser tracker.

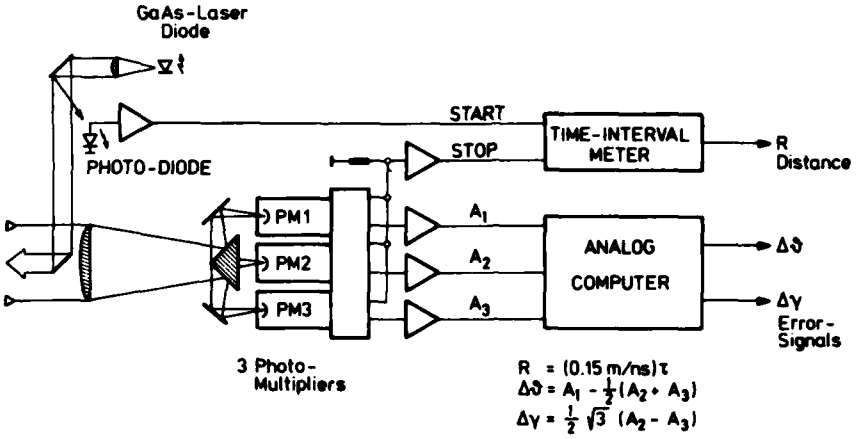

Fig. 3 Block Diagram of the Laser Tracker.

Apart from the optical components, the receiver consists of three multipliers. Before the returned laser pulses hit the three multipliers, the signals are divided into three parts. The intensities of the splitted parts of the laser pulses are equal, when the optical axis of the system is directed exactly towards the target. If the optical axis of the laser tracker is not accurately aligned to the target, the three photo multipliers will be differently illuminated by the returned laser pulse. Thus different signals are derived, and will result in error signals for angle servo-control.

The range is determined by measuring the travel times of the laser pulses from the transmitter via the target reflector back to the receiver.

A pedestal which was produced by Krupp, is used as a mount for the laser tracker. The mount includes all electronic parts for servo-control and digital read-out of angle data.

Specifications of the Laser Tracker

wave length	$904 \cdot 10^{-9}$	m
pulse power	80	W
pulse length	30	ns
pulse repetition frequency	400	Hz
receiver band width	$3 \cdot 10^{-9}$	m
(wave length of visual light 420 - $760 \cdot 10^{-9}$ m)		
maximum range	10	km
accuracy (1σ) angle	0.01	°
range	0.5	m

The micro-wave radar and the laser tracker are linked together via a serial data line. While a target is out of range of the laser tracker, the laser tracker is guided by the tracking radar. A computer takes into account the parallax between the tracking radar and the laser tracker. When the target enters the range of the laser tracker, the tracker automatically switches to track mode; this means, that slant range and angle are measured by the laser tracker.

One important part of the reference system is an inertial navigation system on board the test aircraft. The DELCO Carousel IV A was chosen, because this system is used by the German Lufthansa airline, and its maintenance is done easily by Lufthansa. The advantage of this system is the rotation in azimuth of the stabilized platform.

Thus certain errors can be detected during the alignment procedure, and can therefore be taken into account for navigational computations. Additionally, certain systematic errors are neutralized during the navigation mode.

If no data of the tracking radar or the laser tracker are available, a DME-interrogator is used. This interrogator (Collins DME-700) is able to measure all distances from the aircraft to five different ground stations simultaneously.

The main specification are:

maximum range	600 km
accuracy (1σ)	100 m
(determined by DFVLR)	

3. DETERMINATION OF THE REFERENCE TRAJECTORIES

A combination of positions measured by the ground sensors and the navigational results of the inertial navigation is used in order to determine the reference trajectories. Fig. 4 shows a typical error plot of azimuth measurements taken by the tracking radar. These errors were obtained with the aid of a second tracking radar which was set up about 300 km west of Braunschweig. It is clearly visible that the azimuth error consists mainly of a relatively high frequency noise. The same error behaviour is expected as far as the laser tracker is concerned, but the standard deviation will be much smaller. These high-frequency errors of the laser tracker, or the tracking radar DIR can be smoothed with the aid of least squares polynomial fitting. The disadvantage of this method is, however, that the error noise, as well as high-frequency movements of the test aircraft, are smoothed out, too.

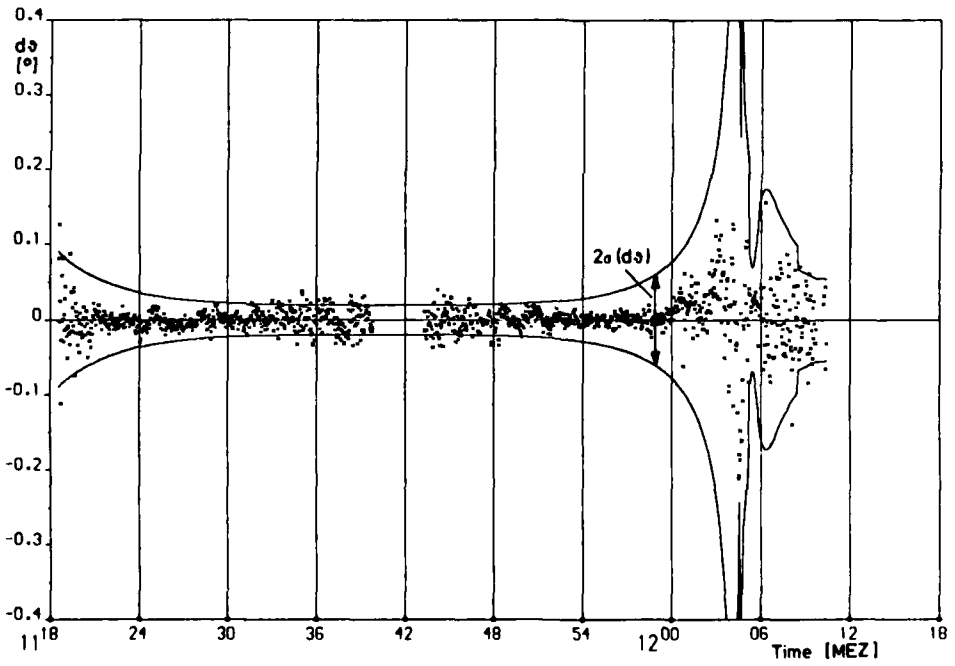

Fig. 4 Typical Azimuth Errors of Tracking Radars.

An inertial navigation system (INS) is able to eliminate this disadvantage. Thus the error noise of the ground equipment can be separated from the manoeuvres of the test aircraft. The INS has low-frequency position errors so that it seems quite logical to combine them with the ground sensors in order obtain a high-precision reference system. This combination is achieved on board the test aircraft by means of a Kalman filter. The filtered reference trajectories are found by adding the INS errors which have been determined by the Kalman filter, to the navigational results measured by the INS.

One great advantage of this method is that the flight-path trajectories and the velocity can be measured with a high degree of accuracy. The same is true as far as the time intervals between the measurements of the ground sensors are concerned. Flight-path trajectories can even be obtained, when neither the tracking radar nor the laser tracker can track the aircraft for a certain time. In this case the flight-path is determined by the INS, where the errors predicted by the Kalman filter have been considered.

The principle of the filtering process is shown in Fig. 5. The accuracy (1σ) of the reference system can be seen as a solid line. In this case, the INS is supported only by the tracking radar. This Figure also shows that radar data are appearing after about eight minutes. The dashed lines show the accuracy (1σ) of the tracking radar data which was calculated from the a priori accuracy data of the radar (angle 0.03°, range 5 m). Thus this value depends on the distance between the test aircraft and the tracking radar. The curve consisting only of noise represents the differences between the reference trajectories and the tracking radar data. In this case the accuracy which was reached is approximately 2 - 4 metres.

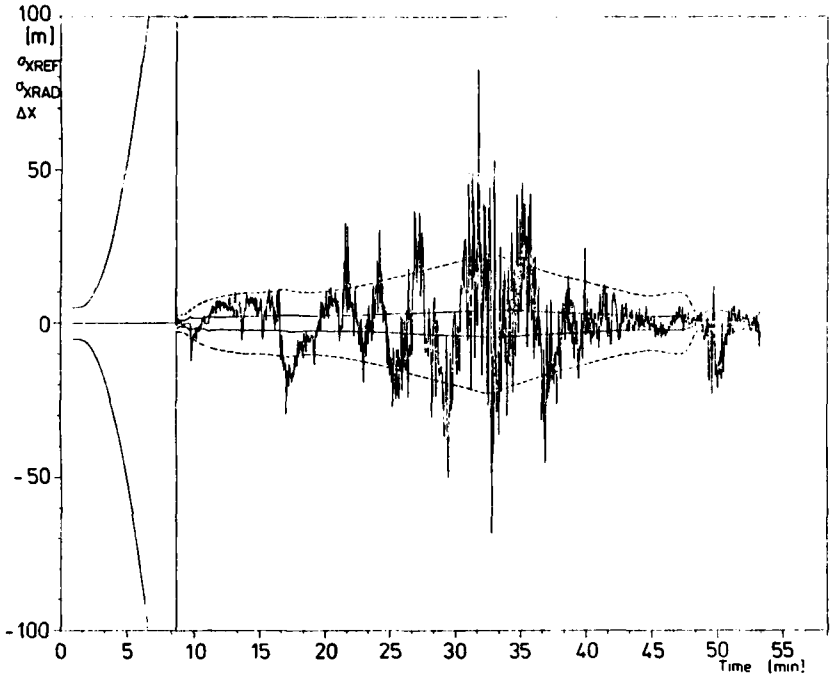

Fig. 5 North-South Error Behaviour of the Reference System.

4. DETERMINATION OF THE REFERENCE TRAJECTORIES WITH INCREASED ACCURACY

When taking a Kalman filter, no future but only actual and previous measurements by the ground sensors can be used. The greatest accuracy can be reached by using all measurements. For this purpose the "Rauch-Tung-Striebel-Algorithm" is used. Obviously, it can only be calculated off-line. Therefore, a great number of data has to be stored during a test flight. The "Rauch-Tung-Striebel-Algorithm" consists of a normal Kalman filter and a backward smoother. In the AFES software this is used in a stabilized form:

Kalman filter:

$$x(k)^- = \phi(k,k-1)\, x(k-1)^+$$
$$x(k)^+ = x(k)^- + K(k)\,(y(k) - H(k)\, x(k)^-)$$
$$P(k)^- = \phi(k,k-1)\, P(k-1)^+\, \phi(k,k-1)^T + Q(k-1)$$
$$K(k) = P(k)^-\, H(k)^T\, (H(k)\, P(k)^-\, H(k)^T + R(k))^{-1}$$
$$P(k)^+ = (I - K(k)\, H(k))\, P(k)^-\, (I - K(k)\, H(k))^T + K(k)\, R(k)\, K(k)^T$$

$x(k)$: state vector
$x(k)^-$, $x(k)^+$: filteres estimates of $x(k)$ immediately before and after measurement k
$P(k)^-$, $P(k)^+$: covariance matrices of $x(k)^-$ and $x(k)^+$
$K(k)$: optimal gain of forward filter.

Backward smoother:

$$x(k,N) = x(k)^+ + C(k)\,(x(k+1,N) - \phi(k+1,k)\, x(k)^+)$$
$$C(k) = P(k)^+\, \phi(k+1,k)^T\, (P(k+1)^-)^{-1}$$
$$P(k,N) = (I - C(k)\, \phi(k+1,k))\, P(k)^+\, (I - C(k)\, \phi(k+1,k))^T + C(k)\,(P(k+1,N) + Q(k))\, C(k)^T$$
$$x(N,N) = x(N)^+ \qquad P(N,N) = P(N)^+$$

N : total number of iterations
x(k,N) : smoothed estimate
P(k,N) : error-covariance matrix of smoothed estimate
C(k) : optimal gain of backward filter.

The smoothing process consists of two different steps:

1. The Kalman filter equations are solved for the flight being tested. The results are estimates of the state vector containing the INS errors and the covariance matrices accordingly.

2. The backward smoother equations are solved (backward) in time using and improving the estimates for the state vector of the forward filter. This algorithm is initialized with the last estimate for the state vector of the forward filter and the corresponding covariance matrix.

The accuracy due to the use of the backward smoother is normally 50 % higher than the usual Kalman filter. The greatest improvement is achieved during time intervals, when no measurements are available from the ground sensors.

5. USE OF DME MEASUREMENTS

The high degree of position accuracy, which can be reached by using the tracking radar or the laser tracker, is not really necessary for many tests. In such a case, the INS can be supported by DME measurements from different ground stations. Usually five stations are used.

The cycle time of the Kalman filter is two seconds. Only one DME measurement is used for each cycle. When interrogating five DME-stations, a complete sequence takes ten seconds. The DME data are measured by one DME interrogator being able to track five different ground stations at the same time. The Kalman filter in the on-board computer can estimate the DME biases which refer to the individual ground stations. Therefore, the filter has five additional elements in the state vector.

Many flight tests made in North Germany have proved that there are enough ground stations. When reaching an altitude of more than 4500 ft, the distances to at least five different stations could be measured.

6. ERROR MODELS

A simplified error model is used for the inertial navigation system (INS). The state vector contains the following elements:

$\Delta\lambda$, $\Delta\varphi$: the position errors in eastern or northern direction, respectively,

Δv_x, Δv_y: the velocity errors in eastern or northern direction,

α, β, γ: the misalignment angles of the platform.

A block diagram of the error model is shown in Fig. 6. It contains the Schuler loops, couplings of earth rate, velocity and acceleration. The gyro drifts are modelled as random walk processes. Earlier flight tests have shown that this simplified error model is sufficient for the case in question.

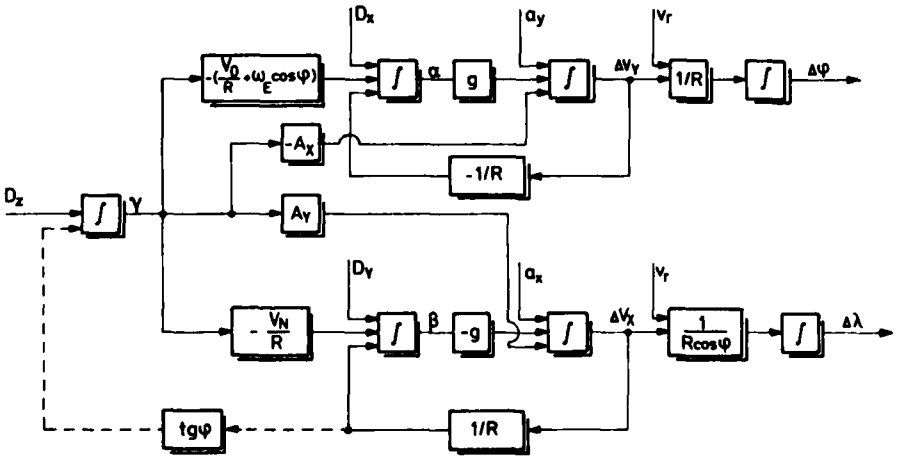

Fig. 6 Simplified INS Error Model.

As far as the tracking radar or the laser tracker is concerned, only random measurement noise is modelled. The systematic errors of the ground sensors are determined precisely. Therefore, there is no need for including elements for these errors in the state vector.

Regarding DME measurements, a bias error and a random noise error are taken into account. A great number of DME data from test flights are available to DFVLR. The standard deviation (1σ) of the DME errors was always approximately 100 m. The standard deviation of the systematic errors of the various ground stations was about 150 m. These values have also been checked by other organisations [1].

One important measurement is taken before each test flight. In order to do so, the test aircraft stays at an accurate surveyed marker. At this particular point, the preflight alignment of INS is made. When using the backward smoother, this surveyed marker is also a precise position update, if the test aircraft stops there.

7. DESCRIPTION OF THE TOTAL SYSTEM

Fig. 7 shows a block diagram of the total system. Immediately after the test aircraft takes off, the tracking radar as well as the laser tracker switch over to track mode. The data of these two ground sensors are checked and transformed to geographical co-ordinates. In addition, the covariance matrices of the measured positions are determined. These data are then transmitted to a computer in the central station, and from there by telemetry to the aircraft. The on-board computer being programmed with the Kalman filter uses these data to support the INS.

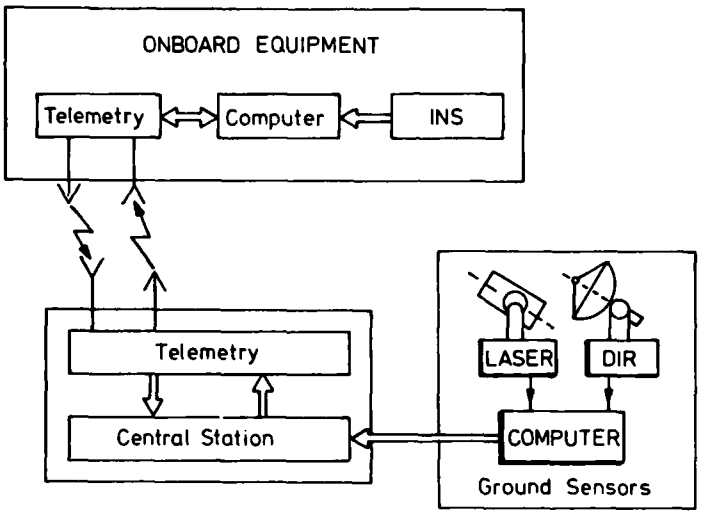

Fig. 7 AFES Block Diagram.

The positions being transmitted from the INS are given in units of about 0,05 nm. This resolution is not sufficient for the determination of the reference trajectories. Therefore, the integration of the INS velocity components is repeated in the on-board computer. The integration interval is 0.05 seconds. This means that the positions are calculated at a rate of 20 Hz. As already mentioned before, the cycle time of the Kalman filter is 2 seconds. Only the prediction of the two elements of the state vector, representing the position errors is made at a rate of 20 Hz.

The results of the on-line Kalman filtering process are used to correct the positions of the INS. These corrected positions are transmitted to the central station via a telemetry down-link, and used for quick-look presentations.

The different data on board the aircraft are acquired with the aid of the interface system called MUDAS (Modular Universal Data Acquisition System). MUDAS enables fast transfers of data, between the different data sources, and the on-board computer. All MUDAS functions are controlled by a processor. Apart from the functions for the total test system, MUDAS can also accept data from the avionic systems to be tested. For this purpose, the interface system MUDAS is equipped with some extra input/output modules. These modules are suitable for the following data formats:

- ARINC 429,
- Synchro signals,
- parallel digital data,
- analogue voltages.

During the test flights, all significant data are recorded on magnetic tapes. Immediately after each test flight, it is possible to use the recorded data for improving the on-line trajectories by using the Rauch-Tung-Striebel backward filter algorithm.

The computer in the central station is mainly used for calculating all relevant values for quick-look presentations. The most important peripheral devices are four x-y plotters.

Typical plots are:

1. flight track,
2. position errors of the tested system in northern and southern direction,
3. diagnostic plot.

The diagnostic plot shows the status of all sub-systems, e. g. the status of tracking radar.

Table 1 indicates the accuracy of the reference system. The errors refer to a polar co-ordinate system. Its origin is in the laser tracker. The correlation time of these errors is relatively long (more than 1 min.). Therefore, it is possible to monitor high-frequency errors of navigation systems, which are smaller than those shown in Table 1.

Distance [m]	Distance [m]	Azimuth [°]
0	-	-
500	0.5	0.010
1 000	0.5	0.006
2 000	0.5	0.003
3 000	0.5	0.004
5 000	0.5	0.005
10 000	0.5	0.005
20 000	5.0	0.008

Table 1 Accuracy of the Reference System.

8. CONCLUSIONS

DFVLR has developed an Avionics Flight Evaluation System (AFES). It can be used for testing of practically all avionic systems. Since there are computers at different locations, real time evaluation is possible. Thus the test results can be judged already during test flights.

When testing navigation systems, it is particularly important to determine the error behaviour. Therefore, AFES comprises a system for determination of reference trajectories. This is the most important sub-system and consists of a laser tracker, a tracking radar, and an inertial navigation system on board the test aircraft.

The data of all these sensors are integrated with the aid of a Kalman filter. As far as short distances from the ground sensors are concerned (up to 10 km), the following accuracies are reached (1σ, north-south or east-west directions):

position : 1 m
velocities : 0.1 m/s .

The interface system (MUDAS) on board the test aircraft contains input and output modules for the avionic systems which are to be tested.

The Avionics Flight Evaluation System has already been used when testing inertial navigation systems and attitude and heading reference systems.

Moreover, it will be used especially for the following purposes:

- testing of a precision distance measuring system (DME/P),
- testing of Global Positioning System (GPS) receivers.

9. REFERENCES

[1] RAWLINGS, R.C.,HARLOW, R.A.; "Flight Trials to determine the overall System Performance of Distance Measuring Equipment". Royal Aircraft Establishment, Technical Report 79140, November, 1979.

[2] RAWLINGS, R.C.; "The Flight Assessment and Applications of DME/DME". The Journal of Navigation, Vol. 34, No. I, January, 1981.

[3] GELB, A. (Ed.); "Applied Optimal Estimation". MIT Press, Cambridge, 1974.

[4] HURRASS, K., WINTER, H.; "A High Precision Reference System for Aircraft Position and Velocity Measurements". DGON-Vierteljahresmitteilungen II/III, 1976.

[5] HURRASS, K.; "Some Investigations on DME Overall Accuracy and Navigation Accuracy". Internal DFVLR-Report, IB 153-79/03.

[6] LATHAM, R.; "Aircraft Positioning with Multiple DME". Navigation: Journal of the Institute of Navigation, Vol. 21, No. 2, 1974.

[7] WINTER, H.; "Experiences in Flight Testing Hybrid Navigation Systems". AGARD Lecture Series No. 82, May 1976.

[8] BROKOF, U., HURRASS, K.; "A Simple Integrated Navigation System Based on Multiple DME". NAECON Proceedings, Dayton, Ohio, May, 1979, pp. 591 to 599.

REFERENCE SYSTEMS FOR THE EVALUATION OF DEAD-RECKONING NAVIGATION EQUIPMENT

by

R. F. Stokes and S. G. Smith
Royal Aircraft Establishment
Farnborough
Hampshire
GU14 6TD
United Kingdom

SUMMARY

Aircraft dead-reckoning navigation systems present particular problems in their assessment, and diagnosis in development where a continuous measurement of their error pattern is required. The inherent accuracy of modern inertial and Doppler equipment is such that there are few direct methods of measuring the system errors to the required precision.

The need for long range, long duration flights over both land and sea with a continuous high accuracy reference has led to the development by RAE of an integrated navigation system in which the outputs of a number of inertial navigation systems are recorded in parallel with those of Doppler radar, DME, Decca, Loran C and Omega. The recorded data is processed post-flight in a Kalman filter which is used to estimate the inertial system errors. The final reference is formed by compensating the inertial outputs for these errors and has the properties of high accuracy, low noise, and continuous availability.

Although simple in concept the implementation of such a scheme is complex. The major problem lies in constructing suitable mathematical models of the various equipments, and the technique of pre-processing is described. The second difficult area is that of obtaining the statistical information regarding the performance of the equipments in a form suitable for inclusion in the models.

Although the reference is produced off-line the techniques can be implemented on-line.

1 INTRODUCTION

1.1 History

Work on reference systems for evaluating navigation equipment for aircraft started at RAE Farnborough at least as early as the mid-1950s. At that time the Inertial Navigator (IN) for a guided bomb was being developed and the navigation of the aircraft to the target used a combination of the weapon IN, Doppler radar and position fixing. An output of the navigation process was a calibration of the weapon IN.

Development of this sytem included flight trials in RAE and A&AEE aircraft using the Decca Navigator chains in Southern England for position reference. The same method was used in the development of the IN intended for the TSR2 which took place in 1960/63. On these trials an early airborne digital computer on board the trials aircraft enabled Decca, Doppler and the IN information to be recorded and processed in flight in a form suitable for post flight analysis using a ground digital computer. This technique formed the basis for producing the reference navigation system which has been used for all our subsequent trials. The production of a position, velocity and attitude reference system for trials of inertial and other navigation systems has formed a major objective for RAE work on integrated navigation since that time.

Through the late 1960s and the 1970s UK IN systems for Harrier, Phantom, Tornado and Jaguar were developed, with RAE playing a major role in the trials of development systems, diagnosis of error sources and the accuracy assessment for operational use. As time progressed the equipments grew more and more accurate and it became increasingly difficult to provide reference data of greater accuracy than the systems under test. This has led to more and more sophisticated techniques being used, and the addition of other navigation aids, such as DME, Loran and Omega, into the mix.

The most stringent accuracy requirements came with the development of IN systems for maritime patrol aircraft in the late 1970s. Here it was necessary to know the position of the trials aircraft to a few tens of yards, at any time in a sortie of several hours duration, and at any place - including low level, over the sea, several hundred miles from the coast. This was needed in order to investigate the subtle effects of flight manoeuvres on the accuracy of the IN systems under operational conditions.

1.2 Early developments of the reference system

As mentioned above, the early trials of IN used the Decca Navigator as a position reference. When the systems under development had accuracies of five to ten miles per

hour, Decca, with errors of a quarter to half mile, was perfectly adequate to measure the system accuracy, but to be able to determine the error sources in the IN the random point to point errors in Decca were a nuisance. To overcome this Doppler ground speed and drift angle were combined with IN heading to provide North and East velocity components. These were then integrated (in the mathematical sense) to obtain the aircraft's position in latitude and longitude. This position information was recorded twice per minute along with the readings of the Deccometers. After flight the Decca readings were processed to give the Decca version of aircraft position, also in latitude and longitude, and the two versions compared.

A plot of latitude and longitude differences as a function of latitude and longitude enabled the main errors in the Doppler system to be determined, viz the heading error, bias and drift error, and scale factor error. The effects of these errors could then be calculated for each recorded time, and the Doppler position corrected. The resulting position had low noise (due to the integration process used on Doppler velocity information) and the long term accuracy of the Decca.

This technique proved adequate when flight trials could be based on simple profiles, mostly straight legs along the Decca bisectors. However in 1964 a new generation of IN arrived. The accuracy of these systems approached one nautical mile per hour, and the intended operation meant that flights of longer duration and range had to be flown. Decca was no longer suitable as the sole position level data source as the aircraft had to be operated in regions outside the Decca cover. For operational reasons the optimum trials route was from Boscombe Down via Shannon to Argentia in Newfoundland. Loran C was used as the position reference over the North Atlantic with Decca at each end of the route. The IN itself provided the most accurate heading information, so this was used for the Doppler/heading based position calculations.

Data processing was done in stages. In flight the Doppler/heading system gave one version of position, the Decca and/or Loran C a second version, and the IN itself a third version. All the data was recorded twice per minute on punched paper tape. Post flight this was processed to provide plots of the differences in latitude and longitude between the various systems as functions of time, and these plots were smoothed by curve fitting using a least squares method.

The IN error plot was often used to correct the position data obtained from Doppler and the radio aids. For example it was found that Loran C had a systematic error which was a function of position and grew to significant levels near Newfoundland. This was detected by the IN error plot having a form unlike typical IN errors, and being consistent from flight to flight. This form of error could be allowed for and was incorporated into the analysis on subsequent stages of data processing to produce the aircraft datum position.

1.3 The modern system

In the 1970s IN equipment had developed to the stage where current datum methods were no longer accurate enough. The only radio aid with sufficient accuracy for our purposes was DME, used in a range/range mode. However DME is a relatively short range aid and it was necessary to modify trials routes to give sufficient cover. One or two exercises were carried out in the USA in order to obtain sufficiently long flight paths for trials purposes. At this time the aircraft were fitted with commercial IN which were incorporated into the datum system, and enabled a reference to be obtained during the periods of flight when radio data was not available. This was done by mathematically modelling the IN errors and correcting for them using the information from the periods when external data was available.

As may be appreciated the process of obtaining reference positions for any particular flight was long winded and very labour intensive, since vast amounts of computation was needed, with human interpretation of the results at most stages. In order to automate the process Kalman filter techniques were developed. This involved designing accurate mathematical models of all the navigation systems employed in the reference system, and devising means whereby faulty data could be eliminated before the results were applied to the filter.

These techniques have been developed over the past five years or so and have found application in the most recent work, that associated with the development and assessment of an IN system for maritime patrol aircraft applications.

2 KALMAN FILTERING

The term Kalman filtering is used somewhat loosely in this paper and is intended to cover techniques descended from the original work by Kalman rather than a direct implementation of his original ideas.

2.1 Advantages of Kalman filtering

The Kalman filter algorithms are very suitable for any application where data has to be processed and results provided in real time, because the incoming data is used sequentially and then discarded. The results present in the Kalman filter at any time reflect the nett total of all information received to date. Thus the 'best' answer is continuously available and there is no requirement for the storage of input data from earlier times.

The form of the Kalman filter equations makes it very easy to combine data from sensors that operate in different coordinate systems and to infer the values of data items that cannot be measured directly. For example it is easy to combine the data from an IN with outputs of position in latitude and longitude, velocity components north and east, and heading, with range fixes from a DME, and ground speed and drift angle from a Doppler velocity sensor, to produce more accurate estimates of position, velocity, and heading.

A further consequence of the form of the Kalman filter algorithm is that data from various sensors can be accepted intermittently and yet still be used in an optimal way. For example, the Doppler ground speed data could be used asynchronously from the drift angle values, and the DME fixes taken at yet other times.

The data from individual sensors are, to a large extent, processed independently of each other, and so it is relatively easy to change the manner in which the inputs from one sensor are treated without affecting the processing of data from other sensors.

As with all good things there is a price to be paid, and in the Kalman filter this is manifest in the requirement for a detailed knowledge of the characteristics of the individual sensors.

2.2 Assumptions

The basic principles of the Kalman filter are based on a number of assumptions:

(1) The process to be modelled in the Kalman filter can be adequately represented by the values of a set of coefficients.

(2) The values of the coefficients at a future time can be predicted from their values at an earlier time and a knowledge of the dynamics of the process. These dynamics have to be reduced to a set of linear differential equations.

(3) The statistical properties of these coefficients are known.

(4) It is possible to measure the value of some combination of the coefficients.

(5) The uncertainty of the measurement quantities are known.

The Kalman filter algorithms then provide a sequential recursive procedure for determining values for the coefficients that are statistically optimum in the sense that they have minimum probable error.

2.3 Kalman filter procedure

The steps in the Kalman filter procedure are as follows:

(1) Assuming a set of values for the coefficients or state elements of the system at some time t, the values of the state at some future time $t + dt$ are predicted.

(2) Using the known statistical properties of the state elements, their uncertainties at time $t + dt$ are also predicted.

(3) The value and probable error of some measurable combination of the state elements is then also predicted.

(4) An observation is made of this measurement quantity, with the observation having a known uncertainty. The difference between the predicted and observed values of the measurement quantity is used to adjust the values of the state elements. The Kalman filter equations yield optimum weighting factors that are used to distribute the difference between the various state elements.

(5) The estimate of the uncertainties is also adjusted to take account of the fact that extra information has also been added to the estimates of the elements, thus reducing their uncertainty.

In the case of the Navigation Reference System the generalised form of the Kalman filter takes the form of the block diagram shown in Fig 1. The state elements are the set of error sources sufficient to characterise the errors in the outputs of the various navigation sensors being used. The prediction process is carried out by mechanising a set of linear differential equations, with time varying coefficients, that describe the behaviour of the error sources in the absence of external disturbances.

2.4 Prerequisities of the filter

There are two aspects of a navigation system's behaviour that it is vital to understand before the system can be successfully incorporated into the Kalman filter. The dynamics of the error propagation must be modelled, as a set of linear differential equations, with sufficient precision to enable the predicted error values to be calculated with acceptable accuracy. In addition the statistics of the system errors have to be known, together with the statistics of any approximations that have been made in the dynamic model. It is often a major task to obtain the information needed to formulate these models, particularly the statistical ones. It can involve analytical studies, and detailed analysis of flight trials results. Often special flights have to be conducted

to collect the required basic data. In the past Kalman filters have been considered to require large computing resources, but this is no longer the case when viewed against the power of modern processors. An integrated navigation system based on the RAE Reference System could be implemented using currently available 32 bit microprocessors.

3 FORM OF THE RAE REFERENCE SYSTEM

The RAE system has been built around the data from an IN which provides the basic outputs of position, velocity, attitude and heading. The Kalman filter is used to estimate the errors in the IN data by comparing it with the outputs of a number of other navigation systems. The various sensors are modelled in terms of their errors in order to simplify the prediction process and reduce the computational load.

Because of the fundamental importance of the deterministic and statistical error models, these have always been derived from, or verified against, flight trials data. In practice the error sources included as state elements do not fully describe the behaviour of a given system because of practical limitations on the number of state elements and a lack of knowledge of the precise details of the error dynamics. An attempt is made to compensate for this by extensive modelling of the uncertainties in the prediction and measurement processes.

It has been found that the processing of the data from individual sensors can best be split into two stages, with a stage of data conditioning or preprocessing being applied before the data is fed to the main Kalman filter.

3.1 Preprocessing

The preprocessing of data from individual sensors serves to reduce the total computing task and simplifies the software design. Three main functions are undertaken:

(1) The incoming sensor data is checked for consistency and reasonableness. Much of this function is easier to perform in the preprocessing because data can be taken at a much higher rate than would be possible in the Kalman filter, although the cross checking of data between systems is best left until the filter.

(2) The outputs of individual sensors are corrected for predictable errors, given the knowledge of the aircraft trajectory from the Kalman filter output and inputs from the operator concerning the conduct of the flight and other environmental data. Examples of these corrections would be lag compensation of outputs of sensors with a low frequency response, and compensation of Doppler ground speed and drift angle for the errors produced when flying over water.

(3) The outputs of some sensors can be averaged to provide inputs to the filter that can be represented by a reduced set of state elements. For example the multiple range position lines available from each Omega ground station can be reduced to a single range value. The error statistics used in the uncertainty prediction and measurement processes are often computed as a function of the flight profile, or of some secondary output from the sensor such as signal to noise ratio.

3.2 Features of the filter

The use of preprocessing techniques makes it possible to use a relatively simple set of error sources for the Kalman filter state vector with considerable benefits in terms of reduced computation. The prediction and measurement processes are mechanised in terms of errors and are linearised with respect to the aircraft trajectory as defined by the output of the integrated navigation system. The Kalman filter makes optimum use of the fixes from any combination of sensors and data rates, and there are further checks on the consistency of the input data before a measurement is used to update the filter's estimate of the individual system errors. This is most important because the filter has a long memory and can be upset for a long period by the inclusion of inconsistent measurements.

A mechanisation of the Kalman filter equations has been used that has been shown to have very good numerical stability, and this has meant that few problems have been experienced in this area where considerable difficulties have been experienced in some other applications.

The general form of the integrated navigation system is shown in Fig 2, with the Kalman filter box containing the elements shown in Fig 1.

4 REFERENCE DATA

Reference data is required for two basic types of trial, which have rather different requirements. Assessment trials require the best absolute accuracy from the reference data, while error source identification requires the data to be free from errors of a similar form to those of the system under test. Because the errors of a navigation system are frequently dependent upon the flight profile, a wide variety of routes have to be flown. This produces a requirement for a reference system with very broad capabilities.

Full three dimensional reference data at position, velocity, and orientation level (nine parameters in all) is needed so that the behaviour of any of the test system's

navigation outputs can be examined. The trials objectives and nature of the test systems dictate that this data be continuously available. High data rates are required in two main applications: for assessing the characteristics of any system outputs required at a high rate, and for investigating error sources that manifest themselves during manoeuvres. This overall set of requirements precludes reliance upon range data from radars or kinetheodolites because they cannot provide all of the quantities or the wide coverage required.

The approach to obtaining the required reference data has been based upon using multiple IN to provide the basic nine parameters. The data from IN has very low noise and a good frequency response, it is however subject to a build up of errors with time and manoeuvre. These errors can be corrected by mixing the inertial data with fixes from radio navigation aids having good long-term accuracy. The aids used for position fixes are Decca, DME, Loran C, Omega, and ground based tracking radar; while velocity fixes are obtained from a Doppler radar velocity sensor.

4.1 Inertial Navigator

Examples of the position and velocity errors of an IN are shown in Figs 3 and 4. The main features of interest are the characteristic periods of oscillation whose amplitude and phase change only slowly with time and aircraft manoeuvres. The observed errors are due to a multitude of sources within the IN, some of which are substantially constant over a number of flights and others of which change from flight to flight or even during the course of one flight. The preprocessing can be used to correct for the result of any error sources that are identified as being constant over a number of flights, and the filter is used to estimate the errors that change. The Kalman filter uses 10 state elements to characterise the IN.

The preprocessing scheme contains a very comprehensive model for predicting the statistics of the IN error states as a function of the aircraft trajectory and uses some 28 statistical error coefficients. These statistical coefficients allow for the changes in the values of the error states due to causes such as acceleration dependent gyro drifts, scale factor errors, and component misalignments.

4.2 DME

Fig 5 shows a typical set of errors in DME range data. The most significant features of these errors are:

(1) The noisy nature of the fixes, compared with the smooth position data that is obtained from the IN.

(2) For the data from any one beacon, apart from the noise, the errors are of the form of a slowly changing bias.

(3) The bias can change significantly from one beacon to another.

DME errors are modelled in the Kalman filter as a bias on the DME range readings, with the process statistics set to acknowledge that the bias can change slowly with time. The DME data is used in the filter by forming as a measurement quantity the difference between the observed DME range and the equivalent quantity predicted from the IN position corrected by the Kalman filter's estimate of the IN position errors.

In order to minimise the number of errors being estimated by the filter, only one DME range bias is modelled for each DME receiver. When the receiver is tuned to a new beacon the bias estimate and its uncertainty are reset. The values of bias and uncertainty for the old beacon are preserved, so that if that beacon should be retuned later in the flight, the filter estimates can be reset incorporating the information gained earlier in the flight.

There is little true preprocessing done on the DME range data, other than to check its validity. If a particular beacon is found to give a consistent bias over a number of flights, then this bias is removed before the data is fed to the Kalman filter. The DME data is ignored when the aircraft is very close to, or very distant from a beacon, because the assumptions of a slowly changing bias error tend not to be valid under these conditions.

A rather special case of preprocessing arises with the treatment of the position data for the DME beacons, and also for the ground stations of the other radio fixing aids. In order to fully realise the potential accuracy of the integrated navigation system it is necessary to ensure that all position data used is referenced to the same geodetic datum. Frequently, the latitude and longitudes of navigation beacons are quoted with respect to the geodetic datum of the country in which the ground station is sited. For any particular flight, a single datum has to be selected, and all position data is transformed to be with respect to the one datum.

4.3 Decca and Loran C

It may seem surprising, but there are many similarities between the significant characteristics of DME and those of Decca and Loran C, if the data from the latter two aids is considered in terms of their hyperbolic position lines, rather than as a

position fix. The position line data is the most suitable form for the Kalman filter because it leads to the simplest individual models for the errors and their uncertainties.

Fig 6 illustrates the errors from a typical set of the Decca red position lines over a number of Decca chains. It can be seen that it too can be represented as a slowly changing bias, although the rate of change of bias is rather more rapid than for the DME data. The Decca position line data is handled in the filter in an exactly analogous way to that used for the DME data, except that the readings are ignored when the aircraft is very close to either master or slave station, and the distant data is rejected on the basis of the width of the Decca zones.

Errors from a Loran C position line are similar to those of Decca. However the data has a new feature compared with the other radio aids, in the discontinuities associated with the 10 microsecond jumps in the output of the Loran receiver. The 10 microsecond jumps can be detected by comparing the observed Loran reading with the equivalent values predicted from the corrected IN positions, and then corrected before the data is passed to the filter. Loran C errors are modelled as a bias that changes only very slowly. Their uncertainty is a function of whether ground or sky waves are being tracked, and of the number of 10 microsecond corrections being applied.

4.4 Tracking radar

The use of data from ground based tracking radar presents a rather different set of problems compared with the other fixing aids. This is because the fixes are much more accurate, and so the estimation of their biases is less significant.

However, because these fixes are given such a high weighting in the filter, it is most important to ensure that the probable error of the measurement quantities are estimated correctly. This is the main task of the preprocessing of the radar data. The fixes are used in terms of the range and bearing from the radar, and a number of factors are used in predicting their probable errors:

(1) The elevation of the radar beam is important because it is very often close to grazing incidence with the surface of the earth.

(2) The actual bearing can also be significant because of the varying terrain surrounding the radar head.

(3) The magnitude of range is significant if the aircraft is not fitted with a transponder.

(4) The accuracies are such that the quantising of digital data and the timing delays associated with the ground and airborne recording systems can introduce significant uncertainties that are a function of the relative positions and velocities of the aircraft and radar.

4.5 Doppler radar

At first sight the errors of Doppler, when operating over the sea, seem very large. This is illustrated in Fig 7. There are large fluctuations in error between successive data points, coupled with large biases that alter with changes in aircraft position and heading. The errors can be largely corrected using a number of stages of preprocessing to correct for deterministic error sources. These error sources are:

(1) Lags in the Doppler information due to its mechanisation which appear as errors in ground speed and drift angle when the aircraft is manoeuvring.

(2) Errors due to distortion of the Doppler spectrum when flying over water.

(3) The effect of the motion of the sea surface.

The IN gives a very good measure of the aircraft manoeuvres and this information can be used to correct for lag induced errors.

Motion of the sea surface can be predicted from knowledge of surface wind. When the aircraft is flying at low altitude, say below 2000 feet, the velocity from the integrated system can be used to measure the wind at the aircraft and this vector can be reduced to sea level to give the surface wind that can be used in the correction algorithms. The accuracy of the corrections vary with the conditions of surface wind and aircraft manoeuvre and the knowledge of these conditions can be used to calculate the uncertainty of the Doppler ground speed and drift angle data at each time.

Fig 8 gives an example of the reduction in Doppler errors produced by the preprocessing.

The residual Doppler errors are represented by four error sources in the Kalman filter, viz Doppler scale factor, drift angle bias, and residual sea motion errors north and east. The changing uncertainties of these four error sources are modelled by the terms calculated in the preprocessing. The Doppler data is introduced into the Kalman filter via two measurement quantities formed as the difference between the filter and the Doppler's indications of ground speed and drift angle.

4.6 Omega/VLF

The Omega equipment produces its output in two forms: as a position in latitude and longitude derived from a combination of data from a number of ground stations, or as number of position lines with respect to the individual ground stations.

Typical examples of the errors in the latitude and longitude data from Omega are shown in Fig 9. The most significant error characteristics are the short term variations coupled with quite long period changes which have a small mean value. Over a long period, these characteristics are complementary to the errors of an IN, except that both systems have errors with oscillatory periods of about 24 hours.

The errors of either type of Omega output are modelled in the filter as a slowly changing bias. The choice between outputs is a difficult trade-off between accuracy, redundancy, and computing load. The latitude and longitude outputs require the smaller computing power because only two error states are needed, but it is hard to predict the probable rate of change of bias because the positions are derived from an ever changing combination of individual position lines. At the other extreme, the individual position lines - up to 25 of them - much more closely meet the assumptions implicit in the error model, but would impose a heavy computing burden.

Two methods of using Omega/VLF data have been examined: firstly, the use of the latitude and longitude outputs in a straightforward manner; secondly, the use of position line data with preprocessing to combine a number of lines and to calculate their likely uncertainties.

This latter preprocessing is another interesting example of how the technique can be used to reduce the size of the filter. The data from each ground station is available as a reading of the range between the aircraft and station measured on each of the transmitted frequencies. Since each of these multiple range measurements is made along a very similar propagation path, it is reasonable to form a single average range measurement to each ground station. The uncertainty of the average range may be calculated from a number of factors: the observed signal to noise ratio gives an indication of the quality of the individual range measurements; the aircraft position plus time and date enables the form of the propagation path to be determined, and from this the uncertainty in the propagation corrections may be calculated.

5 OFF-LINE PROCESSING

All of the features discussed so far are appropriate to an integrated navigation system that is required to produce its results in real time. The creation of reference data for flight trials is a special case in that the maximum accuracy is not required until after the flight. Under these conditions another convenient feature of the Kalman filter algorithms can be used to enhance the accuracy of the final results. Because the propagation equations are linear, the filter can easily be made to run backwards with respect to time to produce a new set of estimates of the IN's errors. Thus at any time we have estimates of the IN errors based on all the information available before that time and an independent estimate derived from all of the information available after that time. The uncertainty of each of these estimates is also available. Thus the two versions can be merged to give a single best estimate based on all of the available information. This technique of forward-backward filtering is especially beneficial for preserving accuracy in areas with poor fixing aid coverage.

6 REFERENCE SYSTEM ACCURACY

The reference data produced by the process described above has all of the desired characteristics stated at the start, and its overall accuracy, when operating without the benefit of fixes from tracking radar may be summarised as follows:

(1) Reference position accuracy 0.07 nautical miles (130 m) rms.

(2) Reference velocity accuracy 0.3 knots (0.15 m/s) rms.

(3) Heading accuracy 0.05 deg rms.

These errors were measured by comparing the results obtained with and without the radar fixes being included. In any given area the accuracy will depend upon the coverage available from the fixing aids and the behaviour of the IN which is itself influenced by the manoeuvres being performed.

It should be noted that the data processing techniques employed to produce the reference system provide a ready means for examining the behaviour of every navigation system used on the flight. The results thus obtained are used to continually refine and update the parameters of the models for each system, and the Kalman filter mechanisation provides a very convenient mechanism whereby this new knowledge can be incorporated for future flights; usually by amendments to the preprocessing corrections or to the calculation of the various uncertainties.

7 LESSONS LEARNED

The Kalman filter approach really does work and its use is justified by its ability to handle diverse and intermittent data and the ease with which it can accommodate

changes to the individual sensor models. The integrated systems have yielded accuracies that could not have been achieved by individual navigation sensors, and have demonstrated the ability to make good use of the complementary features of various equipments.

The price to be paid is in the detailed knowledge required of the characteristics of the individual sensors. This knowledge has led to a more informed use of the data from the sensors and has had wider application than just the integrated systems, in that it has assisted the general improvement of the individual sensors.

If integrated navigation techniques are to be applied more widely there is a need for the flight trials of individual equipments to produce more pertinent data as a matter of course. Too often it has been found that past trials have not produced information in a form appropriate to integrated navigation applications and it has been necessary to conduct special trials to gather the required data. It is highly desirable that future equipment trials should consider the possible use of the equipments in integrated systems and attempt to gather the appropriate basic information.

8 ACKNOWLEDGMENTS

The authors would like to acknowledge the contribution made to the work by their associates, particularly those outside the immediate group at RAE. Firstly Navigation and Radio Division at A&AEE, Boscombe Down, with whom they have worked from the earliest days on trials of navigation equipment, secondly the Racal-Decca Group who have developed models for Doppler to be incorporated in the filter and preprocessing algorithms, and lastly Stephen Howe Ltd who have done much of the general implementation of the Kalman filter. Stephen Howe are providing A&AEE with a version of the RAE integrated navigation software which will be used by Boscombe for future navigation trials.

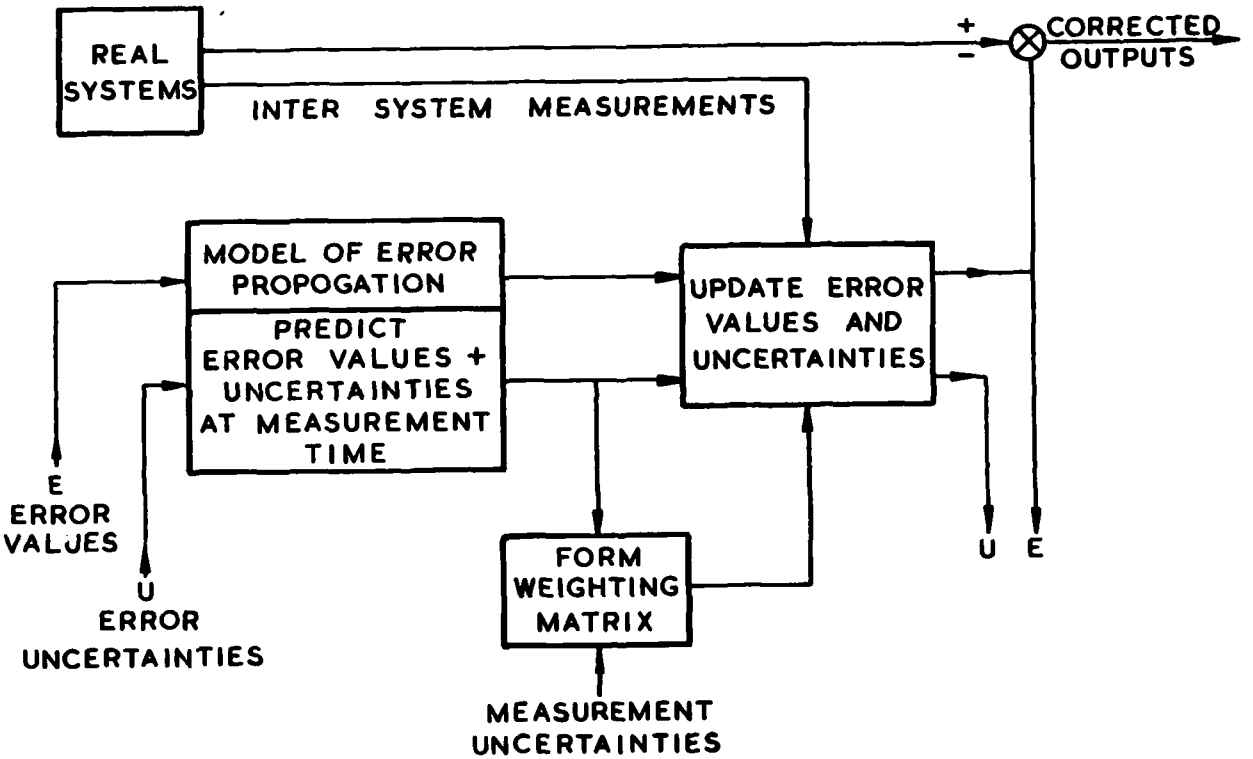

PRINCIPLES OF THE KALMAN FILTER

FIG 1

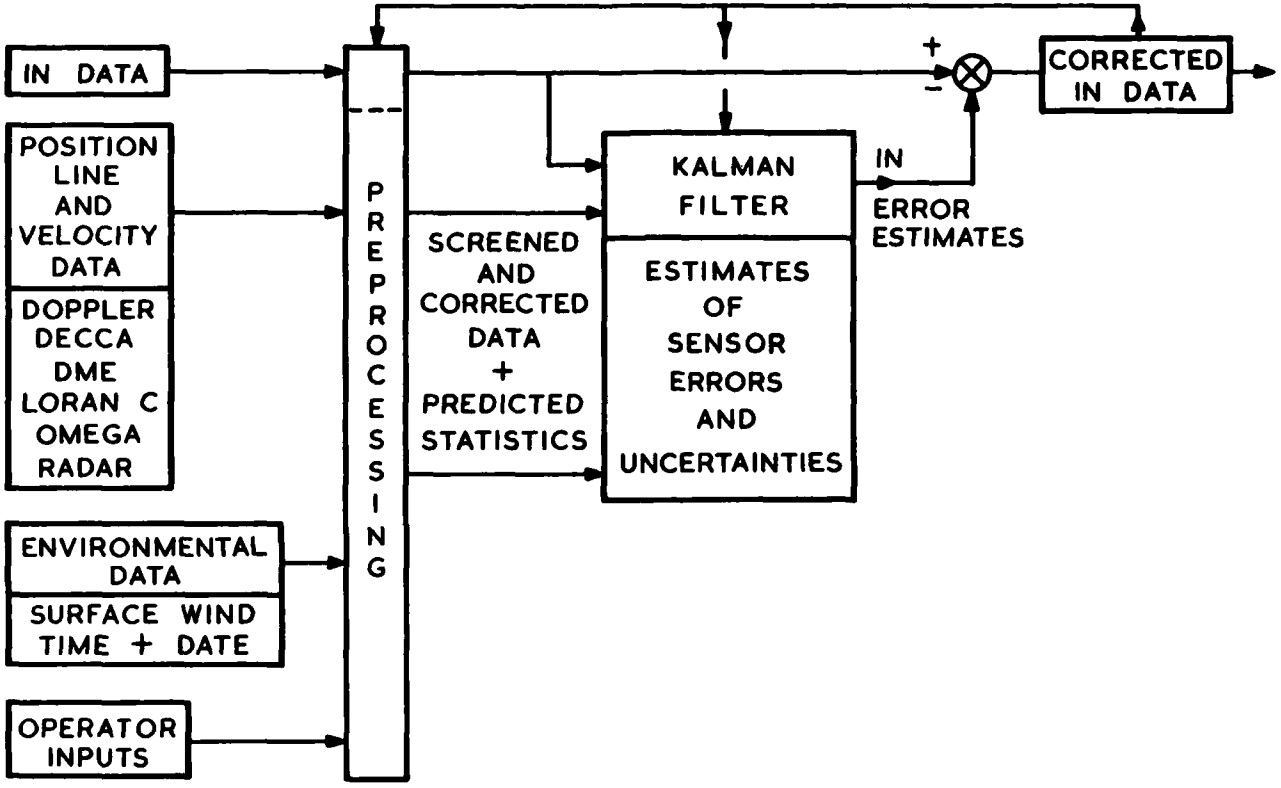

FORM OF THE INTEGRATED NAVIGATION SYSTEM

FIG 2

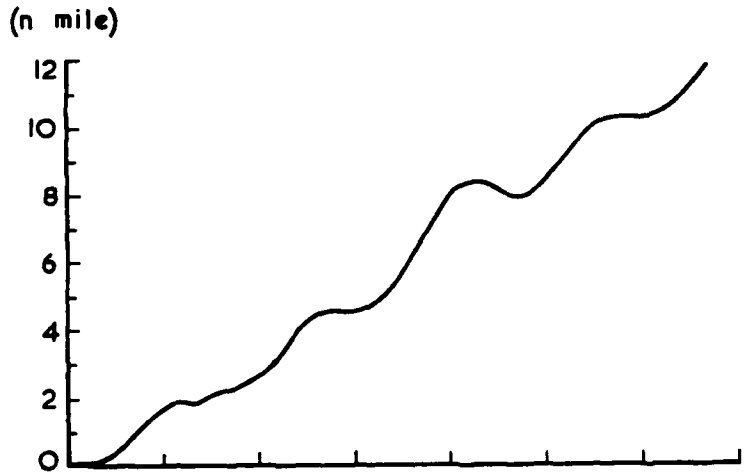

NORTH POSITION ERROR

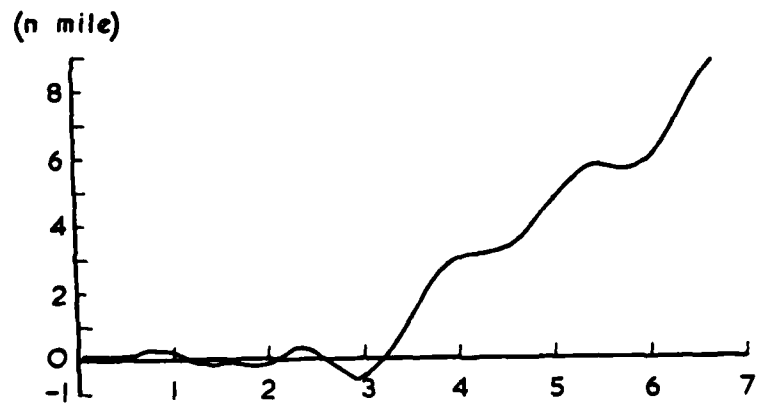

EAST POSITION ERROR

TYPICAL INERTIAL NAVIGATOR POSITION ERRORS

FIG 3

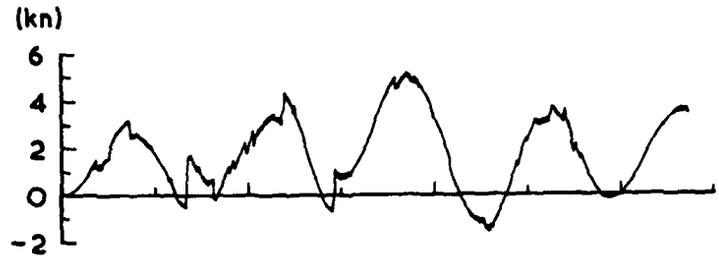

NORTH VELOCITY ERROR

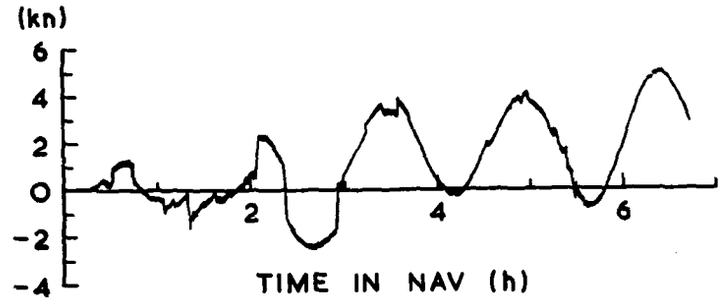

EAST VELOCITY ERROR

TYPICAL INERTIAL NAVIGATOR
VELOCITY ERRORS

FIG 4

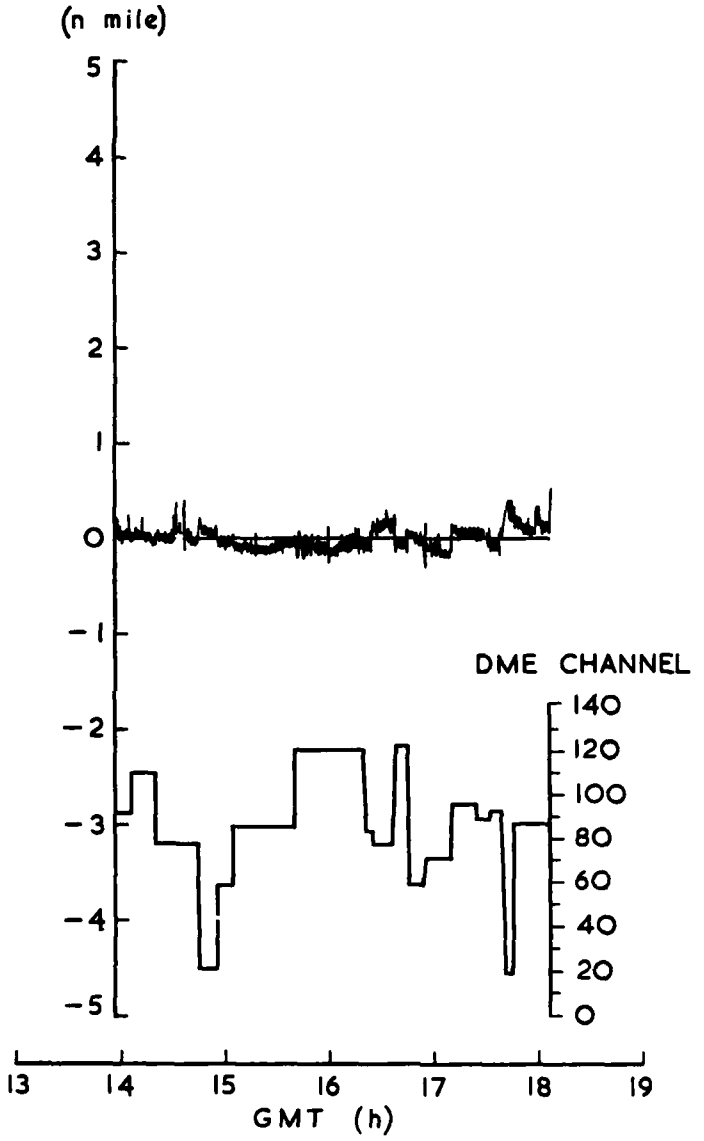

TYPICAL DME RANGE ERRORS

FIG 5

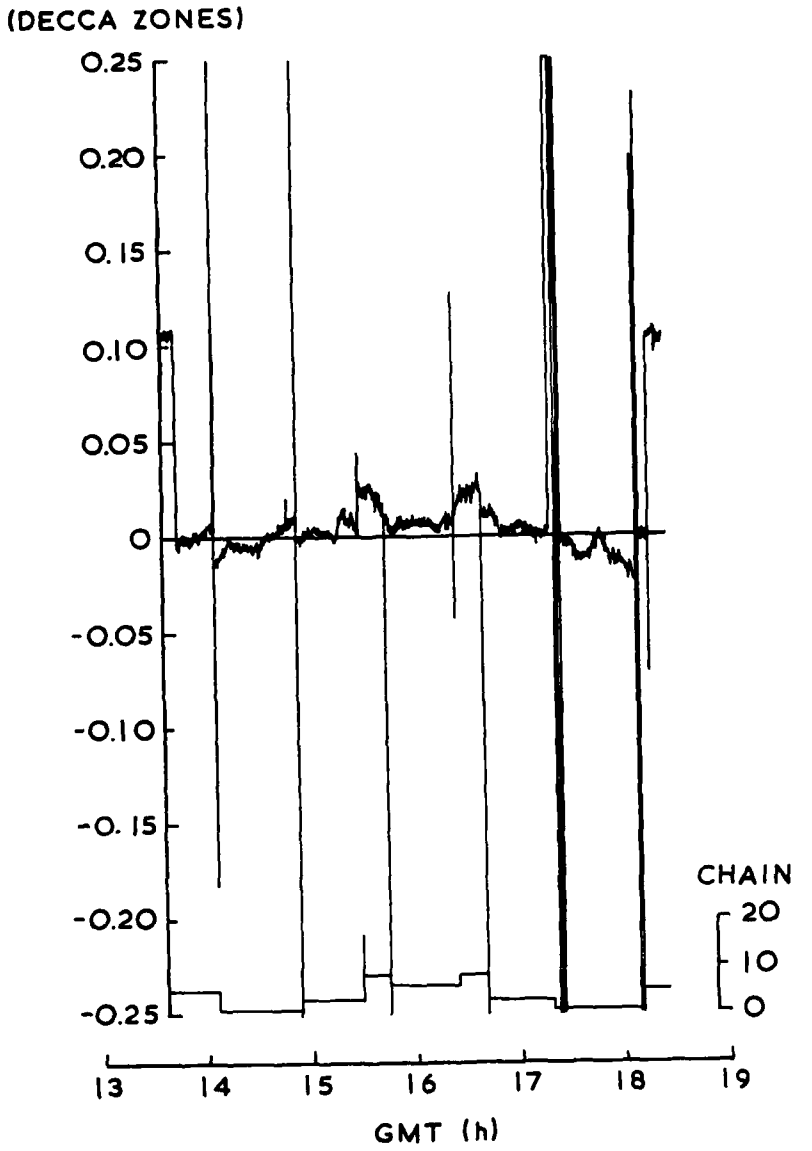

TYPICAL DECCA NAVIGATOR PHASE ERRORS

FIG 6

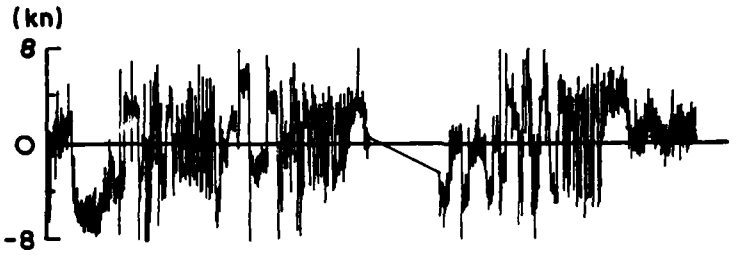

GROUND SPEED ERROR

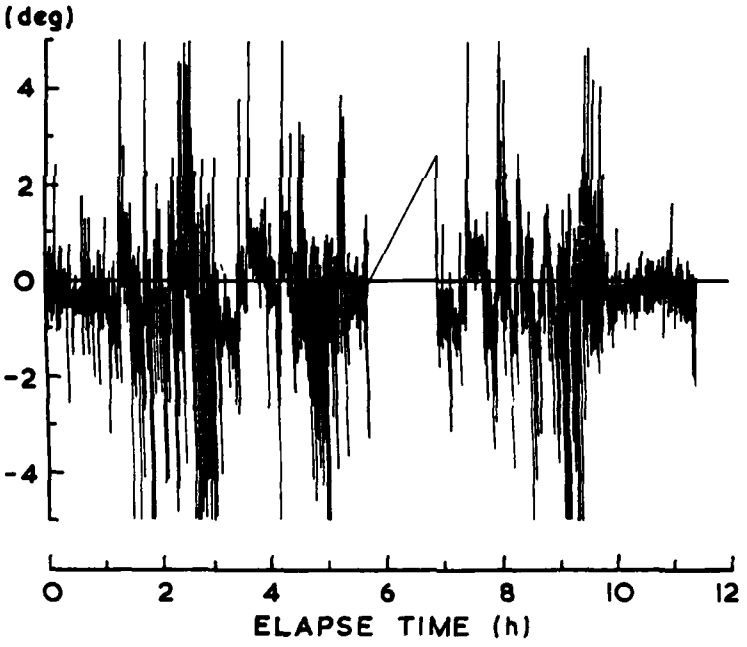

DRIFT ANGLE ERROR

TYPICAL RAW DOPPLER ERRORS

FIG 7

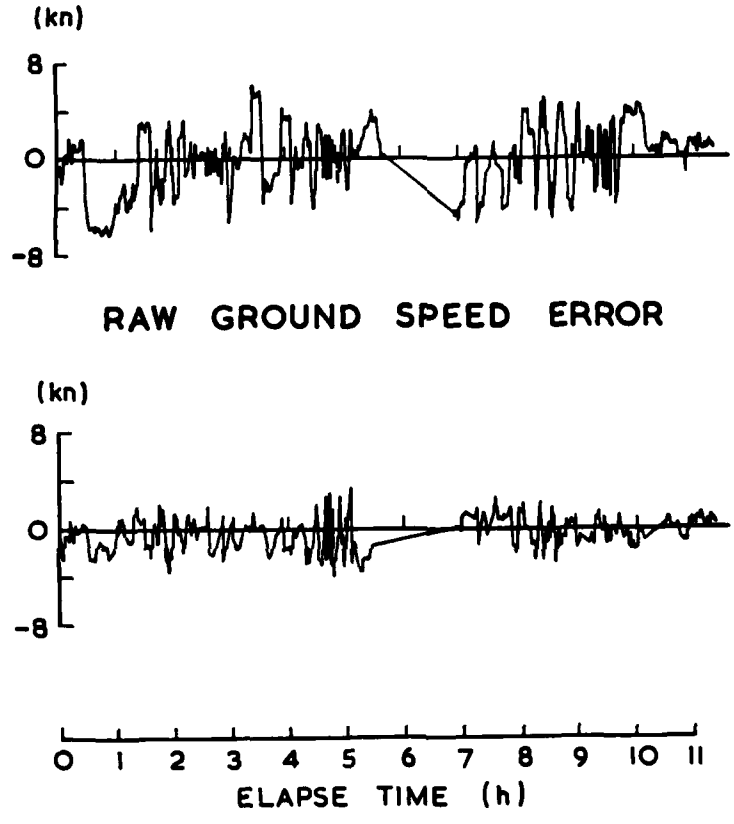

RESULTS OF DOPPLER
DATA PREPROCESSING

FIG 8

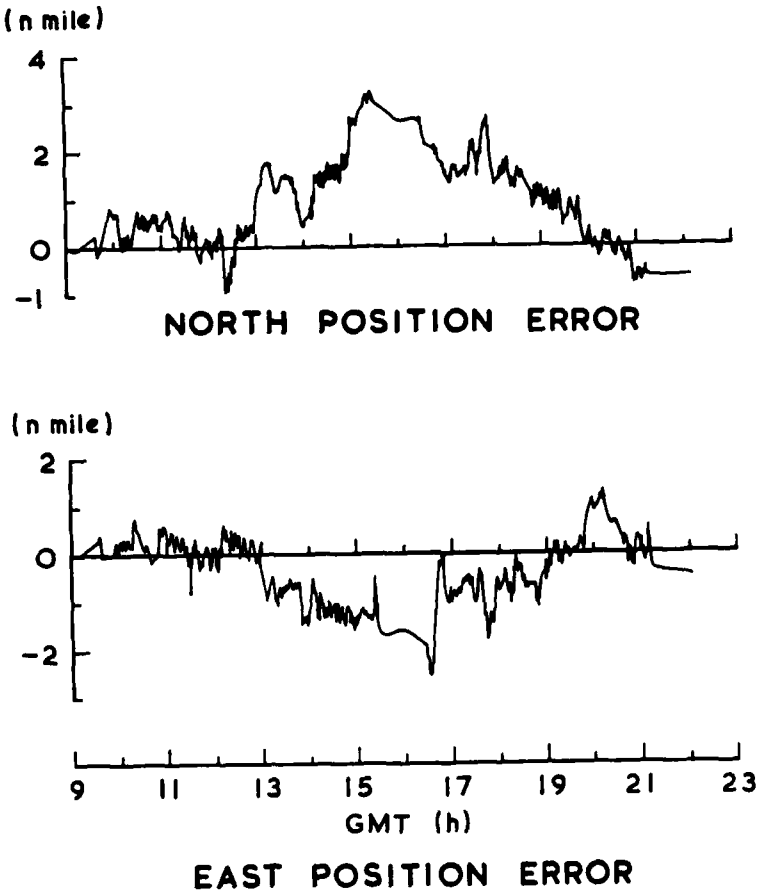

TYPICAL OMEGA POSITION ERRORS

FIG 9

AIR COMBAT SIMULATION
– METHODS, MODELS, TRENDS –

by

G.Wunderlich, H.P.Fehrenz, IABG/SOL
Einsteinstrasse 20
8012 Ottobrunn
W. Germany

SUMMARY

This paper describes briefly various methods to evaluate weapon system parameters needed during air combat. The influences and connections between unmanned and manned combat simulation are derived as well as the main differences between 1 vs 1 and m vs n combat including relevant pilot behaviour. Finally some studies performed with unmanned and manned m/n air combat simulations are described and it is shown how both methods support each other thus broadening the validity of application and results.

1. INTRODUCTION

Before discussing in any detail the wide field of air combat simulation a short view on the background shall be done to understand the reasons to start combat simulations:
A vital part during evaluation of weapon systems, especially in early design phases, is the question dealing with survive-resp. successprobability with respect to its expected threat. Therefore designer as well as user of weapon systems look for suitable methods to estimate these above mentioned parameters. To simplify the problem of air combat it can be cut into two sections, i.e. into the phase before combat (early warning, air battle situation, fighter assignment, fighter guidance, detection etc) and the combat itself. The latter one than principally can be evaluated by various methods shown on figure 1 which should be handled in an integrated manner.

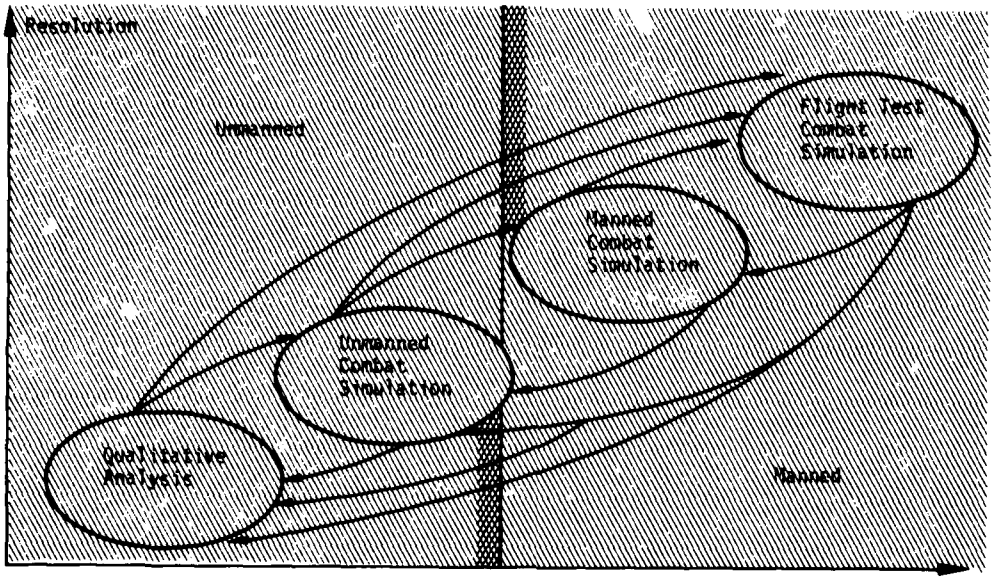

Fig. 1: Simulation Methods

2. METHODS OF COMBAT ANALYSIS

2.1 QUALITATIVE ANALYSIS

Air combat requires certain features with respect to acceleration, turn capability, visibility, size/ colour, radar reflection etc. In a threatening situation on excellent turn capability may be of vital importance while in case of chasing an opponent probably a high longitudinal acceleration is required. This type of analysis may be successful to a certain (low) degree if the nerformance of the weapon systems to be evaluated is quite different. It will become rather uncertain and no more usable if the performance parameter develope adverse, e.g. one aircraft has the better acceleration while the other has the superiour turn performance (figure 2).

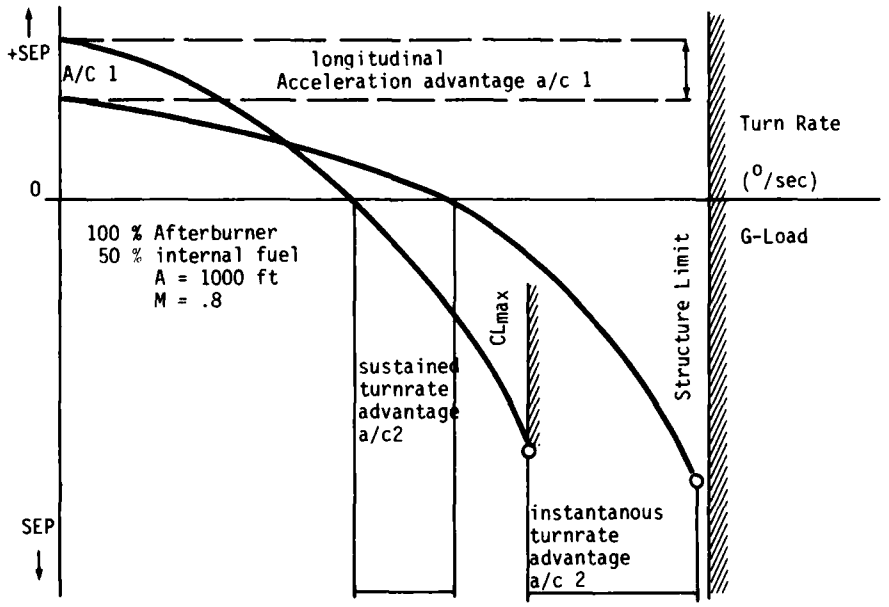

Fig. 2: Qualitative Analysis (Example)

In those cases the problem of weight occurs. Due to the interdependence of many parameters and due to the change of the importance of a certain parameter depending on the environment (threat, weather, armament etc) no weighting function can be developed. This tells that the qualitative analysis has to be supported by quantitative methods as shown on figure 1.

2.2 QUANTITATIVE ANALYSIS

2.2.1 GENERAL

Modern weapon systems are of such expensiveness that expensive evaluation methods are justified. Modern computers are outstanding means (big storage, fast execution) to simulate complicated events occuring during air battles.

Basically three methods can be offered (fig. 1): A complete abstract (unmanned) simulation, a mixed type (manned) simulation and a flight test (manned) simulation. These three methods are based on different modelling resp. hardware and therefore have differing topics, different expenses and different efficiencies. Mainly with respect to the different application areas it is obvious that they must not be seen in competition but in completing each other.

2.2.2 UNMANNED COMBAT SIMULATION

The unmanned simulation needs, as a key element, the simulation of the pilot, his decisions, his time dependend behaviour, the processes of developing movements to handle his aircraft due to his impressions etc. The pilot can either be simulated by some optimizing mathematical equations (e.g. time to achieve a certain position is minimized) or, more realistic, by logical expressions based on intensive dialoques between scientists constructing the simulation model and pilots to develop a decision tree in an iterative manner. This will be discussed later in some detail.

2.2.3 MANNED COMBAT SIMULATION

The main problem of the unmanned simulation is solved by putting the pilot into the loop. But beside the expensive hard- and software and the need to give the pilots very good impressions of the environment (visual cues, handling qualities, g-forces, black-out, noise etc) this requires the simulation in real time (unmanned simulations are up to 5o times faster than real time), a detailed pilot familiarization/training and sufficient replications of the combats to filter out pilotbased dispersion which has the consequence that a rather limited number of parameters and starting conditions can be varied. Additionally most simulators are limited to a rather small number of participants. The resulting effect will be discussed later.

2.2.4 FLIGHT TEST COMBAT SIMULATION

The newest combat simulation method shall be discussed briefly at the example of the USAF/USN-studies AIMVAL/ACEVAL. The purpose of ACEVAL was mainly to find the effects of various force sizes while AIMVAL evaluated the effectiveness of various missile designs. Several aircraft are equipped with autonomous data generation pods giving all flight data to ground stations which calculate the flight-pathes of all participating aircraft. The flightpathes on one hand will be projected on screens to give a detailed view of the combat which serves as an outstanding debriefing system; on the other hand they areused for missile inrange and fly-out calculations serving missile designs as well as pilots to learn something on missile parameters used/needed in combat.

Additionally to the above mentioned methods more factors have to be included in terms of hardware (real aircraft), uncertainties like weather effects and safety aspects, human mistakes and competition as well as effects put on the avionics like sun, clouds, clutter etc.

This type of combat simulation is undoubtedly the most realistic but also the most expensive method. Additionally it is limited to existing aircraft, i.e. the evaluation of future systems is limited to missiles, probably to a certain extend to avionics.

3. PILOT SIMULATION

Fig. 1 showed the methods using manned or unmanned simulation. As mentioned before in case of manned simulation a rather sophisticated simulation of the environment is needed, which shall not be discussed further in this paper. On the other hand some details of pilot simulation are of some interest which may contribute here.

Basically a pilot performs the following tasks:
He watches his environment, builds up decision criteria (estimates due to target behaviour, range, range rate, heading, energy and armament status, noise, avionics information etc) and builds up decisions how to move his aircraft controls taking into account the capabilities of his and the opponents weapon system.

The same is done by a computerized pilot:
As an output of intensive discussions between scientists and pilots decision criteria are agreed and a set of mathematical tests and question series is developed to generate adaequate commands to the aircraft resp. missile. These commands (e.g. g-load, bank angle, power setting, missile launch etc) are compared with the technical feasable values and will be reduced if necessary. Using these (reduced) commands the aircraft/missile flightpath can be integrated for the next timestep.

The main difficulty of this method deals with the pilot, who has to describe his behaviour, to unterstand the resulting formula and to judge the resulting combat. This is only possible by using an interactive method. The pilot has to be informed as detailed and precise as possible on the combat history developing on the basis of his inputs given into the formula. Then he can criticize the program and change his decisions to improve the synthetic pilot as often as necessary to be satisfied. The only suitable method to fulfil this purpose is the use of real time dynamic graphics on displays. Our experience, especially in case of developing the many - on - many unmanned air combat model SILKA in cooperation with major german aerospace industry (BGT, DO, MBB, VFW, IABG) prooved this. We worked more than one year by using extensively various graphic programs which enabled the whole team to develop the combat model by careful iterations and modifications.

Basically no pilot is able to describe his behaviour exactly in all possible situations. Therefore no pilot model can be constructed, which is free of pilot errors. Consequently it does not make sense to exaggerate the precision of other submodels of a combat simulation or of the timestep for example. Additionally a single air combat obviously cannot be representative due to the mentioned weaknesses in the pilot model - it is necessary to evaluate mean values out of 4o - 5o combats, and relative results are to be prefered over absolute numbers.

An immense improvement was the step from an one-vs-one to a much more realistic m-vs-n simulation additionally including more sophisticated avionics, missile etc. The basic idea was that the pilot uses certain parameters which are known to him (range, look angle, target heading) to calculate a "threat-value" against each (detected) opponent. These values vary between 0 and 1 and take into account sensor data, weapon data, geometry etc (see fig. 3).

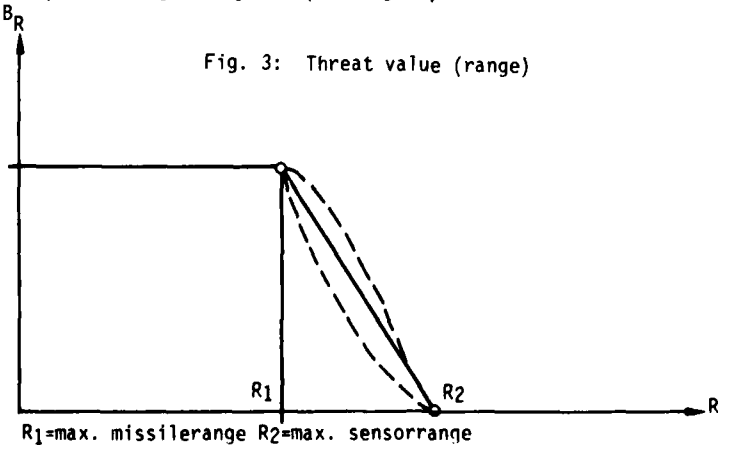

Fig. 3: Threat value (range)

R_1=max. missilerange R_2=max. sensorrange

By multiplying the three components

$$B_{Total} = B_R \times B_\varphi \times B_\psi$$

and adding a weighting function to implement the pilot's capability to extrapolate a "threat matrix" is found which enables the computer pilot to sort out the most attractive resp. the most threatening opponent. This is repeated every time step and leads to one-on-one resp. one-on- few duels of a rather short time period (5 - 20 sec) followed by a duel with changed combattants (see fig. 4.).

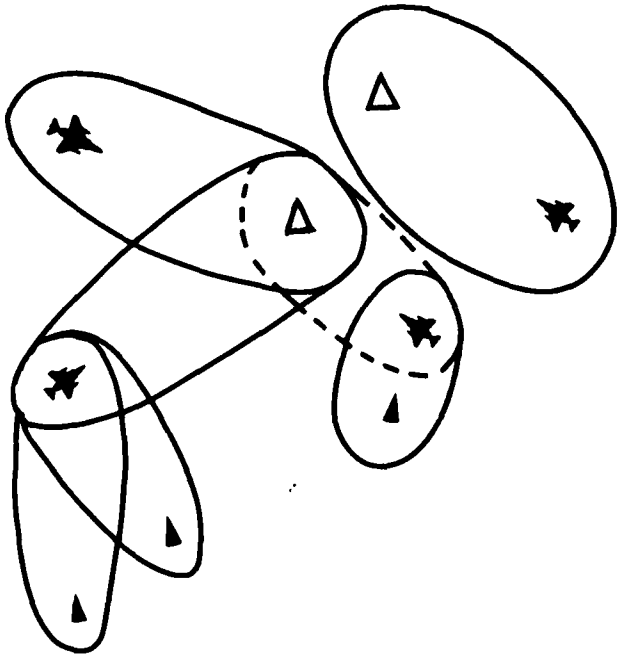

Fig. 4: Attachment of various combattants

4. VERIFICATION AND FINDINGS

4.1 ONE-VS-ONE-COMBAT

Due to the fact that unmanned simulations are contested sometimes as many verifications as possible are necessary. In our case we could use some flight test data (fig. 5) as well as a special comparison study between our one-vs-one unmanned model LULU and our manned simulation DFS (fig. 6 and 7):

Taking into account that the computerized pilot is much more couraged flying low altitudes the results are in sufficient accordance; similar agreement was found for other parameters like airspeed, g-load etc.

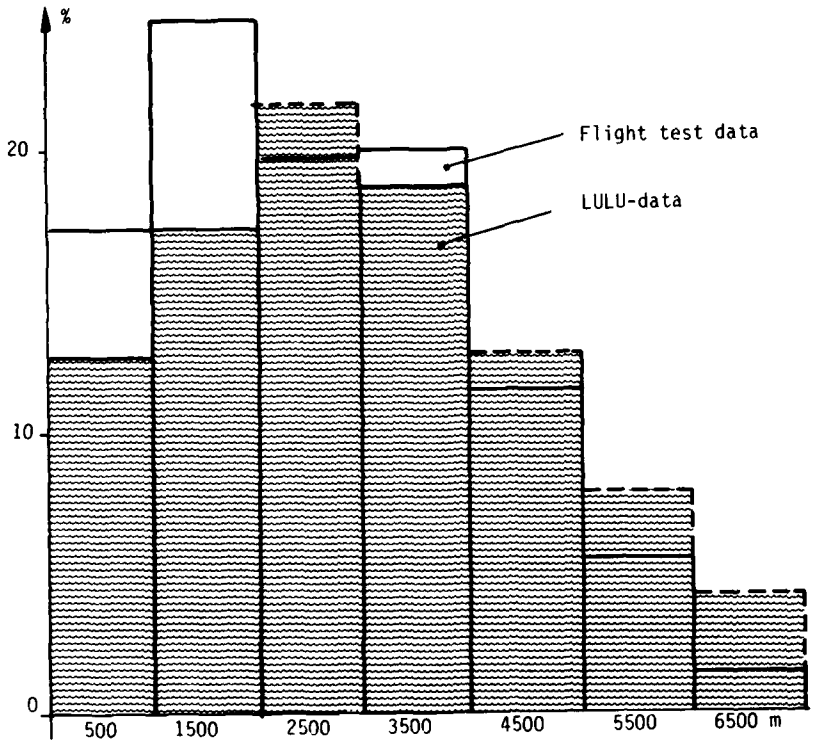

Fig. 5: Comparison LULU-flight test data
example: altitude

A special study was performed to compare LULU and DFS by evaluating combats between F-104 against F-4

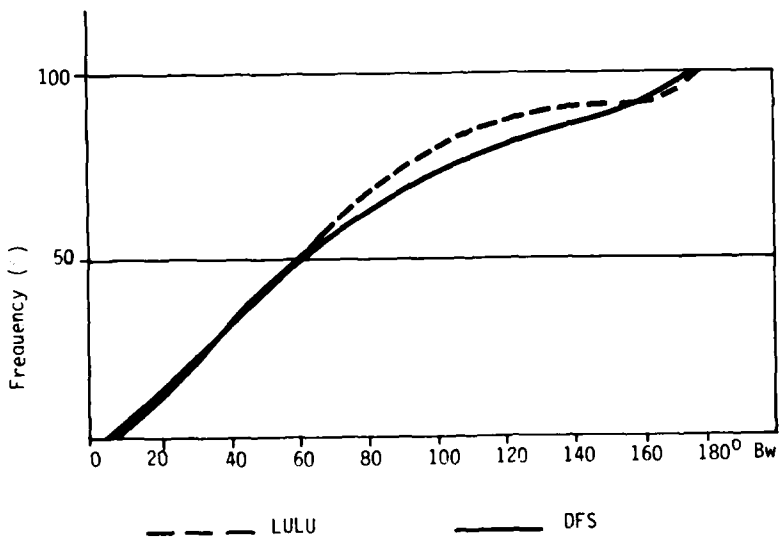

Fig. 6: Comparison LULU-DFS:
= example: off-the-tail-angle

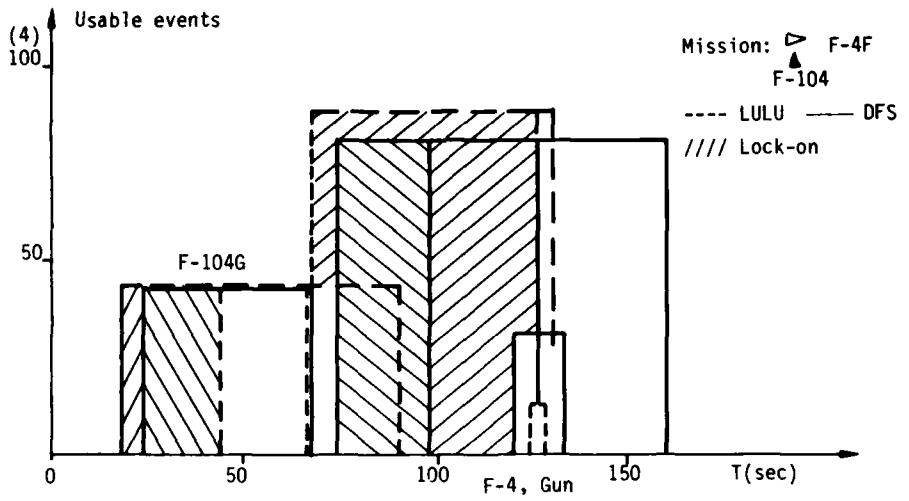

Fig. 7: Comparison LULU-DFS: time in envelope

Comparing parameters like angles, altitude, speed etc. results as shown on fig. 6 were found which show a rather sufficient accordance. Fig. 7 summarizes the mean values of beam-attacks of the F-104 against the F-4 by adding up all time intervalls inside the missile envelope with or without fire control lock-on including the gun. Again a very good agreement was found in terms of total time in envelope and first launch opportunities. The lock-on-times in case of LULU were longer due to the fact that in case of LULU both missile and gun could stay in lock-on simultanously while in case of DFS the pilot had to switch to only one mode.

4.2 MANY-ON-MANY-COMBAT

So one can say that sufficient accordance was found in case of one-vs-one simulations. But first experiences from the unmanned m/n-simulations indicated basic differences between 1/1-and m/n-combats. In section 3 we discussed the relative short lifetime of a 1/1-attachment. This points out the vital importance of a sophisticated threat selection which overrules the maneuvring. This requires an intensive surveillance and search procedure. Exactly these parameters are not included in a 1/1-engagement: The knowledge of the isolated situation effects the combat;it leads to a fixation on the only present opponent, for there is no need to search for other targets. These missing ingredients of a realistic environment do not only lead to an overestimate of certain technical parameters but to a special (unrealistic) 1/1-behaviour. For these reasons the extrapolation from 1/1-engagements to m/n-combats is illegal.

4.3 INFLUENCE ON MANNED COMBAT SIMULATION

The above discussed effects had remarkable influence on the manned simulation by implementing unmanned targets to achieve a m/n-simulation: On one hand some fighterbombers were included to add the tasks of search, target designation and target priority. They are simulated in a very simple manner as listed below (fig. 8).

Fig. 8: UNMANNED FIGHTERBOMBERS
UFB

PURPOSE:

. To incorporate a more realistic Mediumrange-Scenario including Multi-Target-Capability

PROCEDURE:

. UFB'S will fly in formation with one manned escort fighter
. UFB'S only exist as radar targets
. UFB'S only exist if the escort exists
. UFB'S are unarmed
. UFB'S and escorts generate identical radar signals, i.e. the attacking fighter can not discriminate escort/UFB'S
. UFB'S have to be identified

On the other hand, and more important, are the ZULU'S, additional combattants with a simplified technique, but armed and therefore dangerous (fig. 9).

Fig. 9 Z U L U

Zusätzlicher Luftkampfgegner

(Additional opponent)

PURPOSE:

To eliminate the "1/1-effect", i.e.

- to know that only one opponent is present; this leads to a fixation on this single target
- to keep the pilot permanently looking for further opponents, i.e. "attention getter".

PROCEDURE:

- ZULU'S enter combat randomly with respect to time and geometry
- ZULU'S are armed with Air-to-Air missiles
- ZULU'S have to be identified.

By appearing randomly they force the pilot to an intensive surveillance of his environment. i.e. he has no more the chance to stay with one opponent undisturbed for a long time interval. The environment is therefore much more realistic.

During a recent study, the first one including unmanned combattants, the ZULU'S were scaled to an appearance - and successfrequency to keep the pilot alert but not to disturb the final results, i.e. a kill rate by ZULU'S of 10 % was accepted (fig. 10).

Kills by ZULU	10 %
ZULU'S appeared	.9 per combat
ZULU'S Killed	.4 per combat
$\frac{\text{ZULU'S Killed}}{\text{ZULU'S appeared}}$	44 %
ZULU'S engaged	63 % (37 % surprise)

Fig. 10: ZULU - influence

The last column shows that about 37 % of all ZULU'S could achieve a surprise attack which seems to be realistic and again indicates the importance of searching permanently.

First experiences lead to very positive results and pilot comments. Within other effects the so-called "air combat arena", an area described by certain g-loads and speeds, which by some institutions using manned 1/1 simulation was found to be shifted down to very low speeds now returns to an area of increased agility ($0.6 \leq Ma \leq 1.2$).

5. STUDY EXAMPLES

5.1 GENERAL

As mentioned earlier the different methods shall be used in a supporting manner as shown in some detail on fig. 11. Additionally this figure shows the influences found in unmanned m/n simulations included into the manned simulation: On one hand a possibility was implemented to fight in a more realistic m/n-environment in case of manned simulation, on the other hand an improved familiarization and training possibility is needed based on the increased requirements and pilot workload as indicated on fig. 12 showing the training-syllabus present in use.

Fig. 11 AIR COMBAT SIMULATION

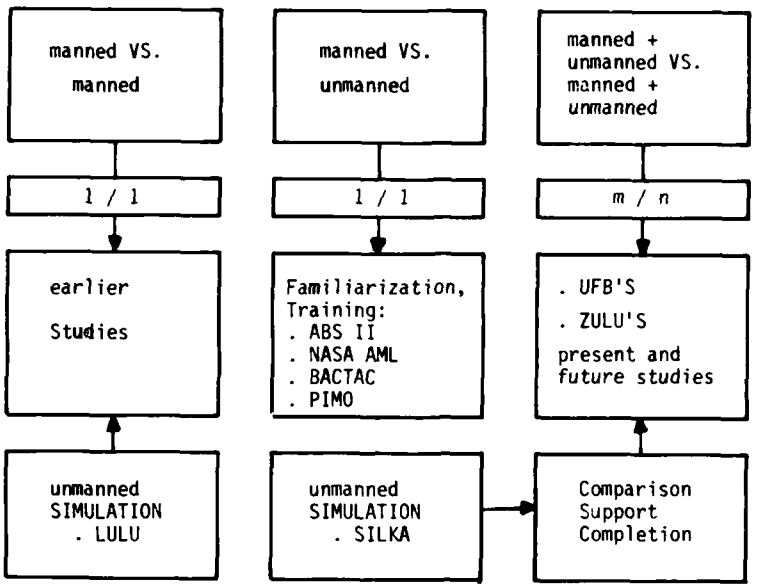

Fig. 12: SYLLABUS

. AIRCRAFT	: SRM-combat excercises
+	
. RADAR	: Familiarization to performance, handling, modes of operation
+	
. HMS/FLIR	: Familiarization to performance and handling
+	
. IFF	: Familiarization to visual/FLIR/electronic IFF
+	
. MISSILES(1)	: First contact to new generation missiles (MRM, SRM)
+	
. UFB'S	: Blue radar shows multitargets (UFB'S and escorts); fight in multitarget environment
+	
. MISSILES(2)	: More information on missiles is available; various tactics to get familiar with the different ranges (r = f (speed, altitude...), the use of inrange indication (R1= range vs nonmaneuvring target, R2- range vs maneuvring target) and the effect of missile-avoidance
+	
. SOJ	: Influence of ECM on radar performance
+	
. ZULU	: Introduction of ZULU; tests on frequency of appearance, visibility, colour code, killprobability etc
+	
. GEOMETRY	: Familiarization to the starting geometry derived from the SILKA-Scenario, random choice

This syllabus indicates the need to improved training methods as well as a possibility to pursue the increasing pilot capabilities. This is necessary to sort out the pilots flying any production runs and to find out the correct time to finish the training and start the production, i.e. to find the pilot capabilities no more changing. Besides other tasks NASA can use their AML (adaptive maneuvring logic), Mc Donnell their ABSII (Air Battle Simulation) and British Aerospace Corporation (BAC) their BACTAC (BAC air combat) for those purposes. All three methods enable combats between human pilot and computerized pilot. In our company an adaequate possibility named PIMO (Pilotenmodell), which will be specifically generated for the discussed purpose, is under development in cooperation with DORNIER.

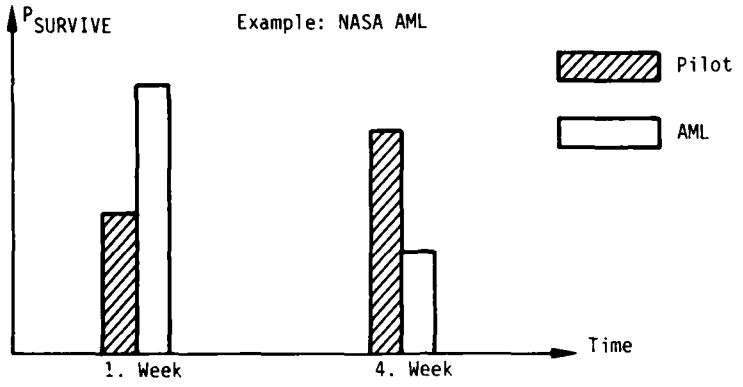

Example: PIMO (not yet implemented)

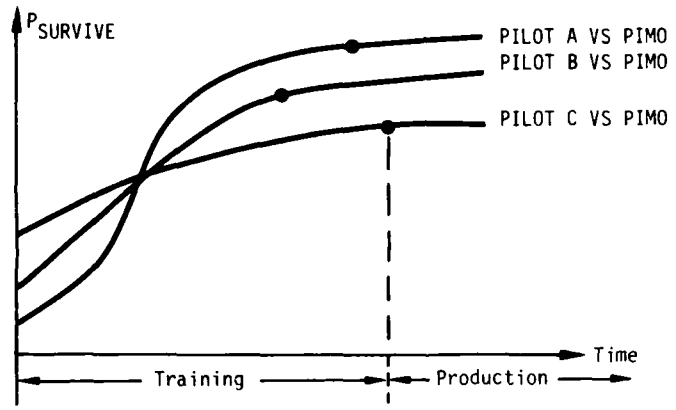

Fig. 13: Familiarization/Training

5.2 UNMANNED SIMULATION

The following example shall inllustrate some possibilities of the m/n - unmanned simulation in use in our company. It will be completed within the next section giving an example of an integrated, i.e. unmanned/ manned simulation study.

The task was to find out the survive-capability of fighterbombers depending on various avionics, jamming, armament and weather conditions.

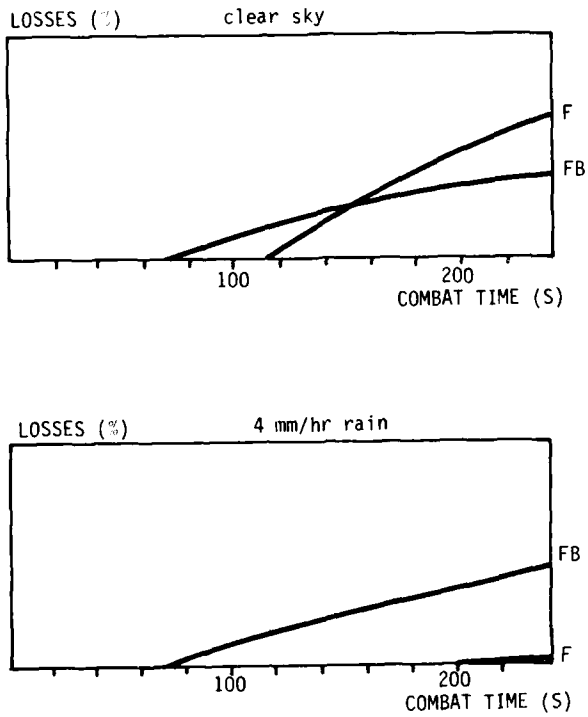

Fig. 14: Effect of rain

Fig. 14 shows the losses for both the fighterbombers (FB) and the attacking fighters (F). The effect of rain was found as a dominating factor decreasing the radar range remarkable in case of fighter and drastically in case of fighterbomber which had an other frequency spectrum.

An other driving factor was ECM. Modern ECM methods, i.e. deception jammers like range gate stealer and multiple target generator were implied and effected the various radar modes (single target track, track while scan) as well as the different missiles (semiactive, data link) in a distinctive manner. For example, a range gate steeler may cause a break lock between lock-on and launch of a missile thus preventing the launch and forcing the radar back into a search status. A multiple target generator may lead to ghost tracks thus generating wrong inrange resp. launch decisions. Additionally it may lead to an increased miss rate due to the fact that the missile may follow a ghost target for a certain time, and later is no more able to catch the designated target.

The results change drastically in case of rain as discussed before. Beside these important findings the study told something on various jamming effects, the influence of different missile performance and the effect of escorting a FB mission.

For certain reasons like weather, ECM, force sizes etc as well as time and money constraints this study was performed with unmanned simulation only. The next example will discuss a study using both methods.

5.3 UNMANNED AND MANNED SIMULATION

5.3.1 GENERAL

This study dealed with air-to-air-missiles designed to fulfil a NATO-requirement describing the threat, operational problems, operational capabilities, performance, priorities etc. The first step was the design of a study scheme (fig. 16) which combines all necessary items including industrial and operational activities: On one hand the industrial parts are the design of various solutions, the analysis of subsystems, flightpath simulation etc.while the operational parts, the area of major interest for this paper, includes the scenario, the air combat simulation and the analysis of results.

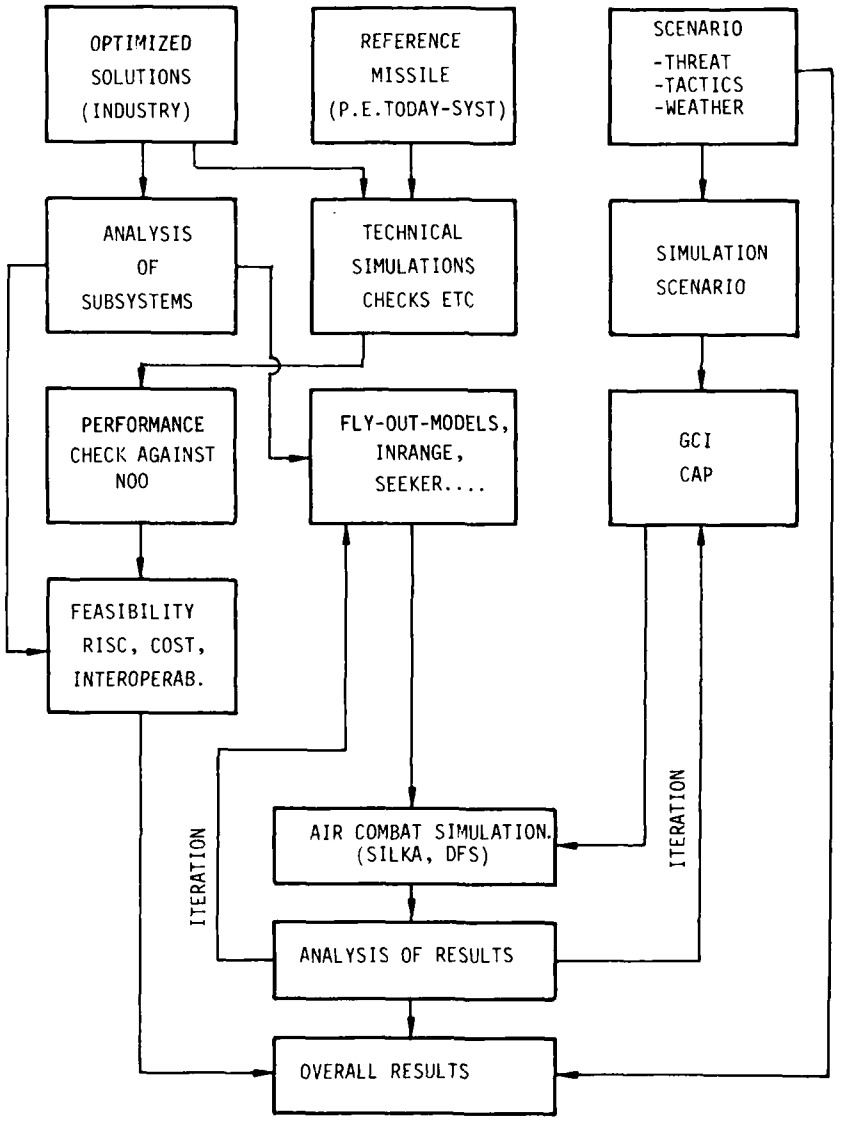

Fig. 15: Study schema

5.3.2 SCENARIO

First the environment conditions (geography, airfields, threat situation, weather conditions, force size etc) are discussed and defined. They lead to a simulation scenario (fig. 16) which is run through pre-combat-models simulating the phase between scramble of the defending aircraft and detection (models simulating controlled intercepts or combat air patrol).

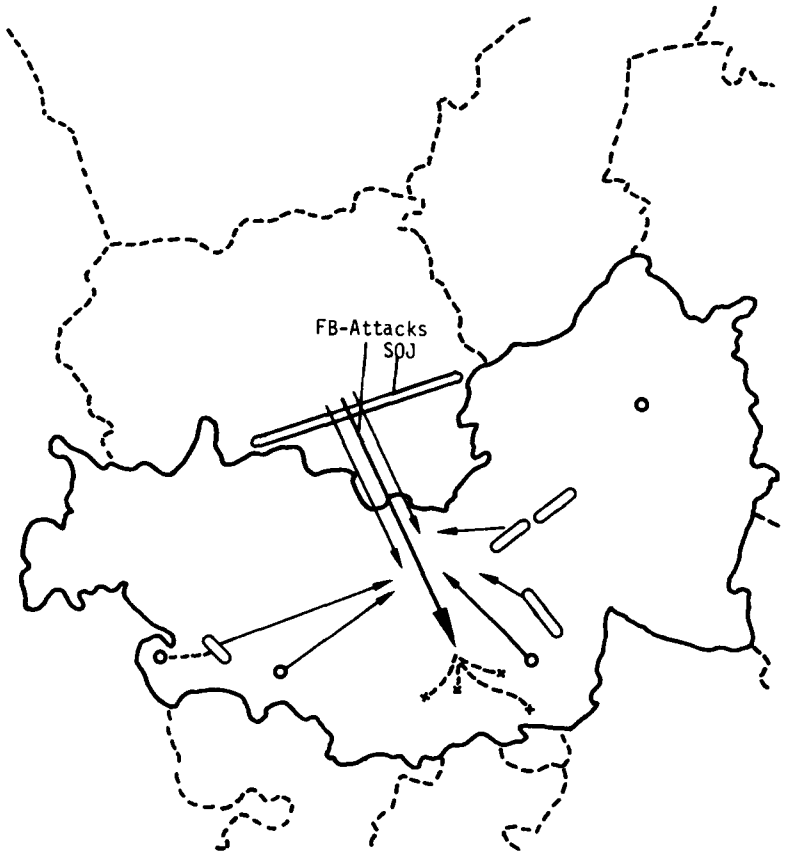

Fig. 16: Simulation Scenario

The results of these pre-runs are geometric conditions serving as inputs for the combat phase. Fig. 17 shows an example gained by GCI - simulations.

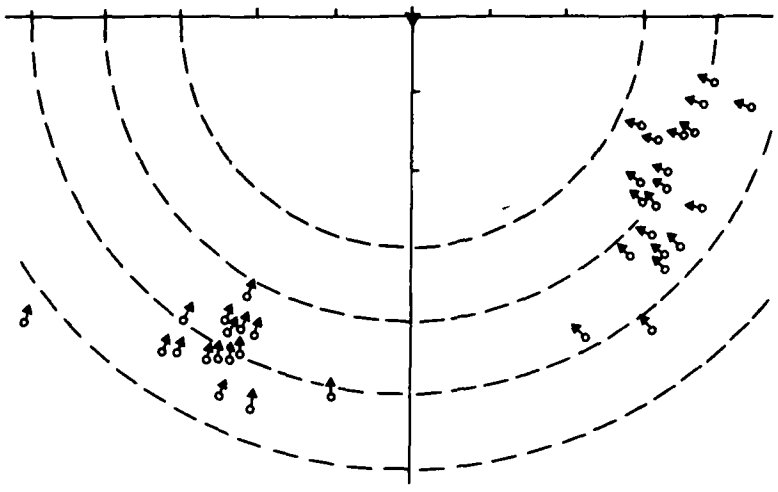

Fig. 17: Starting conditions (GCI)

It was required to use both unmanned and manned simulation. For this reason as much input data and procedures as possible had to be kept identical. Obviously the real-time flying of all 50 starting conditions derived from the scenario was not possible. Therefore 6 representative cases were extracted for the manned simulation (fig. 18).

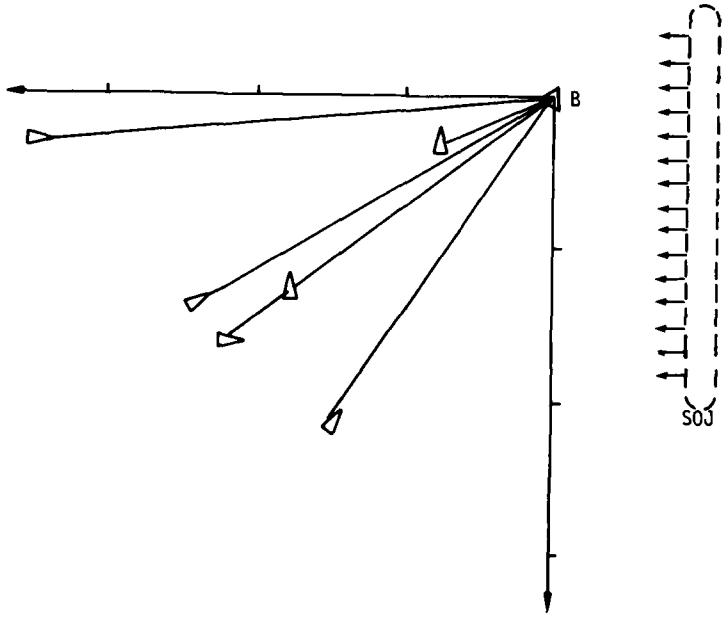

Fig. 18: Starting Conditions MANNED COMBAT SIMULATION

To put as much realism into the environment as possible those 6 starting conditions occured in a random sequence and were randomly reflected at the x-axis. In this way the pilots were not able to start with "canned maneuvers"; the only informations they got were in case of GCI, i.e. two cases. Thus they were forced to search autonomously and additionally to be aware that a ZULU could enter the combat.

5.3.3 RESULTS FROM UNMANNED SIMULATION

First phase of the study was performed with the m/n model SILKA. Some extracted results may illustrate the type of results which are mainly losses, taking into account missile types, ECM, force size etc. They are summarized on fig. 19 to 21.

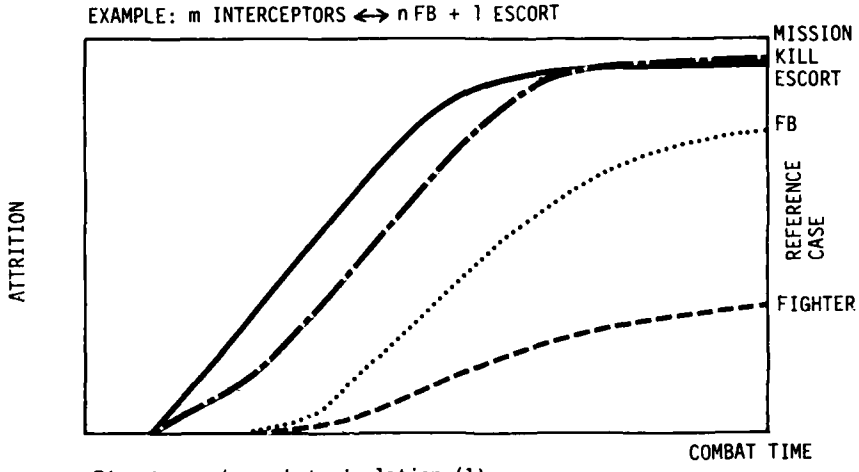

Fig. 19: m/n combat simulation (1)

Fig. 19 shows the combat between m interceptors and n fighterbombers escorted by 1 fighters. Obviously the defenders have a superiour armament which is to be seen at the earlier losses of the opponents and at the relatively low own losses; the latter one is additionally based on the common "defender advantage", i.e. the knowledge out of early warning, which partly enables optimum heading, speed, altitude etc.

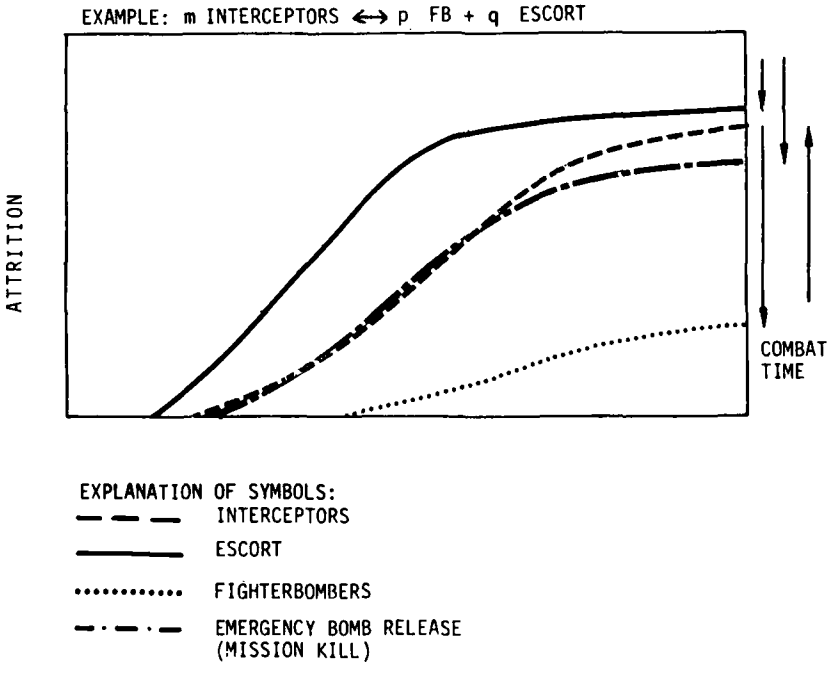

Fig. 20: m/n combat simulation (2)

The next figure 2 discusses the effect of force size:
Instead of n fighterbomber + 1 escort the threat was increased up to p + q.

The arrows at the right edge show the resulting changes. Corresponding to those loss curves missile consumption curves were produced. They show the number of missiles fired as well as the number of missiles which will be lost still on board of the killed aircraft. These curves can be used to evaluate the weapon mix (how many missiles type A/B/C should be carried), the number of missiles to be purchased etc.

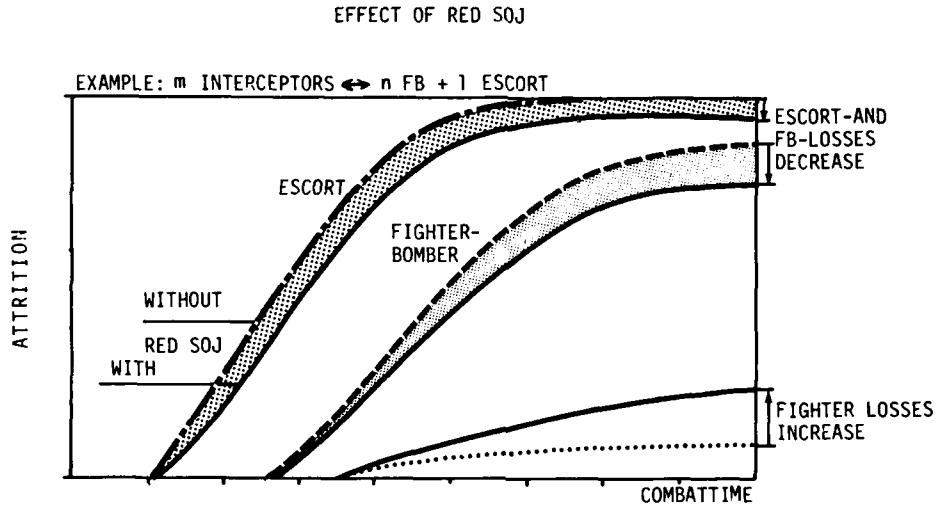

Fig. 21: m/n combat simulation (3)

Finally fig. 21 shows the effects of a stand-off-noise-jammer supporting the penetrating force: The penetrators losses decreased remarkable, the defenders losses were increased by a factor of 2.5.

5.3.4 RESULTS FROM MANNED SIMULATION

For the purpose of this paper there is no need to give detailed results from the second phase of the study, the manned simulation. We will come back to some general results in the next chapter.

Basically the results showed similiar trends as found in the unmanned simulation, but much smaller differences for the various missile candidates to be evaluated. This was discussed in detail and led to the hypothesis that the difference in missile performance should be more efffective if more targets are available, i.e. at higher force sizes. The hypothesis was proven by some additional SILKA-runs showing on one hand the missile launch ratio (fig. 22) of three candidates compared to the reference missile M1 and on the other hand the corresponding loss rates (fig. 23).

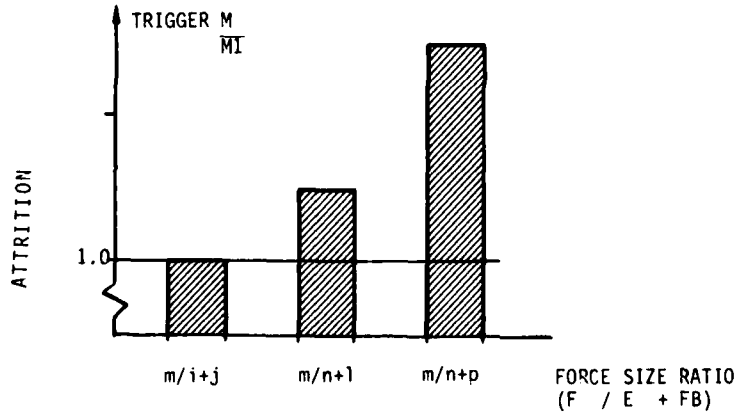

Fig. 22: Force size influence (1)

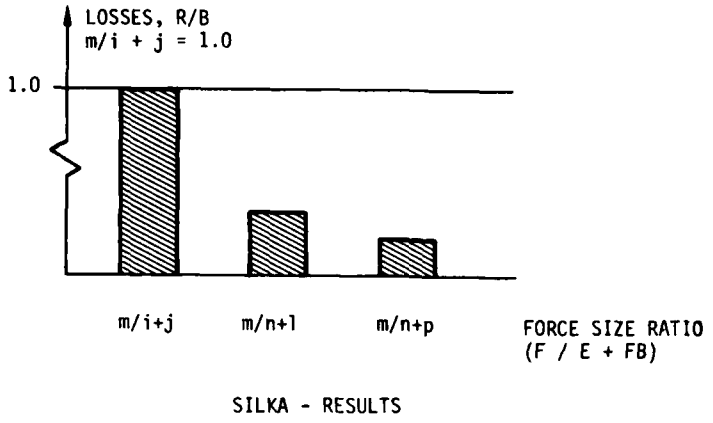

SILKA - RESULTS

Fig. 23: Force size influence (2)

5.3.5 INTEGRATED RESULTS UNMANNED/MANNED SIMULATION

5.3.5.1 LAUNCH STATISTICS

Basically six different missile designs were offered. An improved effectiveness was mainly found in cases of candidates with improved range in the front hemisphere. This is to be explained by looking into the missile launch statistics. The trend of using high aspect angles was already found in other studies and also in various flight test simulations.

The missile launch statistics shows other important indications and enables the designer to draw conclusions concerning the importance of the offered parameters, e.g. the question if the inner boundary is sufficient, or the obvious interdependance between off-boresight angle with aircraft turn rate or avionic limitations (gimbal angle, scan rate, time lags etc).

Another evaluation might be the definition of the seekerhead-look-angle which has to be a compromise between loss of target (if the angle is small) and too many false targets (if the angle is large).

If analyzing the miss reasons important hints can be found to improve the inrange algorithm and to discuss questions like: should the actual target g-load be included or would a set of assumptions concerning certain target behaviour make more sense?

Other results give indications due to power setting resp. temperatures resp. Infra-red-signature-reduction which are of some interest for the design of seekerheads.

Again of some interest is the missile flight time resp. missile average speed concerning possible target maneuvring which influences the inrange calculation.

So obviously the missile launch resp. hit/miss statistic is an important result to evaluate missile and avionic design.

It was found a rather good agreement betwenn both methods comparing the curve shapes and certain values. This portion was agreed by pilots and roughly fits to the surprises achieved by the ZULU (chapter 4.3, fig. 10).

There are many other parameters (altitude, power setting, depression angle, range etc) which show similar trends for both unmanned and manned simulation, i.e. $\pm$ 10 % differing values which is a rather close accordance.

5.3.5.2 LOSS RATE

As mentioned in chapter 5.3.3 a difference was found in comparing the losses for both unmanned and manned simulation. Therefore the hypothesis that the force size has a dominating influence was proven by additional SILKA runs. Comparing now unmanned and manned simulation on the basis of equal force size ratios again a rather good agreement was found (fig. 24).

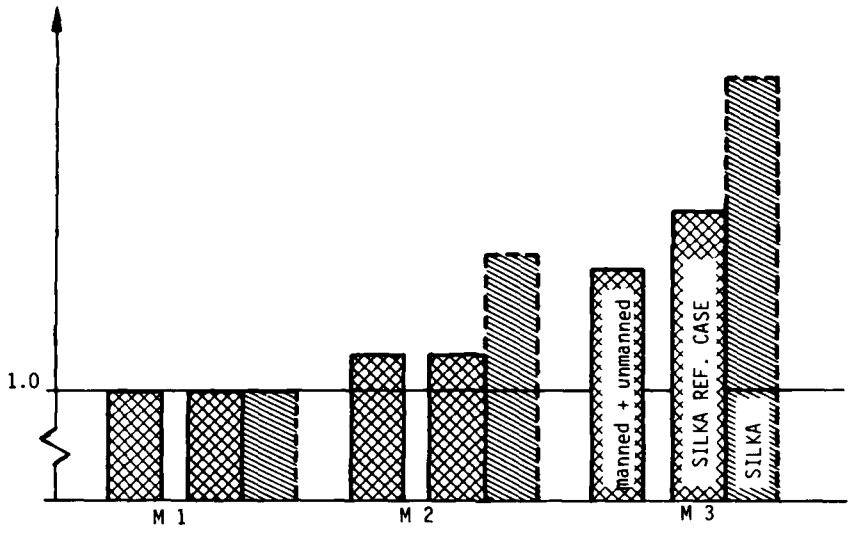

Fig. 24: Total Losses R/B
- unmanned/manned simulation -
(comparison)

Scaling the results on the basis of "1.0" for the reference missile M1, the operational effects of the improved designs (M2, M3) can be seen. In all three cases the first column shows the results of the manned simulation (including the unmanned combattants); the second column shows the results of unmanned simulation with comparable force size and the last column gives the results for higher force size used in SILKA.

5.3.6 CONCLUDING REMARKS

Discussing the use of unmanned and manned m/n-combat simulations it is found that on one hand both methods have their special areas to deal with, on the other hand they support each other.

The discussed study for example shows very well that a large force size has an remarkable influence which could not be found in case of manned simulation. Other important results cannot be gained by the use of unmanned simulation only. So finally one can say that using both methods is widening the field of use increasing the validity of the results.

REFERENCES

(1) Wunderlich, G. — Luftkampf auf dem Computer, Jahrbuch der Luftwaffe 1973

(2) Birkhold, E.; Polis, R.; Pfeifer, M.; Wunderlich, G. — Mehrfachduellmodellierung, Systemanalysen für die Luftrüstung, 1978

(3) Platzöder, L.; Munser, H.J.; Fa. Dornier — Digitales Rechnerprogramm Manöverpilot DGLR-Presentation, 5./6.12.1977, Porz-Wahn

(4) Jones, I. — BACTAC, a combat-worthy computerized opponent, AGARD-Presentation, 3. - 6.9.79, München

(5) — Digital Air Battle Simulation (ABSII) MC-Donnell-Paper GP 74-0946-39, 1976

(6) Hankins, W. — Engagement between Human Pilots and a Computer driven Opponent, NASA-Langley, LWP-1127, Aug. 1973

(7) Wunderlich, G.; Braun, R. — Air-to-Air-Engagement Simulation, AGARD-Presentation Nr. 268, 1979, Paris

(8) Wunderlich, G. — Various papers presented at BwAK/Wehrtechnik, Mannheim und CCG, Oberpfaffenhofen, 1980-1983

(9) Wunderlich, G.; Fehrenz, H.P. — Various IABG-Reports, confidential, 1979-1983.

GROUND EVALUATION OF HELICOPTER AIR-TO-AIR WARFARE

G. CATANI
Avionics and Systems Group
AEROSPATIALE DH
F-13725 Marignanne Cedex, France.

The department «System analysis» of Aerospatiale, Helicopter Division, has,for principal aim,theoretical definition and evaluation of helicopter-borne systems. It's mainly involved during program definition phases or pre-project. Our objective is here to illustrate,with a particular subject system analysis,means and methods implemented at Aerospatiale. The elected subject is helicopter air-to-air warfare. So the purpose of this paper is to give a survey of the work done by Aerospatiale for several years in the field of helicopter air-to-air warfare studies. One will not find here a description of air-to-air systems implemented on board of Aerospatiale helicopters but rather a presentation of means and general methods which are used to define, evaluate and develop air-to-air helicopter fire control and, more precisely, means and methods implemented during fire control pre-project and definition phases. (Fig. 1)

We intend first to show the context of air-to-air helicopter warfare and the requirements of our customers, then we'll describe the means of studies already done by Aerospatiale to meet those requirements.

Finally,we'll present examples of results obtained by simulation technics in the particular case of air-to-air gun fire control. (Fig. 2)

1. CONTEXT-SPECIFIC FEATURES

Given the increasing use of armed helicopters, combat helicopter units are a major component of maneuver forces. In particular, they represent a substantial threat to tanks. This situation creates two problems :

- the protection of friendly tanks against enemy anti-tank helicopters,
- the protection of friendly anti-tank helicopters against enemy fighter helicopters. (Fig. 3)

From this angle, it had become a'must'for the helicopter to have an air-to-air capability.

A quick survey of the situation shows that the problem is new and original. (Fig. 4)

- it is new : in fact experience in the field of helicopter air-to-air warfare is very limited,
- it is original : indeed helicopters have a very specific flight envelope which includes hovering flight. Moreover they can be operated in NOE flight, that is low-altitude flight amidst obstacles, which makes them difficult to spot.

Finally, air-to-air weaponry - missiles, but especially guns - can be made mobile on its support, so that it's possible to make the pointing of the weapon independent of the orientation of the aircraft.

2. WORK DONE AT AEROSPATIALE IN THE FIELD OF AIR-TO-AIR WARFARE STUDIES : REQUIREMENTS AND AIMS

The general requirement described above finds its expression in two different types of requests from military customers.(Fig. 5)

1) The fabrication of simple systems that can be developed in little time. They usually center around a gun, are available on a short-term basis,and are not specific to specialized helicopters.

2) The definition of air-to-air advanced firing systems.

These have better performance, comprise gun and air-to-air missiles and are intended for specialized aircraft.

The general purpose of studies performed at Aerospatiale for several years already is to meet these requirements by harmonizing them, i.e. by allowing, as far as possible, an evolution of simple systems toward higher performance systems.

In all cases, and particularly at a definition level, the objective is to set up coherent fire control by putting a special emphasis on the characteristic air-to-air warfare parameters, which concern target and fighter, and by quantifying the performance of the various systems via the following data :

- reaction time,viz.the time between detection and firing, (Fig. 6)
- accuracy, viz. the target destruction probability.

Such a method stems from the intuitive realization that, in first approximation, two conditions have to be satisfied, are very important, if you want to meet with victory in an air-to-air battle :

1) to fire before the foe,

2) to hit the foe if you have succeeded in firing first.

Of course,those two conditions are neither necessary norsufficient, but they're very important,so that reaction time and accuracy appear to be the best parameters to quantify the quality of a fire control at a definition level.

3. GENERAL MEANS AND METHODS IMPLEMENTED

These different types of means are implemented to set up a fire control during the life of a program.

- **In the definition phase,** the studies stay on simulation technics and are adjusted through the application of realistic figures derived from sighting and firing experiments or supplied by vendors. The data are used to quantify identification of target aircraft, time and range at which intervisibility occurs, acquisition time and range, fire time and range. Another important kind of data concern the fighter flight qualities and perturbations. These simulation procedures can feature the various possible systems. (Fig. 7)

  From a functional point of view, they implement the two following models : (Fig. 8)

  - Hardware models :
    - fighter helicopter
    - target evolutions
    - sensors : airspeed measuring subsystem, navigation subsystem, sighting and telemetry
    - weapons : gun and air-to-air missiles
    - trajectories of shells and missiles.
  - Software models : they feature the software of the future fire control computer, which will be the heart of the fire control system. These models are essentially :
    - statistical filtering for evaluating target maneuvers. Kalman algorithms have been developed to improve accuracy and response time.
    - calculation of weapon pointing, which is used to control the gun turret or to put missiles in their operating range.

  Because digital simulations cannot represent perfectly the reality in the development phase, the systems which have been primarly defined are evaluated on a helicopter simulator including men in the loop. These manned simulations allow to acquire information about ergonomic data and cooperation between pilot and copilot and to optimize real time fire control algorithms. Finally, the optimized fire controls are evaluated by in flight experiments which include prototype equipments. (Fig. 9)

4. EXAMPLES OF RESULTS : NATACHA FIRE CONTROL (1)

Now we are going to illustrate the use of these means during a definition phase. We take the particular case of a gun fire control including the following equipments : (Fig. 10)

- **Copilot sight** to observe, identify, track the target and give distance measurement.
- **Pilot clear vision sight** supporting the pilot aid data.
- **Copilot and pilot helmets sights** for the designation of a target spotted with the naked eye.
- ***Navigation and airspeed sensors.***
- **Gun mounted** on a **turret** providing large field of fire.

This system comprises different modes of use :

- **Principal mode** *which is through the copilot's sight.*
- **Degraded modes** using pilot sight or helmet sights.

In these degraded modes the gun is used in a degraded accuracy, but they enable the pilot to deliver suppressive fire when the copilot is occupied or disabled and the copilot using his helmet sight to fire on a threatening short-range target, without maneuvers.

The following results are given in the case of the principal mode. This mode is estimated with typical scenarios. We give an example in a two dimensional case : (Fig. 11)

t = 0	Fighter	X = 0	Y = 0	Speed = 150 Km/h
	Target	X = 0	Y = 500 m	Speed = 200 Km/h
		maneuvering after t = 0		

(1) H.A.P. fire control.

Three steps are implemented in the simulation : (Fig. 12)

- **First step,** the trajectories of the target and fighter are calculated including speed and acceleration, fighter's pitch roll and yaw angles, fighter's angular rates. All these parameters are put on files.
- **In the second step** of simulation, the filed parameters are used as inputs of the sensors models and the program gives outputs of the sensors (copilot sight, navigation and airspeed subsystem). Outputs are also put on files.
- They are used in the **last step of simulation.**

In this step, one determines the time of firing, for which a certain number of conditions must be met :

- correct sighting,
- gun within its operating range,
- *converging algorithms.*

These conditions are given by a *firing decision module.*

Then filtering and gun-pointing algorithms, using outputs of sensors, are implemented and results are expressed in term of shells/ target miss distance versus time and impact traces left by the shells in the target.

Figure 13 shows the miss distance in the case of the scenario taken in our example. Two types of filtering have been compared :

- classical filtering,
- Kalman filtering.

Figure 14 shows the results of two firing bursts of 10 shells, one at $t \simeq 5$ seconds and the other, $t = 10$ seconds. In both cases we indicate the gain brought about by the Kalman filtering which makes it possible to concentrate the fire on the target with high destruction probability.

Briefly, such results are collected from simulations of several scenarios to quantify the performance of the sensors and of the whole fire control. So we determine the nature and the characteristics of the sensors involved in principal and degraded modes of this fire control, and also the influence of helicopter flight quality on air-to-air combat.

In particular, one shows on one hand the importance of measuring (Fig. 15)

parameters given by the copilot sight :

- o line of sight angles,
- o line of sight rates,
- o fighter/target range.

parameters given by the airspeed subsystem :

vertical, lateral and longitudinal airspeed, from a three axis sensor are essential for gun fire control. They are used by the algorithms in the solution of weapon's pointing equations.

Finally, parameters given by the navigation subsystem :

- o fighter's pitch and roll angles,
- o fighter's angular rates.

On the other hand, the studies make it possible to give first specifications on flight qualities of the fighter and tolerable vibration level and bore-sighting errors.

In the case of the principal mode of gun fire control taken is our example, simulations of several scenarios allow us to quantify response time and accuracy and to finalize filtering and weapon pointing algorithms. So azimuth and elevation errors can be expected less than 4 mrd rms over a large spectrum of fighter and target flight and motions and of wind and distance conditions.

In the next phase, which concern manned simulations, real equipments will be used or simulated and fire control will be real time evaluated. Manned simulations will be necessary to analyse the behaviour of the crew and to finalize real time algorithms.

CONCLUSION

Air-to-air capability has become a necessity for armed helicopters. This problem is new, complex and shows specific features such as hovering flight or mobile weaponry. In this framework, the need of military users finds its expression in a large spectrum of various systems : from simple systems, cheap and available on a short-term basis to high integrated systems, aimed to short reaction time and optimized accuracy.

In order to meet those different requirements, Aerospatiale implements ground means of evaluation based on simulation studies.

These simulation models allow theoretical evaluation of given air-to-air fire controls through a large area of air-to-air scenarios. During definition phases, they represent a powerful mean of building and ground testing every fire control. On the other hand

they provide away to increased efficiency during the development phases, as they make it possible to avoid expensive in-flight tests of non optimized systems.

Moreover, the models become more realistic during the life of the program, because they are adjusted through experimental data, as soon as measurements are available.

Until now, Aerospatiale has used those means of system testing within two important fields of application :

- evaluation of simple gun pilot fire control systems,
- definition and evaluation of complex gun / missiles fire control systems. In this particular case, the principal results achieved concern HAP fire control (NATACHA), whose one of the major feature is the use of Kalman target second order estimation to improve accuracy and response time.

AN EXAMPLE OF SYSTEM ANALYSIS

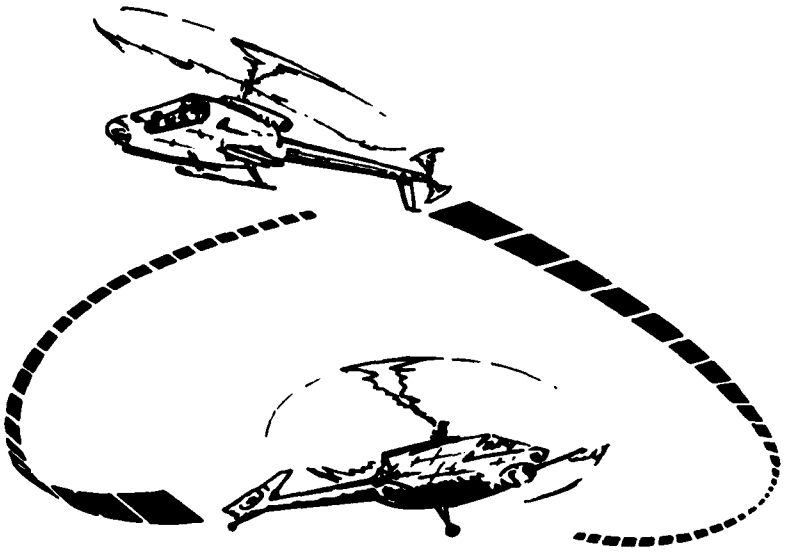

FIGURE 1

HELICOPTER AIR-TO-AIR WARFARE

- CONTEXT : REQUIREMENTS
- AEROSPATIALE MEANS OF STUDY
- EXAMPLE OF RESULTS : GUN FIRE CONTROL

FIGURE 2

HELICOPTER AIR-TO-AIR WARFARE

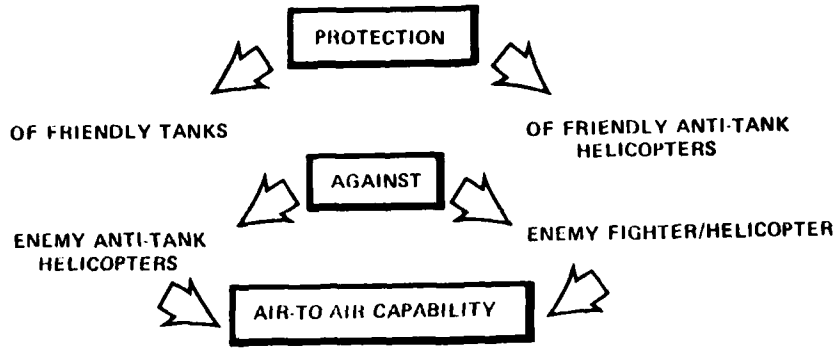

FIGURE 3

HELICOPTER AIR-TO-AIR WARFARE

THE PROBLEM IS :

- NEW : PRESENCE OF AN AIR THREAT

- ORIGINAL : NOE FLIGHT
  SPECIFIC WEAPON

FIGURE 4

HELICOPTER AIR-TO-AIR WARFARE

REQUIREMENTS OF THE CUSTUMERS

① SIMPLE SYSTEMS → SHORT TERM AVAILABILITY
→ NOT SPECIALIZED HELICOPTERS

AND/OR

② HIGH PERFORMANCE SYSTEMS
→ SPECIALIZED HELICOPTERS

FIGURE 5

HELICOPTER AIR-TO-AIR WARFARE
PERFORMANCE EVALUATION

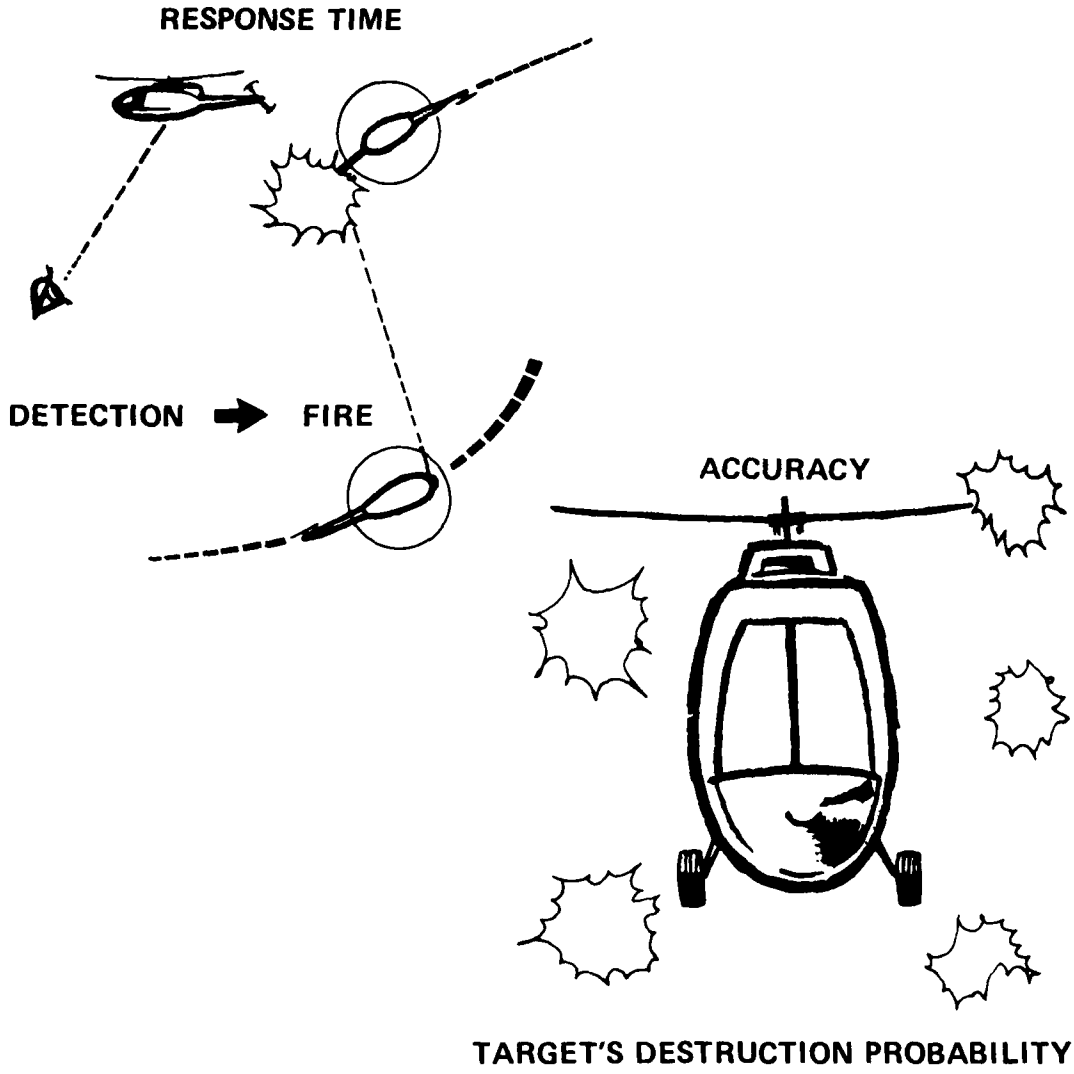

FIGURE 6

HELICOPTER AIR-TO-AIR WARWARE

MEANS AND METHODS OF STUDY

DEFINITION
FORE PROJECT
} PHASES

- MODELS
- SIMULATION
- EXPERIMENTS RESULTS
- VENDORS INFORMATION

FIGURE 7

HELICOPTER AIR-TO-AIR WARFARE

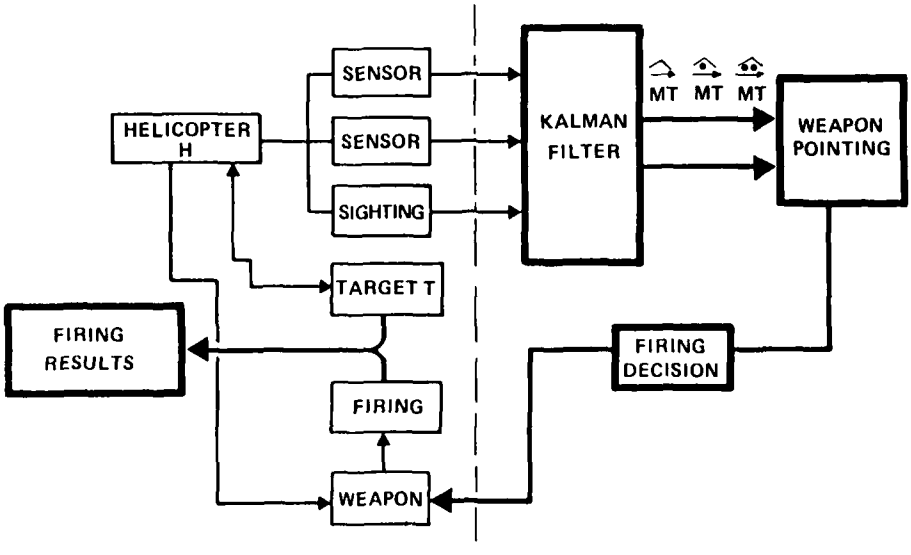

FIGURE 8

HELICOPTER AIR-TO-AIR WARFARE

MEANS AND METHODS

DEVELOPMENT PHASE

- MANNED SIMULATIONS
- IN FLIGHT EXPERIMENTS

→ PROTOTYPE EQUIPMENT

FIGURE 9

HELICOPTER AIR-TO-AIR WARFARE

EXAMPLE OF STUDY

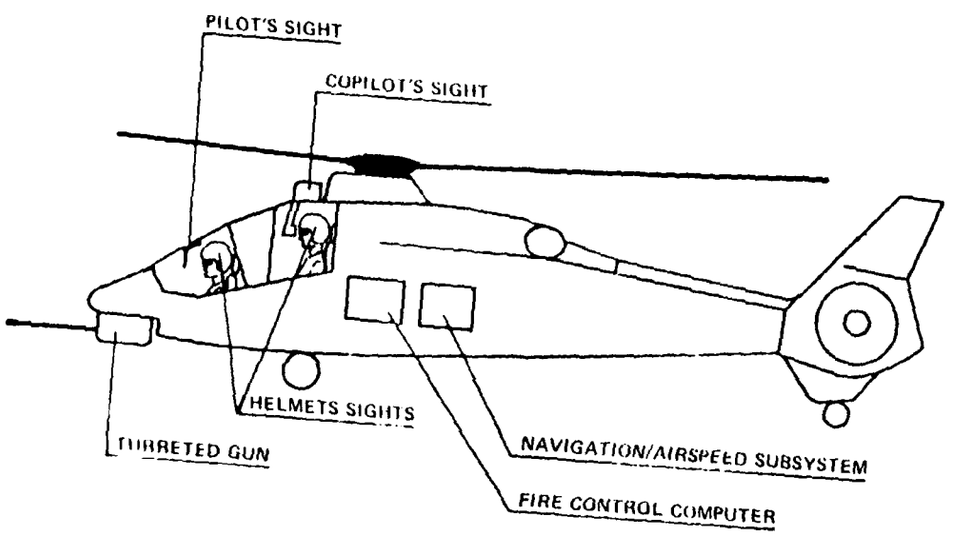

AIR-TO AIR GUN FIRE CONTROL

FIGURE 10

HELICOPTER AIR-TO-AIR WARFARE

EXAMPLE OF SCENARIO

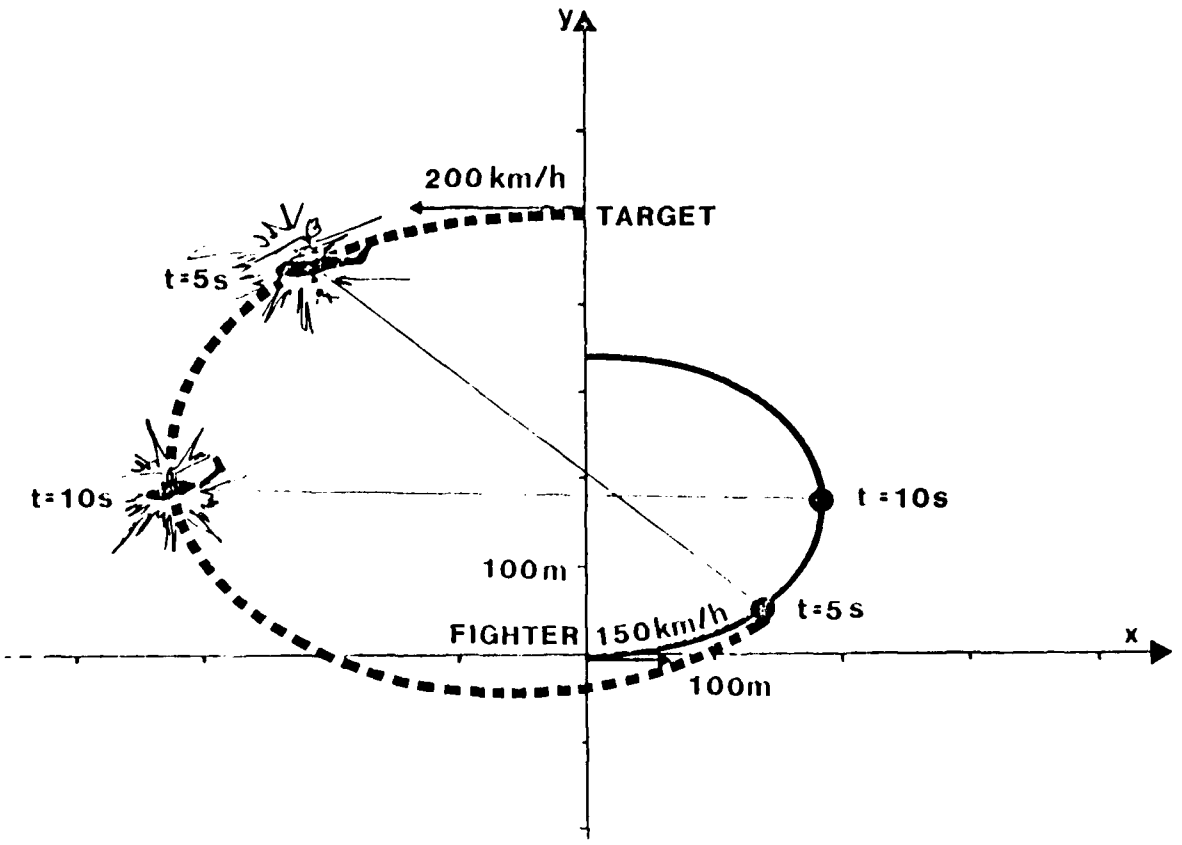

FIGURE 11

HELICOPTER AIR-TO-AIR WARFARE

GUN FIRE CONTROL : STEPS OF SIMULATION

STEPS	INPUTS	OUTPUTS
① TARGET AND FIGHTER MOTIONS	INITIAL CONDITIONS	POSITIONS, SPEEDS, ACCELERATIONS PITCH, ROLL, YAW ANGULAR RATES
② SENSORS SIMUALTION		MEASURED PARAMETERS
③ GUN POINTING FIRE		SHELLS/TARGET MISS DISTANCE IMPACT TRACES

FIGURE 12

HELICOPTER AIR-TO-AIR WARFARE

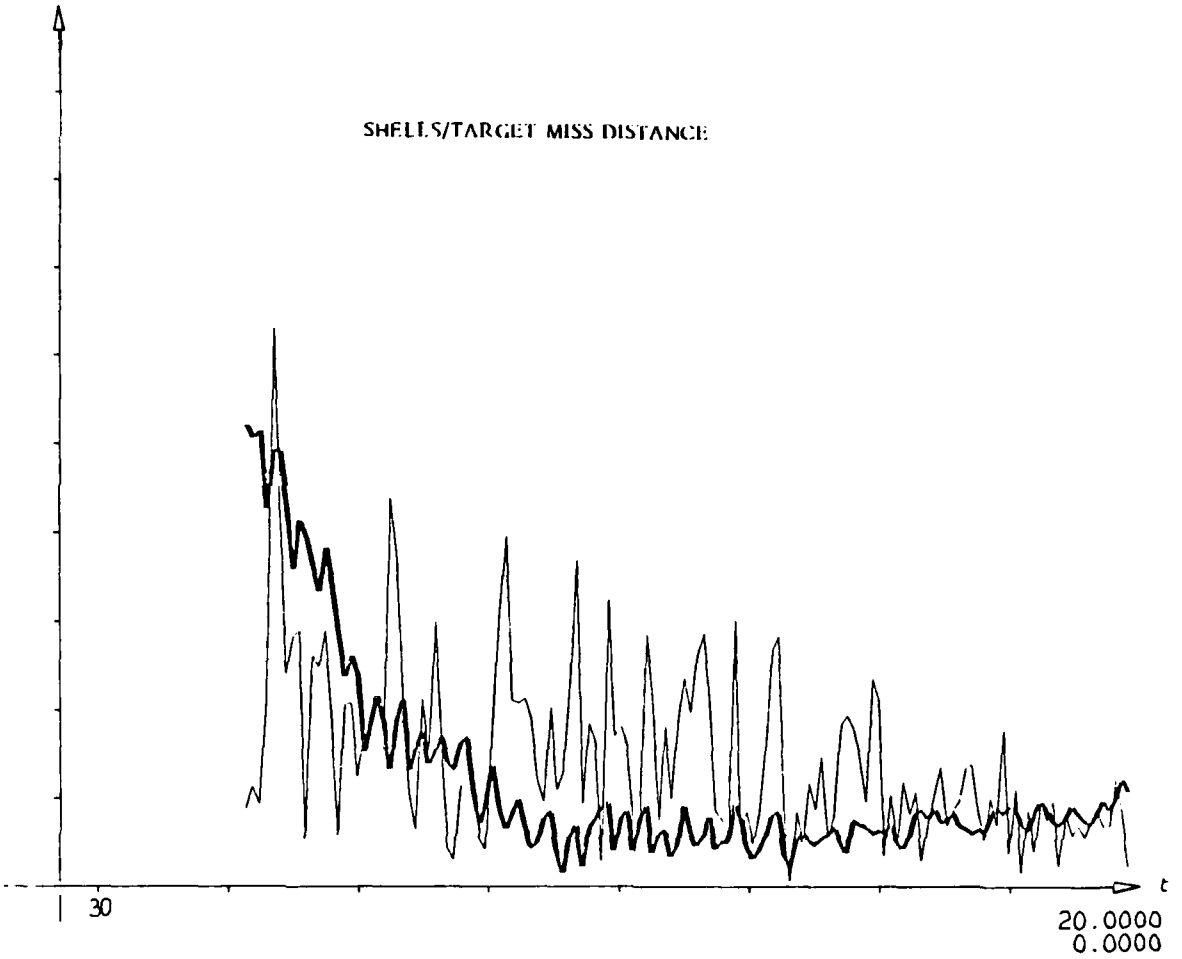

FIGURE 13

HELICOPTER AIR-TO-AIR WARFARE

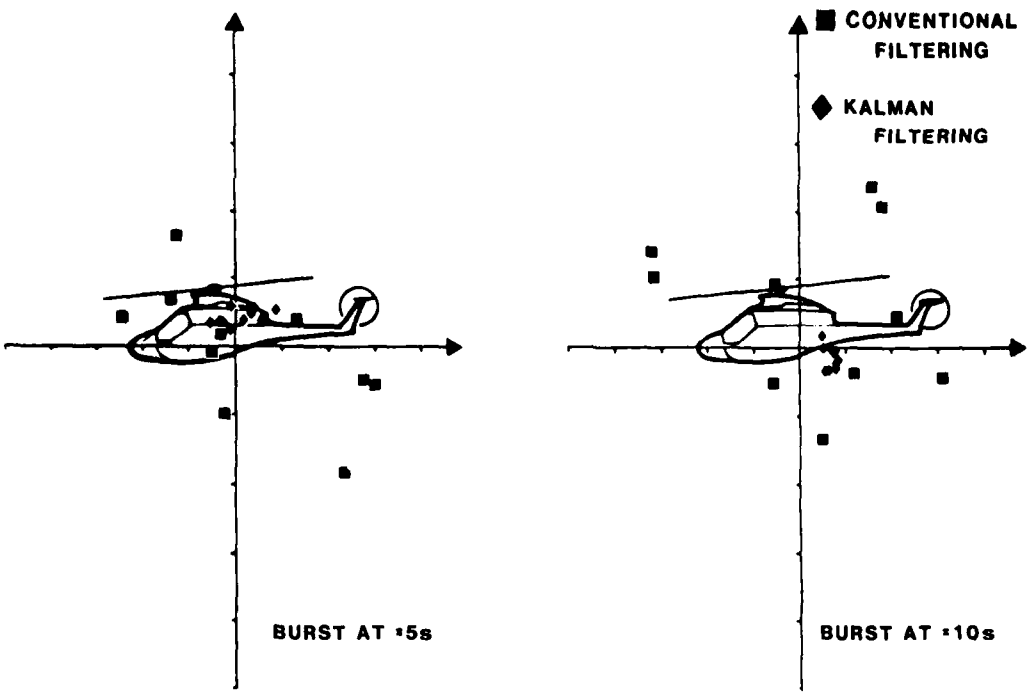

FIGURE 14

HELICOPTER AIR-TO-AIR WARFARE

GUN FIRE CONTROL : SIGNIFICANT DATA

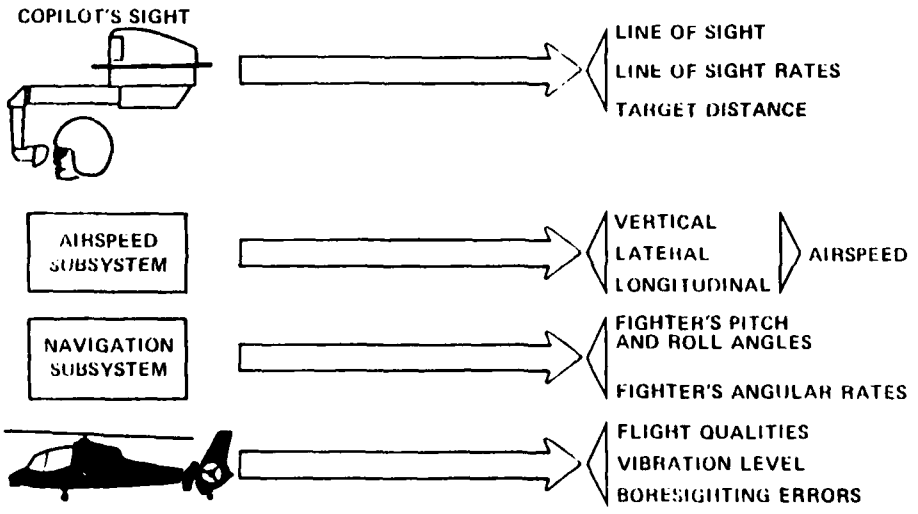

FIGURE 15

TESTING OF THE DIGITAL FLIGHT CONTROL SYSTEM OF THE GERMAN CCV FIGHTER EXPERIMENTAL AIRCRAFT

by
Udo Korte, CCV-Program manager
Messerschmitt-Bölkow-Blohm GMBH
Military aircraft division
P. B. 801160, 8000 Munich 80, FRG

SUMMARY

Our next generation fighter aircraft will probably exhibit those features as relaxed static stability and full authority digital flight control. In such aircraft the pilot ist totally dependent on the FCS and malfunctioning of this system might be catastrophic. Thorough testing of the FCS is therefore mandatory.

This paper outlines the necessary steps in testing a complex digital redundant FCS based on the experiences made with the German CCV fighter experimental aircraft.

INTRODUCTION

Flight Control systems are flight critical. Reliability requirements are in the region of 10^{-7} for overall mission reliability. As component reliability cannot be made high enough to fulfil this requirement, it is common practice to use hardware redundancy. In a redundant system the components (functions) of the system are replicated so that failed units can be detected by comparison and corrected in their effect by use of remaining or alternate paths. With regard to testing this means that not only the components and functions of one channel have to be tested but the communication with other channels, the failure detection, indication and isolation as well.

With the advance of digital computers for flight control system application a new problem has arisen: that of software reliability. The computational capabilities of digital flight control computers have made it possible to fulfil the rapidly growing demands on guidance and control systems of modern fighter aircraft.

A large number of different tasks like Preflight Check, Inflight monitoring, Control Law Computation, Autopilot, Attack Modes etc. can be incorporated leading to large programs with complex software with the increased possibility of software errors.

Redundancy does not help against these errors because if each computer of the replicated system runs identical software errors cannot be detected. Therefore proper verification of software plays an important role in FCS development and testing.

THE GERMAN CCV PROGRAM

The German CCV program was launched in Dec. 1974. It is funded by the German MOD. The objectives of this program were to develop and flight test an advanced, integrated guidance and control system for naturally unstable fighter aircraft.

From Dec. 1977 to Nov. 1981, 118 flights with the new digital flight control system have been conducted. As testbed served a modified single-seater F-104 G supersonic combat aircraft (Fig. 1).

The aircraft was flown in five different configurations reaching an instability of 22 % MAC in the most unstable canard configuration.In a follow on program another 42 flights (until Dec. 1983) have been made with the flight control computer program enlarged for a simple back up software and integrated autopilot modes.

In spite of numerous program changes no accident ever occurred. This demonstrates the effectiveness of ground test methods.

GENERAL DESCRIPTION OF THE FCS

To fulfil the program objectives it was decided to choose a digital FBW-system with 100 % authority. Safety reasons and the operational requirements led to a quadruplex system with parallel signal processing where failures are detected, localized and isolated by majority vote. Fig. 2 gives a system overview.

The four identical computers are the heart of the system. They are 16 bit computers with 16 K (later 32 K) core memory and 2 K RAM. They run identical software and communicate with each other via fast data lines (direct memory access). Each computer performs the following functions:

- Stabilization and control
- Autopilot
- (Back up control)
- Air data computation
- Inertial Navigation (Strap down)
- Preflight check out
- Redundancy management

As can be seen from Fig. 2 not only the computers have been quadruplexed but the other components (sensors, interfaces etc.) as well. In case of the series actuators - they are used in conjunction with existing power actuators and had to be developed new to give full authority for the FBW-system - a triplex solution with self monitoring of each lane is used.

The necessary signals for the guidance and control system are supplied by a number of sensors which can be seen in the more detailed picture of Fig. 3.

The Inertial Measurement Unit (IMU) works in conjunction with the flight computer. Body fixed gyro and accelerometer signals are transmitted from the IMU to the computer via a seriell digital interface. There velocities, attitude angles, longitude and latitude, cross track error etc. are computed in a strap down fashion.

From the IMU-signals, air data signals and pilot pickoffs the desired surface positions are computed and fed via the D/A-converters into the (analog) actuator electronic voting and switching unit. From there the elected signals go to the series actuators.

TEST APPROACH

System design philosophy and system specifications have an important impact on the final testing of the FCS. A straight forward design which avoids unnecessary complexity in hardware and in software can be tested much easier and at lower cost. The main areas in testing are hardware, control laws, software, redundancy management, system installation and operation.

HARDWARE

Hardware testing stands at the beginning of the FCS development and check out. In hardware design and acceptance tests it has to be verified that each individual component fulfils the specified requirements. In case of the CCV many components were common off the shelve hardware, where no special testing was required. This was different with the Redundant Inertial Information and Computation System (RIICS), which was developed by an American supplier after a special specification from MBB. The RIICS consists mainly of the four computers, the four Inertial Measurement Units and a Control and Display Unit (CDU), which enables the communication between the pilot and the system and is a powerful tool in system testing. The CDU will be explained later.

Acceptance tests at the supplier and at MBB included temperature cycling and vibration tests. These burn-in procedures are of special importance in order to provide hardware that is reliable in an aircraft environment.

For other new hardware like series actuators, actuator electronic and switching units, central signal distributor etc. similar design and acceptance tests were made.

CONTROL LAWS

Parallel to the hardware development went a preliminary design of the control laws. After definition of the controller structure the feedforward and feedback coefficients were evaluated for each aircraft configuration for a number of reference points in a Mach, altitude grid. The coefficients are stored in the computer memory. Between the reference points the coefficients are linearly interpolated.

In linear and nonlinear simulations it was checked that satisfactory aircraft behaviour could be reached with the designed control algorithms.

For the final layout a number of hardware test results was necessary. After delivery and installation of the hardware in the aircraft phase and amplitude plots for the computer/actuator paths were made. These measurements were approximated by linear transfer functions plus nonlinearities. Based upon these measurements the controller coefficients were modified.

STRUCTURAL COUPLING

The sensors of the FCS do not only respond to the rigid body motions but to structural oscillations as well. Control surfaces, deflected in response to sensor signals produce oscillatory aerodynamic and inertia forces which depending on their phasing, tend either to damp or to amplify structural vibrations. A self-excited oscillation may result which is simular to flutter. The energy to sustain this oscillation is partly supplied by the control system.

On the ground where aerodynamic forces are absent a servo-elastic instability may occur which is excited by the inertia forces due to control surface accelerations. The energy is again supplied by the control system.

As the aerodynamic forces usually tend to damp structural coupling the ground resonance is the decisive problem. How severe the interaction between control augmentation system and airframe dynamic can be may be illustrated by an example: One modern European

fighter could be seen jumping around in the hangar when its control system was activated for the first time because of ground resonance.

To avoid such surprises structural coupling ground tests were made for the CCV aircraft with the FBW-control system installed. The first tests were made open-loop, followed by closed loop tests. The test arrangements are shown in Fig. 4 and 5.

In the open-loop case the loop was cut open between computer and actuator electronics. The computer output due to a harmonic excitation input with different frequencies (frequency sweep) at the actuator electronic box was measured and analysed with respect to amplitude and phase. For a phase lag of 180° the amplitude ratio of ouput to input must be smaller than one to have a stable closed loop system (Nyquist criterion).

Different to the theoretical computations the first coupling test showed a strong feedback in the pitch loop for the frequency of the first fuselage bending mode (≈ 10 Hz). The location of the rate gyros (IMU's) in the nose cone of the aircraft is detrimental to the suppression of structural oscillations because the structural displacements due to fuselage bending are largest at the nose.

After introduction of a digital filter for the pitch rate signal the response amplitude was reduced to 32 % (Fig. 6). This corresponds to a gain margin of 10 dB which was considered sufficient. Later the first filter was replaced by a digital notch filter which gave further amplitude reduction.

The same filter was used for the roll rate signal. No filter was necessary for the yaw axis.

SOFTWARE VALIDATION

It has already been mentioned that in digital FCS's we have the new problem of generic software errors which cannot be overcome by redundancy because each channel contains the same error. In a naturally unstable aircraft the dependance upon software is absolutely because a direct (mechanical or electrical) link is not possible. This underlines the importance of software test methods.

In case of the CCV-FCS software testing was done in several steps. The flight computer software consists of a large number of modules as for example

Operating + Priority System
Initialization
Synchronization Comp/Comp
Error detection + Indication
Failure Elimination
Air Data Computation
Incidence Sensor Service
Mode Control
Control Laws + Scheduling
Data Transfer (DMA) Computer/Computer
I/O-Handling
Strap down Computing
Auto Nav Computing
CDU-Service
} written by RIICS Supplier
Telemetry service
and others

The software modules were written in assembler using a cross assembler that has been specially developed for a PDP 11/70. The whole program is block structured with a dedicated check sum for each block. Program changes are reflected in check sum changes.

The first step in software validation was static testing in the laboratory. Each new program was loaded into a real flight computer and then checked for different input signals. A special test set consisting of a PDP 11 computer, a key board with CRT, a typewriter and a Control and Display Unit (CDU) enabled the programmer to check the operations of this program step by step (each memory location can be displayed in coded form on the screen). Thus it could be ensured that the mathematical equations and logic paths had been programmed in the right way and provided the required results.

If possible the software modules were tested together with the specific specialist, for example the modul "control laws + scheduling" was tested from the software engineer under assistance of the control engineer.

The CCV flight control computers use fixed point processors. Therefore scaling of signals and coefficients was necessary and special emphasis had to be laid on the definition and test of maximum possible values to avoid overflow.

After static software testing closed loop , real time simulations followed with the flight computer in the loop where pilots flew the digitally simulated aircraft from a fixed base cockpit (Fig. 7).

In these simulations proper operation of the control functions was tested in dynamic situations in the whole flight envelope. For control law design a nonlinear simulation program had been written for a VAX 11/780. This simulation was purely digital, no analog inputs or outputs were possible. The program (aircraft equations of motion and controller) was written in Fortran whereas in the aforementioned closed loop simulation program SL 1 was used for the aircraft and assembler for the controller (flight computer program).

As both simulations were using the same set of aerodynamic data it was possible to check the controller part for programming errors by comparing simulation results for the same step or ramp inputs. So for this part of the program kind of dissimilar software testing was used.

TEST OF THE REDUNDANCY MANAGEMENT

Due to limited funding no iron-bird ground test rig could be built. This was a limitation which could be accepted here because flight testing of the CCV-FCS began in a stable configuration where the mechanical system of the F-104 G could be used as back up.

For future aircraft which will fly naturally unstable from the beginning the requirement for a FCS ground test rig cannot be abandoned.

As there was no ground test rig for the CCV-FCS the aircraft itself with all four systems installed was used as a rig to test redundancy procedures, safety routines and limitations. To a large extent this kind of testing was done using the CDU (Fig. 8).

In the upper part of the CDU there is the failure warning (left side) and identification field (right side). If there is for example a first failure of one of the series actuators the four F a i l 1 sectors A, B, C, D will be red illuminated showing that all four computers have recognized a fault. On the right side where the four main failure types can be indicated the display "ACT" will be yellow illuminated.

If more detailed information about the failure is wanted the Status "ADV"-button has to be pressed. Then all failures found in the system by the computers will be displayed on the two - 8 digit displays in abbreviated form (for example: RAR = roll actuator right) with a sequence of 1 s.

By deliberately introducing failures or failure combinations - for example by switching off one of the four power lanes - it was checked whether the failure indication and failure blocking was as desired.

Failure detection in the CCV-system is made by majority vote. Each computer sends one set of signals it has received from its A/D-interface to the three other computers. So each computer has four sets of data available in its memory and can compare them. If the differences between two or more channels trespass given thresholds the failed components and lanes are recognized by a stored failure pattern and indicated via the master caution flash light and the CDU warnings. The values of the failure thresholds were ground tested as well.

Selection of the position "Memory" with the mode rotary switch on the CDU provides the capability to read out any location of memory and through the use of a coded command sequence to be able to modify the contents of any location in the unprotected memory area. It was therefore possible to modify the flight computer program for special tests. Restoration of the original program after test was verified by check sum comparison.

SYSTEM INTEGRATION TESTS

After modification of the CCV test aircraft and installation of all new hardware it had to be tested that all systems worked properly in the aircraft environment and that the functional relationships were as designed. Sensors, IMU's, Computers, actuators, actuator electronics, interfaces, air data converters, power supplies, emergency batteries, central signal distributor, tape recorder, telemetry assembly, cockpit instruments, CDU etc. were tested within the whole system. Electrical connections and switches as for example weight on wheels switches were checked. Especially important for a FBW-System were the electromagnetic compatibility tests. These were done with external power and internal power (engine running). During these tests all electrical systems were working and the FBW control system activated to see whether there were any mutual influences. Additionally a 40 W transmitter was operated with different frequencies in the near neighbourhood of the computer compartment with the cover open during pitch, roll and yaw inputs. Similar tests were done to check for insensitivity of the actuator electronics by transmitting into the rear antenna junction on the fuselage. The frequency spectrum was chosen such that the usual frequencies of radar and VOR stations were covered.

CONTROLLER GROUND TEST

Prior to first flight and after each larger program change a ground test was conducted where the errorfree operation of the control system was checked concerning control surface deflections for defined stick and pedal inputs, fading routines, control law scheduling, control authority, trimming with and without attitude feedback, speed dependent authority limitations,damper functions (gyro feedback), incidence sensor service (skewed sensors) and logic functions. Fig. 9 shows a simplified linearized block diagram of the longitudinal control path.

On the ground the actual values of α , w_y and ϑ are zero and only the demanded values α_d, w_{yd}, η_D (ϑ_d is not active on the ground) provide a $\delta\eta$ -signal.

These values are proportional to Δn_{zd} and therefore to stick deflection. For test the stick is pulled to a specific position and held there. From the dedicated currency of the electrical stick pick-off which can be readout on the CDU in the cockpit the commanded Δn_{zd} can be evaluated. From Δn_{zd} the theoretical values of α_D , w_{yD}, η_D and $\delta\eta$ and η can be derived and compared with the actual values in the computer memory which are readout on the CDU in coded form. If the actual stabilizer position which is shown in degree on a cockpit instrument is the same as the theoretical one (for different stick inputs) everything is okay if not, the control path can be checked step by step with the help of the internal values. Analog to pitch, roll and yaw are tested.

The same test procedure is also used to check the Mach, Altitude scheduling and interpolation. For this purpose a pressure transducer test unit (TTU) is connected to the pilot static tubes of the aircraft to simulate speed and altitude. A Mach number and altitude between the reference points of the controller coefficients is chosen. Here for definite stick and pedal inputs the actual control surface positions are checked with the theoretical ones.

The control path for ϑ_d and ϕ_d and the feedback coefficients K_ϑ, K_ϕ can be checked by heaving up the airplane to actuate the weight-on-wheel switch. If additionally a change in altitude is simulated the attitude feedback becomes active. Each stick deflection then provides a dedicated run away of stabilizer or ailerons.

The right use of the feedback signals α , β and the incidence sensor program can be checked by positioning the four skewed vanes and reading out the values of CDU-α and β and checking of the positions of the control surfaces.

Logic functions and fading routines are checked as well.

The whole test takes about 45 min.

PREFLIGHT CHECK OUT

The CCV aircraft has stored in its flight computer a preflight checkout program which checks for operational readiness. The program which is run before each flight consists of the following routines:

- Failure detection (Inflight program)
- Power Test
- Instrumentation Test
- Actuator Test
- Single test programs

The inidividual test routines are chosen and operated via the Control and Display Unit.

The routines are divided into different test steps. The chosen test routine and test step number are displayed on the CDU. Each test step is activated by pressing the Ent(er)-button. If the checked values are within their limits there is a "CO" (continue) on the display otherwise a "F" (failure). See Fig. 10.

For the limit checking the earlier described failure detection routine of the operational program (inflight program) is used. Therefore the failure lamps of the "failure warning field" will be illuminated as well.

In the inflight program the following tests are run continuously

- CPU (computer) monitoring
- memory monitoring
- I/O-monitoring
- fault and synchro monitoring for analog and digital information
- power monitoring
- hydraulic monitoring
- actuator and actuator electronics monitoring

These subroutines of the inflight monitoring program are equally used in the pre-flight check out.

FLIGHT TESTING OF THE CCV-FCS

Main points in flight testing of the flight control system were

- System reliability and redundancy management
- Aircraft dynamics (parameter identification)
- Stabilization and Handling within the whole flight envelope
- Structural damping (oscillations and structural loads)

All signals, logic events and internal values necessary for a detailed analysis of possible problems were tape recorded on board for all four computers. Additionally each flight was supervised by the flight conductor and system engineers from a quick-look station at the MBB flight test center. Here the main parameters which describe the flight state, system status and failure status are transmitted via telemetry to the ground and displayed with the help of plotters, system key board displays (SKD), light bars and event lamps.

The light bars for example are used to show each system parameter of all four channels in direct comparison. Each discrepancy can be seen by one "quick look" and it can be decided whether actions have to be taken by the pilot. This supervision part works independent of the failure indication logic.

For failure monitoring one of the SKD's is used. It has already been described that each failure is displayed to the pilot in the cockpit on the CDU. If, however, several failures should occur detailed information about all failures can only be given to the pilot in sequence not in parallel at the same time. Here the SKD is more powerful because all this informaion is available at once.

Various plotters (8 channels each) are used to give information about the aircrafts flight parameters in pitch, roll and yaw and about structural vibrations. As an example the plotter channels for pitch are given:

1. Indicated airspeed
2. Stick pitch
3. Stabilizer position
4. Normal acceleration
5. Angle of attack
6. Rate pitch
7. Attitude pitch
8. Mach number

If there is for example a serious decrease in pitch damping with increasing airspeed the flight conductor can stop further trials at higher airspeed.

As the digital FCS which was developed for the CCV aircraft was a completely new system flight testing was made in several steps beginning with the normal stable configuration of the F-104 G. This test phase was used to gather experience and to gain confidence with the multi-channel FBW-system.

As in this configuration the aircraft could still be flown with the basic mechanical system, which was retained as a back up, the first take-offs and landings were made in mechanic switching to FBW in safe height.

This was not possible in the Canard configurations. As simulations had shown a dangerously strong pitch up at take-off in MEC the first flight had to be made in FBW. The mounting of the canard changed the aerodynamics considerably and gave practically a new aircraft. But this new aircraft could now be tested with a FCS already known from previous flights without canard. (The basic structure of the control system remained unchanged for all five configurations.)

Before proceeding to the unstable canard configurations - the first canard configuration was weakly to neutrally stable - parameter identification flights were made to get a better description of the aircrafts behaviour with canard at high dynamic pressure. Flights at higher airspeeds had shown much less pitch damping than it had been expected from simulation.

Other problems like low amplitude limit cycles in roll due to hysteresis, handling deficiencies in pitch and roll due to too much phase lag in the command path and some drift problems due to numerical inaccuracies and hardware differences had been eliminated before.

Some software problems were detected by flight testing which had not been found in ground test. These were no programming errors but problems introduced by "wrong thinking"

or human interface problems. "Wrong thinking" means the introduction of logic functions, scaling factors or quick program changes which had not been considered in all consequences.

In this context the otherwise so valuabel flexibility of the digital system was kind of dangerousbecause changes from one flight to the next - just to try something new - could be made so easily.

CONCLUSION

The methods and tools used to test the new digital flight control system of the German CCV aircraft during development and flight test have been described. The usefulness of the test methods (and the effectiveness of the redundancy concept) is demonstrated by the fact that in 160 flights no accident ever occurred in spite of numerous software changes.

REFERENCES

1. Kubbat, W. "A Quadruredundant Digital Flight Control System for CCV Application" Agard-Symposium FMP and GCP, Oct. 1974, Paris (MBB-UFE report 1116(Ö))

2. Beh, H. Korte, U. Löbert, G. "Stability and Control Aspects of the CCV F-104 G" Agard FMP-Meeting, Sept. 1978, Ottawa (MBB-UFE report 1337(Ö))

3. Korte, U. "Flight Test Experiences with a Digital Integrated Guidance and Control System in a CCV Fighter Aircraft" AGARD GCP-Meeting, Oct. 1982, Lisbon (MBB/FE136/S/PUB/84-report)

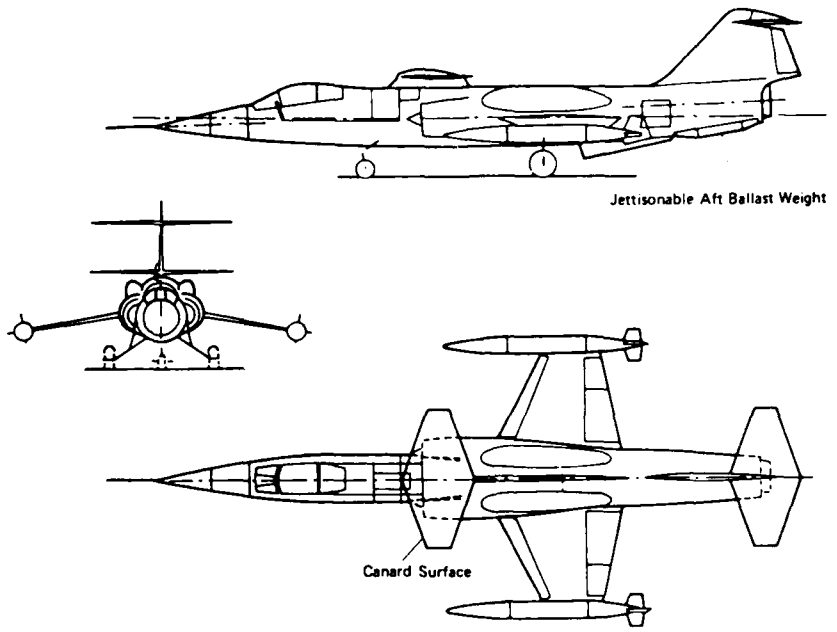

Fig. 1 TEST AIRCRAFT

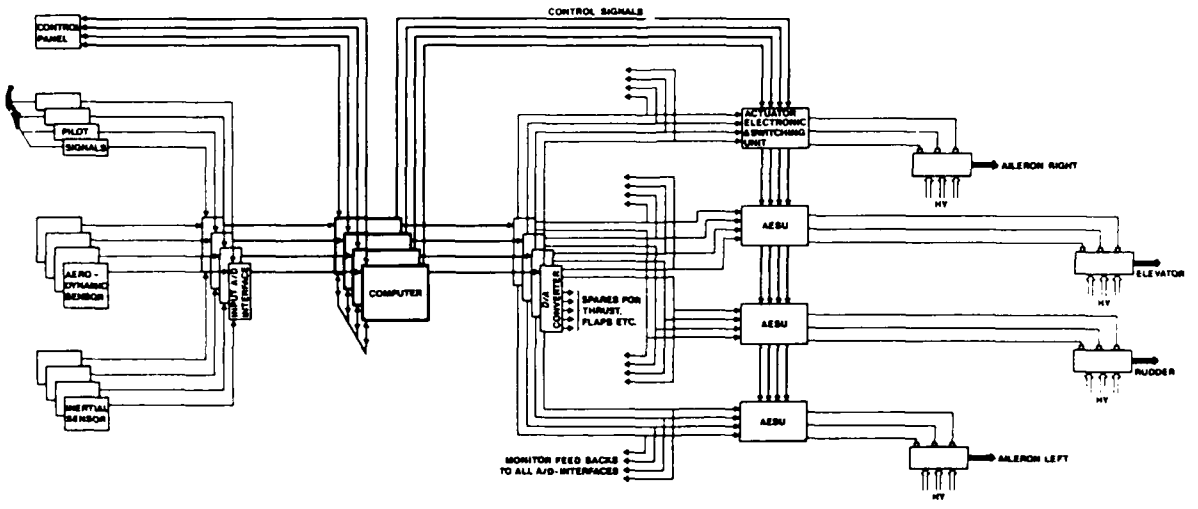

Fig.2 SYSTEM OVERVIEW

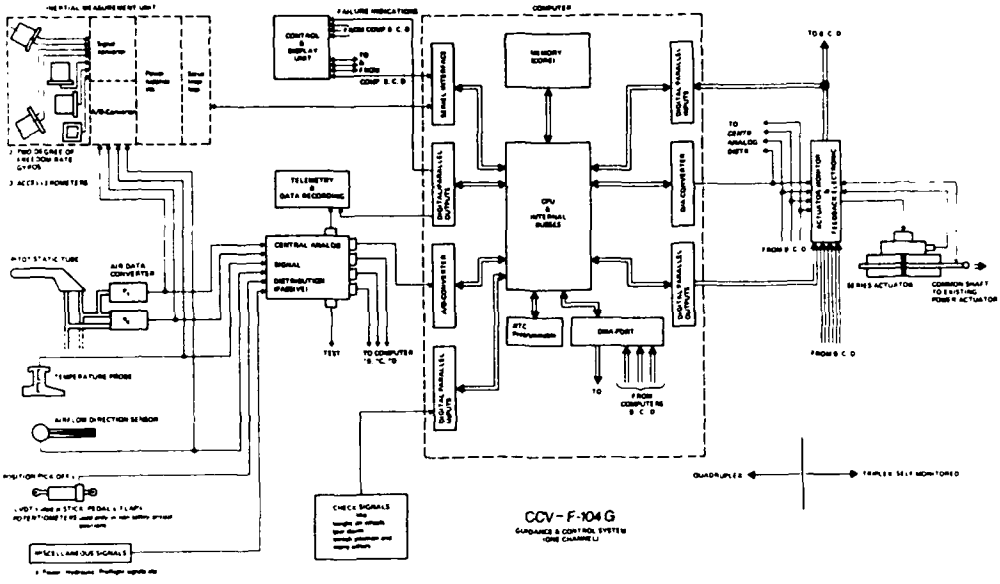

Fig. 3 ONE CHANNEL OF THE GUIDANCE AND CONTROL SYSTEM

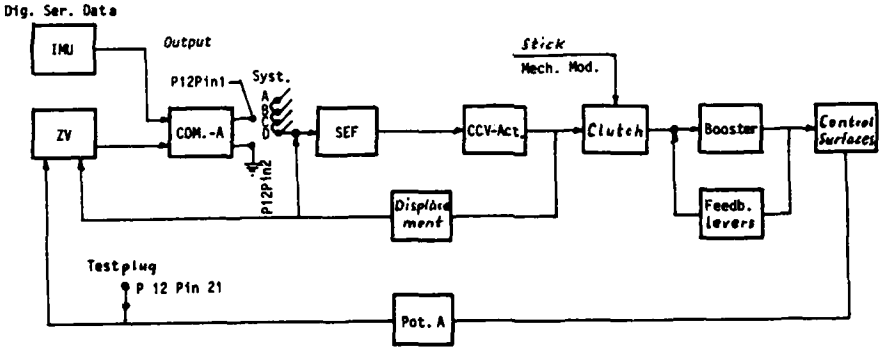

Fig. 4 STRUCTURAL COUPLING GROUND TESTS, OPEN LOOP

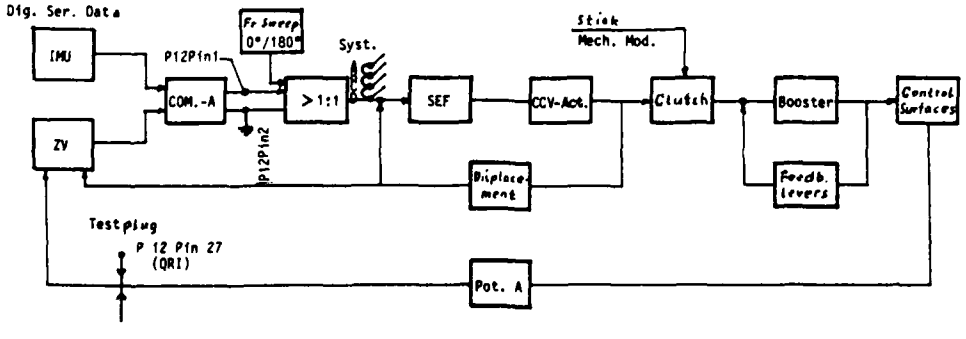

Fig. 5 STRUCTURAL COUPLING GROUND TESTS, CLOSED LOOP

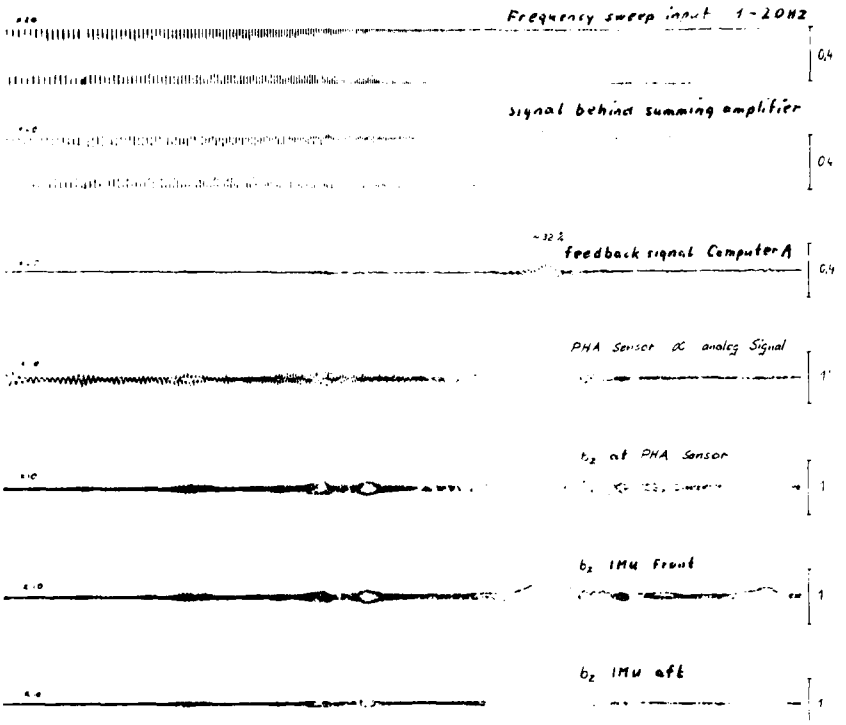

Fig. 6 GROUND RESONANCE TESTS, CLOSED LOOP

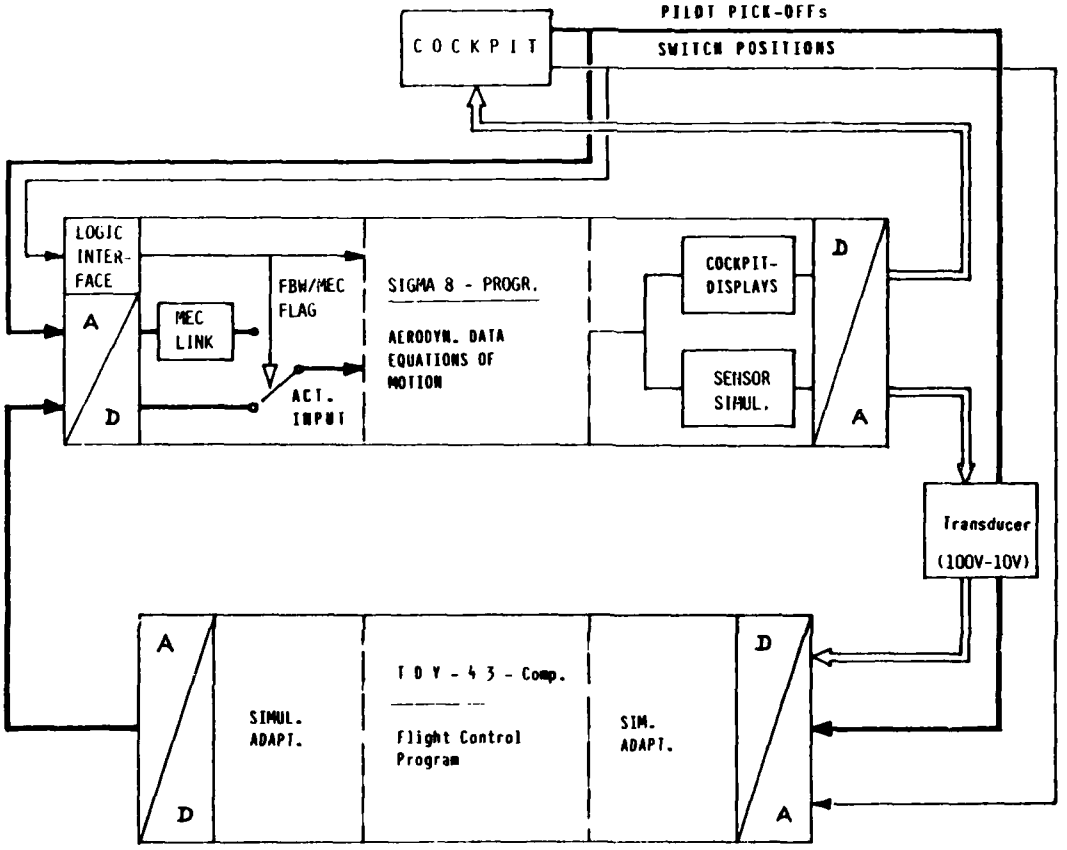

Fig. 7 CLOSED LOOP, REAL-TIME SIMULATION

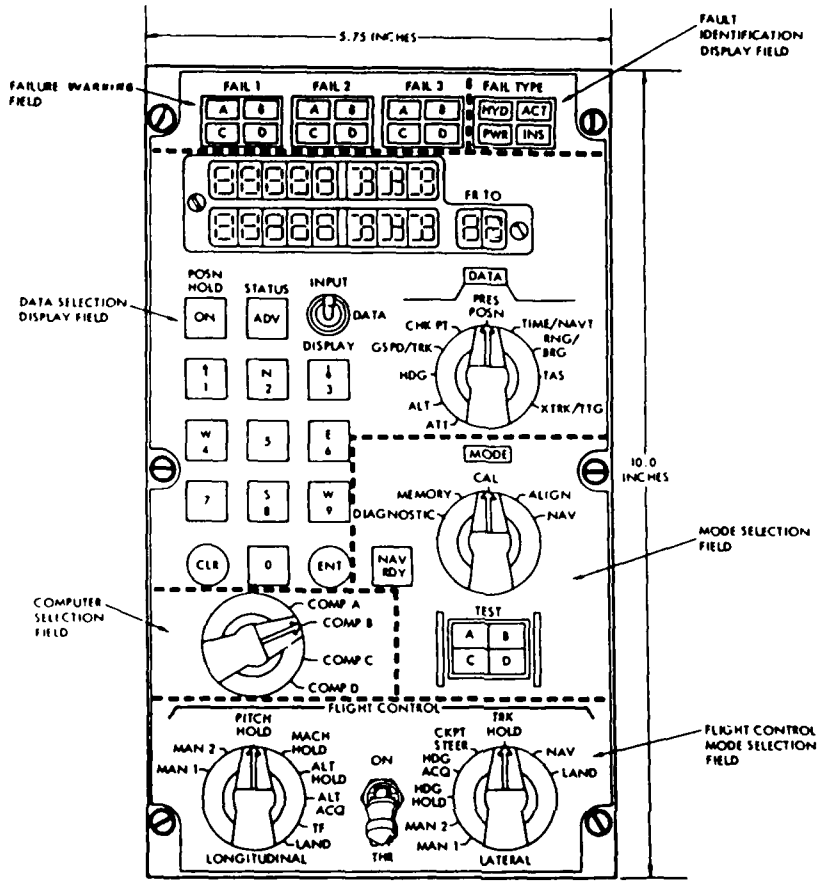

Fig. 8 CDU FIELDS OP OPERATION

PITCH CONTROL (SIMPLIFIED)

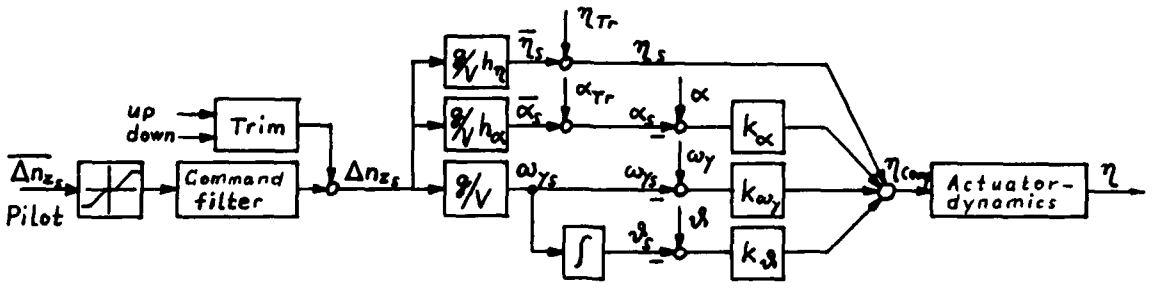

$$h_\alpha, h_\eta = f(Ma, H)$$

$$k_\alpha, k_{\omega_y}, k_\vartheta = f(Ma, H)$$

$$\eta_{Tr}, \alpha_{Tr} = f(Ma, H)$$

Fig. 9 BLOCK DIAGRAM PITCH AXIS

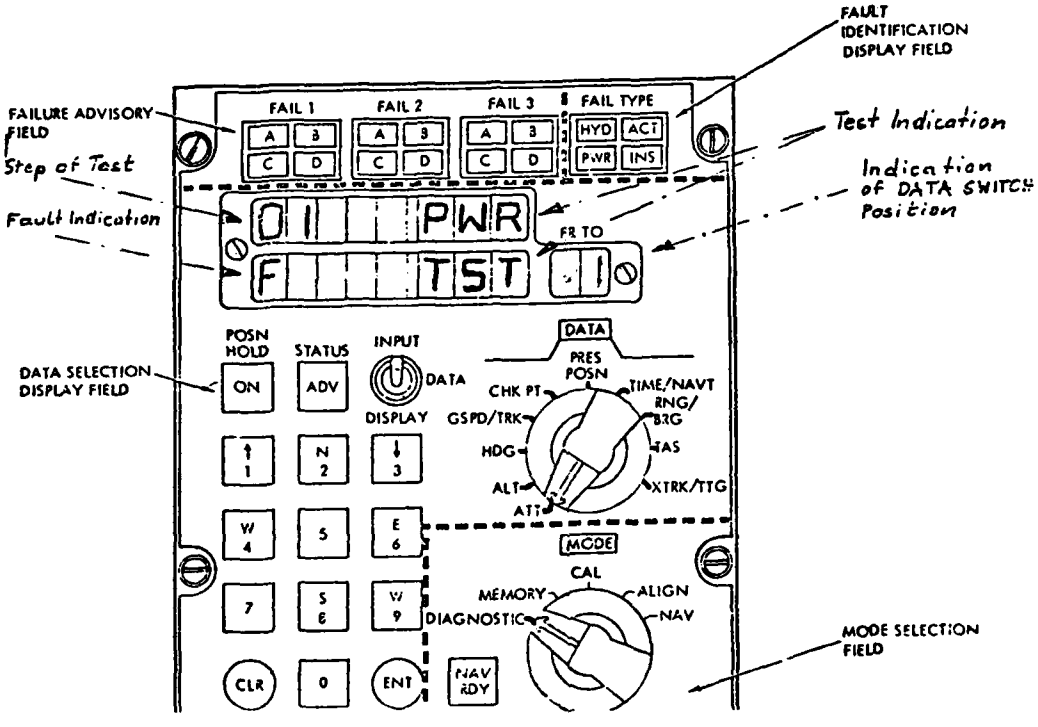

Fig. 10 CDU-DISPLAY FOR PREFLIGHT

AIRLAB: A LABORATORY FOR FLIGHT-CRUCIAL ELECTRONICS SYSTEM RESEARCH

by
H. Milton Holt
Dale G. Holden
Amy O. Lupton
National Aeronautics and Space Administration
Langley Research Center
Hampton, Virginia 23665
USA

SUMMARY

A new laboratory, AIRLAB, recently completed at the NASA Langley Research Center was developed as a focus for conducting research on fault-tolerant electronic systems for flight-crucial applications. The laboratory was conceived and implemented to enhance the utilization of aeronautical research for improving the performance of future aerospace vehicles. Advanced vehicles will require highly reliable digital electronic systems to perform flight-crucial functions which if lost, would cause total failure of the vehicle. The research is actively pursuing development of techniques to form the basis for a validation methodology that can be used to determine the performance and reliability of advanced digital systems. Included in the research are the development of analytical models, emulation techniques, and experimental procedures. The techniques and methods are verified using test specimens of fault-tolerant computers and systems and the capabilities of AIRLAB.

1. INTRODUCTION

Many advances are being made today in aeronautical research that will improve the performance of future aircraft and will allow increased autonomy in manned and unmanned spacecraft. To take advantage of these advances, digital electronic systems will be needed to perform the flight-crucial functions that cannot be performed by existing analog or mechanical systems. These digital electronic systems will include varying degrees of fault tolerance as an approach to meeting the stringent reliability requirements imposed by flight-crucial applications. A typical system designed for flight-crucial applications will have a reliability requirement specifying a probability of catastrophic system failure on the order of 10^{-9} at 10 hours. The design and validation of such highly reliable systems present special problems not found in the design and validation of conventional systems. No longer will exhaustive testing be practical because of the excessive time required and cost incurred to build confidence that the reliability requirements can be met. Also, as the criticality of the function increases and the exposure time increases, classes of errors that were not quantified for inclusion into a formal analytical reliability analysis in the past will now become significant parameters in the analysis. These errors include design flaws in both hardware and software as well as transient and latent faults.

Research is underway at the NASA Langley Research Center to develop the methods and techniques that can aid in determining the performance and reliability of digital electronic fault-tolerant systems without having to rely on exhaustive testing.[1] Fault-tolerant systems are characterized by being able to continue an intended function throughout the mission even in the presence of a fault. Fault-tolerance can be achieved through multiple redundancy in hardware and software in conjunction with the necessary logic for detecting and isolating faults and a capability for removing the faulty component by reconfiguring the system. Since fault-tolerant systems are more sophisticated than existing high reliability systems using triplex, quad, or dual-dual architectures, new techniques and methods are needed to evaluate the performance and reliability of these systems. As shown in figure 1, the work at the Langley Research Center includes development of analytical models for reliability estimation, economic assessment, and software error projection; design proof techniques; emulation capabilities; and experimental procedures leading to the definition of a generic validation methodology. These techniques

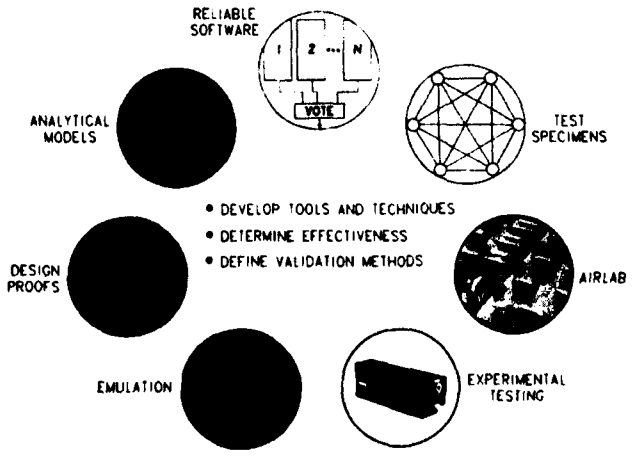

Fig. 1 Fault-tolerant validation technique development.

and methods will be verified and refined by applying them to specimens of fault-tolerant computers and systems using the capabilities of AIRLAB. Candidate tools and techniques will become a part of a proposed validation methodology that will be applied to advanced system concepts or proof-of-concept hardware models in AIRLAB as illustrated in figure 2. Experiments will be conducted to provide information on the effectiveness of the proposed methodology and the candidate tools and techniques. In addition, data on the performance and reliability characteristics of the advanced system test specimen will result.

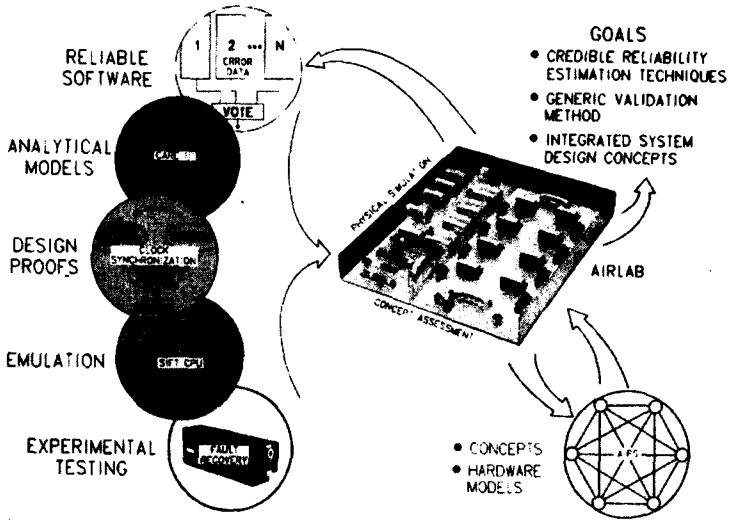

Fig. 2 Fault-Tolerant system validation research.

Some of the complexities that must be considered in analyzing fault-tolerant systems and some of the parameters that must be included when conducting a reliability analysis are illustrated by the fault handling model of figure 3. This model shows the states that must be included in a reliability analysis for a system with no software errors and only permanent faults in hardware. The model shows that system failure can result from several causes. If faults are handled properly and the system proceeds to state A2, system failure can eventual occur due to exhaustion of spare hardware. However, while in the error state, Ae, system failure can occur due to improper handling of the fault. If the fault handling is too slow, a second fault can occur before the active fault is cleared causing the system to go to the failure state, F2. If the fault detection coverage is to small, the fault may not be detected causing the system to go to failure state, F1. The problem becomes much more complex when transient and intermittent faults and software errors are added. Therefore techniques that consider this parameters as well as others are needed.

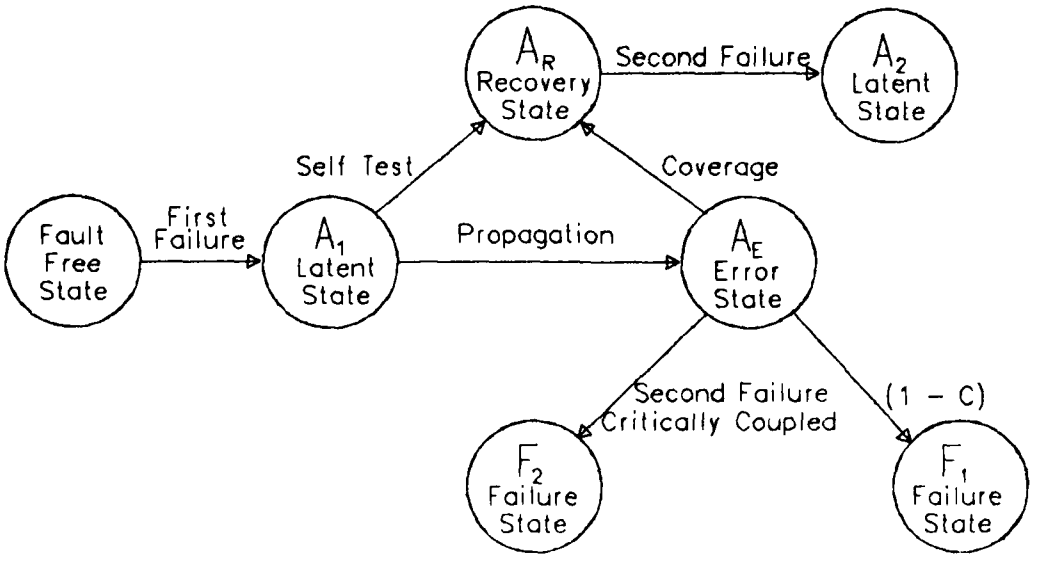

Fig. 3 Fault-handling model.

The goal of research at the Langley Research Center is to provide an effective validation methodology, techniques for conducting comparative analyses of advanced system concepts and guidelines for designing fault-tolerant systems that will be easier to validate. The central focus for the fault-tolerant system research described in this paper is a newly operational laboratory, AIRLAB, at the Langley Research Center developed especially for conducting research on highly reliable electronic

systems. AIRLAB is a national facility that provides many opportunities for cooperative activities between NASA, industry, academia, and other government agencies by researchers who are interested in the design and validation of highly reliable fault-tolerant systems. Discussion of the research using AIRLAB will concentrate on the physical capabilities of the laboratory facility, the development of a validation methodology and the use of advanced system test specimens in defining design guidelines.

2. AIRLAB

AIRLAB became operational at the Langley Research Center in April of 1983 to support research that will become the basis for developing design and validation methodologies. The basic attributes and capabilities of the physical laboratory provided at that time continue to evolve as the requirements for research in the area of fault-tolerant system validation progress. AIRLAB is a 7600 square foot, environmentally controlled laboratory partitioned into three distinct areas as shown in figure 4. The largest area contains eight research work stations and a central-control station. The next largest area is the computer room containing nine VAX 11/750's and a VAX 11/780. Each VAX 11/750 has 2 megabytes of memory and 56 megabytes of local disk storage. The VAX 11/780 has 4 megabytes of memory and 160 megabytes of local disk storage. All 10 of the VAX minicomputers are interconnected with a 256 kilobaud serial digital communication network with DECNET communications software. The third area contains a horizontally microprogrammable Nanodata QM-1 computer that hosts a unique diagnostic emulation algorithm for use in emulating digital devices at the lowest logical level. Each research station is configured with an extensive set of peripherals as well as digital and analog input/output devices. A block diagram for a typical research station is shown in figure 5. Four of the research stations also have MEGATEK 3-D graphic systems with high resolution color monitors.

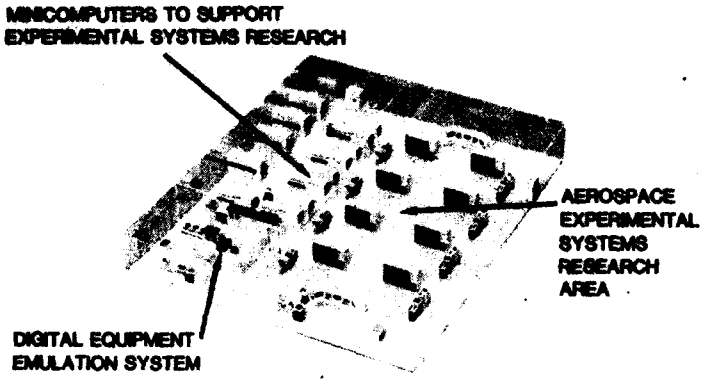

Fig. 4 AIRLAB.

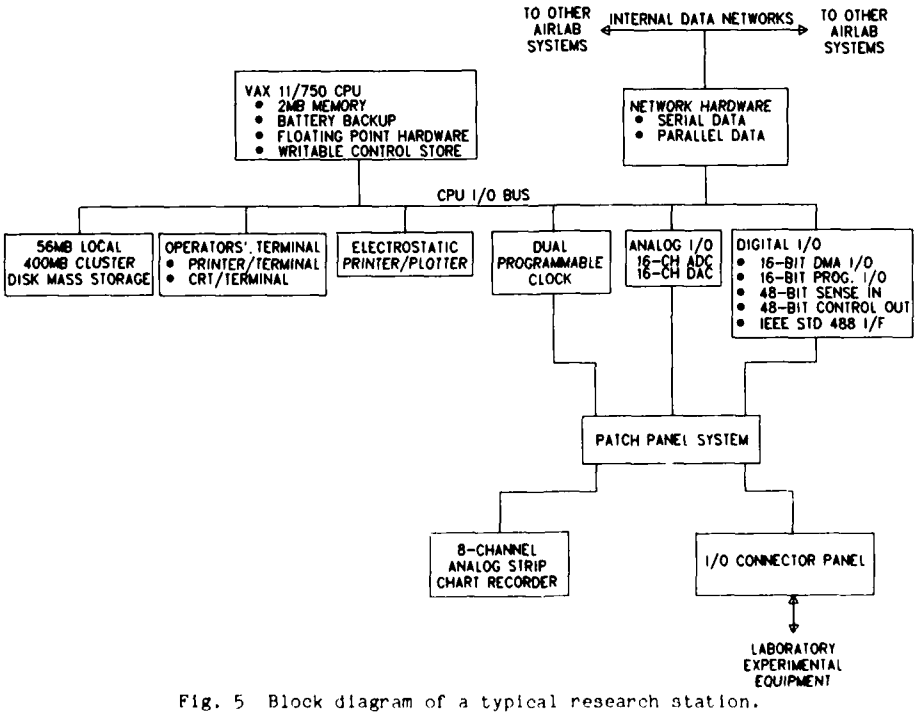

Fig. 5 Block diagram of a typical research station.

AIRLAB provides a capability for conducting experiments without the necessity of each experimenter having to learn the details of the facility hardware and software. A unique software feature of AIRLAB is the Data Management System (DMS) which is the prime interface for experimenters to access information about the laboratories capabilities. A major goal of the DMS is to allow users to be as productive as possible by providing a centralized, easy access to AIRLAB capabilities and research results. The DMS collects data about experiments, organizes it, provides easy access to it, and ensures its integrity. The DMS operating environment, accessible from all AIRLAB VAX computers, is largely menu-driven and offers extensive on-line help. Log-on and log-off procedures are used to track the user's activities on the system and captures as much information automatically as possible. An on-line engineering notebook allows the user to make notes about current work whenever desirable. The user can later search the notes both chronologically and by key words to recall information about the work. Most experimental data collected will initially be kept on-line but will eventually be archived on tape. The DMS provides the capability to facilitate accessing information in archived files using an on-line catalog of all archived files coupled with the ability to browse and search the catalog simply and easily. The DMS also includes a software configuration management system that facilitates the development of user software programs, provides problem reporting and tracking mechanisms, and provides a catalog of all the available software. For those experiments that require access to the VAX operating system, the capability is provided to move easily from the DMS to the operating system and back to the DMS. Other support software currently available is listed in table 1.

- **OPERATING SYSTEM**
  - **VAX/VMS** — **VAX/ELN**
- **LANGUAGES**
  - **FORTRAN** — **VAX - 11 ASSEMBLER**
  - **PASCAL** — **C**
  - **BASIC** — **LISP**
  - **BLISS 32**
- **WORD PROCESSING AND REPORTING**
  - **MASS - 11**
  - **DATATRIEVE**
- **GRAPHICS**
  - **TEMPLATE**
  - **WAND (MEGATEK)**
  - **VERSAPLOT (VERSATEC)**
- **COMMUNICATIONS**
  - **DECNET**

Table I Software products available in AIRLAB.

The design of AIRLAB provides the flexibility to support a variety of research configurations. Figure 6 is an illustration of AIRLAB resources configured for conducting multiple independent experiments. The experiments identified are currently underway in the laboratory. Station 1 is the central control station which is directly connected to the VAX 11/780 and is used for software development and data management. Station 2 is used to demonstrate the diagnostic emulators capability to emulate an avionics microprocessor at the gate level. Stations 3, 4, 5, and 6 are configured for an experiment that is designed to validate assumptions made in the design proof of a fault-tolerant system synchronization algorithm. Two of the stations, 7 and 8, are used in an experiment to investigate the occurrence of software errors. Stations 9 and 10 are each dedicated to supporting one of two fault-tolerant computer system test specimens that are used for developing validation experiments to characterize fault-handling responses. Figure 7 is an illustration of AIRLAB resources configured to support integrated systems experiments. The station assignments are arbitrary, and the data distribution network is experimental and defined by the experimenter. Another possible configuration of the research stations, figure 8, would allow the experimenter to investigate new fault-tolerant computer concepts where redundant elements of the system are simulated at each station.

3. VALIDATION METHODS RESEARCH

A major research thrust in AIRLAB is the development of a validation methodology for fault-tolerant systems with extremely high reliability requirements necessitated by flight-crucial applications. The validation process for advanced electronic systems must begin at the conceptual stage of design and will

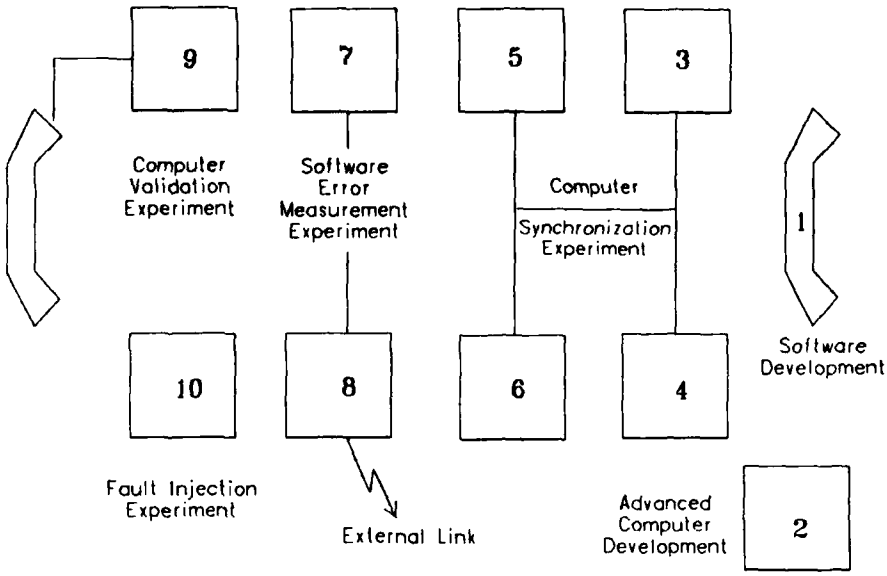

Fig. 6 Experimental stations configured for multiple independent experiments.

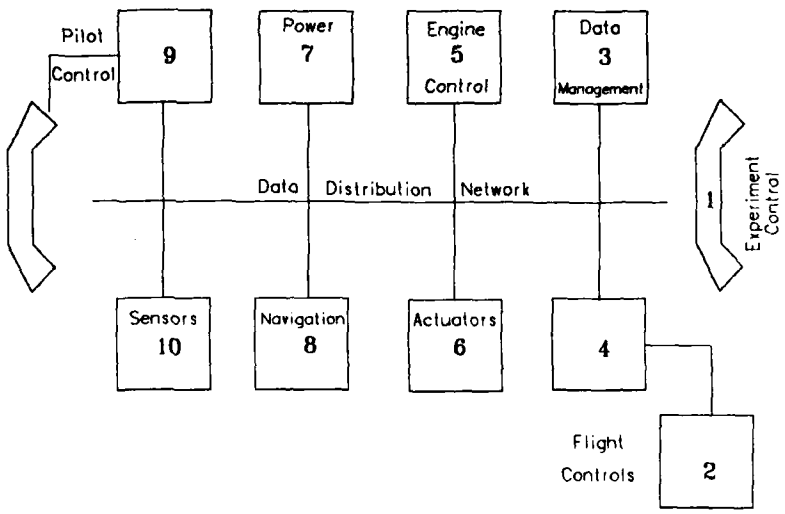

Fig. 7 Experimental stations configured for integrated systems experiments.

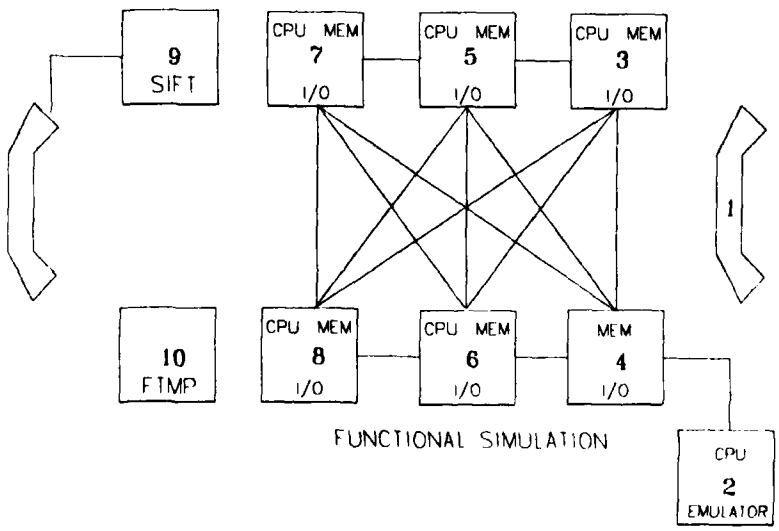

Fig. 8 Experimental stations configured for fault-tolerant systems concept evaluation.

not be completed until some field experience is gained. This process differs from current validation procedures by placing the emphasis on design details at the early stages of system definition and design. In the past, the validation process has focused on establishing that a system meets its intent after the design is complete. Credible reliability estimates for these systems with relatively low reliability requirements have been made using field data collected through life-testing methods. Most existing reliability estimation techniques were developed for systems with significantly lower reliability requirements than needed for advanced aircraft applications and do not allow the analyst to take into account parameters that become increasingly more important as system reliability increases. Indeed, the whole validation process as it exists today is based on relatively simple electronic system configurations. The trend towards more functional complexity in future aerospace applications leads to increases in system design complexity and extreme reliability requirements. Because of such extreme reliability requirements, every system design decision can be a weighty issue in terms of reliability and must be considered very carefully. The validation for such systems requires new analytical techniques, emulation and simulation techniques, mathematical proofs, and experimental testing to provide credible assessments and proofs that a system meets its design intent.

In working group meetings held at the Langley Research Center, experts from industry and academia provided direction and advice for addressing the critical issues in the validation process. Research guidelines were established through the development of a validation framework, and as a result, research in AIRLAB is focused on the development of analytical models, experimental testing, and the development of proof techniques. In March 1979, the first working group meeting was sponsored by NASA as an initial step in defining a validation methodology for evaluating fault-tolerant systems. This working group provided a forum for the exchange of ideas on fault-tolerant avionics and control system validation.[2] The state of the art in fault-tolerant computer validation was examined in order to begin establishing a framework for future discussions of validation research for these systems. The results of the working group and the evolution of AIRLAB by the NASA Langley Research Center provided impetus for a second working group meeting. This second meeting was conducted in October 1979 to identify, beginning with the ideas provided by Working Group I, specific validation tasks that could provide the basis for a validation methodology.[3] To provide an initial focus, validation issues specifically related to two existing fault-tolerant computers, Software Implemented Fault Tolerance (SIFT) and Fault Tolerant Multiprocessor (FTMP), were considered. This working group classified the validation research as shown in figure 9 into three major areas, analytical modeling, logical proofs, and experimental testing, as important to the development of a validation method. The consensus of the participants, which included individuals from universities, industry, and government, was that techniques covering these three areas can be combined to validate highly reliable electronic systems. Work at the Langley Research Center includes development of techniques in all three areas. Several AIRLAB research efforts currently ongoing in these areas are discussed.

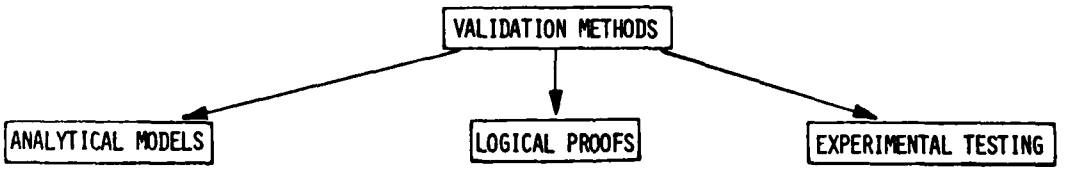

Fig. 9 Validation research.

3.1 Analytical Modeling

To assist experimenters in the development of validation methods, several analytical techniques are being pursued to perform reliability estimations and to measure performance of fault-tolerant systems. One of the unique analytical techniques available in AIRLAB is the Computer-Aided Reliability Estimator (CARE III)[4, 5, 6] program. The CARE III program which is structured as shown in figure 10 allows the

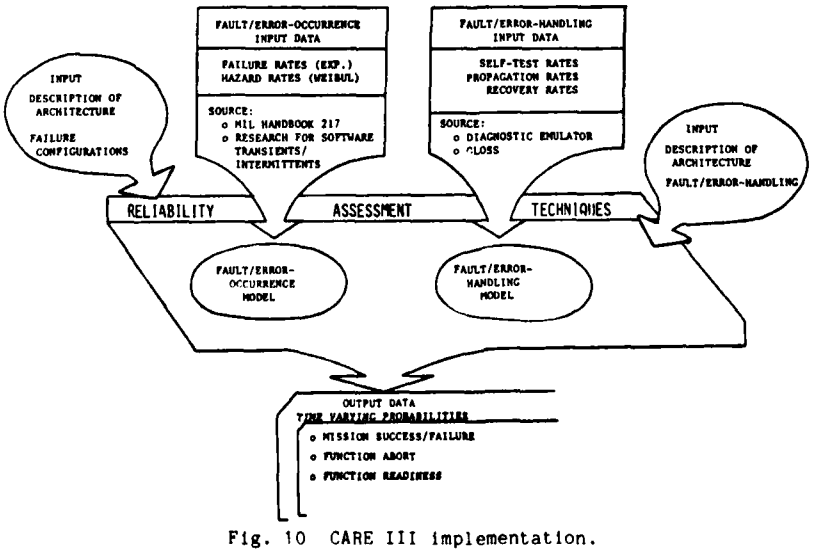

Fig. 10 CARE III implementation.

analyst to more properly account for the systems ability to recover from faults. A unique innovation of CARE III is the state decomposition method used to solve the problem of very large state spaces needed to describe the fault occurrence and fault-handling behavior of fault-tolerant systems. In addition to handling random variables of interest which are exponentially distributed, CARE III is a major departure from conventional approaches in that it also supports nonexponential distributions. Another attribute of CARE III not found in conventional techniques is the ability to model transient faults. This program is a significant advance in reliability modeling technology and was recently released for public use through NASA's COSMIC facility after undergoing a period of testing and validation. A tutorial workshop was conducted in AIRLAB for potential users that focused on the mathematical design and testing of the program and hands-on experience using the program. CARE III will continue to be improved as more experience is gained in its use. Several constraints and limitations of CARE III have already been identified and others will be discovered as the complexity of fault-tolerant systems increase and the reliability requirements of those systems change. As a complement to CARE III, the Semi-Markov Unreliability Evaluator (SURE) program[7] allows the analyst to compute upper and lower reliability bounds very quickly. SURE is based on a new mathematical theorem which uses simple algebraic formulas to efficiently compute accurate bounds for the system failure state probabilities of a large class of semi-Markov models.[8]

Other analytical modeling activities are being pursued in AIRLAB to develop capabilities that provide more accuracy in modeling complex systems. One such effort under a grant with Duke University is the design of a hybrid automated reliability predictor (HARP) which decomposes the problem into a fault-occurrence model and a fault-handling model similar to CARE III.[9] The fault-occurrence model is solved analytically while the fault-handling model is solved by simulation of the model. The simulation is implemented in a form that has the potential for providing more accuracy than the CARE III approach to modeling fault-handling mechanisms. One of the distinct features to be developed for HARP is the ability to make automatic sensitivity analysis of system reliability as a function of various reliability parameters. HARP will allow time varying failure rates to be specified and will provide sensitivity analysis of time dependent transition rates.

An analytical modeling research effort underway in AIRLAB by the University of Michigan is the development of performance models for the evaluation of real-time multicomputer control systems. The goal of the research identified in figure 11 is to systematically classify real time multicomputer systems into groups, develop approximate analytical models for each class, validate the models against performance data from SIFT and FTMP in AIRLAB, and refine the models as a result. Recent success in a preliminary effort has been in the development of a new performance measure referred to as dynamic failure which is defined as failures caused by the system not responding fast enough to hard deadlines.[10]

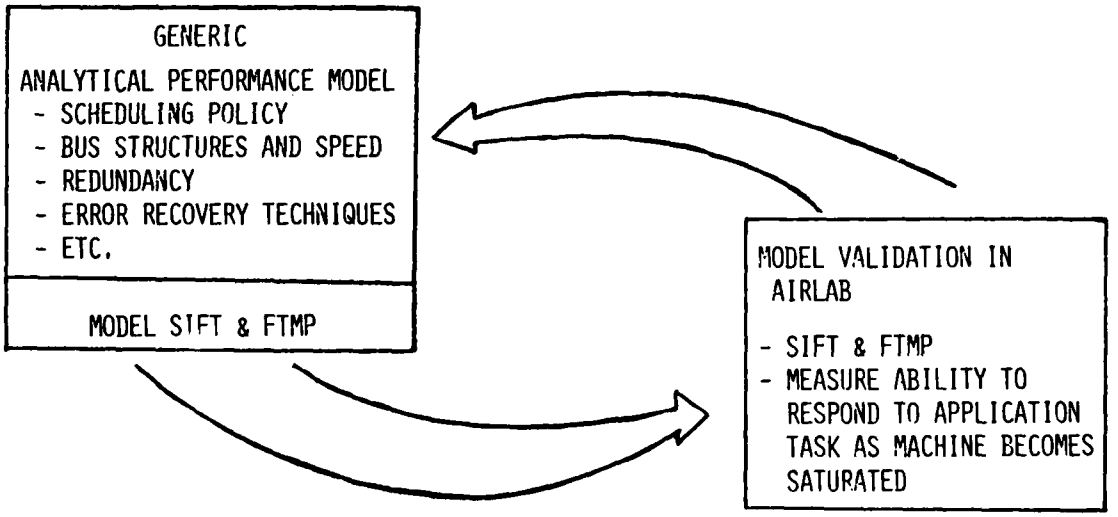

Fig. 11 Analytical performance modeling experiment.

3.2 Logical Proofs

Formal verification techniques can have a major impact on the credibility of the methodology used for the validation of highly reliable fault-tolerant systems. Mathematical techniques to prove that the implementation of a system design is consistent with the design intent would be ideal. A major question concerning analytical modeling of complex systems is the accuracy of the model. A technique for mathematically proving that models are accurate representations of the system being modeled is absolutely necessary to establish the credibility of performance and reliability analyses made using new complex models of highly reliable systems. SRI International identified a method for performing formal proofs[11] and applied the method to a portion of the SIFT operating system. Because of limitations to the generality of formal proof techniques used by SRI, constraints in design flexibility of the SIFT computer system were necessary to accommodate application of the proof process. A peer review workshop on formal proofs with an objective to assess the role of the techniques in system validation with emphasis on the tools developed by SRI was recently sponsored by NASA. Although some progress has been made, formal proof technology is very limited and is currently in the early stages of development. Significant research is required to bring the level of usefulness up to the point of application in the validation process. However, formal proofs appear to be an integral and necessary part of the process and a concentrated effort is needed to bring the technology to fruition.

3.3 Experimental Testing

Results of Working Group Meeting II indicated that testing alone provides a very weak basis for system validation when high reliability is required.[3] However, experimental testing is required for collecting data on the software error process, for verification of new techniques, and for collecting statistically significant data on the fault-handling properties of fault-tolerant systems. NASA is sponsoring the development of validation experiments for fault-tolerant computer systems using AIRLAB resources and the SIFT and FTMP computers as test specimens.

In digital systems the software component in a system reliability analysis is usually considered to be perfect. However, there is no guarantee that the software will be error free even after extensive testing has been accomplished. This uncertainty must be taken into account when performing a reliability analysis of flight-crucial electronic systems. There are several software error models in the literature which might be used for that purpose, however, no consensus exists on which of these models accurately portrays the software error process. Software error rate experiments are being conducted in AIRLAB with the objective of acquiring more information on the software error process. Data from these experiments are needed to either lend credence to or refute assumptions made in the development of the existing models.

An initial experiment design developed by NASA and Boeing[12] was refined, expanded, and implemented in AIRLAB by the Research Triangle Institute. The current experiment design is shown in figure 12. Three independently designed programs, based on a common set of program specifications, are subjected to a series of acceptance tests for a suitable length of time before being declared ready for application. After completion of acceptance tests the three programs are executed simultaneously with common random inputs to each program. The program outputs are voted or compared to detect program errors. Upon observance of an error the process is stopped and the software error is examined in detail, labeled, and returned to the programmer for correction. After the error is corrected, the acceptance test is performed again until the program is again declared ready for application. Upon completion of the acceptance tests the program execution begins again with all three program outputs being compared to detect the next error. This process is continued until a stopping rule is satisfied. The stopping rule is a function of the number of errors observed, number of inputs executed, and the history of interfailure times. When the stopping rule is satisfied each program is returned to the original version that passed the first series of acceptance tests. The process of program execution, error detection, and error correction is repeated until the stopping rule is again satisfied. Replication of the process continues until enough observations are made to achieve the desired level of accuracy. Data collected in this experiment will contribute significantly to our knowledge about the software failure process.

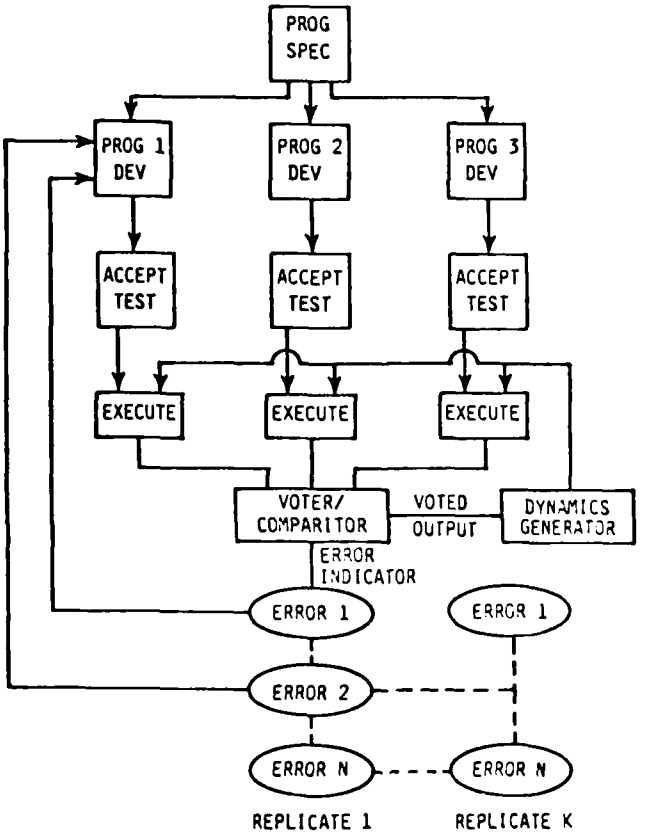

Fig. 12 Software error experiment.

An area that requires verification of new experimental techniques is the determination of the fault-free behavior of a digital system. The first series of experiments under development by Carnegie-Mellon University (CMU) will determine fault-free static properties of fault-tolerant computer systems. These

experiments shown in figure 13 will provide baseline measurements such as time to execute an operating system call, measurements of processor performance such as the time required by the hardware to do simple logical, arithmetic, and control functions and frame utilization or workload measurements. Other fault-free experiments are defined to measure architectural efficiency such as time to transfer varying blocks of data, bus transaction rate, and voting overhead. Performance parameters measured by these experiments are fundamental in determining computer performance. These parameters are likely to change in the presence of faults and are therefore useful in determining when faults are present in the system and when system failure may be imminent. In addition, CMU experiments will address fault handling questions such as time to detect and reconfigure from various faults, software overhead for fault detection, and the efficiency with which the architecture can continue operation in the presence of faults. The experiments are primarily used for characterizing the fault-free performance of a system. Fault-free characteristics are needed as a baseline for determining the performance of a system which is operating under faulty conditions. The experiments can also be used for comparing the performance of competing system designs.

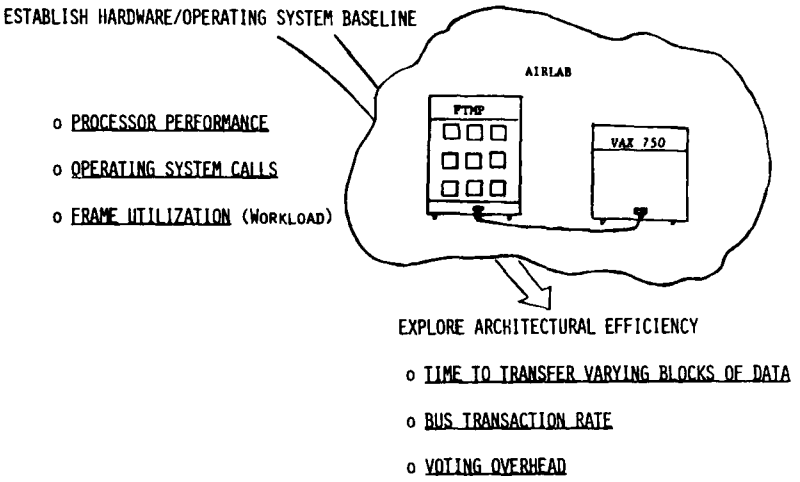

Fig. 13 Fault-free performance experiment.

Another new technique that has been developed and is being verified in AIRLAB is a methodology for validating fault tolerant clock synchronization algorithms. The methodology is a combination of formal proof verification of the algorithm and experimental testing to validate the correctness of the axioms postulated in the proof. The formal proof provides a precise statement of the properties of the system to be measured. Major parameters to be determined experimentally are the maximum clock skew, maximum error in reading another processor's clock, and the maximum drift rate between two clocks. System reliability requirements determine the level of confidence at which these parameter values must be determined. For extremely high reliability requirements classical statistical estimation theory would require a prohibitive number of data samples to establish the level of confidence needed, therefore a nonparametric statistical method of parameter estimation is used. A paper on this methodology will be presented at the IEEE/AIAA 6th Digital Avionics Conference to be held in December of 1984.

One example of experimental testing that will collect data on the fault-handling properties of fault-tolerant systems, is an in-house experiment that will result in techniques for measuring fault-recovery rate distributions. The goal of the experiment is to determine the most promising method for making comprehensive measurements of fault-recovery rates of the FTMP and to improve the analytical model for estimating the reliability of FTMP. As shown in figure 14, faults are injected at the integrated circuit pin level and measurements are made of those parameters that contribute significantly to the fault-handling behavior and hence the reliability of the FTMP. Currently only stuck-at faults are being injected on single pins. One of the major concerns of AIRLAB research is the adequacy of the fault model being used to generate statistical data. It is obvious that stuck-at faults are not truly representative

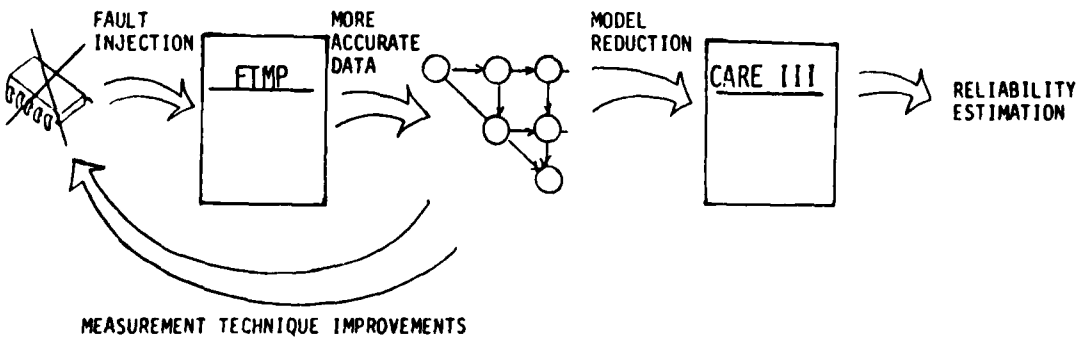

Fig. 14 FTMP fault recovery rate distribution experiment.

of all system faults, but their occurrence is possible and they are the most convenient to model. Additional research is needed to properly define fault models for the integrated circuit pin level. Likewise, transient and intermittent fault models need to be defined. Once fault models are clearly defined, data from fault-injection experiments will be more meaningful in terms of reliability parameter accuracy.

A common problem with advanced reliability techniques such as SURE and CARE III is the requirement for input data that is not readily available and indeed may even be specific to the application. Components of system fault recovery and recovery rate distributions are typical parameters that are not available. One approach for obtaining the input data needed for reliability estimations is to emulate the system at a level sufficient to describe fault-propagation characteristics. The diagnostic emulator shown in figure 15 provides the capability to emulate digital systems to the gate level at a very fast rate that is nominally 2.6 million gates per second. The diagnostic emulator can be used as a system surrogate to observe and analyze behavior and provide empirical data for systems selected for mathematical analysis.

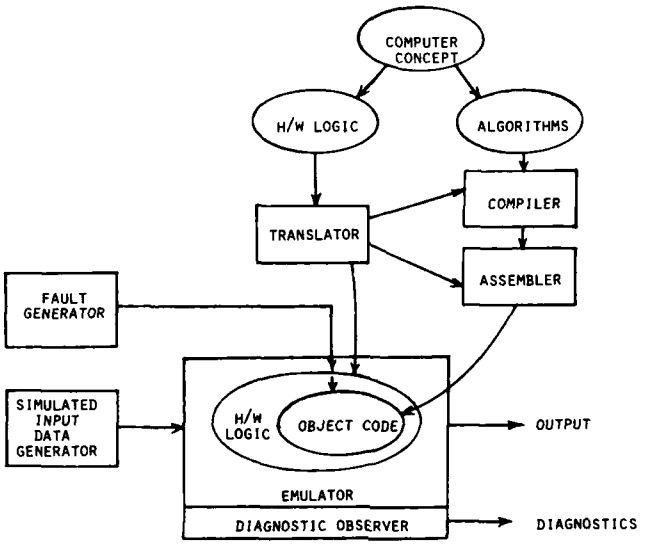

Fig. 15 Diagnostic Emulator.

4. DESIGN GUIDELINES RESEARCH

The application of validation techniques to advanced system concepts as discussed in the introduction and illustrated in figure 2 provides an opportunity to identify guidelines that will be helpful in designing fault-tolerant systems that are validatable. Experiments that may provide information on design considerations are being conducted on fault-tolerant computer test specimens SIFT and FTMP that exist in AIRLAB and experiments are being defined for several advanced architectures that are planned to be available in AIRLAB in the future. Examples of AIRLAB activities to be conducted in the near future include an implementation of fault-tolerant software on the SIFT computer and the definition and development of validation techniques and assessment methodologies for an Integrated Airframe/Propulsion System Architecture (IAPSA) and for the Advanced Information Processing System (AIPS).

The two fault-tolerant computer systems that are currently installed in AIRLAB to be used as test specimens are SIFT and FTMP. As the name implies, the SIFT computer shown in figure 16 isolates faults

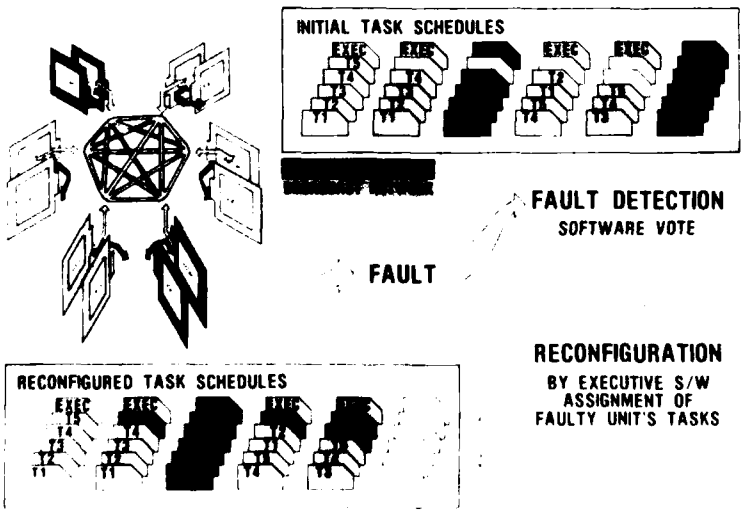

Fig. 16 Software Implemented Fault Tolerance Computer.

primarily with voting techniques implemented in software. Upon detection of an error using a software voter the operating system software decides which element of the system is faulty and invokes a reconfiguration task to eliminate the faulty element. The detailed design and operation of SIFT are discussed in reference 13. The FTMP computer has a very different architecture from SIFT as seen in figure 17. FTMP initially detects faults in a hardware voter and error detector. The FTMP operating

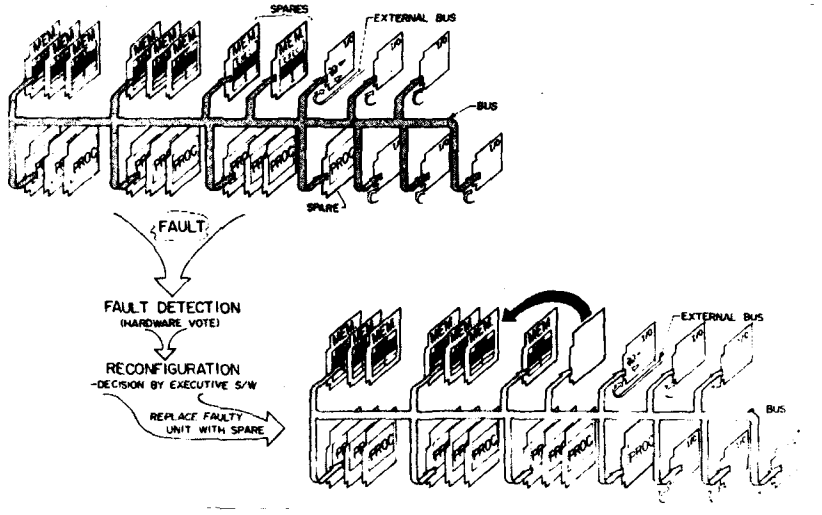

Fig. 17 Fault-Tolerant Multiprocessor.

system software also invokes a reconfiguration task to eliminate the faulty elements of the system.[14] Both the SIFT and FTMP computers are available for developing validation experiments and analytical procedures. An example of experiments currently being conducted using SIFT and FTMP is the collection of input data required by analytical performance and reliability techniques. Results from the SIFT and FTMP experiments will be applied to the development of a methodology for validating any advanced fault-tolerant computer system concept.

The objectives of implementing fault-tolerant software on the SIFT computer are to evaluate the impact of fault-tolerant software on computer design and to estimate the reliability gains to be obtained. The activity involves the application of a modified recovery block technique[15] to a part of the operating system of SIFT. The recovery block technique in software is similar to a hardware system with a standby spare. When the primary software module fails, an alternate module that is dissimilar to the primary module is substituted for the primary module. The structure for the experiment on SIFT consists of a primary algorithm, a single alternate, and an acceptance test. The initial objective of the experiment is to gain experience in applying fault-tolerant software on a real time flight control computer and to determine how to collect data that is needed for examining possible reliability gains. This work is a precursor to efforts discussed below on the Critical Activating Technology program and is primarily to gain hands-on experience in preparation for that program.

The IAPSA program provides an opportunity to define validation techniques applicable to an integrated electronic control system during the initial design phases. The first phase of the IAPSA effort including simultaneous studies by two airframe manufacturers has been completed. The objectives of the studies were to define the requirements for an integrated digital control system architecture for 1990's high performance aircraft, define candidate architectures to meet the requirements, and select the most promising concept for further investigation and implementation.[16,17] The second phase of this work involves performing a detailed system design and implementation. The major issue to be addressed in this effort is system validation. Therefore, the design and implementation process will be a major departure from the traditional approach in that performance and reliability models are to be developed first, followed by the development of a validation plan. A system will then be designed to realize the models and AIRLAB experiments will be used to aid in resolving design issues. The next step will be to implement an engineering model of the system and test the model in AIRLAB according to the validation plan.

The AIPS program provides a system architecture against which emerging validation techniques and software design methods can be evaluated. The thrust of the AIPS development is to provide a system architectural design composed of a set of core building blocks that can be configured and assembled for a variety of applications ranging from spacecraft to civil aircraft. Design methodology, system modularity, hardware/software architecture, and validation processes are major elements of the program output. Current plans include building a proof-of-concept (POC) system to demonstrate system applicability and to provide a test specimen in AIRLAB for the development of validation and assessment methodologies specific to the AIPS architectural designs. Although the POC system will not be delivered to AIRLAB for several years, a plan is being implemented that will utilize some of the individual architectural building blocks to simulate the AIPS concept in AIRLAB at a level detailed enough to address design issues, especially those that might facilitate system validation. Initial experiments will be conducted using FTMP and a Fault Tolerant Processor (FTP) which are major building blocks for the AIPS architecture. Supplementary to the AIPS program is the Critical Activating Technology (CAT) program which includes as a major element the investigation of the applicability of fault-tolerant software to the AIPS concept. The thrust of this work is to determine the impact on system hardware and software design of incorporating fault-tolerant software and to determine the gains to be expected in software reliability with fault-tolerant software included.[18] AIRLAB experiments are being developed to address the question of what reliability gains might be obtained.

AD-A153 254 GROUND AND FLIGHT TESTING FOR AIRCRAFT GUIDANCE AND CONTROL(U) ADVISORY GROUP FOR AEROSPACE RESEARCH AND DEVELOPMENT NEUILLY-SUR-SEINE (FRANCE) R ONKEN ET AL. 3/3

UNCLASSIFIED DEC 84 AGARD-AG-262 F/G 1/4 NL

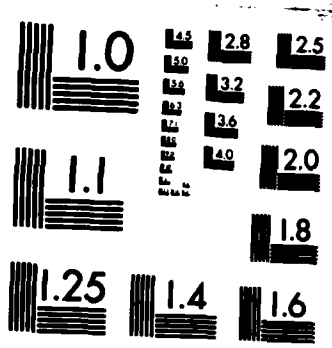

5. CONCLUSIONS

NASA'S AIRLAB provides a unique capability for pursuing new methods for designing and validating fault-tolerant systems that will be required to meet the requirements imposed by flight-crucial applications in advanced aircraft and spacecraft designs. Since AIRLAB is a national facility, cooperative research activities between NASA, industry, academia and other government agencies that take advantage of the laboratories features are encouraged. Using the AIRLAB capability and research sponsored by NASA, new reliability techniques such as CARE III and SURE have been developed. Procedures for collecting fault-occurrence and fault-handling data are being generated using fault-injection techniques at the pin level on hardware test specimens FTMP and SIFT and at the gate level on the diagnostic emulator. Some progress has also been made in improving formal proof-of-correctness techniques and a procedure has been developed to verify assumptions made in the proof of a clock synchronization algorithm. In addition, experiments are underway that will lead to the development of techniques for measuring the performance of fault-tolerant systems. Other experiments have provided data on the occurrence of errors in software. The techniques and procedures resulting from these experiments will become the basis of a validation methodology for enhancing the ability to evaluate fault-tolerant electronic systems. Experiments for evaluating the effectiveness of the proposed validation methodology will also lead to establishment of guidelines applicable to the design of advanced electronic systems. The availability of effective validation methods will pave the way for more confidently using fault-tolerant electronic systems in applications with flight-crucial requirements. The availability of validatable fault-tolerant systems will enable the continued expansion of ideas for improving the performance of future aerospace vehicles beyond what may be possible today.

5. References

1. Holt, H. Milton: Validation Methods for flight-crucial Systems. 1983 SAE Aerospace Congress and Exposition Conference on Aerospace Behavioral Engineering Technology, Long Beach, CA. October 1983.

2. Validation Methods for Fault-Tolerant Avionics and Control Systems--Working Group Meeting I. NASA CP-2114, 1979.

3. Validation Methods for Fault-Tolerant Avionics and Control Systems--Working Group Meeting II. NASA CP-2130, 1979.

4. Stiffler, J. J., et al.: CARE III Final Report Phase I, Vols. 1 and 2. NASA CR-159122 and NASA CR-159123, 1979.

5. Bavuso, S. J.: Trends in Reliability Modeling Technology for Fault Tolerant Systems. AGARD Conf. Proc. No. 261 on Avionics Reliability, Its Techniques and Related Disciplines, April 1979.

6. Stiffler, J. J.; and Bryant, L. A.: CARE III Phase II Report, Mathematical Description. NASA CR-3566, 1982.

7. Butler, R. W.: The Semi-Markov Unreliability Range Evaluator (SURE). NASA TM 86261, 1984.

8. White, Allan L.: Upper and Lower Bounds for Semi-Markov Reliability Models of Reconfigurable Systems. NASA CR-172340, 1984.

9. Geist, R.; Trivedi, K.; Dugan, J.; and Smotherman, M.: Design of the Hybrid Automated Reliability Predictor. Proceedings of the 5th IEEE/AIAA Digital Avionics Systems Conference, Seattle, WA, November 1983.

10. Krishna, C.M.; and Shin, K.G.: Performance Measures for Fault-Tolerant Multiprocessor Controllers for Critical Processes. Proceedings of the 20th Annual Allerton Conference on Communications, Control, and Computing, University of Illinois, October 1982.

11. Levitt, K. N. et al.: Investigation, Development, and Evaluation of Performance Proving for Fault-Tolerant Computers. NASA CR-166008, 1983.

12. Nagel, P. M.; and Skrivan, J. A.: Software Reliability: Repetitive Run Experimentation and Modeling. NASA CR-165836, 1982.

13. Goldberg, J., et al: Development and Analysis of the Software Implemented Fault Tolerance (SIFT) Computer. NASA CR-172146, 1984.

14. Smith, T. B., III, et al.: Development and Evaluation of a Fault-Tolerant Multiprocessor (FTMP) Computer, Volume I-FTMP Principles of Operation. NASA CR-166072, 1983.

15. Hecht, Myron; and Hecht, Herbert: Fault-Tolerant Software Modules for SIFT. NASA CR-165874, 1982.

16. Stern, A.D.; and Carlin, C.M.: Study of Integrated Airframe/Propulsion Control System Architectures, (IAPSA) Volumes I, II, and III. NASA CR-172173, NASA CR-172174, and NASA CR-172175, 1983.

17. Bangert, L.H.; Henke, K.R.; Grommes, R.J., and Kerr, W.B.: Study of Integrated Airframe/Propulsion Control System Architectures. NASA CR-172167, 1983.

18. Slivinski, T.: Study of Fault-Tolerant Software Technology. NASA CR-172286, 1984.

REPORT DOCUMENTATION PAGE

1. Recipient's Reference	2. Originator's Reference	3. Further Reference	4. Security Classification of Document
	AGARD-AG-262	ISBN 92-835-1482-3	UNCLASSIFIED

5. Originator Advisory Group for Aerospace Research and Development
North Atlantic Treaty Organization
7 rue Ancelle, 92200 Neuilly sur Seine, France

6. Title GROUND AND FLIGHT TESTING FOR AIRCRAFT GUIDANCE AND CONTROL

7. Prepared at the request of the Guidance and Control Panel of AGARD.

8. Author(s)/Editor(s)	9. Date
Various	December 1984
10. Author's/Editor's Address	**11. Pages**
Various	204

12. Distribution Statement This document is distributed in accordance with AGARD policies and regulations, which are outlined on the Outside Back Covers of all AGARD publications.

13. Keywords/Descriptors

Flight testing	Ground testing
Active controls	Wind tunnel testing
Fuel conservation	Helicopter warfare
Digital control systems	Avionics flight testing

14. Abstract

Prepared at the request of the Guidance and Control Panel of AGARD, the purpose of this AGARDograph is to yield a survey of number of major test facilities/techniques and their benefits in evaluating new guidance and control components and systems.

AGARDograph No.262 Advisory Group for Aerospace Research and Development, NATO GROUND AND FLIGHT TESTING FOR AIRCRAFT GUIDANCE AND CONTROL Edited by R.Onken and H.A.Rediess Published December 1984 204 pages Prepared at the request of the Guidance and Control Panel of AGARD, the purpose of this AGARDograph is to yield a survey of number of major test facilities/techniques and their benefits in evaluating new guidance and control components and systems. ISBN 92-835-1482-3	AGARD-AG-262 Flight testing Active controls Fuel conservation Digital flight control systems Ground testing Wind tunnel testing Helicopter warfare Avionics flight testing	AGARDograph No.262 Advisory Group for Aerospace Research and Development, NATO GROUND AND FLIGHT TESTING FOR AIRCRAFT GUIDANCE AND CONTROL Edited by R.Onken and H.A.Rediess Published December 1984 204 pages Prepared at the request of the Guidance and Control Panel of AGARD, the purpose of this AGARDograph is to yield a survey of number of major test facilities/techniques and their benefits in evaluating new guidance and control components and systems. ISBN 92-835-1482-3	AGARD-AG-262 Flight testing Active controls Fuel conservation Digital flight control systems Ground testing Wind tunnel testing Helicopter warfare Avionics flight testing
AGARDograph No.262 Advisory Group for Aerospace Research and Development, NATO GROUND AND FLIGHT TESTING FOR AIRCRAFT GUIDANCE AND CONTROL Edited by R.Onken and H.A.Rediess Published December 1984 204 pages Prepared at the request of the Guidance and Control Panel of AGARD, the purpose of this AGARDograph is to yield a survey of number of major test facilities/techniques and their benefits in evaluating new guidance and control components and systems. ISBN 92-835-1482-3	AGARD-AG-262 Flight testing Active controls Fuel conservation Digital flight control systems Ground testing Wind tunnel testing Helicopter warfare Avionics flight testing	AGARDograph No.262 Advisory Group for Aerospace Research and Development, NATO GROUND AND FLIGHT TESTING FOR AIRCRAFT GUIDANCE AND CONTROL Edited by R.Onken and H.A.Rediess Published December 1984 204 pages Prepared at the request of the Guidance and Control Panel of AGARD, the purpose of this AGARDograph is to yield a survey of number of major test facilities/techniques and their benefits in evaluating new guidance and control components and systems. ISBN 92-835-1482-3	AGARD-AG-262 Flight testing Active controls Fuel conservation Digital flight control systems Ground testing Wind tunnel testing Helicopter warfare Avionics flight testing

AGARD
NATO OTAN
7 RUE ANCELLE · 92200 NEUILLY-SUR-SEINE
FRANCE
Telephone 745.08.10 · Telex 610176

DISTRIBUTION OF UNCLASSIFIED AGARD PUBLICATIONS

AGARD does NOT hold stocks of AGARD publications at the above address for general distribution. Initial distribution of AGARD publications is made to AGARD Member Nations through the following National Distribution Centres. Further copies are sometimes available from these Centres, but if not may be purchased in Microfiche or Photocopy form from the Purchase Agencies listed below.

NATIONAL DISTRIBUTION CENTRES

BELGIUM
Coordonnateur AGARD — VSL
Etat-Major de la Force Aérienne
Quartier Reine Elisabeth
Rue d'Evere, 1140 Bruxelles

CANADA
Defence Scientific Information Services
Dept of National Defence
Ottawa, Ontario K1A 0K2

DENMARK
Danish Defence Research Board
Ved Idraetsparken 4
2100 Copenhagen Ø

FRANCE
O.N.E.R.A. (Direction)
29 Avenue de la Division Leclerc
92320 Châtillon

GERMANY
Fachinformationszentrum Energie,
Physik, Mathematik GmbH
Kernforschungszentrum
D-7514 Eggenstein-Leopoldshafen

GREECE
Hellenic Air Force General Staff
Research and Development Directorate
Holargos, Athens

ICELAND
Director of Aviation
c/o Flugrad
Reyjavik

ITALY
Aeronautica Militare
Ufficio del Delegato Nazionale all'AGARD
3 Piazzale Adenauer
00144 Roma/EUR

LUXEMBOURG
See Belgium

NETHERLANDS
Netherlands Delegation to AGARD
National Aerospace Laboratory, NLR
P.O. Box 126
2600 AC Delft

NORWAY
Norwegian Defence Research Establishment
Attn: Biblioteket
P.O. Box 25
N-2007 Kjeller

PORTUGAL
Portuguese National Coordinator to AGARD
Gabinete de Estudos e Programas
CLAFA
Base de Alfragide
Alfragide
2700 Amadora

TURKEY
Department of Research and Development (ARGE)
Ministry of National Defence, Ankara

UNITED KINGDOM
Defence Research Information Centre
Station Square House
St Mary Cray
Orpington, Kent BR5 3RE

UNITED STATES
National Aeronautics and Space Administration (NASA)
Langley Field, Virginia 23365
Attn: Report Distribution and Storage Unit

THE UNITED STATES NATIONAL DISTRIBUTION CENTRE (NASA) DOES NOT HOLD STOCKS OF AGARD PUBLICATIONS, AND APPLICATIONS FOR COPIES SHOULD BE MADE DIRECT TO THE NATIONAL TECHNICAL INFORMATION SERVICE (NTIS) AT THE ADDRESS BELOW.

PURCHASE AGENCIES

Microfiche or Photocopy
National Technical
Information Service (NTIS)
5285 Port Royal Road
Springfield
Virginia 22161, USA

Microfiche
ESA/Information Retrieval Service
European Space Agency
10, rue Mario Nikis
75015 Paris, France

Microfiche or Photocopy
British Library Lending
Division
Boston Spa, Wetherby
West Yorkshire LS23 7BQ
England

Requests for microfiche or photocopies of AGARD documents should include the AGARD serial number, title, author or editor, and publication date. Requests to NTIS should include the NASA accession report number. Full bibliographical references and abstracts of AGARD publications are given in the following journals:

Scientific and Technical Aerospace Reports (STAR)
published by NASA Scientific and Technical
Information Branch
NASA Headquarters (NIT-40)
Washington D.C. 20546, USA

Government Reports Announcements (GRA)
published by the National Technical
Information Services, Springfield
Virginia 22161, USA

Printed by Specialised Printing Services Limited
40 Chigwell Lane, Loughton, Essex IG10 3TZ

ISBN 92-835-1482-3

END

FILMED

6-85

DTIC